Synthesis and Characterisation of Ferrite-Ferroelectric Composites with Rare Earth Substitution

Thesis Submitted for the

Award of the Degree of

Doctor of Philosophy

by

Renu Rani
(Regn. No. 900912019)

to

School of Physics and Material Science
Thapar University,
Patiala-147004, India

April - 2013


Dedicated
To
My
Family

CERTIFICATE

This is to certify that the thesis entitled **"Synthesis and Characterisation of Ferrite - Ferroelectric Composites with Rare Earth Substitution"** which is being submitted by **"Ms. Renu Rani"** in fulfillment of the requirement for the award of degree of Doctor of Philosophy to Thapar University, Patiala, is a record of candidate's own work carried out by her under our supervision and guidance.

The matter presented in this thesis has not been submitted in part or full for the award of any degree in any other University or Institute.

Supervisors

.....

Dr. Chandra Prakash
Directorate of ER&IPR, DRDO,
DRDO Bhawan, New Delhi-110105

Sangeeta 25/10/12

.....

Dr. Sangeeta Singh
Department of Physics,
G.V.M. Girls Colllege, Sonepat-131001

31/10/2012

.....

Prof. K.K. Raina
School of Physics and Materials Science
Thapar University, Patiala-147004

ACKNOWLEDGEMENT

Despite having only one name on the cover, this thesis would not have been possible without the input of others whose assistance has been invaluable. Firstly, I express my deepest and sincere gratitude to my supervisors ***Dr. K. K. Raina,*** *Thapar University, Patiala,* ***Dr. Chandra Prakash****, DRDO, New Delhi and* ***Dr. Sangeeta Singh****, G.V.M. Girls College, Sonipat for their continuous support and guidance in my research efforts. It is really difficult to express in words my indebtedness to them for everything they have done for me. Without the guidance of their previous work, much of what accomplished in this thesis would not have been possible.*

I wish to express my deepest and sincere gratitude to ***Dr. J.K. Juneja****, Hindu College, Sonipat for the constant guidance, motivation, support and freedom throughout the course of this work. I am thankful to him for giving me enough time and attention during research, while writing manuscripts and thesis.*

I must acknowledge ***Dr. Abhijit Mukherjee****, Director Thapar University, Patiala, for granting me the permission to register for Ph.D. programme in his meritorious institute. I would like to recognize the contribution of* ***Dr. Kulbir Singh****, Head, SPMS, Thapar University, Patiala, for his persistent help in overcoming the bureaucracy issues that would have impeded completion of my Ph. D. work. I also appreciate the time and efforts of* ***Dr. O.P. Pandey****and* ***Dr. Puneet****Faculty SPMS, devoted in analyzing my research work.*

I am also thankful to ***Dr. O.P. Pruthi****, President, managing committee, G.V.M. Girls College, Sonepat and* ***Dr. JyotiJuneja****, Principal, G.V.M. Girls College, Sonepat, for providing excellent research facilities and working atmosphere in Electroceramic Research Laboratory (ERL), G.V.M. Girls College, Sonepat. Without their co-operation it wouldnot have been possible for me to complete my research work.*

I oblige the co-operation of ***Dr. R. P. Pant*** *(NPL, New Delhi) for permitting me to record XRD patterns for this study and* ***Dr. R.K. Kotnala****(NPL, New Delhi) for carrying out magnetic measurements in his lab.It is my pleasure to thank* ***Dr. R.S.***

Kunduand***Dr. Rajesh Punia***, G.J.U. Hisar, for their kind permission to undertake structural measurements related to this work.

I cannot explain how thankful I am to my seniors as well as my friends ***Dr. Praveen Kumar***, ***Dr. PratibhaSingh***,***Ravi Shukla***, ***Rekha Rani***and***Dipti***for creating a homely atmosphere at the work place and extending all possible help for performing experiment.I have always found them to be ready to help at any moment, may be either in the field of research or in any day-to-day problems. I specially thank tomy friends and all lab members***Ramneek***, ***Gurpreet***, ***Rishi*** and ***Supreet*** in Material Research Lab, Thapar University, Patiala for their co-operation in every manner.

I would like to thank CSIR, PSCST and CICS for their financial support for present my work in UNSW, Sydney, Australia, in International Conference on Electroceramics, Dec 12-16-2011.

I would like to thank my Mummy, Papa and Brother***Mr. RakeshDahiya*** for their continual love and unconditional support. I would like to extend special thanks to my Bhabhi***Mrs.Geeta*** for her persistent moral support, encouragement and their forbearance of my hectic schedule in completing my research work.I thank my fiancé***Vishal Khatri***, for his unstinted support and love during past two years, without which it would have not been possible for me to complete my work in time.

Finally, I would like to thank God for giving me most precious family, relatives and close friends, who shared with me every moment of joy and despair, by their immense patience and moral supports.

(Renu Rani)

ABSTRACT

The materials exhibiting at least two of the three properties (ferroelectricity, ferromagnetism and ferroelasticity) are termed as multiferroic materials. Magnetoelectric materials, which simultaneously exhibit ferroelectricity and ferromagnetism, have been drawing attention of the researchers due to their multifunctionality and thereby finding applications in a number of devices. Researchers found a lot of interest in these materials not only because they have the properties of their parent compounds i.e. ferrite and ferroelectric phase, but also due to their unique property, Magnetoelectric (ME) effect. The magnetoelectric effect is a coupled two-field effect in which induction of electric polarization by applying an external magnetic field and induction of magnetic polarization by applying an external electric field. Magnetoelectric materials can be realized in single phase and two phases (composite form). In single phase materials, ME is due to the coupling of magnetic and electric orders but almost all single phase magnetoelectric materials have temperature constraint i.e. they show ME effect at low temperatures and the effect is weak. Due to this, these materials have very limited use.To overcome the deficiency of single-phase multiferroics and to provide new approach to the magnetoelectric coupling mechanisms, recent work concentrates on the class of composite-type magnetoelectric materials. In magnetoelectric composite the origin of magnetoelectric effect is due to mechanical coupling between magnetostriction effect in ferrite phase and piezoelectric effect in ferroelectric phase i.e. stress-strain coupling. These composite-type material have high ME coupling response even above room temperature and due to their high value of ME coefficients, these materials have various advantages over single-phase magnetoelectric materials.So many researchers are getting attracted towards the investigations of magnetoelectric composite materials not only due to their large value of ME coefficient but also due to their wide range of applications in electronic devices like sensors, wave guide, transducers, actuators, phase invertors, radio electronics, optoelectronics, microwave electronics, transducers in instrumentation and fiber communication technology. For the present work, composites of Ni-Zn ferrite (NZF) and barium strontium titanate (BST) were studied and efforts have been made to improve their dielectric, ferroelectric, piezoelectric, magnetic and magnetoelectric properties.

In the present work following series were prepared for detailed and systematic study

Series A		$(1-y)Ba_{0.9}Sr_{0.1}TiO_3 - (y)\ Ni_{0.8}Zn_{0.2}Fe_2O_4$	(y = 0 - 0.15in step of 0.05)
Series B	Series B1	$Ba_{0.9}Sr_{0.1}Zr_xTi_{1-x}O_3$	(x = 0 - 0.16 in step of 0.04)
	Series B2	$(1-y)Ba_{0.9}Sr_{0.1}Zr_{0.04}Ti_{0.96}O_3 + (y)\ Ni_{0.8}Zn_{0.2}Fe_2O_4$	(y = 0 - 0.15 in step of 0.05)
	Series B3	$0.95Ba_{0.9}Sr_{0.1}Zr_xTi_{1-x}\ O_3 + 0.05Ni_{0.8}Zn_{0.2}Fe_2O_4$	(x = 0 - 0.16 in step of 0.04)
Series C	Series C1	$Ba_{0.9-3x/2}Sr_{0.1}La_xTiO_3$	(x=0 - 0.02 in step of 0.005)
	Series C2	$(1-y)Ba_{0.9-3x/2}Sr_{0.1}La_{0.005}TiO_3 + (y)\ Ni_{0.8}Zn_{0.2}Fe_2O_4$	(y = 0 - 0.15 in step of 0.05)
	Series C3	$0.95Ba_{0.9-3x/2}Sr_{0.1}La_{0.005}TiO_3 + 0.05\ Ni_{0.8}Zn_{0.2}Fe_2O_4$	(x=0 - 0.02 in step of 0.005)
Series D		$(1-y)Ba_{0.9}Sr_{0.1}Zr_{0.04}Ti_{0.96}O_3 + (y)\ Ni_{0.8}Zn_{0.2}Fe_2O_4$	(y = 0 - 0.15 in step of 0.05)

Note: Samples of series A, B and C were sintered in conventional furnace and those of series D were sintered using microwave furnace

The research work carried out for the Ph.D. thesis has been divided into seven chapters as summarized below briefly: -

Chapter IThe introduction and importance of the individual phases and magnetoelectric composites are discussed in this chapter. The aim of carrying out the present work including the criteria of selection of individual phases (ferrite and ferroelectric), scope of these investigations have also been discussed. We also describe a brief review of the research and development work that has been carried out till recently in magnetoelectric composites. **Chapter II** deals with methods of sample preparation and characterization techniques used for studying various properties (like structural, dielectric, ferroelectric, ferromagnetic and magnetoelectric) of ceramics. The details of experimental techniques, various characterization equipments and their working details are also given in this chapter. Optimization of sintering temperature of $0.1Ni_{0.8}Zn_{0.2}Fe_2O_4$ – 0.9 $Ba_{0.9}Sr_{0.1}TiO_3$ composite and results of (1-y) $Ba_{0.9}Sr_{0.1}TiO_3$ + $(y)Ni_{0.8}Zn_{0.2}Fe_2O_4$ (series A) composite are discussed in ***Chapter III.*** In ***Chapter IV*** we are reporting the effect of Zr content on $Ba_{0.9}Sr_{0.1}Zr_xTi_{1-x}O_3$ (BSZT) for x = 0.00 to 0.16 in steps of

0.04 (Series B1) for optimization of Zr substituted ferroelectric phase for composite. For x = 0.04 in BSZT, we observed best dielectric and ferroelectric properties. So for composite system, we selected ferroelectric phase as $Ba_{0.9}Sr_{0.1}Zr_{0.04}Ti_{0.96}O_3$ and vary the second phase i.e NZF (Series B2). In this chapter we are also reporting the effect of Zr content on composite system by keeping fixed ratio of both phases (series B3). In ***Chapter V*** we are reporting the effect of La content on $Ba_{0.9-3x/2}Sr_{0.1}La_xTiO_3$ for x = 0.00 to 0.02 in steps of 0.005 ($Ba_{0.9}Sr_{0.1}TiO_3$) for optimization of La substituted ferroelectric phase for composite. For x = 0.005 in BSLT we observed best dielectric and ferroelectric properties. So for composite system we select the ferroelectric phase as $Ba_{0.9-3x/2}Sr_{0.1}La_{0.005}TiO_3$ and vary the second phase i.e NZF (Series C2). In this chapter we are also reporting the effect of La content on composite system by keeping fixed ratio of both phases (series C3). In ***Chapter VI*** we are reporting the structural, dielectric, ferroelectric and ferromagnetic properties of (1-y) $Ba_{0.9}Sr_{0.1}TiO_3$ + (y)$Ni_{0.8}Zn_{0.2}Fe_2O_4$ composites prepared by microwave sintering and the properties of micro wave sintered composites are compared with those prepared by conventional solid state sintering are also presented in this chapter. ***Chapter VII*** includes the conclusion and summary of the results. Recommendations for the future work have also been given in this chapter.

LIST OF PUBLICATIONS

A *In Refreed Journal*

1) *Dielectric and Ferroelectric Properties of BST and Ni-Zn Ferrite Composites*, **Renu Rani**, Parveen Kumar, Sangeeta Singh, J.K. Juneja, Chandra Prakash and K.K. Raina, *Integrated Ferroelectrics*, **122** (2010) 38-44.

2) *Dielectric properties of Zr substituted BST ceramics*, **Renu Rani**, Sangeeta Singh, J.K. Juneja, Chandra Prakash and K.K. Raina, *Ceramic International*, **37** (2011) 3755-3758.

3) *Effect of Two-Stage Sintering on Dielectric Properties of* $BaTi_{0.9}Zr_{0.1}O_3$ *Ceramics*, RekhaRani, **Renu Rani**, Parveen Kumar, Sangeeta Singh, J.K. Juneja, Chandra Prakash and K.K. Raina, *Phase Transition*, **84** (2011) 843-849.

4) *Influence of Zr Substitution on Ferroelectric Properties of BST Ceramics*, **Renu Rani**, Parveen Kumar, Sangeeta Singh, J.K. Juneja, Chandra Prakash and K.K. Raina, *Ferroelectric Letters*, **38** (2011) 108-113.

5) *Structural and Dielectric properties of Ba0.9Sr0.1ZrxTi1-xO3+ 5%* $Ni_{0.8}Zn_{0.2}Fe_2O_4$*Composite*, **Renu Rani**, Sangeeta Singh, J.K. Juneja, Chandra Prakash and K.K. Raina, *Ferroelectric letters*, **38** (2011) 134-140.

6) *Effect of Sintering Temperature on Dielectric Properties of Iron Deficient Nickel Ferrite*,**Renu Rani**, Sangeeta Singh, J.K. Juneja, K.K. Raina and Chandra Prakash, *American Institute of Physics*, **1372** (2011) 216-219.

7) *Improved Dielectric Properties via Mechano- Chemical Activation in* $Ba_{0.80}Pb_{0.20}TiO_3$ *Ceramics*, Parveen Kumar, **Renu Rani**, Sangeeta Singh, J.K. Juneja, Chandra Prakash and K.K. Raina, *American Institute of Physics*, **1393** (2011) 339-340.

8) *Structural, Electrical, Magnetic and Magnetoelectric properties of (y)* $Ni_{0.8}Zn_{0.2}Fe_2O_4$ + *(1-y)* $Ba_{0.9}Sr_{0.10}Zr_{0.04}Ti_{0.96}O_3$ *Composites*, **Renu Rani**, Sangeeta Singh, J.K. Juneja, Chandra Prakash and K.K. Raina, *Advances in Condensed Matter Physics* ***(accepted)***

9) *Structural, Electrical and Magnetic Properties of Microwave Processed* $Ni_{0.80}Zn_{0.20}Fe_2O_4$,**Renu Rani**, Sangeeta Singh, Chandra Prakash and K.K. Raina, *Journal of key engineering Materials*, **547** (2013)25-30.

10) *Dielectric and Ferroelectric Properties of Sr Substituted BaTiO3 and Mn-doped Ni-ZnFerrite*

*Composites,***Renu Rani**, Parveen Kumar, Sangeeta Singh, J.K. Juneja, Chandra Prakashand K.K. Raina, *Bulletin of Material Science* ***(communicated)***.

11) *Structural, Dielectric and Ferroelectric Properties of* $Ba_{0.9}Sr_{0.1}TiO_3$ *and Mn doped* $Ni_{0.8}Zn_{0.2}Fe_2O_4$ *Composites*, **Renu Rani**, Parveen Kumar, Sangeeta Singh, J.K. Juneja, Chandra Prakash and K.K. Raina ,*Ceramic International* ***(communicated).***

12) *Dielectric, Ferroelectric, Magnetic and Magnetoelectric Properties of* $0.05\ Ni_{0.8}Zn_{0.2}Fe_2O_4$-$0.95\ Ba_{0.9-3x/2}Sr_{0.1}La_xTiO_3$ *Magnetoelectric Composites,* **Renu Rani**, Sangeeta Singh, J.K. Juneja, Chandra Prakash and K.K. Raina***(To be Communicated)***

B *In Conferences*

(i)International Conferences

1) *Structural and Dielectric Properties of BST Ceramics Prepared by Microwave Processing,***Renu Rani**, Rekha Rani, Parveen Kumar, Sangeeta Singh, J.K. Juneja, Chandra Prakash and K.K. Raina, *International Symposium on Nanostructured Materials: Structure, Properties, and Applications (ISNM-2009)organized by KanyaMahavidyalaya, Jalandhar, Punjab,* ***Oct 28-29, 2009***.

2) *Dielectric and Ferroelectric Properties of BST and Ni-Zn Ferrite Composites,***Renu Rani**, Parveen Kumar, Sangeeta Singh, J.K. Juneja, ChandraPrakash and K.K. Raina "*International Conference on Electroceramics, New Delhi,* ***December 13-17,2009***.

3) *Dielectric and Ferroelectric Properties of Strontium Substituted* $BaTiO_3$ *and Mn-doped Ni-ZnFerrite Composites,***Renu Rani**, Parveen Kumar, Sangeeta Singh, J.K. Juneja, K.K. Rainaand Chandra Prakash, *International Workshop & Symposium on the Synthesis and Characterisationof Glass/Glass Ceramics, C-MET Pune,* ***July 7-10, 2010***.

4) *Improved Dielectric Properties via Mechano-Chemical Activation in* $Ba_{0.80}Pb_{0.20}TiO_3$*Ceramics*, Parveen Kumar, **Renu Rani**, Sangeeta Singh, J.K. Juneja, Chandra Prakash and K.K. Raina, *International Conference On Advanced in Condensed Nano Materials(ICACNM-2011) Panjab University, Chandigarh,* ***Feb 23-26, 2011***.

5) *Structural, Electrical and Magnetic properties of Microwave processed Ni-Zn ferrite* **Renu Rani**, Chandra Prakash and K.K. Raina, *International Conference on Electroceramics, Sydney, Australia,* ***December 12-16, 2011***.

6) *Impedance studies of (1-y)$Ba_{0.9}Sr_{0.1}TiO_3$ + (y) $Ni_{0.8}Zn_{0.2}Fe_2O_4$ Composite*, **Renu Rani**, SangeetaSingh,J.K. Juneja, K.K. Rainaand Chandra Prakash, *International conference and workshop on nanostructured ceramics and other nanomaterials (ICWNCN), Delhi* ***March 13-16,2012***.

(ii)National Conferences

1) Attended *National Seminar on Condensed Matter, High Energy and Nuclear Physics*, organised by Deptt. of Physics, JMI, New Delhi , ***March 23-24, 2009***.

2) *Dielectric Behaviour of Microwave Sintered BST Ceramics*,**Renu Rani,**Rekha Gandhi, Parveen Kumar, Sangeeta Singh, J.K. Juneja, Chandra Prakash and K.K. Raina, *Recent Trends in Multifunctional Oxide Materials, Osmania University, Hyderabad,* ***July 17- 18,2009.***

3) *Dielectric Properties of Substituted Barium Titanate Processed by Novel Techniques*ParveenKumar, **Renu Rani**, Sangeeta Singh, J.K. Juneja, Chandra Prakash and K.K. Raina, *National Symposium On Microwave Processing Of Materials (NSMWP-2010), Indian Institute of Technology, Delhi*,***November 28, 2010.***

4) *Effect of Sintering Temperature on Dielectric Properties of Iron Deficient Nickel Ferrite*,**Renu Rani**, Sangeeta Singh, J.K. Juneja, K.K. Raina and Chandra Prakash, *National SeminarOn Ferroelectrics and Dielectrics(NSFD- XVI), Guru GhasidasVishavidyalaye, Bilaspur, Chattisgarh,* ***December 2-4, 2010***.

5) *Dielectric Properties of Substituted Barium Titanate Processed by Novel Technique*,Parveen Kumar, **Renu Rani**, Sangeeta Singh, J.K. Juneja, Chandra Prakash and K.K Raina,*National Seminar On Ferroelectrics and Dielectrics (NSFD- XVI), Guru GhasidasVishavidyalaye, Bilaspur, Chattisgarh,* ***December 2-4, 2010***.

6) *Dielectric Properties of La Substituted $Ba_{0.90}Sr_{0.10}TiO_3$ Ceramics***Renu Rani**, SangeetaSingh, J.K. Juneja, ChandraPrakash and K.K. Raina,*National Symposium On Materials For Advanced Technology" NSMAT, Banasthali,* ***March 27- 29, 2011.***

7) *Comparison of Dielectric Properties of Conventional and Microwave sintered 50%$Ba_{0.9}Sr_{0.1}TiO_3$+ 50% $Ni_{0.8}Zn_{0.2}Fe_2O_4$ Composites*,**Renu Rani**, Sangeeta Singh, J.K. Juneja, Chandra Prakash and K.K. Raina, *National seminar on advanced material and devices, GVMGC, Sonipat,* ***July 3-4, 2011.***

8) *Ferroelectric and Ferromagnetic properties of* $Ba_{0.9}Sr_{0.1}Zr_xTi_{1-x}O_3$ *+ 5% NZFComposite,***Renu Rani**, Sangeeta Singh, J.K. Juneja, Chandra Prakashand K.K. Raina, *National seminar on advanced material and devices, GVMGC, Sonipat,* ***July 3-4, 2011***.

9) *Electrical and Magnetic Properties of BSZT+NZF Composite,***Renu Rani**, Sangeeta Singh, J.K. Juneja, K.K. Rainaand Chandra Prakash, *National Symposium on Advanced Materials, Sharda University, Greater Noida,* ***July 6, 2011***.

10) *Effect of Lanthanum Substitution on Electrical Properties of BST Ceramics,***Renu Rani,**Sangeeta Singh, J.K. Juneja, K.K. Rainaand Chandra Prakash, *23rd AGM of MRSI, Functional materials for sustainable energy and advance technology Thapar University, Patiala,* ***Feb 13-15, 2012***.

11) *Electrical and Magnetic Properties of Ferrite-Ferroelectric composite,***Renu Rani**,Sangeeta Singh, J.K. Juneja, K.K. Rainaand Chandra Prakash*, National Conference on Recent advanced in Material Science(NCRAMS-2012), Dyal singh College, Karnal,****Feb 25-26,2012****.*

12) *Multiferroic Properties of Microwave Processed BSZT+NZF composite,* **Renu Rani**, Sangeeta Singh, J.K. Juneja, K.K. Rainaand Chandra Prakash, *National ConferenceOn Functional Materials (NCFM-2012), G.V.M. G.C. Sonipat,* ***Sep 24-25, 2012***.

13) *Multiferroic Properties Of BSLT+NZF Composite,***Renu Rani**,Sangeeta Singh, J.K. Juneja, K.K. Raina and Chandra Prakash, *National Symposium on Materials and Processing (MAP- 2012), BARC, Mumbai,* ***Oct 10-12, 2012***.

14) *Multiferroic Properties of Ni0.8Zn0.2Fe2O4 -Ba0.9-3x/2Sr0.1LaxTiO3 ME-Composites, Parveen Kumar,* **Renu Rani**, Sangeeta Singh, J.K. Juneja, K.K. Raina and Chandra Prakash, *24th AGM of MRSI, Advanced Materials For Energy Applications,****Feb 11-13,2013.***

15) *Modification in ME composite properties via different preparation techniques,* **Renu Rani**, Sangeeta Singh, J.K. Juneja, K.K. Raina and Chandra Prakash, *National Conference On Advanced Materials and Devices (NCAMD-2013),* ***Feb 27-28, 2013***

Awards/Prize/Achievements

1) Paper entitled “Electrical and Magnetic properties of Ferrite ferroelectric composite” was selected for**Best Third Paper Presentation award** in NCRAMS-2012 held on Feb 25-26, 2012 at Dyal Singh College,Karnal.

TABLE OF CONTENTS

LIST OF FIGURES

Chapter III Synthesis and Characterizations of NZF - BST Composites

Chapter IV Synthesis and Characterizations of Zr Substituted NZF– BST Composites

Chapter V Synthesis and Characterizations of La Substituted NZF– BST Composites

Chapter VI Synthesis and Characterizations of Microwave Sintered NZF– BSZT Composites

LIST OF TABLES

Chapter - I

Introduction

Chapter I

Introduction

Ferrite-ferroelectric composites consisting of two phases viz. magnetic and ferroelectric are called magnetoelectric composite. Now a days, many researchers are getting attracted towards the investigations of magnetoelectric materials not only because of their academic interest, good electrical and magnetic properties but also due to their potential applications in electronic devices like sensors, wave guide, transducers, actuators and phase invertors etc. [1-2]. These materials show the unique property i.e. magnetoelectric effect which is not shown by any individual component. The magnetoelectric (ME) effect is generally the appearance of electric polarization on applying a magnetic field or appearance of magnetization on applying an electric field.

Main aim of the present work is concentrated on the synthesis and characterization of Barium Strontium Titanate- Nickel Zinc Ferrite (BST-NZF) composites. In this context, in the following sections ferroelectricity, ferromagnetism, ferrite-ferroelectric composite (magnetoelectric composites) and their applications are going to be discussed.

1.1 Ferroelectricity

In this section an introduction to the field of ferroelectric, their structural aspects and a brief review of piezoelectric properties are presented.

Ferroelectricity is a property of certain non-conducting crystals or dielectrics that exhibit spontaneous electric polarization which can be reversed in direction by application of an external electric field. The first ferroelectric material was Rochelle salt

($KNaC_4H_4O_6 \cdot 4H_2O$) which was synthesized more than 400 years ago. Initially, ease in preparation of single crystal of Rochelle salt made it interesting for the study, but its water solubility made it technologically unattractive [3-4].The first technological breakthrough in ferroelectricity came with the discovery of barium titanate ($BaTiO_3$) during the Second World War [5-8]. Before the discovery of barium titanate, the most widely used materials for capacitors were steatite, mica, TiO_2, $MgTiO_3$ and $CaTiO_3$ with dielectric constant of $\leq$ 100 whereas the dielectric constant of barium titanate is more than 1100, which is very high as compared to the previously reported materials. Ferroelectricity in crystals can be explained on the basis of symmetry operations. It is found that symmetry operations can be combined in 32 different ways, resulting in 32 different crystal classes. These thirty-two point groups can be further classified into (a) crystals with a center of symmetry and (b) crystals without center of symmetry.

Crystals with center of symmetry, include 11 point groups which are labeled as centrosymmetric. These point groups do not show polarity. The remaining 21-point groups which do not have a center of symmetry are known as non-centrosymmetric. This non-centrosymmetric class can further be divided into two classes i.e. piezoelectric (ability to develop an electrical charge when mechanical stress is applied) and pyroelectric (ability to change polarization with temperature). Ferroelectrics are subclass of this piezoelectric and pyroelectric class. All ferroelectric crystals necessarily possess both the properties. However, pyroelectrics are not necessarily ferroelectrics [9]. Although the polarization of ferroelectric is similar to the polarization of pyroelectric but there is a difference between two polarizations because the ferroelectric polarization is reversible by an external applied electric field.Thus the materials which can be defined as ferroelectric must have two characteristics: The presence of spontaneous polarization and reversibility of the polarization under electric field [10].

The main applications of ferroelectric materials is their use in high dielectric constant capacitors, piezoelectric sonar, ultrasonic transducers, radio and communication filters, medical diagnostic transducers, stereo tweeters, buzzers, gas igniters, positive temperature

coefficient (PTC) sensors and switches, ultrasonic motors, thin-film capacitors, and ferroelectric thin film memories etc.[11-13].

In the group of ferroelectric materials there are four subcategories:

- Tungston Bronze ($PbNb_2O_6$)
- Pyrchlore ($Cd_2Nb_2O_{7)}$
- Layer Structure ($Bi_4Ti_3O_{12}$)
- Perovskite group {BaTiO3, PZT, PLZT}

Among these, the perovskite group is the most important and thus the most widely studied. Most of the useful ferroelectrics, such as barium titanate (BT), barium zirconate titanate (BZT), barium strontium titanate (BST), lead titanate ($PbTiO_3$), lead zirconate titanate (PZT) and potassium niobate ($KNbO_3$), have perovskite structure. A brief explanation about perovskite structure is given in the next section.

1.1.1 Perovskite Structure

Perovskite is the mineral name of calcium titanate ($CaTiO_3$). Its simplest structure is cubic. A typical ABO_3 unit cell structure is shown in *figure 1.1(a)* and complete lattice is shown in *figure 1.1 (b)*. The larger A cations, monovalent or divalent metal (A: Na^+, K^+, Ca^{2+}, Ba^{2+}, Pb^{2+} etc.) are on the corners of the unit cell represented by bigger sphere in this figure. The smaller B cations, tetravalent or pentavalent metal (B: Ti^{4+}, Zr^{4+}, Sn^{4+}, Nb^{5+}, Ta^{5+}, W^{6+} etc.) are at the body center represented by small sphere in the figure. The oxygen atoms are at the face centers of the cube represented by red sphere [3]. The negatively charged oxygen ions exert an electrostatic force on the positive cations, causing distortion of the crystal structure (*figure 1.1(c)*). The arrows depict the stretching motion due to the electrostatic force. The result is the electrically polarized material shown in *figure.1.1 (d)*. Ferroelectricity is characteristics of compound with distorted perovskite structure.

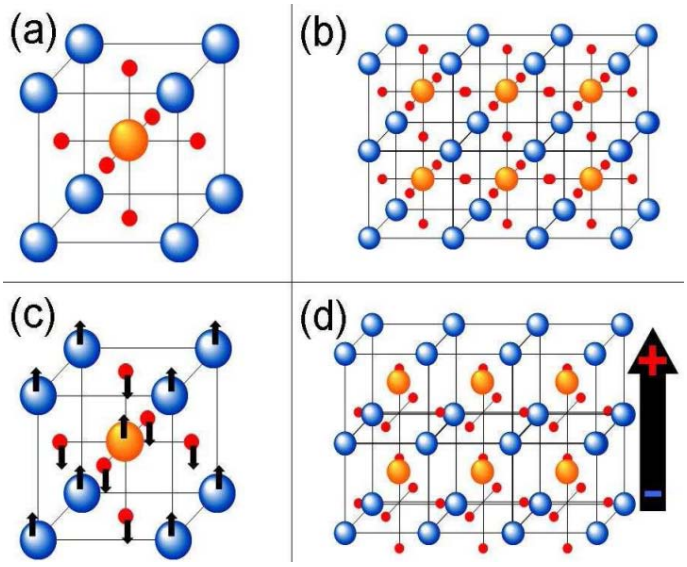

Figure 1.1 Schematic of the ferroelectric effect for a perovskite. (a) A perovskite unit cell. (b) A perovskite lattice. (c) Crystal structure distortion due to electrostatic forces between the ions. (d) Resulting electric polarization of the crystal.

1.1.2 Ferroelectric Curie point and Phase Transitions

Ferroelectric Curie point (T_c) is an important characteristic of ferroelectrics. When the temperature decreases through the Curie point, most ferroelectric materials undergo a structural phase transition from a paraelectric phase to a ferroelectric phase. The paraelectric phase always has a higher symmetry than the ferroelectric phase. The temperature of the phase transition is called as the Curie temperature (T_c). At a temperature above T_c, the crystal does not exhibit ferroelectricity; on the other hand, when the temperature is below T_c, the crystal exhibits ferroelectricity. At Curie temperature ferroelectric material shows anomalies in their properties. For example, dielectric constant has a very high value near the Curie point of ferroelectric materials. This phenomenon is usually called the 'dielectric anomaly'. Curie temperature is different for different ferroelectric materials In the case of a common ferroelectric, $BaTiO_3$, the Curie temperature T_c is 120°C [14-15].

1.1.3 Ferroelectric Domain and Hysteresis Loop

Ferroelectrics possess regions with uniform polarization, known as ferroelectric domain. Within a domain, all the electric dipoles are aligned in the same direction. There may be many domains in a crystal separated by interfaces called domain walls [10]. A single domain can be obtained by domain wall motion, by the application of electric field. Strong fields could lead to the reversal of the polarization in the domains known as domain switching. The polarization reversal can be observed by measuring the ferroelectric hysteresis as shown in *figure 1.2*.

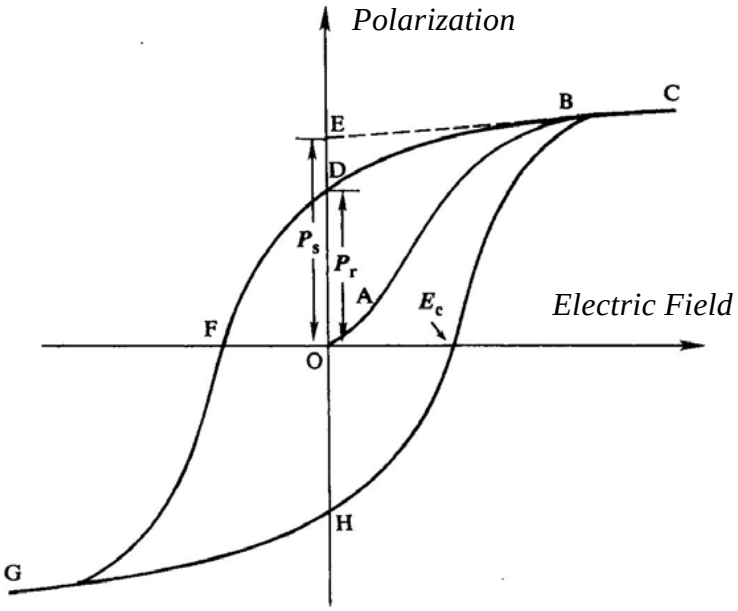

Figure1.2 Ferroelectric (P-E) hysteresis loop

The starting point is assumed to be at H (*figure 1.2*). As the electric field strength is increased, the domain starts to align in the positive direction, giving rise to rapid increase in the polarization. At very high field levels, the polarization saturates. The polarization does not fall to zero when the external field is removed. At zero external fields, some of the domains remain aligned in the positive direction hence the crystal will show a remnant

polarization P_r (OD). The crystal cannot be completely depolarized until a field of magnitude OF is applied in the negative direction. The external field needed to reduce the polarization to zero is called the coercive field strength, E_c. If the field is increased in negative direction, the direction of polarization flips and hence a hysteresis loop is obtained.

1. 2 Electrical Poling

In ferroelectric materials domains are randomly oriented ceramics, and thus the net polarization of the materials is zero. Therefore ferroelectric ceramics can not be used for piezoelectric applications directly. In order to put the materials for piezoelectric applications, domains should be aligned in one direction. This can be done by poling the samples. Poling is a process during which a high electric field is applied on the ferroelectric ceramic samples to force the domains to reorient in the direction of the applied electric field. Representation of domains allignment during poling process is shown in *figure 1.3*.

For domain reorientation, an electric field must be applied on the sample and maintained for certain duration of time. For a given field and poling time, better domain rearrangement is achieved at higher temperature, but lower than T_c because with the increase in poling temperature, crystalline anisotropy and coercive field of the ferroelectric materials decreases. Also, with increasing temperature, space charges, which act against domain motion, decreases in ceramic materials.

However, when the poling temperature is too high, a problem arises because electrical conductivity increases and the consequent increase in leakage current which may result in sample breakdown during poling process. Sample is allowed to cool to room temperature in the presence of applied field and field is removed when it is cooled to room temperature. After poling, a remnant polarization and remnant strain are maintained within the material, and it starts exhibiting piezoelectric effects [16].

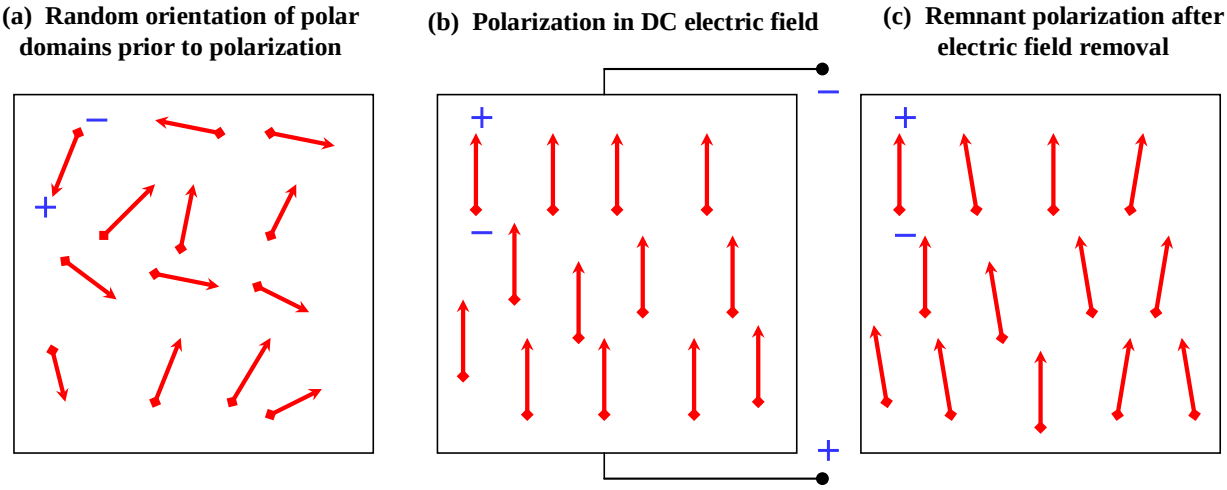

Figure.1.3 Representation of domain alignment during poling process

1.3 Piezoelectricity

The word “piezoelectricity” is originated from the Greek word “piezo” which means to press. Piezoelectric properties of ferroelectric ceramics are important for many applications.

In ferroelectric ceramics two types of piezoelectric effect are observed [17]. The first is direct piezoelectric effect, where the piezoelectric material develops a potential across its boundaries when subjected to a mechanical stress (or pressure) and this property is exploited to make sensors. Second is converse piezoelectric effect where when an electric field is applied to the material, a mechanical deformation takes place and this property can be exploited to make actuator. Thus a piezoelectric material can be used both as sensor and actuator and hence is often referred to as smart material [18].

1.3.1 Mechanism of Piezoelectricity

In a piezoelectric crystal, the positive and negative electrical charges are separated, but symmetrically distributed, so that the crystal overall is electrically neutral. When some stress is applied, this symmetry is disturbed and the charge asymmetry generates a voltage. Converse

piezoelectricity is also revealed by ferroelectrics where application of an electrical field creates mechanical stress (distortion) in the crystal. Because the charges inside the crystal are separated, the applied voltage affects different points within [19] the crystal differently, resulting in the distortion.

1.3.2 Piezoelectric Parameters and their Relations:

1.3.2 (a) Piezoelectric Charge Coefficient (d)

When a piezoelectric material is subjected to stress, electric charge is generated on the surface. The charge generated per unit force is called piezoelectric charge coefficient and is denoted by 'd' which is measured in pC/N. High value of d is required for devices such as sonar, ultrasonic cleaner, transducer etc. Piezoelectric charge coefficient is a directional property and is usually specified with subscripts to identify the conditions under which it is determined for e.g., d_{33} and d_{31}. In these piezoelectric charge coefficients, first subscript corresponds to the direction of the applied stress and second corresponds to the direction of the faces of the ceramic on which charges are developed.

1.3.2 (b) Hydrostatic Charge Coefficient (d_h)

It corresponds to the effect of development of charge when a pressure is applied on the material. Hydrostatic charge coefficient (d_h) is measured in C/N and is related to d_{33} and d_{31} piezoelectric charge constants by the relation:

$$d_h = d_{33} + 2d_{31} \qquad \textbf{…1.1}$$

1.3.2 (c) Piezoelectric Voltage Coefficient (g)

It gives the electric field produced by a stress in a piezoelectric material. Its usual units are meter-volt/Newton. 'g' constant is related to the 'd' constant by the relation:

$$g = d / (\varepsilon \varepsilon_o) \qquad \textbf{…1.2}$$

where g is called the piezoelectric voltage coefficient, ε and ε_o are the dielectric constant of the material and permittivity of the free space, respectively. Corresponding to d_{33} and d_{31} piezoelectric constants, there exist g_{33} and g_{31} piezoelectric voltage coefficients.

1.3.2 (d) Electromechanical Coupling Factor (k)

Another important parameter of piezoelectric material is the electro-mechanical coupling factor k, which reflects the efficiency of a material. It gives us the measure of the part of the applied electrical energy converted into mechanical energy or vice-versa and is determined by resonance method [20-21]. Since conversion of electrical energy into mechanical energy and vice versa is always incomplete hence *k* is always less than unity.

$$k^2 = \frac{\text{Mechanical energy converted in to electrical energy}}{\text{Input mechanical energy}} \qquad \textbf{... 1.3}$$

Depending on the mode of energy conversion, there exist various electromechanical coupling factors, for example k_p, k_t and k_{33}. Here, k_p is planar coupling coefficient, related to the energy conversion, when the applied electric field is perpendicular to the generated mechanical vibrations, which are along the plane. k_t is thickness coupling factor related to the energy conversion, when the applied electric field is in the direction of generated mechanical vibrations and which are along the thickness in the material.

1.4 Ferrimagnetism and Ferrite Materials:

In this section an introduction to the field of ferrite, their structural aspects and a brief review of magneto-striction materials are presented.

A ferrimagnetic material is the one in which the magnetic moments of the atoms on different sublattices opposite to each other but the opposing magnetic moments are unequal and a spontaneous magnetization remains as shown in *figure 1.4(a)*. Let us say A and B atoms are on two different sublattices then in ferrimagnetic materials all “A” atoms (blue)

have their spins aligned in one direction and all "B" atoms (orange) have their spin aligned in the opposite direction. As the magnetic moment of an "A" atom is greater than that of atom "B" hence there is net magnetization M, in the crystal unlike in the antiferromagnetic materials shown in *figure 1.4 (b)* [22]. In antiferromagnetic magnetic moments directed in opposite directions have same magnitudes and thus cancel out each other and as a result of it the crystals possess no magnetization.

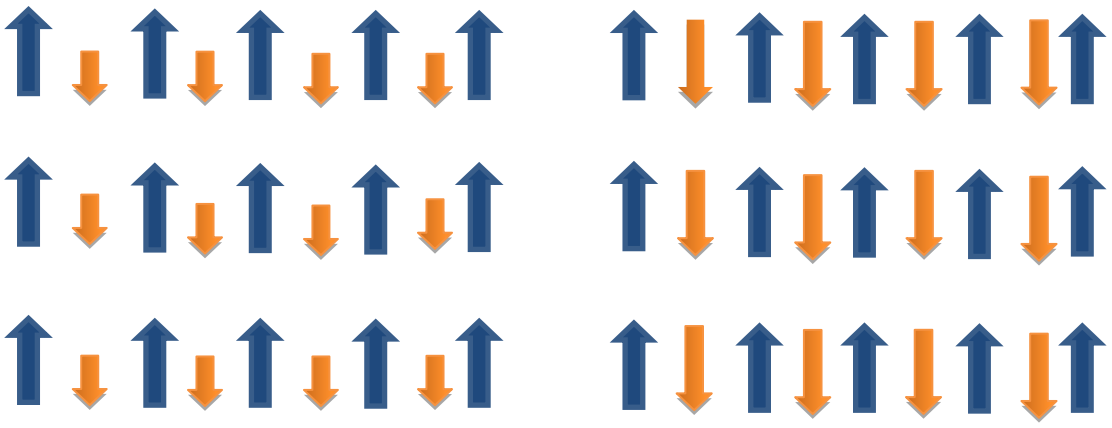

Figure 1.4 (a) Magnetic ordering in ferrimagnetic **(b)** Magnetic ordering in antiferromagnetic materials

Well known example of ferrimagnetic material is ferrites (e.g. Fe_3O_4), which are solid crystalline solution of iron and other metal oxides. The foundation of interest in this magnetic oxides were laid by Snoek [23-24] and his colleagues. Their experimental work, together with the basic theory of ferrimagnetism developed by Neel, was the starting point for rapid expansion of research activity in the field of ferrites [25]. These materials are of considerable scientific interest due to their various high frequency applications. They have been found to be of immense industrial use and their devices have numerous applications in telecommunications, space research, storage devices etc.

Their high electrical resistivity makes them very useful for high frequency work where the eddy current losses become important. In addition to this, these materials have

high dielectric constant of the order of few thousand at low frequencies and falling to about ten to twenty at microwave frequencies. Their Magnetostrictive (ability to produce magnetization when stress is applied) property is very useful in transducer applications.

1.4.1 Composition and Structure of Ferrites:

Ferrites with spinel structure; which is named after mineral spinel $MgAl_2O_4$. The general chemical formula of spinel ferrite is $MeFe_2O_4$, where Me is a divalent ion such as Fe, Mg, Co, Ni, Zn, Cu and Cd or a mixture of these. Each unit cell of spinel ferrite contains eight molecules of $MeFe_2O_4$ having 32 oxygen ions which form a cubic closed packed structure leaving 96 available interstitial sites. Unit cell of ideal spinel structure is shown in *figure 1.5 (a)* where large sphere represent oxygen ions. On close examination of this, structure shows that there are two kinds of interstices. These interstices are referred to as tetrahedral or A sites and Octahedral or B sites shown in *figure 1.5 (b)*. Out of the 96 available interstitial sites 64 are tetrahedral (A) and 32 are octahedral (B) sites and out of which only 8 and 16 respectively are occupied by metal ions. In general, the distribution of ions in ferrite is represented by the expression

$$Me_x^{2+}Fe_{1-x}^{3+}[Me_{1-x}^{2+}Fe_{1+x}^{3+}]O_4^{2-}$$

Where the metallic cations outside the bracket occupy A sites i.e. tetrahedral site and the metallic cation enclosed by square brackets occupy B sites i.e. octahedral site.

On the basis of site occupancy by divalent or trivalent metal ions spinel structure can be classified into three categories namely: Normal spinel, Inverse spinel and mixed spinel.

Normal spinel: Those ferrites in which all the tetrahedral sites are occupied by the divalent metal ions and the octahedral sites are occupied by the trivalent metal ions are called normal ferrites. In the above general formulae x=1 corresponds to normal spinel ferrites. Common examples of these ferrites are Zinc ferrite and Cadmium ferrite with their respective formulae as:

$$Zn^{2+}[Fe_2^{3+}]O_4 \text{ and } Cd^{2+}[Fe_2^{3+}]O_4$$

Inverse spinel: These are the ferrites in which 8 out of 16 trivalent metal ions occupy tetrahedral sites, and remaining trivalent metal ions and divalent metal ions occupy the octahedral sites. In the above general formula x = 0 corresponds to the case of an inverse spinel ferrites. Examples of such ferrites are magnetite and Nickel ferrite with their respective formulae

$$Fe^{3+}[Fe^{2+}Fe^{3+}]O_4^{2-} \text{ and } Fe^{3+}[Ni^{2+}Fe^{3+}]O_4^{2-}$$

Mixed spinel: Ferrites which are neither complete normal nor completely inverse are called mixed ferrites. In these ferrites A and B - sites are randomly occupied by both divalent and trivalent metal ions. In mixed ferrite $0 < x < 1$ correspond to the case of mixed spinel ferrite. The nickel zinc ferrite is the common example of this type of ferrites with the structural formula

$$Zn_x^{2+}Fe_{1-x}^{3+}[Ni_{1-x}^{2+}Fe_{1+x}3+]O_4^{2-}$$

The factors which can influence the distribution of metal ions over A and B sites in ferrites are

- Ionic radii of metal ions
- The electronic configuration
- The electrostatic energy of the spinel [26-30].

Immense studies of many properties of mixed ferrite system have been made. Among this Nickel - Zinc ferrite is an important member of these magnetic materials due to its wide range of applications as the result of its high resistivity, high magnetic permeability, low dielectric loss, high Curie temperature, high mechanical hardness, low porosity, reasonable cost and chemical stability. Mixed Ni-Zn ferrite has been commercially used in radio-frequency circuits, high-quality filters, rod antennas, transformer cores, read/write heads for high speed digital tape and operating devices [31]. So for the present study Nickel-Zinc ferrite is selected as a ferrite phase because it helps to obtain good magnetoelectric coefficient.

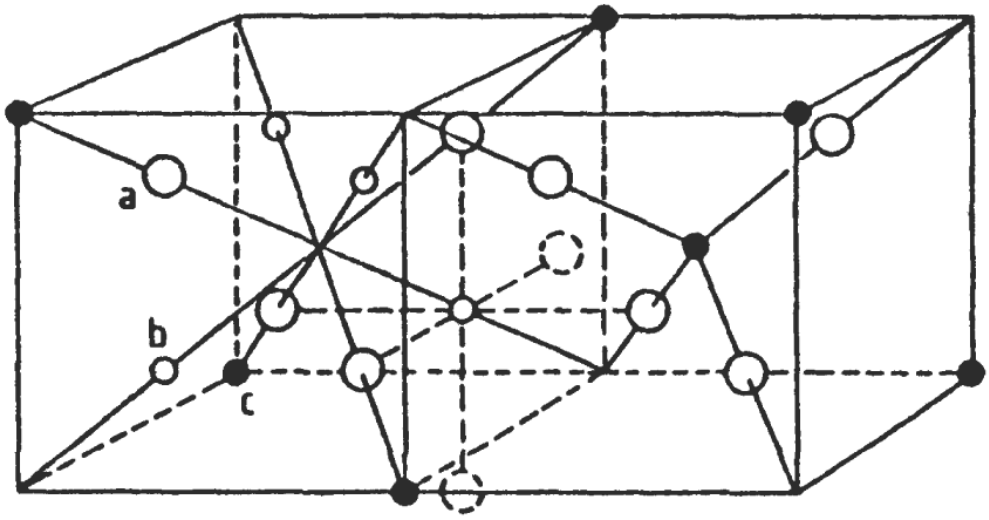

a) oxygen
b) cations occupying octahedral sites
c) cations occupying tetrahedral sites

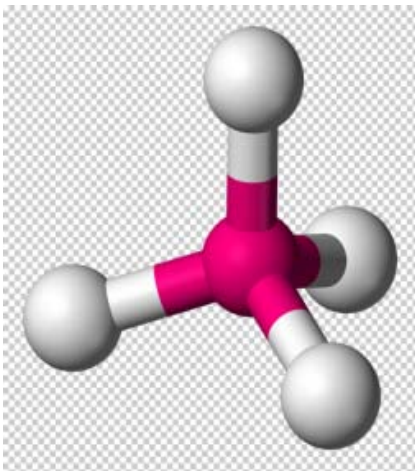

Tetrahedral , A-site

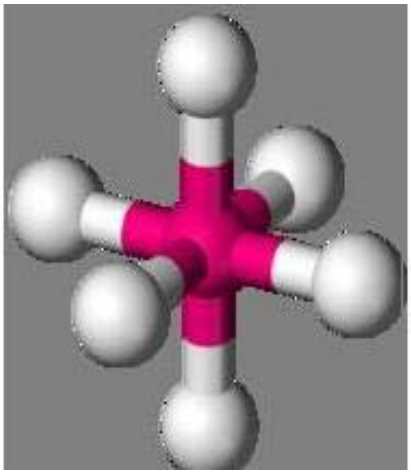

Octahedral , B-site

Figure 1.5 (a) Unit cell of Spinel structure **(b)** Tetahedral and octahedral representation

1.5 Magnetoelectric Materials:

Magnetoelectric materials are the materials, which are simultaneously ferrimagnetic and ferroelectric. Such materials can be used for all the potential applications of ferrimagnetic and ferroelectric materials. In addition, these materials also show the magnetoelectric effect. The magnetoelectric effect is a coupled two field effect in which

induction of electric polarization by applying an external magnetic field and induction of magnetic polarization by applying an external electric field. In the first case, this phenomenon is referred to as the direct magnetoelectric effect while, for the case of a magnetic material in an electric field, it is called the converse magnetoelectric effect [32-33].

The effect can be expressed in the following form

$$P_i = \sum \alpha_{ij} H_j + \sum \beta_{ijk} H_j H_k + \ldots\ldots\ldots \quad \textbf{...1.4}$$

$$M_i = \sum \alpha_{ij} E_j + \sum \beta_{ijk} E_j E_k + \ldots\ldots\ldots \quad \textbf{...1.5}$$

Where P is the electric polarization, M is the Magnetization, E and H are the electric and magnetic field respectively;$\alpha$and β are the linear and nonlinear magnetoelectric coefficient. Magnetoelectric materials can be realized in single phase and two phases (composite form).

1.5.1 Single Phase Magnetoelectric Materials

The first known single phase magnetoelectric material was Cr_2O_3. Some other examples of single phase magnetoelectric materials are Gd_2CuO_4, Sm_2CuO_4, $KNiPO_4$ and $LiCoPO_4$ etc. In single phase, magnetoelectric effect is due to the coupling of magnetic and electric orders. Almost all single phase magnetoelectric materials have temperature constraint i.e. they show the magnetoelectric effect at very low temperature and also they show very low value of magnetoelectric coefficient. So single phase materials have not yet found any technological applications. However research on suitable single phase magnetoelectric materials is being carried out by a large number of research groups. To overcome the deficiency of single-phase multiferroics and to provide new approach to the magnetoelectric coupling mechanisms, recent work concentrates on the class of composite-type magnetoelectric materials. It was observed that composite-type material yield a large magnetoelectric (ME) coupling response even above room temperature.

1.5.2 Two Phase Magnetoelectric Materials : Ferrite-Ferroelectric Composite

Magnetoelectric composites consist of magnetostriction (ferrite phase) and piezoelectric (ferroelectric phase) phases simultaneously and much stronger magnetoelectric

effect could be realized in these composites. The composite materials have been employed to an increasing extent in the recent years to take advantages of the combination of these two materials.

In magnetoelectric composite the origin of magnetoelectric effect is due to interaction between magnetostrictive phase and piezoelectric phase through mechanical coupling i.e. stress-strain coupling. The first discussion on synthesized composite materials was proposed by Van Suchtelen in 1972 [34]. He described the sum and product properties in the composites depending on the property of interest. Unchino et al. [35] organized the resultant properties of the composites into three categories, namely sum properties, product properties and combination properties.

A sum property of the composite is defined as a weighted sum of the contributions of the individual component phases, proportional to the weight/volume fractions of the phases in a composite as shown in *figure 1.6(a)*. The sum property can be observed in simple physical quantities such as density. The dielectric property of a composite can be a sum property if no reaction occurs during the multi-phase mixing i.e. if there is simple mixing of multi phases.

A more interesting result of a composite structure is the product property, which is reflected in the composite structure but is absent in the individual phases as shown in *figure 1.6(b)*. In a biphasic composite material, if one phase exhibits a property $A \rightarrow B$ with a proportionality tensor $dB/dA = X$ (may be a constant or dependent on A or B) and the second phase exhibits a property $B \rightarrow C$ with a proportionality tensor $dC/dB = Y$, then the composite will exhibit a property $A \rightarrow C$ which is absent in either of the initial phases. The property $A \rightarrow C$ is called a product property of the composite. The proportionality tensor is the product of the proportionality functions of the two phases, hence called the product property.

$$\frac{dC}{dA} = \frac{dC}{dB} \times \frac{dB}{dA} = Y.X \qquad \textbf{...1.6}$$

In some cases, the output property of composites exceeds that of each initial phase. This enhancement in the property refers to a combination effect. A simple demonstration of

the combination effect is plotted in *figure 1.6 (c)*. In this case, the property of interest depends on two parameters B and C with the relationship B/C. If variables B and C follow convex and concave type characters as illustrated in *figure 1.6 (c)*. Then combination value B/C will reach a maximum at an intermediate ratio of the two phases.

The Magnetoelectric effect of the ferrite-ferroelectric composite exhibit the product property of the composite [36].

$$\frac{dE}{dH} = \frac{dE}{dX} \times \frac{dX}{dH} = dp \,.\lambda = \alpha \qquad \ldots 1.7$$

where E is the electric voltage, H is the magnetic field, X is the strain produced, d_p is the piezoelectric coefficient, λ is the magnetostriction coefficient, α is the Magnetoelectric coefficient.

Thus the Magnetoelectric effect is a result of the product of the Magnetostrictive effect (magnetic/mechanical effect) in the ferrite phase and the piezoelectric effect (mechanical/electric effect) in the ferroelectrics phase. *Figure 1.7* shows the schematic representation of the ME effect in the composites utilizing the product property

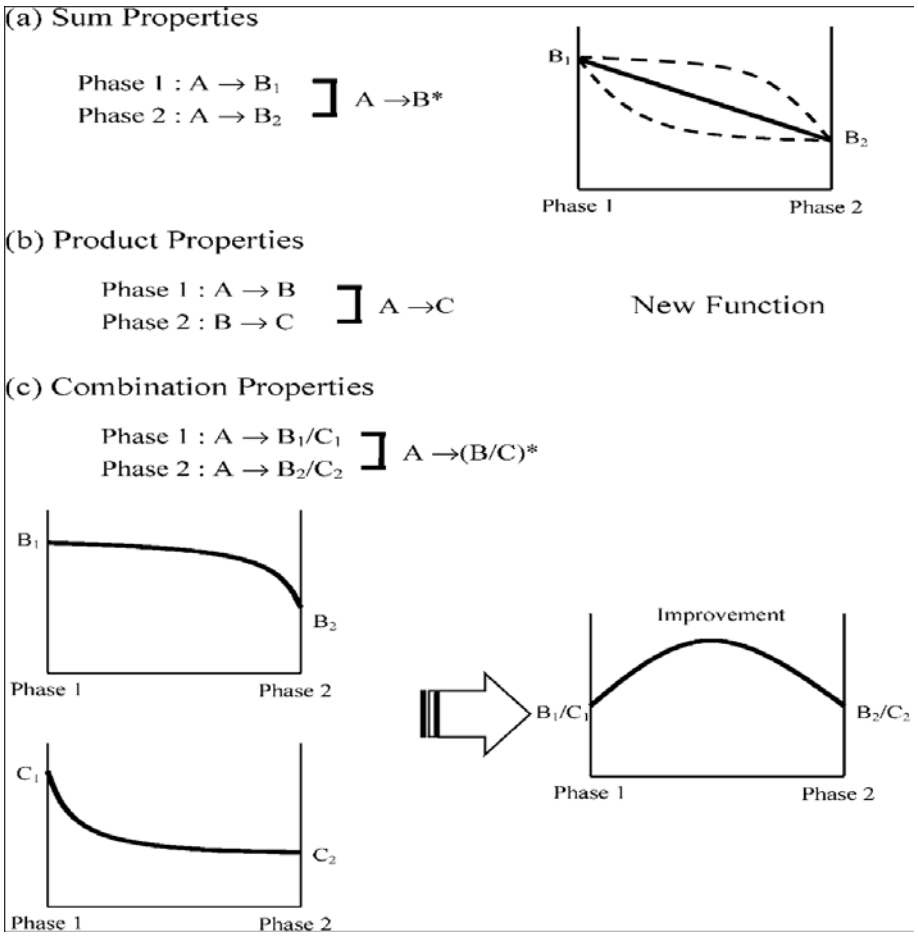

Figure 1.6 Resultant composite properties; (a) sum properties, (b) product properties, and (c) combination properties

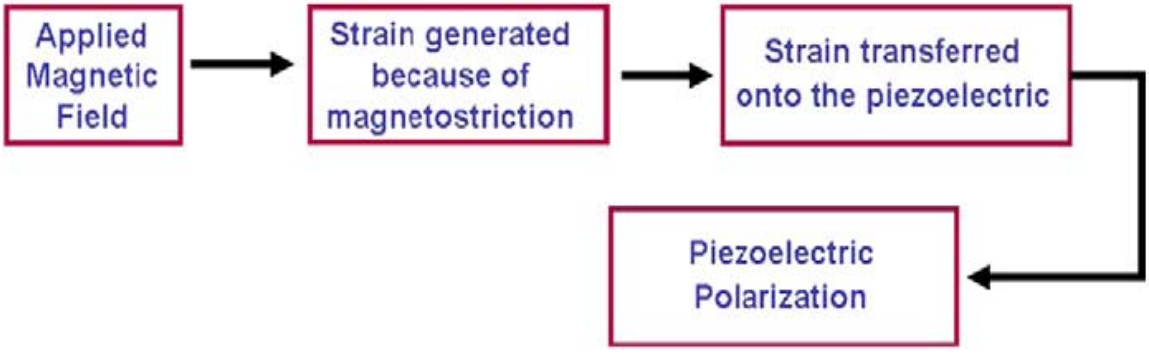

Figure 1.7 Representation of the ME effect in the composites utilizing the product property

1.5.3 Applications of Ferrite- Ferroelectric Composites

The ME effect is a tool for the conversion of energy from magnetic to electric form or vice versa. The ME coupling factor is an important indication of the usefulness of these materials for any devices. Unfortunately, many ME materials have very low ME coupling factors. Nevertheless, many applications have already been proposed by various researchers.

As these materials show magnetoelectric property thus they have received continuous attention as potential sensors for magnetic field measurements and transducers for magnetoelectric conversion and actuators [37-38]. These composites are of interest for a variety of device applications including electrically controlled electro-optic or piezoelectric devices, actuators and magnetoelectric memory devices. These composites also find a lot of technological applications in radio electronics, optoelectronics, microwave electronics and transducers in instrumentation, wave guide, phase inverters, rectifier, modulators, integral optics and fiber communication technology [39-41].

1.5.4 Requirement for Obtaining Good Magnetoelectric Effect

Some requirements for obtaining good ME effect in composites are given by Boomgaard and Born [42] in 1978 which are mentioned below:

- Two phases should be in equilibrium and no chemical reaction should occur between the constituent phases.
- Magnetostriction coefficient of ferrite phase and piezoelectric coefficient of ferroelectric phase should be high.
- Resistivity of the constituent phases should be high to avoid the leakage of the charges developed in the ferroelectric phase during poling.
- Proper polling strategy should be adopted to get higher ME signal.
- The porosity of the sample should be as low as possible to ensure good mechanical coupling between two phases.

1.6 Review on Magnetoelectric Composites

Detailed literature survey was carried out using INSPEC data base and internet. The information collected is summarized below:

The first work on ME effect was done by Curie in 1894 [43]. However, no further work was done until 1958 and in 1958 Landau and Lifshitz [44] proved the possibility of the ME effect in certain crystals on the basis of the crystal symmetry. In 1960 Dzyaloshinskii [45] applied the symmetry argument to antiferromagnetic Cr_2O_3, and it was suggested that the ME effect could be seen in Cr_2O_3. But this was experimentally confirmed by Astrov [46] by measuring of magnetization in presence of external electric field and later by Rado and Folen [47] by measuring electric polarization in presence of external magnetic field. Since then there have been many papers reporting observations and measurements of the ME effect in single phase materials [48–60]. But all materials showed the ME effect at low temperature and there ME response was generally very weak, because of this it is difficult to use these materials for device applications.

To overcome the deficiency of these materials magnetoelectric composites (ME composites) come in to picture. The first work on ME composites was done by Van Suchtelen in 1972 and other researchers at Philips Laboratories in the Netherlands on the composition of the quinary system Fe–Co–Ti–Ba–O [61-65]. In 1978 Boomgard and Born [66] outlined the conceptual points for preparation of good ME composites. At that time, ME composites did not attract attention and the field of ME composite research went dormant for almost 20 years across the world. Then in the early 1990s, Newnham's group [67] and Russian scientists [68-70] prepared particulate ceramic composites of ferrites and $BaTiO_3$ or PZT by a conventional sintering processing but experimental studies of these ME composites in the 1990s did not represent a great step forward. An upsurge in the ME composite research appeared in the early 2000s.

In 2000, R.P. Mahajan et.al [71]. studied the conductivity, dielectric behavior and magnetoelectric effect of $CuFe_2O_4$- Barium Titanate composites. In this the conduction phenomenon was explained on the basis of small polaron hopping model and they reported

the maximum value of magnetoelectric coefficient for 75% ferroelectric phase in composite system. K.K. Patankar et.al. [72] have studied the structural, dielectric and magnetoelectric properties of $CuFe_{1.8}Cr_{0.2}O_4 + Ba_{0.8}Pd_{0.2}Ti_{0.8}Zr_{0.2}O_3$ composite and maximum value of ME coefficient reported by this group was 182.7 μV/cm-Oe. The same properties were also studied by M.B. Kothale et.al. [73] for $Cu_{0.6}Co_{0.4}Fe_2O_4 + Ba_{0.8}Pb_{0.2}TiO_3$ and maximum value of ME coefficient reported by this group was 120 μV/cm-Oe. V.M. Laletin et.al. [74] studied the magnetoelectric effect in composites of nickel ferrite and barium lead zirconate titante. N. Rammanohar Reddy et.al [75] studied the structural, longitudinal modulus and internal friction loss of $Ni_{0.93}Co_{0.02}Mn_{0.05}Fe_{1.95}O_4$-$Ba_{0.8}Pb_{0.2}TiO_3$ prepared by solid state route. S.L. Kadam et.al. [76] studied the conductivity with temperature, dielectric properties and magnetoelectric properties of $Ni_{0.75}Co_{0.25}Fe_2O_4$+$Ba_{0.8}Pb_{0.2}TiO_3$ and the maximum value of ME coefficient obtained by this group was 140 μV/cm-Oe. Structural, resistivity, thermoemf with temperature, dielectric properties and magnetoelectric properties of $Ni_{0.50}Co_{0.25}Fe_2O_4 + Ba_{0.8}Pb_{0.2}TiO_3$ composite was reported by S.L. Kadam et.al. [77] and the maximum value of ME coefficient reported by this group was 302 μV/cm-Oe. Detailed dielectric properties of $Ni_{0.50}Co_{0.50}Fe_2O_4$+$Ba_{0.8}Pb_{0.2}TiO_3$ composite was studied by K.K. Patankar et.al. [78]

C.M. Kanamadi et.al [79] and S.R. Kulkarni et.al [80] studied the structural, dielectric and magnetoelectric properties of $Ni_{0.8}Cu_{0.2}Fe_2O_4$ - $Ba_{0.9}Pb_{0.1}Ti_{0.9}Zr_{0.1}O_3$ and $Ni_{0.8}Co_{0.1}Cu_{0.1}Fe_2O_4 + PbZr_{0.8}Ti_{0.2}O_3$ composites respectively, and maximum value of ME coefficient obtained by these groups were 431 μV/cm-Oe and 375 μV/cm-Oe, respectively. M.B. Kothale et.al. [81] studied the electrical conduction and magnetoelectric effect in $Cu_{0.4}Co_{0.6}Fe_2O_4$ - $Ba_{0.8}Pb_{0.2}TiO_3$ composites and reported that ferroelectric phase transition is of diffused phase type and is affected due to the other phase in composite and they got maximum magnetoelectric coefficient for 85% ferroelectric phase in composite. R.S. Devan et.al. [82] and D.R. Patil et.al. [83] studied the structural, resistivity, thermoemf with temperature, dielectric properties and magnetoelectric properties of $Ni_{0.92}Co_{0.03}Cu_{0.05}Fe_2O_4$ - $BaTiO_3$ and $NiFe_2O_4$ - $Ba0.9Sr_{0.1}TiO_3$ composites, respectively, and maximum value of

ME coefficient obatained by these groups were 536 μV/cm-Oe and 533 μV/cm-Oe, respectively. N. Rammanohar reddy et.al. [84] reported the dielectric, elastic, anelastic and conductivity behavior of $Ni_{0.5}Zn_{0.5}Fe_{1.95}O_4$ - $Ba_{0.8}Pb_{0.2}TiO_3$ composite and they observed that the longitudinal modulus of ferrite phase depends on temperature. Dandon Wu et.al. [85] studied the composite system of nickel ferrite and lead zirconate titanate and they reported the maximum value of ME coefficient for 35% of ferrite phase. R. S. Devan et.al. [86] studied the $BaTiO_3$ and $Ni_{0.94}Co_{0.01}Cu_{0.05}Fe_2O_4$ composite and they reported that composite with 70% ferroelectric phase has intermediate electrical and magnetic properties as compared with the others.

Giap V. Duong et.al. [87-89] studied the $BaTiO_3$ – $CoFe_2O_4$ composite system and they reported the effect of preparation condition and effect of structure on magnetoelectric properties of this composite. This group also reported the mechanism of magnetoelectric effect in $BaTiO_3$ – $CoFe_2O_4$ composite system. J.A. Matutes Quino et.al. [90] studied the synthesis and characterization of nickel ferrite and barium titanate composite and they conclude that composite system with high content of ferroelectric phase is excellent as a candidate for magnetoelectric composite. J.G. Barbosa et.al. [91] studied the temperature dependence of the dielectric permittivity of $BaTiO_3$ – $CoFe_2O_4$ composite and its effective dielctric constant was calculated and fitted using a generalized brick-wall model that took in to account the contributions from the $BaTiO_3$ and $CoFe_2O_4$ phases.

R.S. Devan et.al. [92] reported the magnetoelectric effect and electrical properties in $BaTiO_3$ and $Ni_{0.93}Co_{0.02}Cu_{0.05}Fe_2O_4$ and they reported that maximum static ME coefficient 587.75 μV/cm Oe for 70% of ferroelectric phase at magnetic field of 2.1 kOe. S.Y. Tan et.al [93] studied the $MgFe_2O_4$ and barium titanate composite and they reported the highest ME coupling coefficient for 60% of ferrite phase and they also reported the P-E loop of samples before and after magnetic poling and showed the marked improvement in polarization and confirmed the coupling of electric dipoles with the magnetic applied field. R. Grossinger et.al. [94] reported the physics of magnetoelectric composite and they also

discussed the different measurements methods for determining the magnetoelectric coefficients.

S. R. Kulkarni et.al. [95] studied the electrical and magnetoelectric properties of $Ni_{0.8}Co_{0.1}Cu_{0.1}Fe_2O_4 - PbZr_{0.5}Ti_{0.5}O_3$ composite and they reported the maximum value of ME coefficients for 35 % ferrite phase. S.S. Chougule et.al. [96] studied the structural, dielectric, M-H hysteresis loop and magnetoelectric properties of $Ni_{0.9}Zn_{0.1}Fe_2O_4$ + PZT composite and the value of ME coefficient obtained by this group was 748 μV/cm-Oe. W.H. Tuan et.al. [97] studied the both bulk and multilayered specimens of barium titanate –nickel ferrite composite. C.M. Kanamadi et.al. [98] reported the dielectric and magnetic properties of $CoFe_2O_4$ - $Ba_{0.9}Sr_{0.1}TiO_3$ composites. B.K. Bammanvar et.al. [99] and S. Narendra Babu et.al [100] studied the Structural, M-H hysteresis loop and magnetoelectric properties of $Ni_{0.2}Co_{0.8}Fe_2O_4$ - $Ba_{0.8}Pb_{0.2}Ti_{0.2}Zr_{0.8}O_3$ and $Ni_{0.93}Co_{0.02}Mn_{0.05}Fe_{1.95}O_4$ – PZT composite respectively. The maximum values of magnetoelectric coefficient obtained by these groups were 536 μV/cm-Oe and 110 μV/cm-Oe respectively. R.C. Kamble et.al. [101] studied the $Co_{1.2-y}Mn_yFe_{1.8}O_4$ and $BaZr_{0.08}Ti_{0.92}O_3$ composite and they reported the structural and dielectric properties of this composite system. C. Miclea et.al. [102] studied the magnetoelectric properties of cobalt ferrite and PZT composite and they reported the maximum value of ME coefficient for 40% ferrite phase.

R.C. Kambale et.al. [103] studied the magnetic, dielectric and magnetoelectric behavior of $NiFe_{1.9}Mn_{0.1}O_4$ and $BaZr_{0.08}Ti_{0.92}O_3$ ME composites and they reported that ME coefficient decreases with increase of ferrite content. Abdul Same Fawzi et. al. [104] studied the composite of nickel ferrite and $Pb_{0.93}La_{0.07}(Zr_{0.60}Ti_{0.40})O_3$ and they reported the P-E hysteresis loop as well as M-H hysteresis loop of this composite. S.U. Durgasimi et.al. [105] reported the electrical properties of $Li_{0.5}Ni_{0.6}Zn_{0.15}Fe_2O_4$ and $Ba_{0.5}Sr_{0.5}TiO_3$ composite. They observed that for higher value of ferrite phase, dielectric loss increases with temperature due to conduction loss and they also reported the ME coefficient 1500μv/cm-Oe. Jianglichen et.al. [106] reported the ferroelectric properties and magnetoelectric effect in $Ni_{0.93}Co_{0.02}Cu_{0.05}Fe_2O_4$ and PZT composite they showed that composite exhibit P-E

hysteresis loop as well as M-H hysteresis loop at room temperature. R.C. Kambale et.al. [107] studied the structural, dielectric and magnetoelectric properties of $BaZr_{0.08}Ti_{0.92}O_3$ + $CoMn_{0.2}Fe_{1.8}O_4$ composite. The maximum value of ME coefficient reported by this group was 2 mV/cm-Oe. V.L. Mathe et. al. [108] studied the magnetoelectric properties of particulate and bi-layer PMN-PT/$CoFe_2O_4$ composites. They reported the higher value of ME coefficient for 15 % ferrite phase. B.K. Bammanvar et.al. [109] studied the ME effect of NZF and PZT composite system and they reported the maximum value of ME coefficient is 840 μv/cm Oe for 15 % ferrite phase.

Thus, from literature survey it seems that there is an increasing scientific interest in magnetoelectric phenomenon, which is evident from the rising number of publications in the last ten years and it has also been ascertained from the literature survey that various combinations of ferrite ($CoFe_2O_4$, $CuFe_2O_4$, $NiFe_2O_4$, etc.) and ferroelectric ($BaTiO_3$, $PbTiO_3$, $Ba_{1-x}Pb_xTiO_3$, etc.) phases have been studied. And it is found that work on the ME Composites is limited to the measurement related to dielectric properties, resistivity and magnetic properties only. But properties like ferroelectric (P-E) hysteresis, magnetic (M-H) hysteresis loops and sintering by microwave furnace both were found rarely in literature. So in this context the present work is on investigation of all the properties of ME composites.

.1.7 Objectives of the Present Work:

The first objective was to select a composition of ferroelectric phase and ferrite phase that exhibits good ferroelectric and ferromagnetic properties and composites of that exhibit good magnetoelectric effect. For the present work barium strontium titanate (BST) is selected as a ferroelectric phase due to its high dielectric constant, relatively low dielectric loss and variable Curie temperature depending on the concentration of strontium (Sr^{2+}). Nickel zinc ferrite (NZF) is selected as a ferrite phase due to its wide range of applications as already discussed in section 1.4.1. Composites were prepared by solid state reaction route by considering the fact that this method is the cheapest, simplest and conventional ways to synthesize bulk samples.

So present work entails the following objectives:

- To synthesize modified composites of nickel zinc ferrite (NZF) and barium Strontium titanate (BST) by solid state method.
- Modification was carried out by substituting Zr and La in BST.
- Optimization of process parameters.
- Sintering of samples by conventional and microwave techniques.
- To characterize the materials for structural, electrical and magnetic properties.
- Analysis of results.

Following material series were studied

Series A		$(1-y)Ba_{0.9}Sr_{0.1}TiO_3$ - (y) $Ni_{0.8}Zn_{0.2}Fe_2O_4$	(y = 0 - 0.15in step of 0.05)
Series B	Series B1	$Ba_{0.9}Sr_{0.1}Zr_xTi_{1-x}O_3$	(x = 0 - 0.16 in step of 0.04)
	Series B2	$(1-y)Ba_{0.9}Sr_{0.1}Zr_{0.04}Ti_{0.96}O_3$ +(y) $Ni_{0.8}Zn_{0.2}Fe_2O_4$	(y = 0 - 0.15 in step of 0.05)
	Series B3	$0.95Ba_{0.9}Sr_{0.1}Zr_xTi_{1-x}O_3$ +0.05$Ni_{0.8}Zn_{0.2}Fe_2O_4$	(x = 0 - 0.16 in step of 0.04)
Series C	Series C1	$Ba_{0.9-3x/2}Sr_{0.1}La_xTiO_3$	(x=0 - 0.02 in step of 0.005)
	Series C2	$(1-y)Ba_{0.9-3x/2}Sr_{0.1}La_{0.005}TiO_3$ +(y) $Ni_{0.8}Zn_{0.2}Fe_2O_4$	(y = 0 - 0.15 in step of 0.05)
	Series C3	$0.95Ba_{0.9-3x/2}Sr_{0.1}La_{0.005}TiO_3$ + 0.05 $Ni_{0.8}Zn_{0.2}Fe_2O_4$	(x=0 - 0.02 in step of 0.005)
Series D		$(1-y)Ba_{0.9}Sr_{0.1}Zr_{0.04}Ti_{0.96}O_3$ +(y) $Ni_{0.8}Zn_{0.2}Fe_2O_4$	(y = 0 - 0.15 in step of 0.05)

Note: Samples of series A, B and C were sintered in conventional furnace and those of series D were sintered using microwave furnace. All these samples were investigated for their structural (XRD and SEM), dielectric (dielectric properties with frequency and temperature), ferroelectric, ferromagnetic and Magnetoelectric properties in detail.

Refrences:

1) J. Ryu, S. Priya, K. Uchino and H.J. Kim, J. Electroceramics, **8** (2002) 112.
2) M. Vopsaroiu, J. Blackburn and M.G. Cain, J. Phys. D: Appl. Phys., **40** (2007) 5027.
3) M.E. Lines and A.M. Glass, Principles and applications of ferroelectric and related materials, New York, USA (2001).
4) G.H. Haertling, J. Am. Ceram. Soc., **82 (**1999) 797.
5) P.R. Coursey and K.G. Brand, Nature, **157** (1946) 297.
6) S. Miyake and R. Ueda, J. Phys. Soc. Jpn., **1** (1946) 32.
7) B.M. Vul and I.M. Goldman, Doklady Akademii Nank USSR., **46** (1945) 154.
8) E. Wainer, Trans. Electro. Chem. Soc., **89** (1946) 331.
9) F. John and G. Shirane, Ferroelctric Crystals, New York, Pergamon (1962).
10) D. Damjanovic, Rep. Prog. Phys., **61** (1998) 1267.
11) G. Busch, Ferroelectrics, **74** (1987) 267.
12) W. Kanzig, Ferroelectrics, **74** (1987) 285.
13) G. Busch, Ferroelectrics, **71** (1987) 43.
14) H.D. Megaw, Ferroelectricity in Crystals, Methuen and Co., London (1957).
15) F. Jona and G. Shirane, Ferroelectric Crystals, Pergamon Press, Oxford, USA (1962).
16) B. Jaffe, W. Cook and H. Jaffe, Piezoelectric Ceramics, Academic Press, London (1971).
17) L.B. Kong, J. Ma, H.T. Huang, W. Zhu and O.K. Tan, Mater. Lett., **50** (2001) 129.
18) L.E. Cross and R.E. Newnham, J. Am. Ceram. Soc., **3** (1987) 289.
19) J. Fousek, Ferroelectrics, **113** (1991) 3.
20) ANSI/IEEE Standards on Piezoelectricity, **176** (1987) 1.
21) V.K. Katiyar and S.L. Srivastava, J. Appl. Phys., **76** (1994) 455.
22) William F. Smith, Principles of Material Science and Engineering, Mc Graw Hill Co. (Publishers) New York, USA (1986).
23) J.L. Snoek, Philips Tech. Rev., **8** (1946) 353.

24) J.L. Snoek, New Devlopment in Ferrimagnetic Materials, Elsevier Publishing Comp. New York, USA (1947).

25) L. Neel, Am. Phys., **3** (1948) 137.

26) E.W. Gorter, Philips Research Reports, **9** (1954) 295.

27) G. Blasse, Philips Research Reports, **3** (1964) 1.

28) J. Smit, Solid State Comm., **6** (1968) 745.

29) S. Roberts and A. Von Hipple, J. Appl. Phys., **17** (1946) 610.

30) E.J.W. Verwey and E.L. Heilman, J. Chem. Phys., **15** (1947) 174.

31) Z. Wang, D. Schiferl, Y. Zhao and H. S. C. Oneill, J. Phys. Chem. Solids, **64** (2003) 2517.

32) V.M. Laletin, Phys. Lett., **17** (1991) 1342.

33) M. Mahesh Kumar, A. Srinivas, S.V. Suryanarayana, G. S. Kumar and T. Bhimankara, Bull. Mater. Sci., **21** (1998) 251.

34) J. Van Suchetelene, Philips Research Reports, **27** (1972) 28.

35) J. Ryu, S. Priya, K. Uchino and H. E. Kim, J. Electroceramics, **8** (2002) 107.

36) C. W. Nan, Phy. Rev. B, **50** (1994) 6082.

37) L.P.M. Bracke and R.G. Van Vliet, Int. J. Electron., **51** (1981) 225.

38) J.G. Wan and J. M. Liu, J. Appl. Phys., **93** (2003) 12.

39) M.D. Michelena, F. Montero and Sanchez, J. Magn. Magn. Mater., **242** (2002) 1160.

40) H. Schmid, Bull. Mater. Sci., **17** (1994) 1411.

41) E. Wood and A. E. Austin, Int. J. Magn., **5** (1974) 303.

42) J. Van Den Boomgaard and R. A. J. Born, J. Mater. Sci., **13** (1978)1538.

43) P. Curie, J. Physique, **3** (1894) 393.

44) L.D. Landue and E. Lifshitz, Electrodynamics of Continuous Media, Addison-Wesley, Reading, USA (1960).

45) I.E. Dzyaloshinskii, Soviet Phys.—JETP, **37** (1960) 628.

46) D.N. Astrov, Soviet Phys.—JETP, **11** (1960) 708.

47) G.T. Rado and V.J. Folen, Phys. Rev. Lett., 7 (1961) 310.

48) R.M. Hornreich, Solid State Commun., **7** (1969)1081.

49) R.M. Hornreich, J. App. Phys., **41**(1970) 950.

50) E. Fischer, G. Gorodetsky and R.M. Hornreich, Solid State Commun., **10** (1972) 1127.

51) V.J. Folen, G.T. Rado, and E.W. Stalder, Physical Rev. Lett., **6** (1961) 607.

52) S. Foner and M. Hanabusa, J. Appl. Phys., **34** (1963) 1246.

53) L.M. Holmes, L.G. Van Uitert, and G.W. Hull, Solid State Commun., **9** (1971) 1373.

54) R.M. Hornreich, IEEE Transactions on Magn. **8** (1972) 584.

55) R.M. Hornreich, in Proceedings of the Symposium on Magnetoelectric Interaction Phenomena in Crystals, Seattle,Wash, USA (1973).

56) R.M. Hornreich, A. Freeman and H. Schmid, Eds., Gordon and Breach Science, New York, USA (1975).

57) R. Hornreich and S. Shtrikman, Phys. Rev., **161** (1967) 506.

58) T.J. Martin and J.C. Anderson, Phys. Lett., **11** (1964) 109.

59) T.J. Martin and J.C. Anderson, IEEE Transactions on Magn., **2** (1966) 446.

60) M. Mercier, in Proceedings of the Symposium on Magnetoelectric Interaction Phenomena in Crystals, Seattle, Wash, USA (1973).

61) J. Van Suchtelen, Philips Research Report, **27** (1972) 28.

62) J. Van Den Boomgaard and R.A.J. Born, J. Mater. Sci., **13** (1978) 1538.

63) J. Van Den Boomgaard, A.M.J.G. Van Run, and J. Van Suchtelen, Ferroelectrics **10** (1976) 295.

64) J. Van Den Boomgaard, D.R. Terrell, R.A.J. Born and H.F.J.I. Giller, J. Mater. Sci., **9** (1974) 1705.

65) A.M.J.G. Van Run, D.R. Terrell, and J.H. Scholing, J. Mater. Sci., **9** (1974) 1710.

66) J. Van Den Boomgaard and R.A.J. Born, J. Mater. Sci., **13** (1978) 1538.

67) G. Harshe, J. P. Dougherty and R. E. Newnham, Int. J. Appl. Electromagn. Mater., **4** (1993) 145.

68) S. Lopatin, I. Lopatin and I. Lisnevskaya, Ferroelectrics, **162** (1994) 63.

69) T.G. Lupeiko, I.V. Lisnevskaya, M.D. Chkheidze and B.I. Zvyagintsev, Inorg. Mater., **31** (1995) 1245.

70) M.I. Bichruin, I.A. Kornev, V.M. Petrov and I. Lisenvskaya, Ferroelectrics, **204** (1997) 289.

71) R.P. Mahajan, K.K. Patankar, M.B. Kothale and S.A. Patil, Bull. Mater. Sci., **23** (2000) 273.

72) K. K. Patankar, R.P. Nipankar, V.L. Mathe, R.P. Mahajan and S.A. Patil, Ceramic Int., **27** (2001) 853.

73) M.B. Kothale, K.K. Patankar, S.L. Kadam, V.L. Mathe, A.V. Rao and B.K. Chougule, Mater. Chem. Phys., **77** (2002) 691.

74) V.M. Laletin and G. Srinivasan , Ferroelectrics, **280** (2002) 177.

75) N. Rammanohar Reddy, E. Rajagopal, K.V. Sivakumar, K.K. Patankar and V.R.K. Murthy, J. Electroceramics, **11** (2003) 167.

76) S.L. Kadam, K.K. Patankar, V.L. Mathe, M.B. Kothale, R.B. Kale and B.K. Chougule, Mater. Chem. Phys., **78** (2003) 684.

77) S.L. Kadam, K.K. Patankar, C.M. Kanamadi and B.K. Chougule, Mater. Res. Bull., **39** (2004) 2265.

78) K.K. Patankar, S.S. Joshi and B.K. Chougule, Phys. Lett. A, **346** (2005) 139.

79) C.M. Kanamadi, L.B. Pujari and B.K. Chougule, J. Magn. Magn. Mater., **295** (2005) 139.

80) S.R. Kulkarni, C.M. Kanamadi and B.K. Chougule, Mater. Res. Bull., **40** (2005) 2064.

81) M.B. Kothale, K.K. Patankar, A.V. Rao, V.L. Mathe and B.K. Choughle, Ferroelectrics, **325** (2005) 143.

82) R.S. Devan, D.R. Patil, S.A. Lokare, S.S. Chougule, B.K. Chougule and V.D. Kolekar, J. Phys. Chem. Solids, **67** (2006) 1524.

83) D.R. Patil, S.A. Lokare, S.S. Chougule and B.K. Chougule, Phys. B, **393** (2007) 77.

84) N. Rammanohar Reddy, M. Venkataramana, K. Krishanaveni, K.V. Siva Kumar and V. R.K. Murthy, Bull. Mater. Sci., **30** (2007) 357.

85) Dandan Wu, Weihua Gong, Haijin Deng and Ming li, J. Phys. D Appl. Phys., **40** (2007) 5002.

86) R.S. Devan, S.B. Deshpande and B.K. Chougule, J. Phys. D Appl. Phys., **40** (2007) 1864.

87) Giap V. Duong and R. Groessinger, J. Magn. Magn. Mater., **316** (2007) 624.

88) Giap V. Duong and R. Groessinger, J. Magn. Magn. Mater., **310** (2007) 1157.

89) Giap V. Duong, R. Groessinger and R. Sato Turtelli, J. Magn. Magn. Mater., **310** (2007) 361.

90) Matutes quino, M. E. Botello - Zubiate, V. Corral-Flores, J. De. Frutos, F. Cebollada, A.M. Gonzalez, Int. Ferroelectrics, **101** (2008) 22.

91) J.G. Barbosa, B.G. Almuda, C. Araiyo and J.A. Mendes, Ferroelectrics, **367** (2008) 15.

92) R.S. Devan, Y.D. Kolekar and B.K. Chougule, J. Alloys Compd., **461** (2008) 67.

93) S. Y. Tan, S.R. Shannigrahi, S.H. Tan and F. E. H. Tay, J. appl. Phys., **103** (2008) 094105.

94) R. Grossinger, Giap V. Duong and R. Sato Turtelli, J. Magn. Magn. Mater., **320** (2008) 1972.

95) S.R. Kulkarni, R.S. Devan and B.K. Chougule, J. Alloys Compd., **455** (2008) 336.

96) S.S. Chougule and B.K. Chougule, J. Alloys Compd. **456** (2008) 441.

97) W.H. Tuan and S.S. Chen, Ferroeletrics, **381** (2009) 167.

98) C.M. Kanamadi, J.S. Kun, H.K. Yang, B.K. Moon, B.C. Choi and J.H. Jeong , J. Appl. Phys. A, **97** (2009) 575.

99) B.K. Bammanvar, L.R. Naik, R.B. Pujari and B.K. Chougule, J. Alloys Compd., **477** (2008) L4.

100) S. Narendra Babu, S.V. Suryanarayana and M.T. Bhimasankaram, J. Alloys Compd., **473** (2009) 418.

101) R.C. Kambale , P.A. Shaikh, K.Y. Rajpure, P.B. Joshi and Y.O. Kolekar, Int. Ferroeletrics, **121** (2010) 1.

102) C. Miclea, C. Tansoiu, L. Amarande, C.F. Miclea, C. Plevites, M. Cioangher, L. Trupina and T. Tanasoiu, J. Opto. Adv. Mater., **12** (2010) 272.

103) R.C. Kambale , P.A. Shaikh, C.H. Bhosale, K.Y. Rajpure and Y.D. Kolekar, J. Alloys Compd., **489** (2010) 310.

104) A.S. Fawzi, A.D. Sheikh and V.L. Mathe, Phys. B, **405** (2010) 340.

105) S.U. Durgasimi, S.S. Chougule, B.K. Chougule, C.H. Bhosale and S.S. Bellad, J. Engg. Sci. Tech., **3** (2011) 1446.

106) Jianglischen, Zhuo Xu, and XULU , Ferroelectrics, **410** (2011) 29.

107) R.C. Kambale, Y.A. Park and N. Hur, J. Korean Phys. Soc., **59** (2011) 3385.

108) V.L. Mathe, A.D. Sheikh and G. Srinivasan, J. Magn. Magn. Mater., **324** (2012) 695.

109) B.K. Bammanvar and L.R. Naik , J. Magn. Magn. Mater., **324** (2012) 944.

Chapter - II

Material Synthesis and Characterization Techniques

Chapter II

Material Synthesis and Characterization Techniques

Magnetoelectric composites are important materials due to their wide range of industrial and commercial applications. The performance of these ME composites are closely dependent on their synthesis method as their microstructural, electrical and magnetic properties are sensitive to processing methodology. Therefore, it is important to understand the various processes involved in material preparation. This chapter includes a brief background on the methods of sample preparation and characterization techniques used for studying various properties. Also, a brief description about the experimental techniques used and the characterization equipment's used in the present work are described here.

2.1 Material Synthesis: Solid State Route

A number of techniques (conventional and non-conventional) are used to synthesize ceramic materials [1]. Some of them are i) hydrothermal synthesis, ii) spray drying techniques, iii) wet chemical methods, iv) sol-gel route, v) solid state reaction route. For the present work, solid state reaction route was adopted for synthesizing the samples as this method is cheaper, simpler and conventional way to fabricate bulk samples. A flow chart describing the various steps involved in processing of composites is shown in *figure 2.1*.

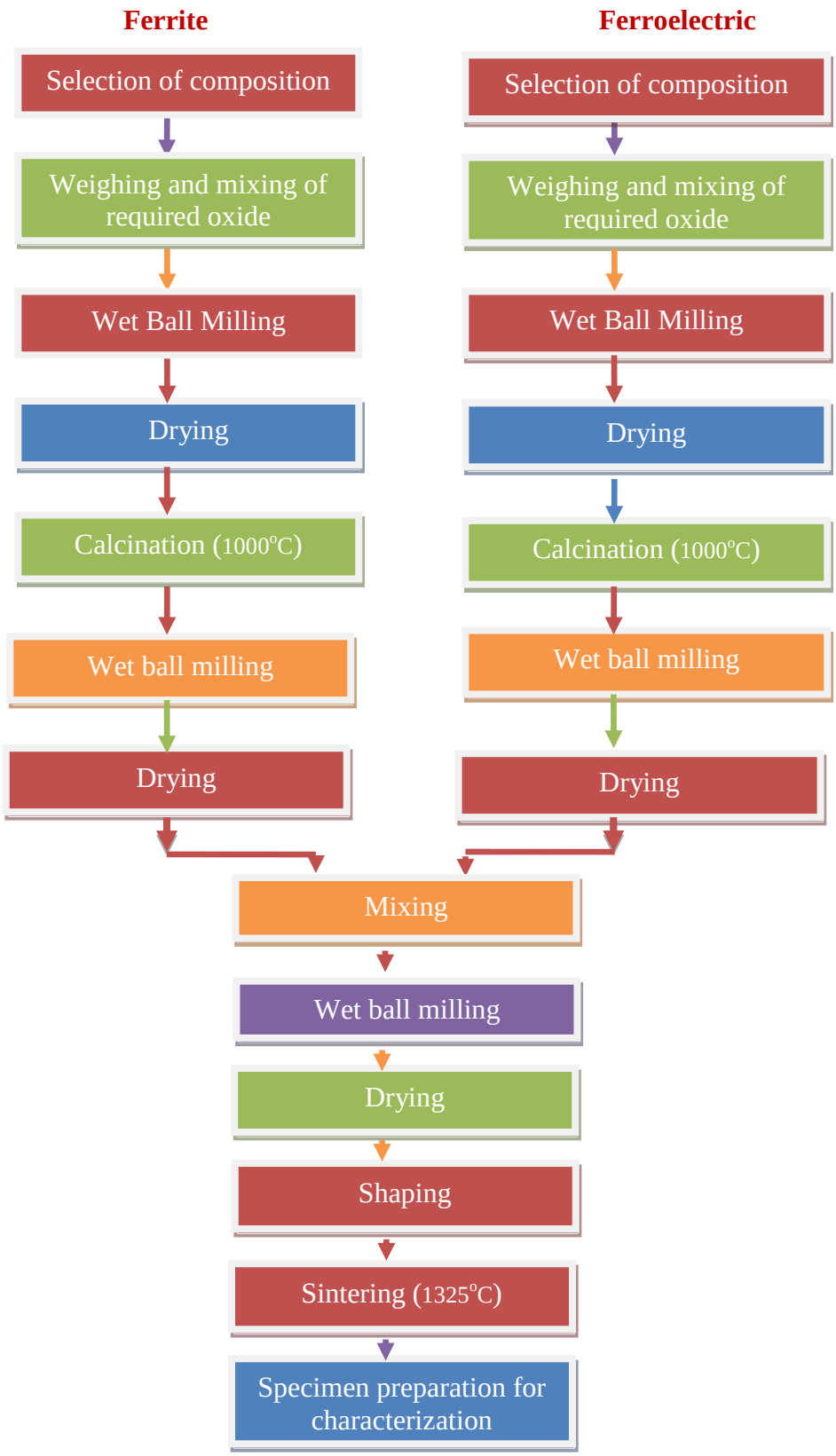

Figure 2.1 Flow chart for conventional solid state route

2.1.1 Raw Chemicals and Ball Milling

Chemical composition is only one aspect of the specification of raw materials. Raw materials are evaluated on the basis of their purity. Impurities in the raw materials affect the reactivity as well as their end product properties [2]. The raw materials used for the present work were $BaCO_3$, ZrO, $SrCO_3$, La_2O_3, TiO_2 for ferroelectric phase and NiO, ZnO, Fe_2O_3 for ferrite phase and all were analytical grade (AR grade, 99.9 % Purity).

These oxide materials were weighed in desired stoichiometric ratio and ball milled. The process of ball milling helps in reducing particle size and eliminating aggregates by means of mechanical force. The ball mill used for the present work with its various specifications is shown in *figure 2.2*. High density zirconia balls and distilled water were used as milling media. For all the samples the ball milling was done for 3 hrs. The wet slurry was then kept in an oven at 120^{o}C for drying purpose.

- **Type: Mini Ball Mill (Two Bowls)**
- **Purpose: For grinding raw materials for synthesis of ceramics**
- **Plate speed: 40 to 500 r.p.m.**
- **Bowl speed: max 1000 r.p.m.**
- **Two samples can be processed simultaneously**
- **R.P.M., time and direction of rotation are programmable**

Figure 2.2 High- energy ball milling with its various specifications

2.1.2 Calcination

The metal oxides usually do not react at room temperature. In order to facilitate the reaction to occur, they are heated to higher temperature. This process is called calcination.

During calcination either partial or complete phase of the compound is formed. Calcination causes the interaction of constituents by interdiffusion of their ions and resulting of homogeneous body hence, it is considered that calcination is a part of mixing process. It also helps in removing the unwanted gases during the decomposition of the constituent compounds. During calcination four physical processes are involved in the raw materials: (i) Linear expansion of the particles (< 400^{o}C) (ii) Solid phase reaction (400-750^{o}C) (iii) Contraction of product (750-850^{o}C) and (iv) Grain growth (> 850^{o}C) [3]. Usually, the calcination temperature is chosen high enough to cause reaction, but low enough to facilitate subsequent grinding. In the materials, having volatile constituents, the calcination temperature must be kept low enough to avoid loss of these volatile constituents.

For the present work both the phases i.e. ferrite phase and ferroelectric phase were calcined in closed alumina crucible at 1000^{o}C and then recalcined at 1100^{o}C for 4 h in a programmable furnace with heating rate of 5^{o}C/min followed by natural cooling. The calcined powder was grounded in agate pestle-mortar and ball milled again for 3 hrs. 30 mins and then slurry was kept in the oven for drying and after drying the reacted powder of both phases were mixed in desired ratio and were ball milled again. The programmable furnace used for the present work with its various specifications is shown in *figure 2.3*.

- **Heating elements : Silicon Carbide**
- **The working area (inside heating zone) : 12″ Depth × 6″ Height × 6″ Width**
- **Maximum operating temperature: 1550 ^{o}C.**
- **Thermocouple Used: R-type thermocouple.**
- **Heating rate and soaking time are programmable**
- **Temperature accuracy: ± 1 ^{o}C**

Figure 2.3 Programmable furnace used for calcination and its various specifications

2.1.3 Shaping

The ball milled powder obtained after mixing of two phases is subjected to shaping. Before shaping, an organic binder is added to the powder for giving sufficient strength to green body so that handling between shaping and sintering may not be difficult. One of the most important requirements of the binder is that it should be possible to remove the binder from the pressed shapes without any disruptive effect. For the present work, dilute solution of polyvinyl alcohol (PVA) was used as binder. There are various shaping methods which include Uniaxial Pressing, Isostatic Pressing, Extrusion, Injection molding, Tape Casting, Slip Casting, Gel Casting [4]

Among these different shaping techniques uniaxial pressing was used for the present work to form circular discs of ~15 mm diameter and 1-2 mm thickness. It was carried out in a die having movable top and bottom. The process involved is shown in *figure 2.4*. A lot of care at various levels of mixing is required while using this pressing technique, usually samples prepared by this technique show mechanical cracks after sintering. Highly polished die and punch surfaces help to reduce wall friction and these are made of hardened steels to minimize wear and tear and maintain surface finish. The hydraulic press used for the present work with its various specifications is shown in *figure 2.5*.

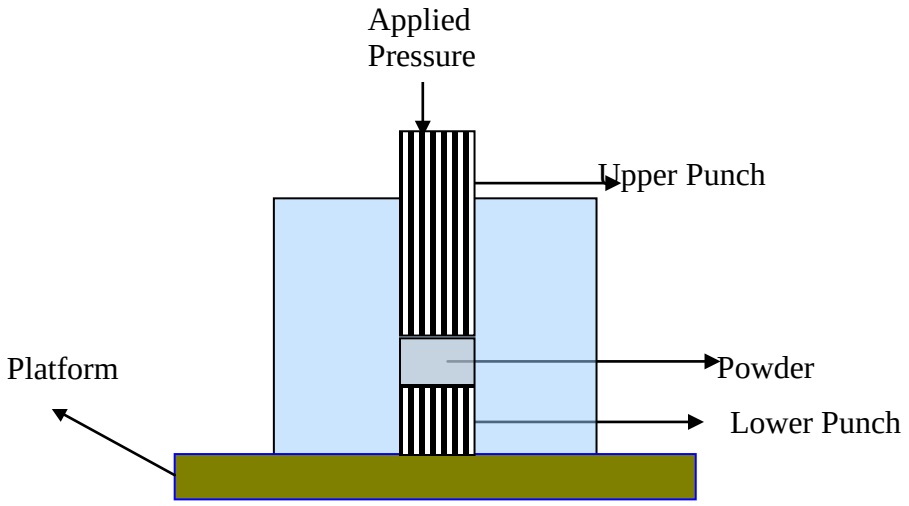

Figure 2.4 Unidirectional pressing

- **Maximum 10 ton pressure can be applied uniaxially**
- **Dies are available for pressing circular discs of various sizes and ring shape**

Figure 2.5 Hydraulic press with its various specifications

2.1.4 Sintering

Sintering is basically a heat treatment given to material for densification at an appreciable temperature hence sintering is the process by which a powder is transformed into a strong and dense body. During sintering the atomic motion is more violent and the area between grains in contact increases due to the thermal expansion of the grains and finally only one interface between two grains remains. This corresponds to a state with much lower surface energy. In this state, the atoms on the grain surfaces are affected by neighbouring atoms in all directions, resulting in dense ceramics with improved properties [5].

At the beginning of the sintering process, the lattice distortion and internal strain are reduced by atomic diffusion but as the temperature increases recrystallization process takes place through atomic diffusion. In the recrystallization stage, grain growth is usually realized through the motion of grain boundaries as shown in *figure 2.6*. In general, higher sintering temperature

and larger soaking time would result in larger grains resulting in highly dense ceramics [6]. There are many factors that affect the sintering process some of them are:

1. Temperature
2. Green density
3. Uniformity of green microstructure
4. Atmosphere
5. Impurities
6. Size distribution
7. Particle size

For the present work sintering was done by using conventional and microwave furnaces.

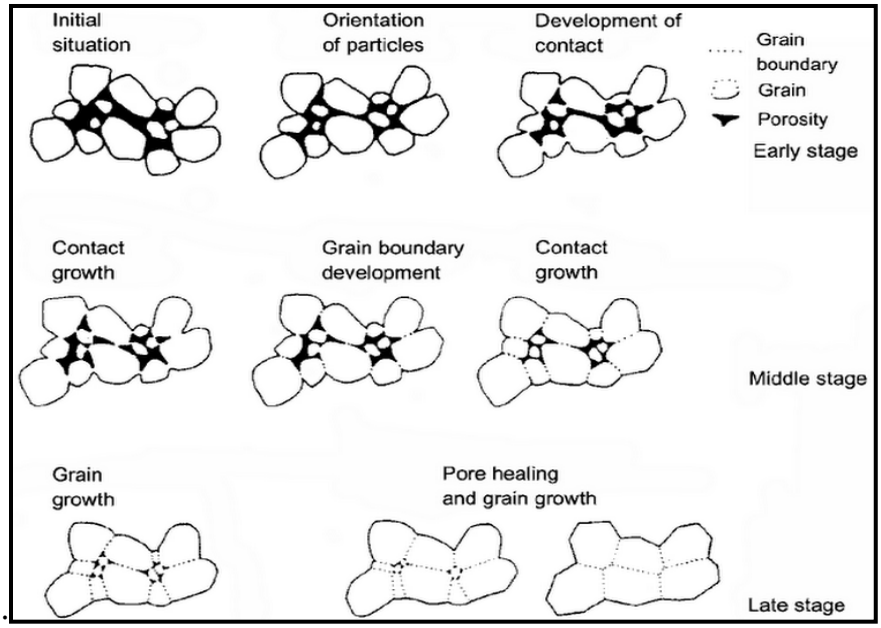

Figure 2.6 Grain growth during sintering

2.1.4 (a) Conventional Sintering (CS)

In conventional thermal processing, heat is transformed to the material through convection, conduction and radiation due to thermal gradients.

For the present work sintering was done by using a programmable high temperature conventional furnace at 1325^{o}C for 4 h with a heating rate of 5^{o}C/min.

2.1.4 (b) Microwave Sintering (MWS)

Microwave processing is an innovative technique in the field of ceramic processing and material synthesis. Excellent reviews have been written on the developments in this rapidly growing field [7-9]. Microwaves are electromagnetic radiations with a frequency range of 300 MHz to 300 GHz. During microwave processing, heat is generated internally within the material instead of originating from external sources, and hence there is an inverse heating profileas compared to conventional sintering. In this case material is heated by energy conversion rather than the energy transfer so the heating is very rapid [10]. Microwave heating of ceramics produce a cold wall furnace, as here, sample itself is a heating element hence microwave heating has many advantages over conventional heating methods [11-14]. Some of these advantages include, time and energy saving, rapid heating rates, considerably reduced processing time and temperature and fine microstructures. The heating process involved in conventional and microwave furnaces are shown in *figure 2.7*.

For the present work the samples were sintered at 1325^{o}C for 20 mins. The sintering profile for microwave and conventional sintering used in the present work is shown in *figure 2.8* and microwave sintering furnace used for the present work with its specifications is shown in *figure 2.9*.

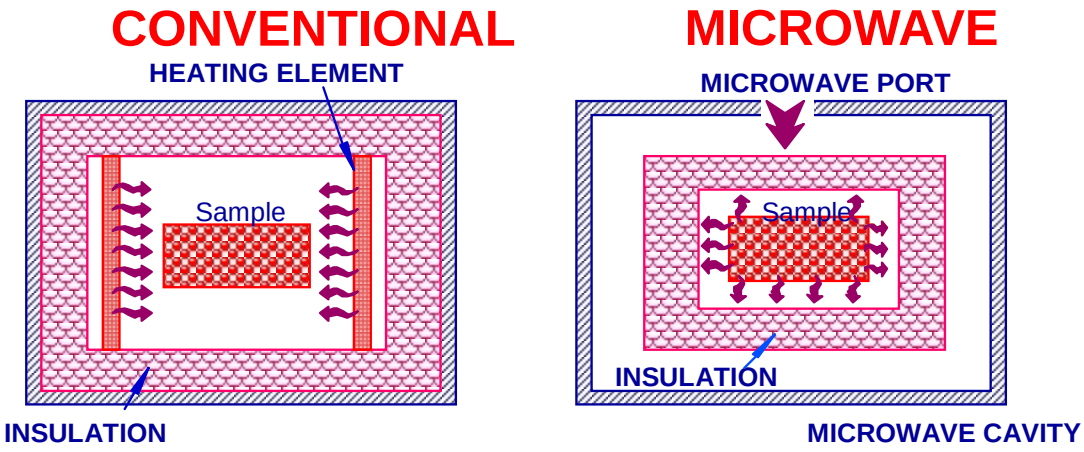

Figure 2.7 Heating process in conventional and microwave

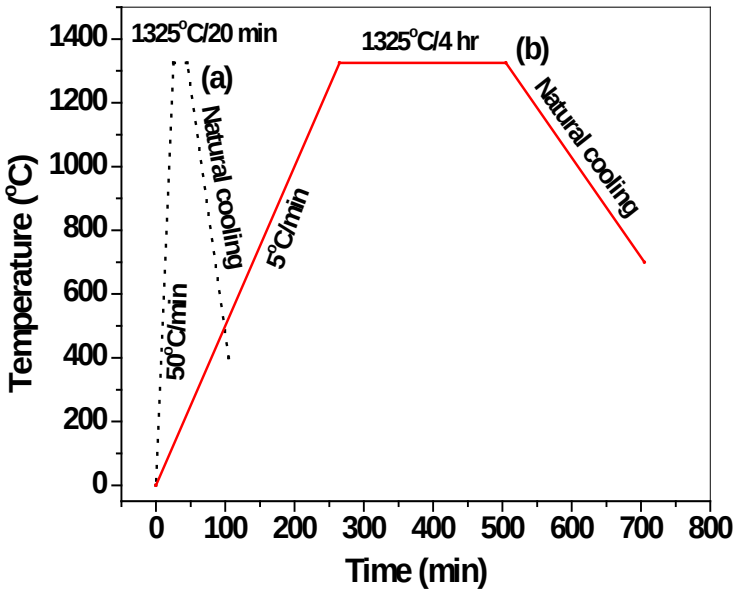

Figure 2.8 Sintering schedule of (a) microwave and (b) conventional sintering

- **Insulation:** High alumina bricks & back up by zirconia blend ceramic fiber
- **Size of sample:** 35 mm max
- **Heating system:** Microwave by magnetron
- **Power output:** 1.5 kW
- **Maximum temp.:** 1650°C
- **Temp. sensor:** IR sensor
- **Heating rate and soaking time are programmable**

Figure 2.9 Furnace used for Microwave sintering and its various specifications

2.2 Characterizations

The samples prepared by solid state reaction route were characterized for their structural, dielectric, ferroelectric and ferromagnetic properties. The various characterization techniques used for the present work are described below.

2.2.1 Density

For the present work the experimental density (d_{exp}) was measured by using Archimedes principle as shown in *figure 2.10*. According to this principle, first the weight of the sample was taken in air, which is referred as $W_{a.}$. After taking the weight of sample in air, the sample was suspended in water with the help of a very thin wire and its weight was taken in water which is referred as W_w. The ratio of W_a and the difference between W_a and Ww gives the experimental density of sintered samples as given in equation 2.1.

$$d_{exp} = \frac{Wa}{Wa-Ww} \times dw \qquad \ldots 2.1$$

Where d_{exp} (g/cc) is the density of the sample and d_w is the density of water which is 1.0 g/cc at room temperature.

Theoretical density, d_{th} (g/cc) was calculated from the lattice parameters using the relation [15]

$$d_{th} = (1\text{-}y)\, d_{th(ferroelectric)} + y\, d_{th(ferrite)}$$

where y is the concentration of ferrite phase.

$$d_{th} = \frac{Z \times M}{Na^3} \qquad \ldots 2.2$$

Where Z is the no. of molecules per unit cell and its value is different for both phases

Z = 8 for ferrite phase

and Z = 1 for ferroelectric phase

M is the molecular weight, N is the Avogadro's number and V is the volume of the unit cell.

Relative density (%) was calculated using the formula 2.3

$$d_{rel} = \frac{dexp}{dth} \times 100 \qquad \ldots 2.3$$

and Porosity (P) was estimated using the relation 2.4

$$P\ (\%) = 1 - \frac{dexp}{dth} \times 100 \qquad \ldots 2.4$$

For good magnetoelectric effect the porosity of the samples should be as low as possible because porosity in excess of 25-30% allows the absorption of moisture leading to many serious problems [1].

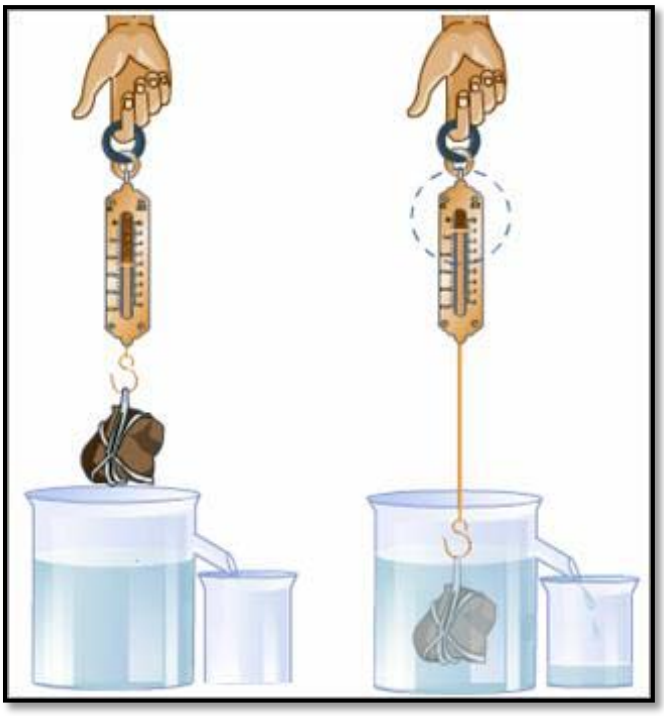

Figure 2.10 Density measurements by Archimedes principle

2.2.2 X-ray Diffraction (XRD)

X-ray crystallography is a technique for determining the arrangement of atoms with in a crystal and lattice parameters. X-rays are electromagnetic radiation with typical photon energies in the range of 100 eV-100 keV. For diffraction applications, only short wavelength X-rays in the range of a few angstroms to 0.1 Å are used because the wavelength of X-rays is comparable to the size of atoms. These are ideally suited for probing the structural arrangement of atoms and molecules in a wide range of materials [16-17]. The basic principle for X-rays is that for a fixed wavelength (λ), the constructive interference occurs for a fixed set of an inter planer spacing (d)

and at an incidence angle (θ) shown in *figure 2.11*. According to Bragg's condition of diffraction:

$$2d \sin\theta = n\lambda \qquad \textbf{…2.5}$$

For a cubic system, the inter planar distance (d) is given by

$$\frac{1}{d^2} = \frac{h^2+k^2+l^2}{a^2} \qquad \textbf{…2.6}$$

Using equation 2.5 and 2.6 we can predict the diffraction angle for any set of planes, For any set of planes, for a given 'λ' if the following condition is satisfied, we can calculate the h,k and l for different values of θ and also we can find out the unit cell parameter.

$$\boldsymbol{Sin^2\theta = \frac{\lambda^2}{4a^2}(h^2+k^2+l^2)} \qquad \textbf{…2.7}$$

Similarly, the relation for a tetragonal system is

$$\boldsymbol{Sin^2\theta = \frac{\lambda^2}{4}\left(\frac{h^2+k^2}{a^2}+\frac{l^2}{c^2}\right)} \qquad \textbf{…2.8}$$

For the present work, the structural analysis of the individual phase and composite was done by XRD using Bruker, D-8 Advance model. Cu-K_α (λ = 1.54056 Å) radiations were used for recording the diffraction pattern. The diffraction angle, 2θ was varied from 20^o to 70^o. All the lattice parameters were calculated using equation 2.5 and powder X software with an error of 0.05 degree in 2θ value.

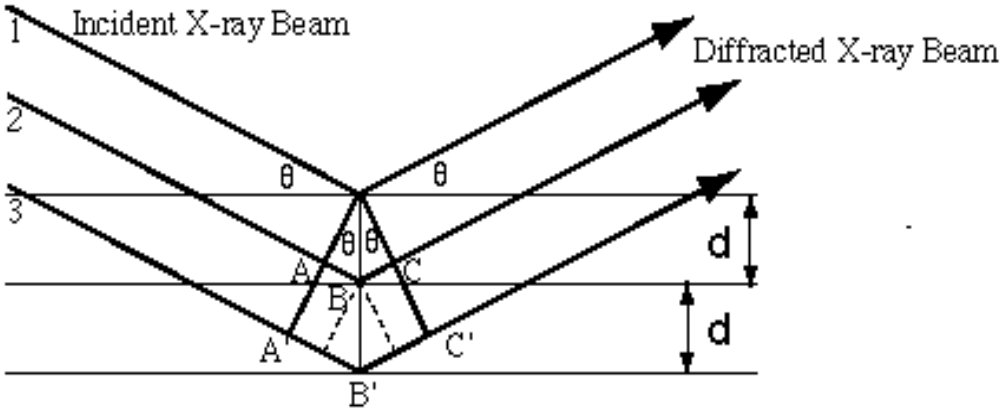

Figure 2.11 Bragg diffraction condition

2.2.3 Scanning Electron Microscopy (SEM)

The scanning electron microscope is a type of electron microscope which is used to determine the average crystallite size and the surface morphology of the samples. It also gives information about the grain evolution and grain size. In SEM a beam of electrons is produced at the top of the microscope by an electron gun. The electron beam follows a vertical path through the microscope, which is held with in a vacuum. The beam travels through electromagnetic fields and lenses, which focus the beam down toward the sample. Once the beam hits the specimen, the secondary electrons, back scattered electrons, auger electrons, characteristic x-rays and several other radiations are released from the specimen as shown in *figure 2.12*. Detectors collect these X-rays, backscattered electrons, and secondary electrons and convert them into a signal that is sent to a screen similar to a television screen. This produces the final image. Generally, the secondary electrons are collected to form the image in the SEM mode.

For the present study, this technique has been used to study the grain size of the samples. The micrographs also help in studying and identifying the porosity and uniformity of the samples. The microstructures of freshly broken sintered samples were studied by scanning electron microscope (JEOL JSM 6510LV, Japan). The broken pieces were placed on brass stubs and then were coated with gold using sputtering techniques. The average grain size of the samples was determined by linear intercept method.

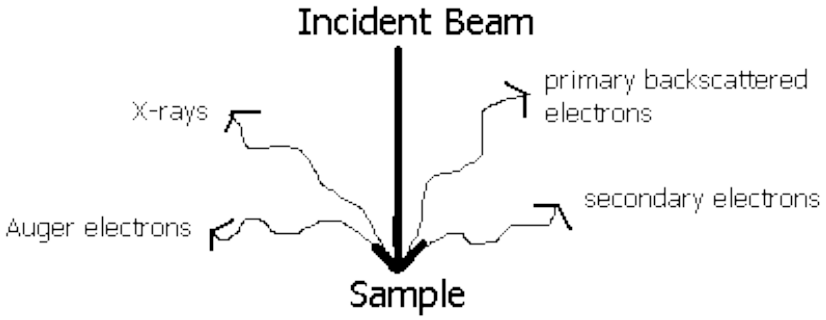

Figure 2.12 Various beam emitted from the specimen

2.2.4 Electroding

After sintering, the samples should be converted in the form of parallel plate capacitor for further electrical characterization. This can be achieved by electroding the samples.

For the present work, for studying the electrical properties of the samples, the electrical contacts were made by depositing silver electrode on both sides of the pellet using silver epoxy. The coated pellets were then put in a furnace in the temperature range 400-500^{o}C for 1 h for firing the silver paste.

2.2.5 Dielectric Properties

The capacitance for a parallel plate capacitor whose area is much greater than the separation distance of the plates is given by [18]

$C = \varepsilon_0 A/d$ Where, ε_0 = permittivity of free space (= 8.854x 10^{-12}F/m)

When a dielectric (electrical insulator) fills the space between the plates, the capacitance of the capacitor is increased by a factor ε', which is called the dielectric constant of the dielectric material. For most applications the dielectric properties are important practical parameters and it provides a great deal of information about the suitability of the material for various applications.

For the present work the dielectric properties of the samples were measured as a function of temperature in the range 30°C to 300°C at discrete frequencies of 1 kHz, 10 kHz, and 100 kHz by using Agilent 4263B LCR meter (Agilent Tech. Ltd) as shown in *figure 2.13* and room temperature measurement of ε and loss tangent ($tan\ \delta$) as a function of frequency (20Hz to 1MHz) were done by using Agilent 4284A LCR meter. For an alternating electric field, the dielectric constant can be expressed in terms of real and imaginary quantities

$$\varepsilon_r = \varepsilon - \varepsilon''$$

Where ε is the real component of the dielectric constant, in phase with the applied field and ε'' is the imaginary component and is 90^{o} out of phase with the applied field. The imaginary part is due to either by resistive leakage or by dielectric absorption [3]. The ratio of imaginary part to real part of the dielectric constant is known as dielectric loss (tanδ)

$$\tan\delta = \varepsilon''/\varepsilon$$

- **The LCR meter is interfaced with instrument controller and hot stage through IEEE–488 and temperature controller through serial port for automatic data acquisition.**
- **The acquired data can be saved in worksheet form for further analysis.**
- **The instrument is equipped with an in-built dc source to supply voltage -40 V to 40 V.**
- **The software allows visualization of an online trace of the measured parameters.**
- **The dielectric constant measures the amount of charge that an electroded disc of material can store, relative to the charge that stored by electrodes separated**

Figure 2.13 Experimental Setup for measurement of dielectric measurement system with its various specifications

2.2.6 a.c. Conductivity

The electrical conductivity is an important material property that not only gives information about how well a metal conducts electrical current but also provides information of the defects, loss and conduction mechanism in the dielectric materials.

For the present work the ac conductivity of the samples were calculated from the dielectric parameters by using the relation [19]

$$\sigma_{ac} = \varepsilon\, \varepsilon_o \omega \tan\delta$$

where ε is the dielectric constant, tanδ is the loss tangent, ε_o is the permittivity of free space (8.854×10^{-12}F/m) and ω is the angular frequency.

2.2.7 Ferroelectric Properties

Polarization reversal (switching) is a characteristics of ferroelectricity, which can be observed by measuring the polarization vs electric field hysteresis loop (P-E hysteresis loop) below Curie temperature. This is usually done by using Sawyer-Tower circuit [20] shown in *figure 2.14*. The method consists of applying an alternating voltage *V* and studying the relationship between the stored charge and instantaneous voltage for test sample. A capacitor C_0 of high value is connected in series with the test sample (C_x). The voltage across this capacitor measures the charge stored on the test sample.

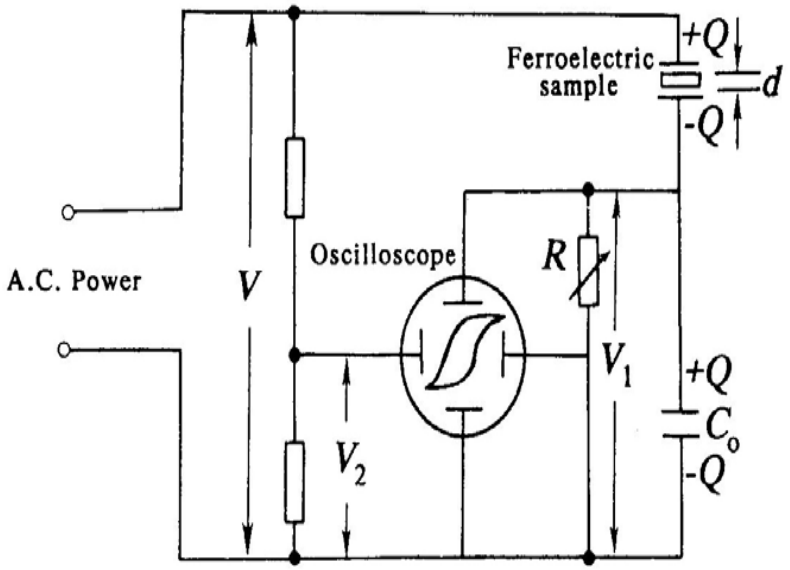

Figure 2.14 Schematic of modified sawyer-Tower circuit

For the present work the ferroelectric nature of the composite samples was analyzed using an automatic PE loop tracer system shown in *figure 2.15*. The P-E loop tracer was based

on Sawyer –Tower circuit and can be operated at discrete frequencies ranging 20-1000 Hz. The system consists of PC, software, programmable voltage source (up to 3 kV). For measurement; specimen was kept in a spring-loaded jig and immersed in silicon oil bath to avoid any sparking or breakdown at high voltage. The loop was recorded by the system and the software calculates all the parameters like P_s, P_r , E_c and E_{max}.

Figure 2.15 P-E Hysteresis Loop Tracer

2.2.8 Poling

Poling is a process during which a high electric field is applied on the sample to force the domains of ferroelectric phase to reorient in the direction of the applied electric field. The ferroelectric phase doesn't possess any piezoelectric properties owing to the random orientation of the ferroelectric domains in the ceramics. After poling, sample starts exhibiting piezoelectric effect. For obtaining good properties, a field higher than coercive field (E_c) must be applied at higher temperature during poling.

For the present work, the poling was done at 150^o C in silicon oil bath by applying field strength of ~15kV/cm for 1 hr. Then the sample was allowed to cool by switching off the heater

in applied electric field and the field was removed at room temperature. The poling set-up used for the present work is shown *figure 2.16*.

Figure 2.16 Poling set up

2.2.9 Vibrating Sample Magnetometer (M-H hysteresis loop set-up)

The magnetic properties of a material are usually characterized by M-H hysteresis loop. This gives the behavior of a material when excited by an external magnetic field. There are many techniques to obtain magnetic hysteresis loops like Vibrating Sample Magnetometer (VSM), superconducting quantum interference device (SQUID), hysteresis graph etc.

For the present work, VSM technique was employed for obtaining the M-H hysteresis loop as shown in *figure 2.17* because it is extremely sensitive with ease of sample mounting and exchange. It is based on change in flux in a coil when a sample is made to vibrate between the electromagnets. Lake shore 735 VSM controller was used for recording M-H hysteresis loops and from these loops the parameters such as saturation magnetization, remenant magnetization and coercivity were measured directly from hysteresis loops.

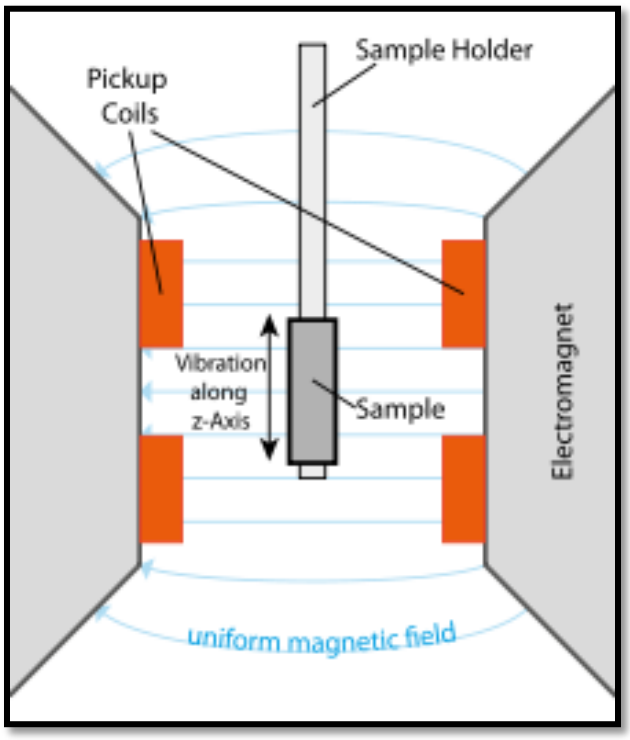

Figure 2.17 Vibrating sample magnetometer (VSM)

2.2.10 M-E Set Up:

The magnetoelectric effect is very important and unique property shown by ferrite-ferroelectric composite. It is coupled two field effect in which induction of electric polarization by applying an external magnetic field and induction of magnetic polarization by applying an external electric field.

For the present work, study of magnetoelectric effect was done by two ways as discussed below:

(i) Using VSM

In this two pieces from a single pellet were taken. Electric poling was done for one piece at 15 kV/cm and room temperature M-H hysteresis loops were taken for both electrically poled and unpoled pieces of composite samples.

(ii) Using ME-Setup

In this way, static magnetoelectric (ME) coupling coefficient (dE/dH) as a function of dc magnetic field (0-1700 Oe) keeping ac magnetic field constant at 10 Oe was studied using ME

setup consisting of lock in amplifier (7265 DSP), electromagnets (10″ poles) and sample holders. Electric voltage was noted from lock in amplifier and magnetoelectric coupling coefficient (mV/cm-Oe) was calculated by using formula.

$$\alpha = \frac{dV}{t} \times \frac{1}{H_{ac}}$$

Where t is thickness of the sample and H_{ac} is the ac magnetic field.

Refrences

1) P. Consin and R.A. Ross, Mater. Sci. Engg. A, **130** (1990) 119.

2) B. Jaffe, W. Cook and H. Jaffe, Piezoelectric Ceramics, Academic Press, London (1971).

3) Y. Xu, Ferroelectric Materials and Their Applications, Elsevier Science Pub, New York, USA (1991).

4) A.J. Moulson and J.M. Herbert, Electroceramics: Materials, Properties and Applications, Chapman and Hall, New York, USA (1997).

5) M.W. Barsoum, Fundamental of Ceramic (1997).

6) K. Uchino, Processing of Ceramics (1982).

7) W.H. Sutton, Am. Ceram. Soc. Bull., **68** (1989) 376.

8) D.E. Clark, W.H. Sutton and D.A. Lewis, Ceram. Trans., **80** (1997) 61.

9) J. Jacob, L.H.L. Chia and F.Y.C. Boey, J. Mater. Sci., **30** (1995) 5321.

10) O.P. Thakur, Chandra Prakash and D.K. Aggarwal, J. Ceram. Process. Res., **3** (2002) 75.

11) R. Roy, S. Komarneni and J.L. Yang, J. Am. Ceram. Soc., **68** (1985) 392.

12) W.B. Snyder, W.H. Sutton, M.F. Iskander and D.L. Johnson, Mat. Res. Soc. Proceed. (1990).

13) R.L. Beatty, W.H. Sutton and M.F. Iskander, Mat. Res. Soc. Proceedings (1992).

14) D.E. Clark, W.R. Tinga and J.R. Laia, Ceram. Trans., **36** (1993) 110.

15) Renu Rani, Sangeeta Singh, J.K. Juneja, Chandra Prakash and K.K. Raina, Ferroelectric Lett., **38** (2011) 134.

16) S.K. Chatterjee, Prentice-Hall of India Private Limited, New Delhi (1999).

17) B.D. Cullity, Addison-Wesley Publication Company, Menlo Park, California.

18) W. F. Smith, Principles of Materials Science and Engg., MC graw -Hill, U.S.A.

19) S.S Choughle and B. K. Choughle, Mat. Chem. and Phys., **108** (2008) 408.

20) C.B. Sawyer and C.H. Tower, Phys. Rev., **35** (1993) 269.

Chapter - III

Synthesis and Characterizations of NZF– BST Composites

Chapter III

Synthesis and Characterizations of NZF – BST Composites

This chapter includes study on the structural, dielectric, ferroelectric, ferromagnetic and magnetoelectric properties of (y) $Ni_{0.8}Zn_{0.2}Fe_2O_4$ - (1-y) $Ba_{0.9}Sr_{0.1}TiO_3$ *(Series A)* composite. This is the subject of investigation for the present thesis. Samples with varying composition (y = 0, 0.05, 0.10, 0.15 and 1.00 by wt. %) were prepared by conventional solid state reaction route. The steps involved in synthesis of composite samples are given in *figure 2.1* and temperature - time sintering profile is shown in *figure 2.9 (b)*. In solid state reaction route, heat treatment at higher temperature significantly influences the system properties [1-2]. The sintering temperature and sintering schedule are very important which influence the material properties and therefore optimization of these is necessary and which is also discussed in this chapter.

3.1 Optimization of Sintering Temperature

In order to select optimum temperature for sintering, composition $0.10Ni_{0.8}Zn_{0.2}Fe_2O_4$–$0.90Ba_{0.9}Sr_{0.1}TiO_3$ was sintered at three different temperatures in the range of 1275^{o}C to 1325^{o}C and this composition was considered as the starting point for further research. Phase identification of sintered pellets was done by using D8 Advance X-ray diffractometer (XRD) (Bruker AXS) in a range of Bragg angles ($20^o \leq 2\theta \leq 65^o$) with step size of 0.02^o. The sintered pellets were lapped and electroded using silver epoxy. Dielectric properties of the samples were measured as a function of temperature in the range 30°C to 200°C at discrete frequencies (1 kHz,

10kHz, 100kHz) using Agilent 4263B LCR meter. P-E hysteresis loops were recorded using automatic P-E loop tracer. M-H hysteresis loops were recorded using Lake Shore 735 VSM .

Figure 3.1(a) shows the XRD patterns of composite samples sintered at different sintering temperatures. All XRD patterns show well defined peaks with specific indices characteristic peaks of both phases. No extra peak was observed other than ferroelectric phase and ferrite phase suggesting that no chemical reaction occur between two phases during sintering and they maintained proper stoichiometry. *Figure 3.1(b)* depicts the porosity of the samples as a function of sintering temperature. As the sintering temperature increases the porosity of sample decreases and has minimum value at sintering temperature of 1325^{o}C. That may be due to better grain growth at higher sintering temperature.

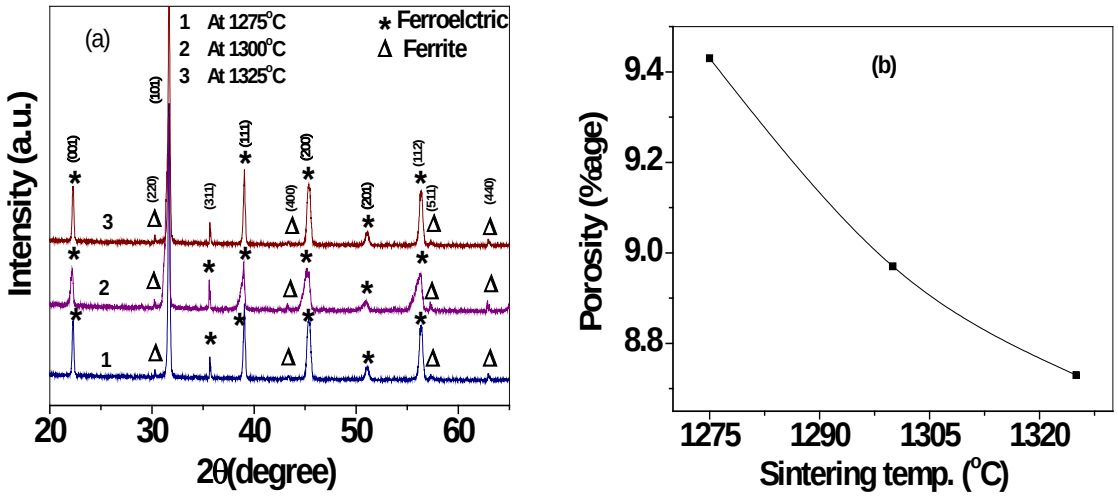

Figure 3.1 (a) XRD patterns, and (b) porosity of all samples as a function of sintering temperature

Figure 3.2 shows the variation of dielectric constant with temperature at different frequencies at all sintering temperature. All samples show a dielectric peak at ferroelectric transition temperature. It is observed that dielectric constant is maximum and dielectric loss is minimum for sample sintered at 1325^{o}C. The value of ferroelectric Curie temperature (T_c), room

temperature dielectric constant (ε_{RT}), dielectric constant at T_c (ε_{max}) and loss tangent for all samples are given in *table 3.1*.

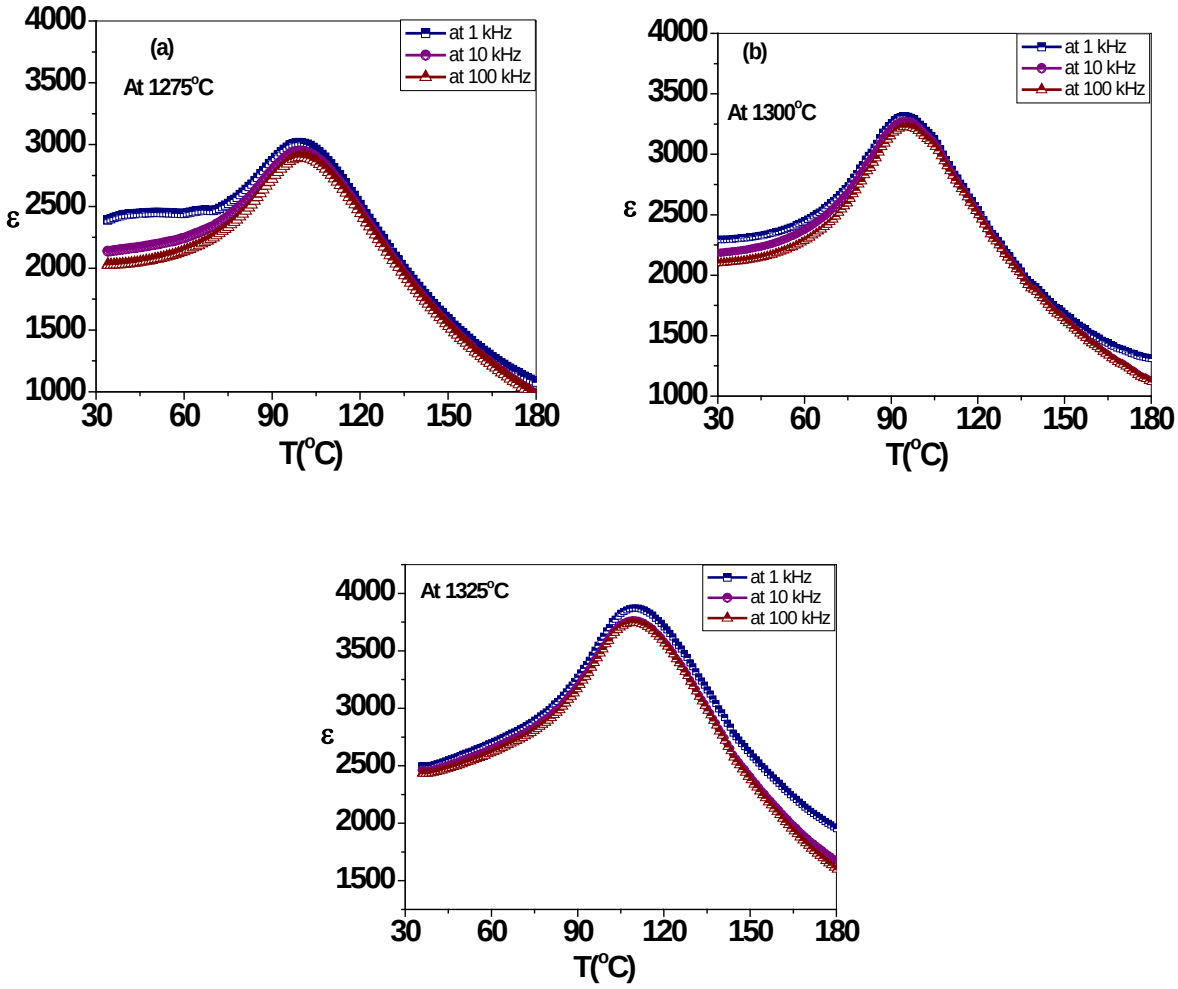

Figure 3.2 Variation of dielectric constant with temperature for different sintering temperatures

Figure 3.3 depicts the P-E hysteresis behavior for samples sintered at different temperature. It shows that as sintering temperature is increased from 1275 to 1325°C, spontaneous polarization (P_s) increases from ~7.77 μC/cm^2 to 9.64 μC/cm^2 and coercive field (E_c) decreases from 4.40 kV/cm to 2.48 kV/cm as given in table 3.2. This can be correlated to the decrease in porosity of sample i.e. increase in density of sample with increase in sintering temperature.

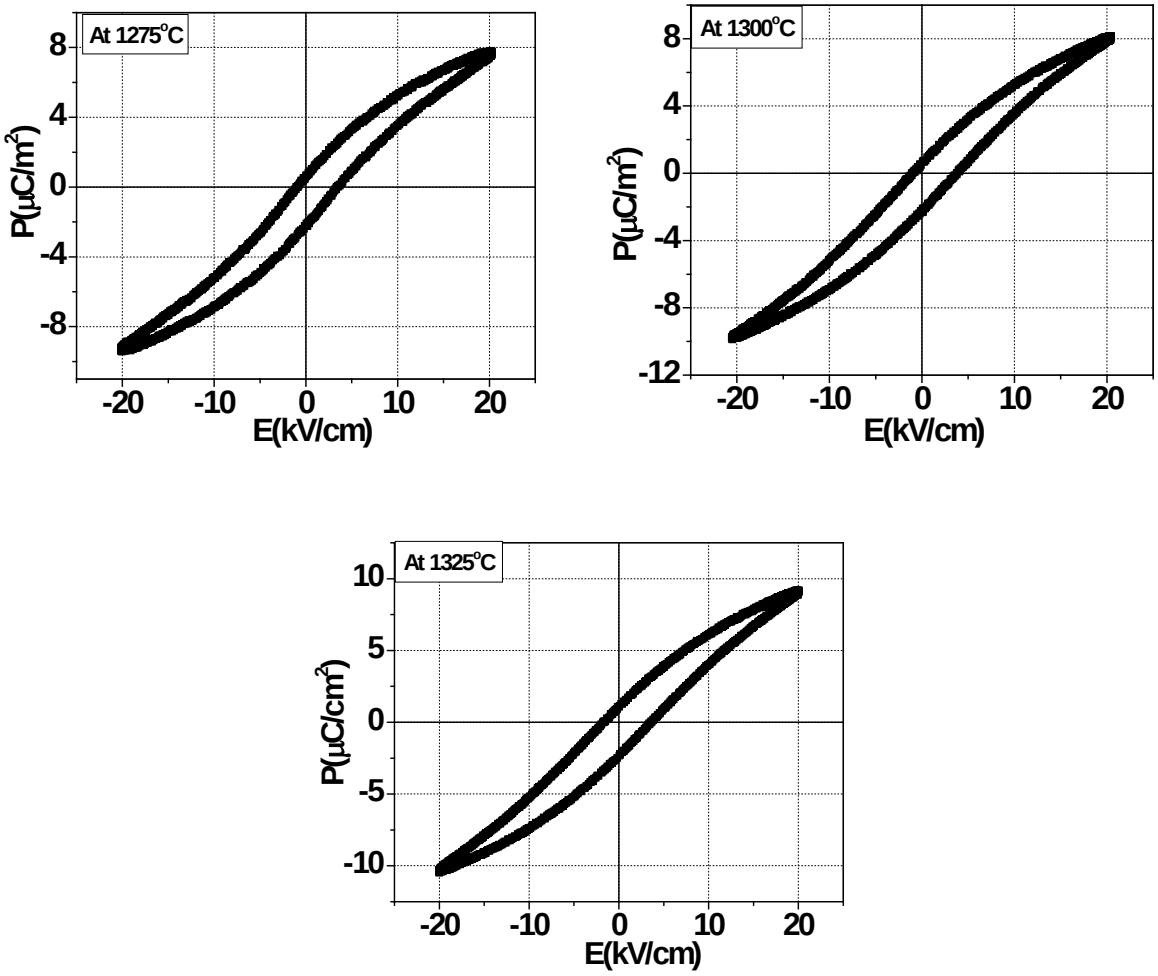

Figure 3.3 P-E hysteresis loops for different sintering temperatures

The room temperature M-H loops for sample sintered at different temperatures are shown in *figure 3.4*. It shows that as sintering temperature is increased from 1275 to 1325°C spontaneous magnetization increases as given in *table 3.2*. The low value of spontaneous magnetization at low sintering temperature can be related to large value of porosity because porosity causes the discontinuity which prevents the movement of domain wall and hence show low value of magnetization.

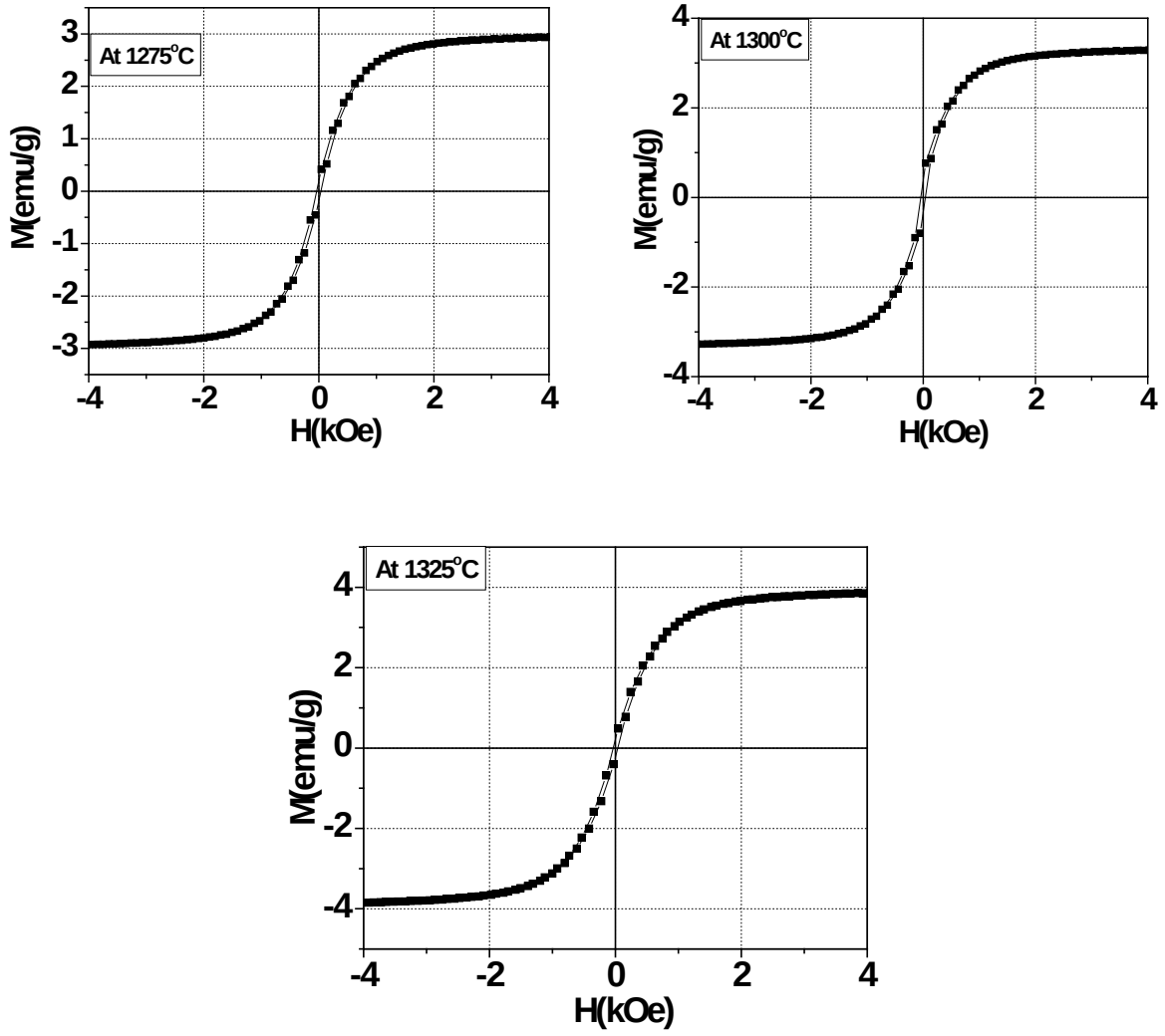

Figure 3.4 M-H hysteresis curves for different sintering temperatures

Table 3.1

Dielectric parameters of 0.1NZF – 0.9 BST at 100 kHz

Sintering Temperature (^oC)	**T_c (^oC)**	**ε_{RT}**	**ε_{max}**	**tanδ $_{RT}$**	**tanδ $_{max}$**
1275	100	2027	2898	0.020	0.038
1300	95	2103	3224	0.015	0.026
1325	109	2423	3744	0.011	0.018

Table 3.2

Ferroelectric and Ferromagnetic parameters 0.1NZF – 0.9BST composite

Sintering temp. (^oC)	P_s ($\mu C/cm^2$)	E_c (kV/cm)	M_s (emu/g)
1275	7.77	4.40	2.92
1300	8.19	4.24	3.34
1325	9.64	2.62	3.88

From the above discussion we can conclude that sintering temperature affects dielectric, ferroelectric, and ferromagnetic properties of the material. The Porosity was observed to be lowest for composition sintered at 1325^{o}C. The spontaneous polarization (P_s), room temperature dielectric constant (ε_{RT}) and spontaneous magnetization were observed to be higher for composition sintered at 1325^{o}C. As sintering temperature is increased to 1350^{o}C, both phases react into each other. Hence, optimum temperature for sintering for composite samples at which dielectric, ferroelectric and ferromagnetic properties are optimized is 1325^{o}C.

3.2 Synthesis of (y) $Ni_{0.8}Zn_{0.2}Fe_2O_4$(NZF) - (1-y) $Ba_{0.9}Sr_{0.1}TiO_3$ (BST)

The individual phases ($Ni_{0.8}Zn_{0.2}Fe_2O_4$ and $Ba_{0.9}Sr_{0.1}TiO_3$) were prepared by conventional solid state reaction route. AR grade NiO, ZnO, Fe_2O_3 $BaCO_3$, $SrCO_3$ and TiO_2 were used as raw materials. The mixing was carried out by ball-milling using zirconia balls and distilled water as milling media for both phases. The slurries of NZF and BST were first dried and then calcined at 1000^{o}C for 4 hrs. The calcined powder was then grounded to fine powder, ball milled again, dried and then recalcined at 1100^{o}C for 4 hrs. The recalcined powder was then grounded to fine powder using pestle mortar, ball milled again and dried. The composites of (y) NZF - (1-y) BST were prepared by mixing the two phases i.e. ferrite and ferroelectric phase by weight. A small amount of diluted PVA was added as binder and the pellets having 2-3 mm thickness and 15 mm diameter were pressed using the uniaxial hydraulic press (pressure = 10 ton). The pellets were sintered at 1325^{o}C for 4 hrs with constant heating rate of 5^{o}C/min.

After sintering experimental density of the samples was determined using Archimedes' principle. Theoretical density of the samples was calculated using the lattice parameters. XRD was done by using Bruker, D-8 Advance model in a range of Bragg angles ($20^o \leq 2\theta \leq 65^o$) with step size of 0.02^o. The micro structures of freshly broken sintered samples were studied by scanning electron microscope (JEOL JSM 6510LV, Japan). For measuring electrical properties, the sintered pellets were lapped and then electroded by using silver epoxy and heated at 400 ^{o}C for 30 min to ensure good ohmic contact. The dielectric properties of the samples as a function of temperature at discrete frequencies were measured by using Agilent 4263B LCR meter and room temperature measurement of ε and loss tangent ($tan\ \delta$) as a function of ac frequency (20Hz to 1MHz) were measured by using Agilent 4284A LCR meter . The ferroelectric nature of the composite samples was analyzed using an automatic PE loop tracer system (Agilent Technologies Ltd.). Electrical poling was done at 150^o C in silicon oil bath by applying field strength of ~15kV/cm for 1 hr. Then the sample was allowed to cool by switching off the heater in applied electric field and the field was removed at room temperature. Lake shore 735 VSM was used for recording M-H hysteresis loops. The magnetoelectric signal (voltage) was determined as a function of increasing DC magnetic field (0–1500 Oe) using 7265 DSP lock-in amplifier in the presence of small AC magnetic field (H_{ac} = 10 Oe). Electric voltage (V) was noted from lock in amplifier and magnetoelectric coupling coefficient (mv/cm-Oe) was calculated by using the formula.

$$\alpha = \frac{dV}{t} \times \frac{1}{H_{ac}} \qquad \ldots\ldots \mathbf{3.1}$$

Where t is thickness of the sample and H_{ac} is the ac magnetic field

3.3 Characterizations of (y)$Ni_{0.8}Zn_{0.2}Fe_2O_4$ - (1-y) $Ba_{0.9}Sr_{0.1}TiO_3$ Composites

3.3.1 Structural Properties

3.3.1 (a) X-Ray Diffraction

The structural analysis of the individual phases and their composites was done by XRD with Cu-K_α radiation in the Bragg angle range of 20^o to 65^o. *Figure 3.5* shows the XRD patterns of individual phases (BST & NZF) and their composite samples for y = 0.05, 0.10 and 0.15. XRD patterns of composite samples show well defined peaks with specific indices characteristics peaks of both phases and it confirms the perovskite structure in ferroelectric phase (BST) and cubic spinel structure in ferrite phase (NZF). No extra peak was observed other than ferroelectric phase and ferrite phase. This suggests that no chemical reaction took place between two phases during sintering and they maintained proper stoichiometry. It is also observed that there is increase in intensity and number of peaks corresponding to ferrite phase with increase in ferrite content (y).

The calculated lattice parameters for all the samples are given in *table 3.3*. From here it is observed that there is slight change in lattice parameters of both phases in composite samples. This may be due to the inhomogeneous stresses exerted on each other by the two phases [3]. A similar random variation in lattice parameters has been reported by many researchers for various composite samples [4-5]. For all the samples experimental density, theoretical density and relative density was calculated by using the formulae as discussed in *section 2.3.1* and all these calculated values are given in *table 3.3*. Relative density was found to decrease for composite samples and it is minimum for y = 0.05. This may be due to lack in connectivity of the two phases with different structure in composite system [6-7].

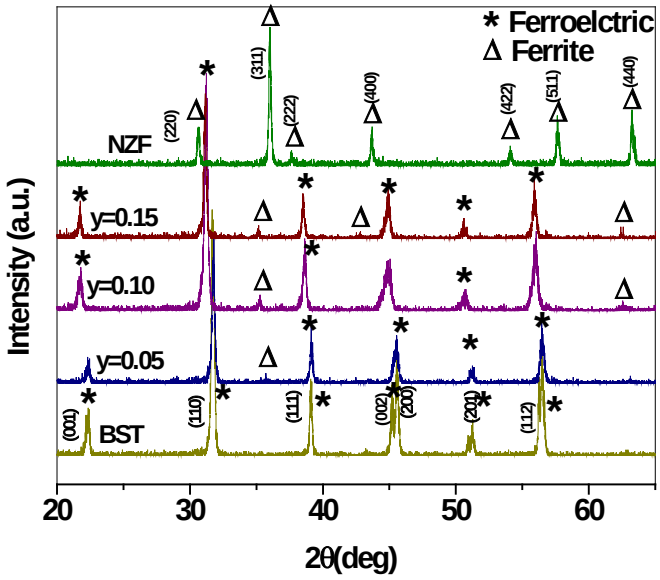

Figure 3.5 XRD pattern for (y) NZF- (1-y) BST **(Series A)** composites for different values of y.

3.3.1(b) Scanning Electron Microscope (SEM)

Scanning electron microscopy was done to study the surface morphology of the composite samples. The SEM images for all the samples are shown in *figure 3.6(a-e)*. The micrographs show closely packed and well oriented grains. The shape, size and distribution of grains confirm the polycrystalline nature. Smaller grains can be seen in case of composite samples but we can't distinguish the grains of two phases individually due to low concentration of ferrite phase.

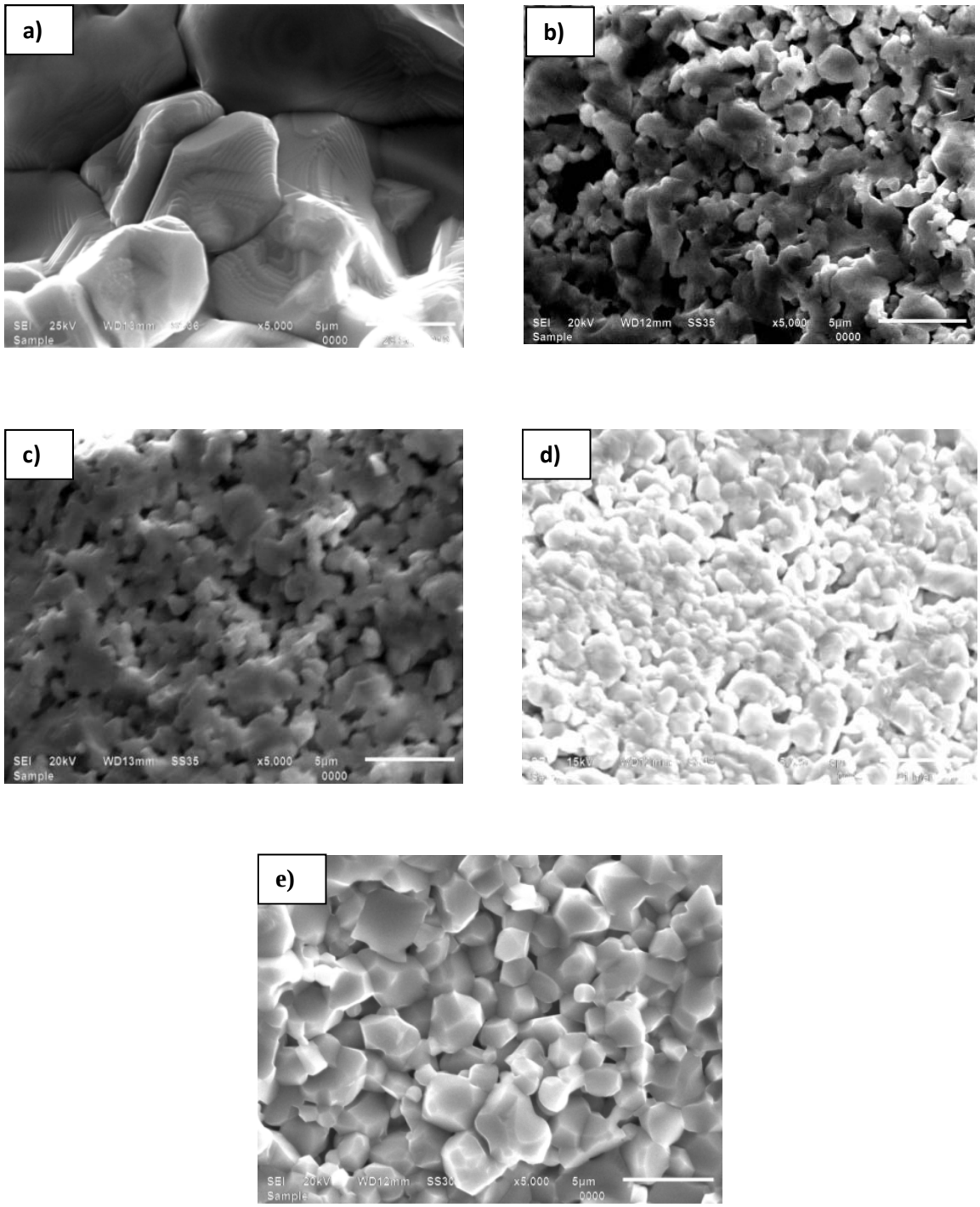

Figure 3.6 SEM micrographs of (y) NZF- (1-y) BST **(series A)** composites for (a) y = 0.00, (b) 0.05, (c) 0.10, (d) 0.15 and (e) 1.00

Table 3.3

Structural parameters of (1-y) BST- (y) NZF **(Series A)**

x	Ferroelectric			Ferrite a (Å)	d_{exp} (g/cc)	d_{th} (g/cc)	Relative density (%)
	a(Å)	c(Å)	c/a				
0.00	3.99	4.00	1.0043	-	5.74	5.96	96.30
0.05	3.98	4.00	1.0044	8.32	5.21	5.93	87.84
0.10	4.03	4.04	1.0042	8.33	5.28	5.79	91.02
0.15	4.02	4.04	1.0045	8.33	5.24	5.82	88.98
1.00	-	-	-	8.34	4.93	5.41	91.12

3.3.2 Dielectric Properties

3.3.2 (a) Variation of ε and tanδ with Frequency

Figure 3.7(a-b) shows the variation of dielectric constant (ε) and dielectric loss (tanδ) with frequency for all samples at room temperature. The value of dielectric constant decreases with increase in frequency because in a dielectric material, polarization occurs due to contributions of electronic, ionic, dipolar and space charge polarization. With the change in frequency, the contribution of different polarization comes into light. At lower frequencies, all types of polarization contribute but the maximum contribution is of space charge polarization due to inhomogeneous dielectric structure and as the frequency increases, contribution of different polarization decreases and only electronic polarization contributes at higher frequencies so the dielectric constant was found to decrease with increase in frequency for all samples.

In case of composites, the high value of dielectric constant at lower frequencies is due to the fact that the ferroelectric regions are surrounded by non ferroelectric regions similar to the relaxor ferroelectric materials. Here non ferroelectric regions are ferrite phase and grain boundaries.

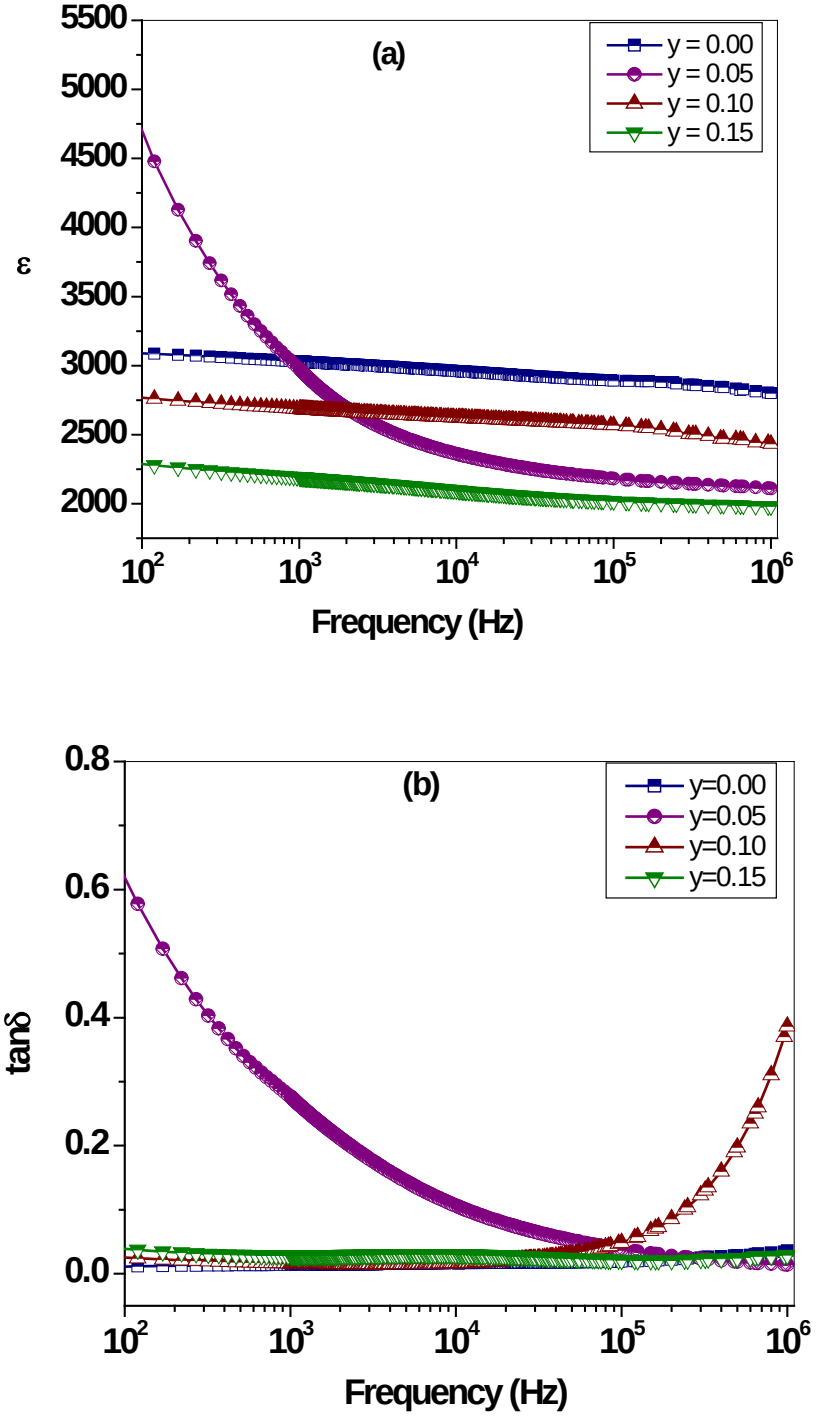

Figure 3.7 Variation of (a) dielectric constant (b) loss as a function of frequency at room temperature for (y) NZF- (1-y) BST **(series A)** composites

This gives rise to interfacial polarization and it can also be related to heterogeneity of the samples like pores, impurities and grain structure in composite samples [8-9]. But for y = 0.05 larger dispersion is observed because of its high porosity which results in large space charge polarization. It is also observed that room temperature dielectric constant decreases with addition of ferrite phase. The dielectric constant remains less dependent at higher frequencies because beyond frequency of external electric field the electron exchange between $Fe^{2+}/Fe^{3+}$and Ni^{2+}/Ni^{3+} in ferrite phase cannot follow the alternating field [10-11]. The variation of loss tangent with frequency for all samples show a similar dispersion as that of dielectric constant with frequency but for y = 0.10 at higher frequencies, dielectric loss increases with frequency that may be due to some extrinsic loss phenomena [12].

3.3.2(b) Temperature Dependence of ε and tanδ at Different Frequencies

Figure 3.8 (a-d) shows the variation of dielectric constant with temperature at different frequencies for all studied samples. All samples show a dielectric peak at a ferroelectric transition temperature. For y = 1.00 dielectric constant and dielectric loss increases with temperature continuously which is the typical dielectric behavior of ferrite materials. Sample having no ferrite content (y = 0.00) is showing normal ferroelectric to paraelectric transition as shown in *figure 3.8 (a).* From the figure, it can be seen that as the ferrite content (y) in the composite increases, the dielectric peaks get broadened and suppressed. This may be due to the incorporation of non-ferroelectric phase (ferrite phase) in the pure ferroelectric phase and it dilutes the ferroelectric properties of the composites, resulting in the reduction of the dielectric constant and broadening of the peak. The broadening of peak may also be due to microscopic heterogeneity in the composites due to presence of two phases [13-15].

From *figure 3.8* it is also observed that for large value of ferrite content, dielectric constant increases at higher temperature. This increase in dielectric constant at higher temperatures is due to the increase in dielectric polarization. This increase in polarization is due to thermally activated electron hopping between $Fe^{+2} \leftrightarrow Fe^{+3}$ ions as well as $Ni^{+2} \leftrightarrow Ni^{+3}$ ions

present in the ferrite phase. The value of dielectric loss also increases with temperature. High values of loss tangent (tanδ) in paraelectric region are attributed to thermal conductivity losses at higher temperature due to presence of ferrite phase and similar behavior has been reported by many workers [16-17]. Due to varying amounts of ferrite phase (y) in composite samples, the crystal structures do not maintain the same lattice parameters as in pure phase resulting in different curie temperatures. Various dielectric parameters like ε_{RT}, ε_{max}, $\tan\delta_{RT}$, T_c and $\tan\delta_{max}$ are given in table 3.4 for all values of y.

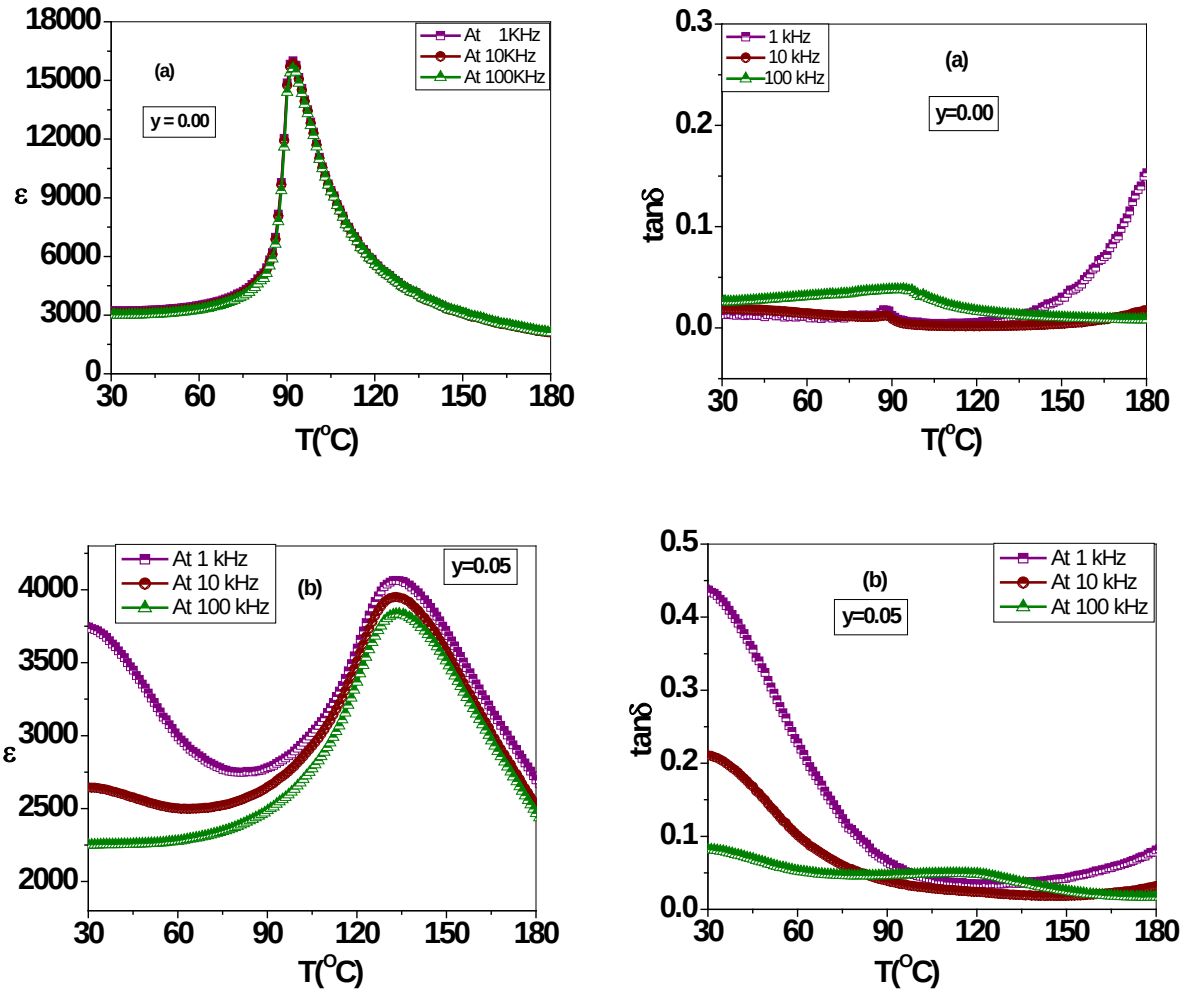

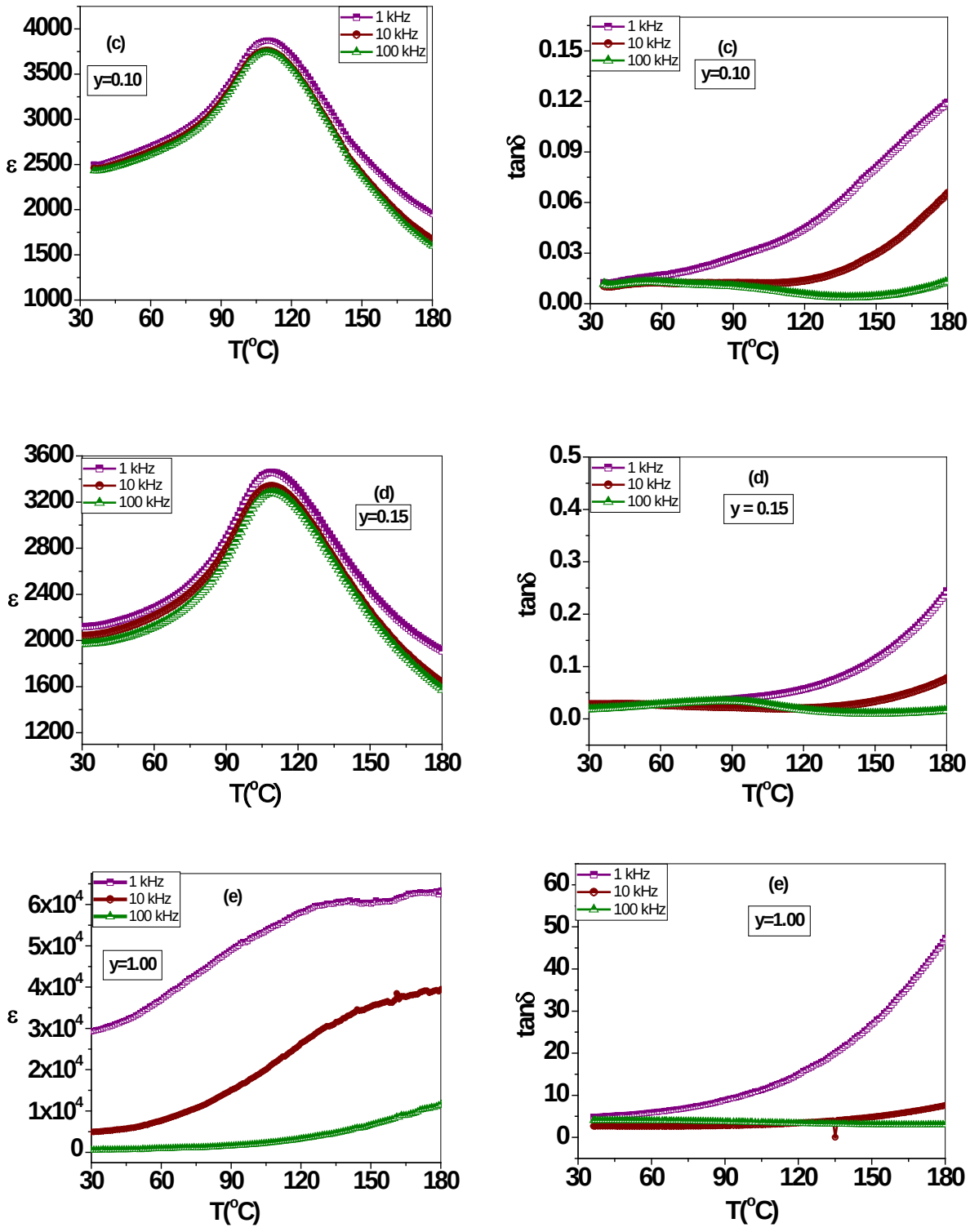

Figure 3.8 Temperature variation of ε and tan δ at different frequencies for (y) NZF- (1-y) BST composites

Table 3.4

Dielectric parameters of (1-y) BST- (y) NZF (**Series A)** composites at 100 kHz

Y	ε_{RT}	ε_{max}	$\tan\delta_{RT}$	$\tan\delta_{max}$	T_c (^oC)
0	3011	15890	0.022	0.028	92
0.05	2251	3834	0.082	0.037	134
0.10	2423	3744	0.011	0.018	109
0.15	1975	3280	0.018	0.023	105

3.3.3 Electrical conductivity:

In order to understand the conduction mechanisms and the type of polarons responsible for conduction, ac conductivity at room temperature was calculated in the frequency range from 20 Hz to 1 MHz. *Figure 3.9* shows the variation of ac conductivity with frequency. From this figure it is clear that conductivity increases linearly with increase in frequency for all the samples and for composite samples, conductivity is high as compared to pure ferroelectric phase that is due to the presence of ferrite phase. The linear variation of ac conductivity with frequency indicates that conduction occurs due to small polaron hopping. These results are similar to the reported by other workers [18-19].

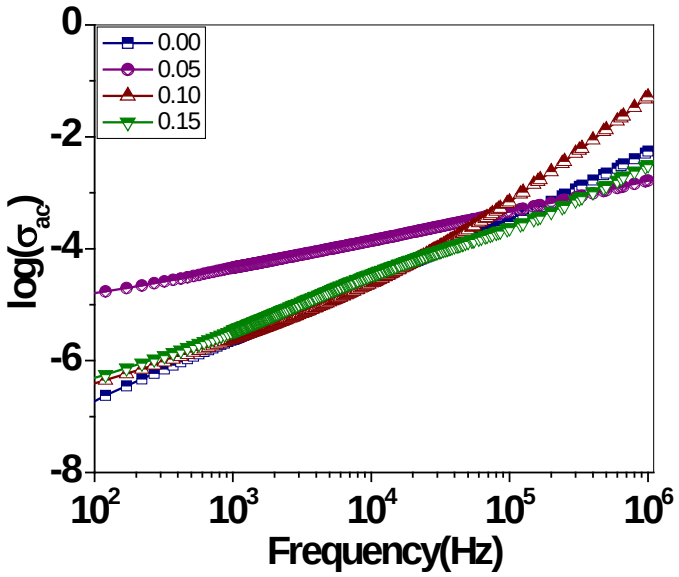

Figure 3.9 Variation of ac conductivity with frequency for (y) NZF- (1-y) BST **(series A)** composites

3.3.4 Ferroelectric Properties (P-E Hysteresis Loop)

To study ferroelectric behavior of composites, room temperature P-E hysteresis loops were taken for all the samples at different electric fields as shown in *figure 3.10 (a-d).* It also confirms the existence of ferroelectric property in composite systems. From figure, it is observed that area of loop increases with the increase in electric field. This is due to the fact that with increase in electric field, the motions of domains become easier and as a result there is increase in P_r and E_c. From figure, it is also observed that the loops for composite samples are slightly asymmetric and this asymmetry is increasing with increase in ferrite content which may be due to internal bias field developed in the ferroelectric phase, electrode/sample interface or due to defects present in the sample [20].

All ferroelectric parameters calculated from P-E hysteresis loops are given in *table 3.5*. From this table it is observed that the values of spontaneous polarization (Ps) of the samples obey the rule of mixtures i.e. goes on decreasing with decrease in ferroelectric content. It means ferroelectric behavior is weakening, which may be due to low internal polarizablity i.e. decrease

in long range ordered behavior of electric dipoles because ferrite particles with spinal structure are incorporated into the ferroelectric phase and act as pores in the presence of applied electric field and break the electric current resulting in the decrease of these electrical parameters with increase in ferrite content [21]. From *table 3.5* it is observed that value of coercive field for y = 0.05 is large as compared to the other samples which may be due to large value of porosity and dielectric loss of this sample.

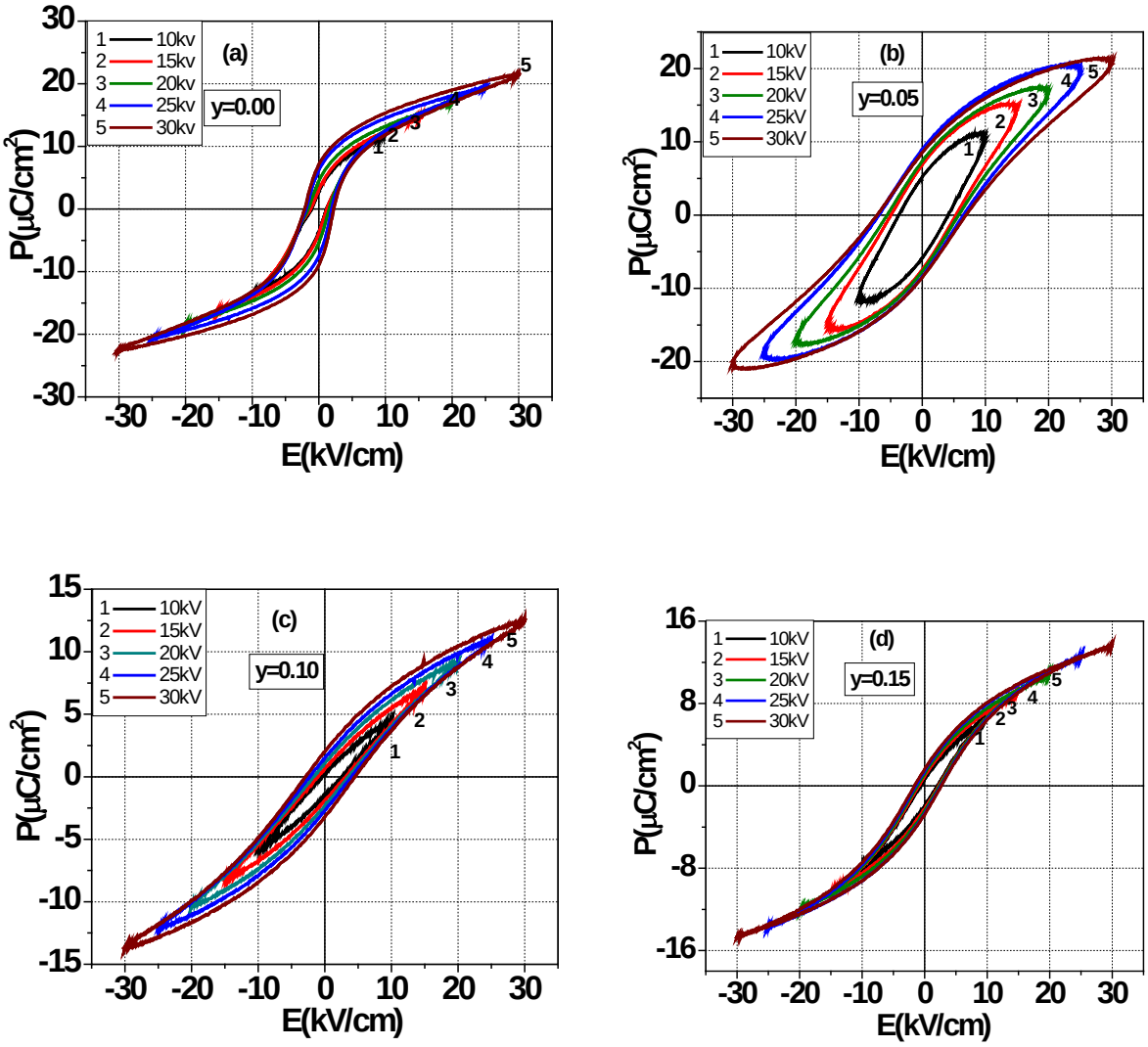

Figure 3.10 Polarization vs electric field (P-E) hysteresis loop at different electric field for (y) NZF- (1-y) BST **(series A)** composites

3.3.5 Ferromagnetic Properties (M-H hysteresis loop)

In order to understand the magnetic nature of composites, magnetic hysteresis loops for all samples were taken. *Figure 3.11 (a-d)* illustrates the magnetic hysteresis loops at room temperature. It also confirms the existence of magnetic ordering in composite system. The value of saturation magnetization is given in *table 3.5*. From table it is observed that saturation magnetization increases with increase in ferrite content i.e. these values also obey the rule of mixtures and it is due to the fact that the individual ferrite grains act as center of magnetization and the saturation magnetization of the composites is vector sum of all these individual contributions. The magnetic contact increases with increase in ferrite content and results in increase of net magnetization [22]. But the value of magnetization in composites is smaller than the pure ferrite phase because ferroelectric material incorporates in to the ferrite phase and acts as pores in the presence of applied magnetic field and breaks the magnetic current resulting in the decrease of these magnetic parameters [23-24].

Table 3.5

Ferroelectric and ferromagnetic parameters of (1-y) BST- (y) NZF **(series A)** composites

y	P_r ($\mu C/cm^2$)	E_c (kV/cm)	P_{max} ($\mu C/cm^2$)	M_r (emu/g)	M_s (emu/g)	H_c (Oe)
0.00	6.85	2.19	20.17	--	--	--
0.05	7.70	7.8	16.00	0.17	1.60	70.39
0.10	1.75	2.62	9.64	0.39	3.88	73.56
0.15	1.70	2.21	8.60	0.83	6.53	79.34
1.00	--	--	--	1.38	40.23	42.4

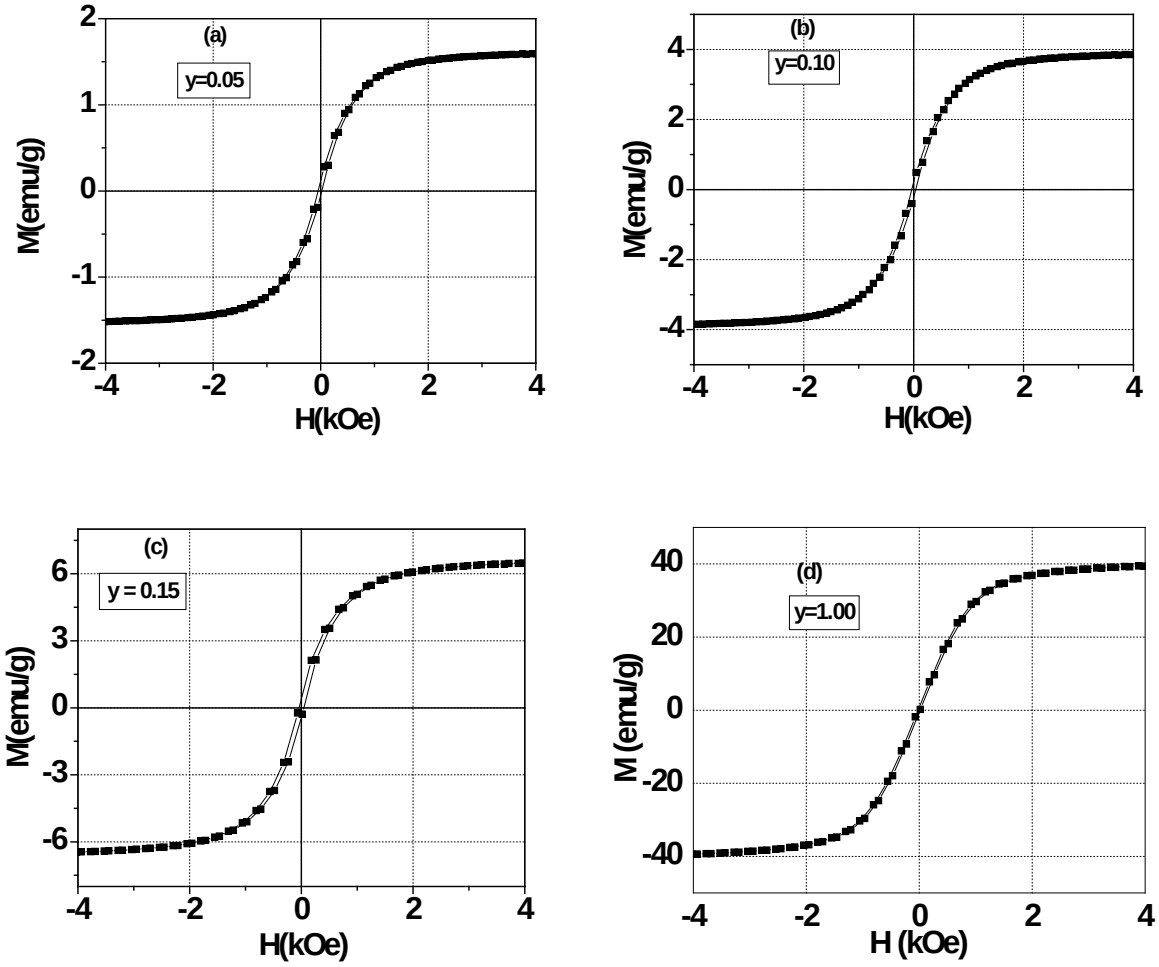

Figure 3.11 M-H loops of (y) NZF- (1-y) BST **(series A)** composites

3.3.6 Magnetoelectric Property

To study the effect of electric poling on ferromagnetic property in composites, two pieces from a single pellet were taken. One piece from each composite sample was electrically poled at 15 kV/cm and room temperature M-H hysteresis loops were taken for both electrically poled and unpoled pieces of composite samples and comparison is shown in *figure 3.12 (a-c)* and values of magnetic parameters for poled and unpoled samples are given in *table 3.6*. From this table it is clear that, remenant magnetization and saturation magnetization for electrically poled samples are higher than those for unpoled samples which is the evidence of ME coupling. The

comparison of poled and unpoled samples has also been reported by S.Y.Tan et.al. for $MgFe_2O_4$-Barium titanate composites to prove multiferroics nature of the materials [25].

Variation of ME coupling coefficient (α) with dc magnetic field was also studied and is shown in *figure 3.12 (d).* The appearance of ME signal in NZF-BST composites is due to the strain induced in magnetostrictive phase (NZF) by applied magnetic field which leads to polarization in the piezoelectric phase (BST). From this figure it is observed that ME coefficient goes on increasing with increase in magnetic field and after attaining a maximum value it decreases with further increase in magnetic field which may be due to fact that after a certain value of magnetic field the magnetostriction coefficient of ferrite phase reaches its saturation value. Hence, the strain produced in the ferrite phase would produce a constant electric field in the piezoelectric phase resulting in decrease in ME coefficient with increase in the applied dc magnetic field. Value of ME coefficient increases with increase in ferrite content (*Table 3.6*). This may be due to increase in magnetostriction phase. However, with further increase in ferrite content the ME coefficient (α) decreases which may be due to low resistivity of ferrite phase as compared to ferroelectric phase resulting in the leakage of the charges developed in the ferroelectric grains due to the presence of conductive ferrite grains [26].

Table 3.6

Ferroelectric and ferromagnetic parameters of (1-y) BST- (y) NZF **(series A)** composites

y	M_r (emu/g)	M_s (emu/g)	H_c (Oe)	M_r (emu/g)	M_s (emu/g)	H_c (Oe)	α (mV/cm-Oe)
	Unpoled			**Poled**			
0.00	--	--	--	--	--	--	--
0.05	0.17	1.60	70.39	0.23	1.69	68.40	0.8
0.10	0.39	3.88	73.56	0.55	4.54	71.52	1.42
0.15	0.83	6.53	79.34	1.13	7.59	82.40	1.2

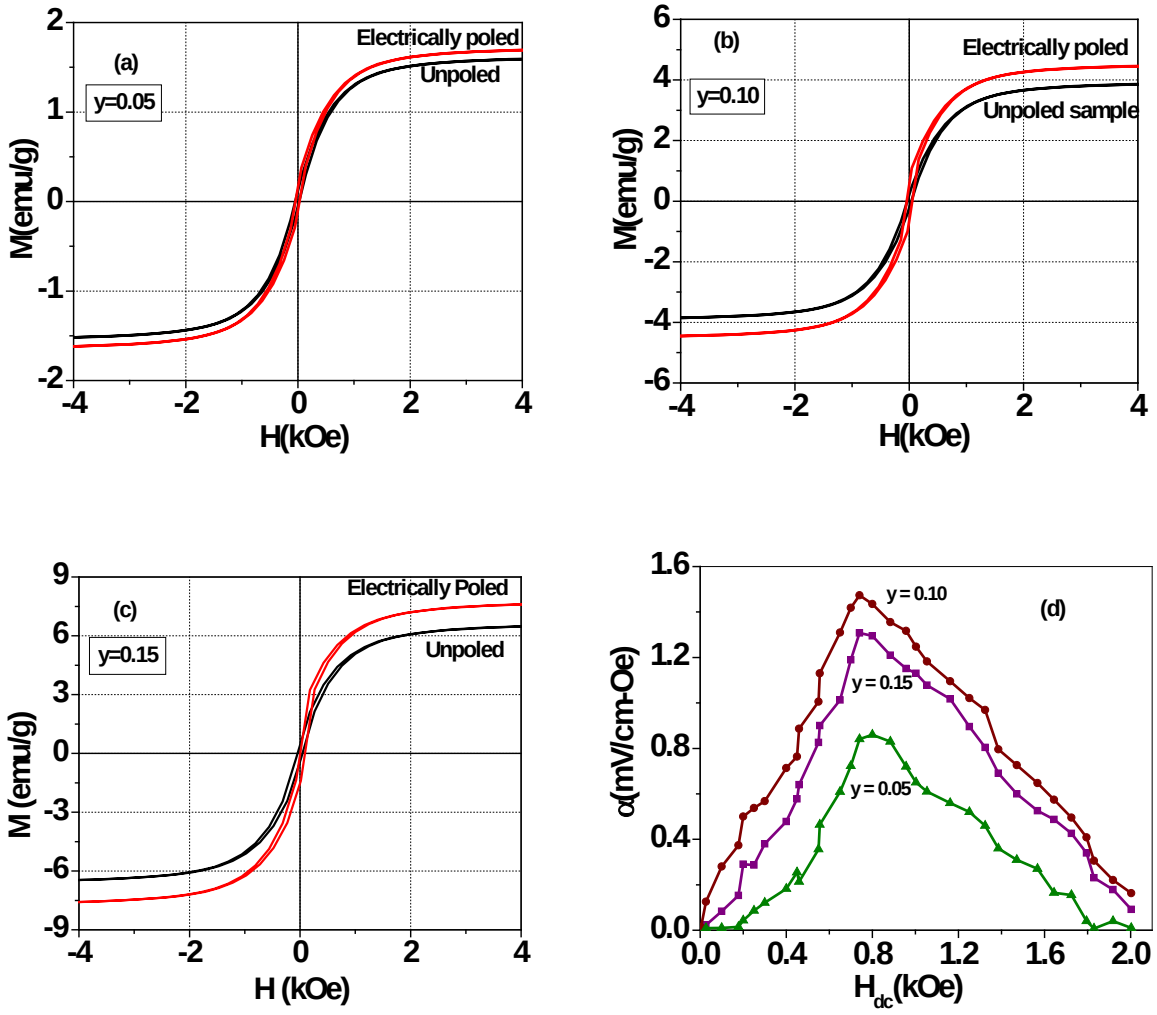

Figure 3.12 Magnetization Vs Magnetic field (M-H) hysteresis loop for electrically poled and unpoled samples of (1-y) BST- (y) NZF **(series A)** composites for (a) 0.05, (b) 0.10, (c) 0.15 and (d) Variation of ME coefficient with magnetic field

Refrences:

1) K. Katayama, M. Abe, T. Akiba and H. Yanagida, J. Euro. Ceram. Soc., **5** (1989) 183.
2) Y. Xu, Ferroelectric Materials and Their Applications, Elsevier Science Pub, New York, USA (1991).
3) Renu Rani, S. Singh, J.K. Juneja, C. Prakash and K.K. Raina, Ferro. Lett., **38** (2011) 134.
4) B.K. Bammannavar and L.R. Naik, J. Mag. Magn. Mater., **321** (2009) 382.
5) S.L. Kadam, K.K. Patankar, C.M. Kanamadi and B.K. Chougule, Mater. Res. Bull., **39** (2004) 2265.
6) S. Upadhyay, D. Kumar and O. Prakash, Bull. Mater. Sci., **19** (1996) 513.
7) R.A. Islam and S. Priya, Int. Ferroelectrics, **82** (2006) 1.
8) C.M. Kanamadi, L.B. Pujari and B.K. Chougule, J. Magn. Magn. Mater., **295** (2005)139.
9) S.M. Pilgrim, A.E. Sutherland and S.R. Winzer, J. Am. Ceram. Soc., **73** (1990) 3122.
10) N. Ponpandian, P. Balay, and A. Narayanasamy, J. Phys. Cond. Matter.,**14** (2002) 3221.
11) M.B. Kothale, K.K. Patankar, S.L. Kadam, V.L. Mathe, A.V. Rao, and B.K. Chougule, Mater. Chem. Phys.,**77** (2002) 691.
12) L.I. Maissel and R. Glang, Handbook of Thin Film Technology, McGraw-Hill, New York, USA (1970).
13) K.K. Patankar and V.L. Mathe, J. Electroceramics, **6** (2001)115.
14) S. Upadhyay, D. Kumar and O. Prakash, Bull. Mater. Sci., **19** (1996) 513.
15) C.M. Kanamadi, L.B. Pujari and B.K. Chougule, J. Magn. Magn. Mater., **295** (2005) 139.
16) J. Paledo, G. Grange, R. Goutte and L. Fyrand, J. Phys. D, **7** (1974) 78.
17) S. Upadhyay, D. Kumar and O. Prakash, Bull. Mater. Sci., **19** (1996) 513.
18) S.A. Lokare, R.S. Devan and B.K. Chougule, J. Alloys Compd., **454** (2008) 471.
19) R.S. Devan, Y.D. Kolekar and B.K. Chougule, J. Alloys Compd., **461** (2008) 678.
20) D.R. Patil and B.K. Chougule, J. Alloys Compd., **470** (2009) 531.
21) S.K. Pandey, O.P. Thakur, Anand Kumar and C. Prakash, J. Appl. Phys., **100** (2006) 014104.
22) K. Carl and K.H. Hardtl, Ferroelectrics, **17** (1978) 473.

23) C.M. Kanamadi, G. Seeta Rama Raju, H.K. Yang, B.C. Choi and J.H. Jeong, J. Alloys Compd., **479** (2009) 807.

24) R.S. Devan, S.B. Deshpande and B.K. Chougule, J. Phys. D: Appl. Phys., **40** (2007) 1864.

25) M.M. Mallapur, M.Phil. Thesis, Shivaji University, Kolhapur, (2003).

26) S.Y. Tan, S.R. Shannigrahi, S.H. Tan and F.E.H. Tay, J. Appl. Phys., **103** (2008) 094105.

Chapter - IV

Synthesis and Characterizations of Zr Substituted NZF– BST Composites

Chapter IV

Synthesis and Characterizations of Zr Substituted NZF – BST Composites

This chapter includes study on the structural, dielectric, ferroelectric, ferromagnetic and magnetoelectric properties of Zr substituted (y) $Ni_{0.8}Zn_{0.2}Fe_2O_4$ - (1-y) $Ba_{0.9}Sr_{0.1}TiO_3$ ((y) NZF-(1-y) BST) composites.

The compositions discussed in the present chapter are:

Series B1 $Ba_{0.9}Sr_{0.1}Zr_xTi_{1-x}O_3$ where x = 0.00, 0.04, 0.08, 0.12, 0.16

Series B2 (y) $Ni_{0.8}Zn_{0.2}Fe_2O_4$ + (1-y) $Ba_{0.9}Sr_{0.1}Zr_{0.04}Ti_{0.96}O_3$ where y = 0.00, 0.05, 0.10,0.15

Series B3 $0.95Ba_{0.9}Sr_{0.1}Zr_xTi_{1-x}O_3 + 0.05\ Ni_{0.8}Zn_{0.2}Fe_2O_4$ where x = 0.00, 0.04, 0.08, 0.12, 0.16

In *series B1*, we have studied the effect of Zr content on $Ba_{0.9}Sr_{0.1}Zr_xTi_{1-x}O_3$ with x = 0.00 to 0.16 in steps of 0.04 for optimizing the best Zr substituted ferroelectric phase for composite system. In *series B1* for x = 0.04, we have observed best dielectric and ferroelectric properties hence for preparing composite samples we have selected the ferroelectric phase as $Ba_{0.9}Sr_{0.1}Zr_{0.04}Ti_{0.96}O_3$. In *series B3* the ratio of both phases (ferroelectric and ferrite) was fixed and content of Zr were changed in ferroelectric phase.

All samples were prepared by conventional solid state reaction method. Samples were sintered at 1325^oC for 4 hrs. at uniform heating of 5^oC/min. After sintering experimental density of the samples was determined using Archimedes' principle. Theoretical density of the samples was

calculated using the lattice parameters. XRD was done by using Bruker, D-8 Advance model at room temperature in a range of Bragg angles ($20^o \leq 2\theta \leq 65^o$) with step size of 0.02^o. The micro structures of freshly broken sintered samples were studied by scanning electron microscope (JEOL JSM 6510LV, Japan). For measuring electrical properties, the sintered pellets were lapped and then electroded by using silver epoxy and fired at 400 ^{o}C for 30 min to ensure good ohmic contact. The dielectric properties of the samples as a function of temperature at discrete frequencies were measured by using Agilent 4263B LCR meter and room temperature measurement of ε and loss tangent ($tan\ \delta$) as a function of frequency (20Hz to 1MHz) were measured by using Agilent 4284A LCR meter. The ferroelectric nature of the composite samples was analyzed using an automatic PE loop tracer system. Electrical poling was done at 150^o C in silicon oil bath by applying dc field ~15kV/cm for 1 hr. Then the sample was allowed to cool by switching off the heater in applied electric field and the field was removed at room temperature. Lake shore 735 VSM was used for recording M-H hysteresis loops. The magnetoelectric signal (voltage) was determined as a function of increasing DC magnetic field (0–1500 Oe) using 7265 DSP lock-in amplifier in the presence of small AC magnetic field (H_{ac} = 10 Oe). Electric voltage (V) was noted from lock in amplifier and magnetoelectric coupling coefficient (mV/cm-Oe) was calculated by using the formula:

$$\alpha = \frac{dV}{t} \times \frac{1}{H_{ac}} \qquad \text{.....4.1}$$

Where t is thickness of the sample and H_{ac} is the ac magnetic field

4.1 Structural Properties

4.1 (a) XRD

Phase analysis of all samples was done by using XRD analysis. XRD pattern of all compositions i.e. for series B1, B2 and B3 are shown in *figure 4.1*, *4.2* and *4.3* respectively. The calculated values of lattice parameters of all samples for *series B1*, *B2* and *B3* are given in *table 4.1*. From XRD patterns of series B1 *(figure 4.1)* we found that all peaks could be indexed and correspond to a perovskite phase, which indicate that samples formed in single phase. Splitting

of peak (002 and 200) at an angle near about 45^{o} confirms the material with tetragonal structure but these two peaks with peak indices (002) and (200) are merging into each other with increase in Zr content. This indicates that the structure of the material is changing and tetragonality of the material is decreasing with increase in amount of Zr content. It is also observed that the diffraction peaks shift towards lower angle with increase of Zr content resulting in the increase in the lattice parameters as expected since Zr^{4+} (0.72 Å) is larger than that of the Ti^{4+} (0.605 Å) [1].

Figures 4.2 and *4.3* show the XRD patterns of composite samples (*Series B2* and *B3*) and their individual phases. XRD patterns of composite samples exhibit the characteristic peaks of both phases i.e. (110) for ferroelectric phase and (311) for ferrite phase confirming the presence of both phases. For all samples all the peaks could be indexed and no extra peaks were observed hence it is clear that no chemical reaction took place between two phases and they maintained proper stoichiometry. From *figure 4.2* it is observed that the intensity and number of ferrite peaks increase with increase in ferrite content (y) hence the present composite system follow the rule of mixture and from *figure 4.3* it is observed that the intensity of ferrite phase peak is very low which is due to very small percentage of ferrite phase. From the calculated values of lattice parameters of *series B2*, it is observed that there is slight change in lattice parameters of both phases in composite samples as compared to pure phases individually. This may be due to stress exerted on each other by the two phases [2]. Many researchers have reported similar changes in lattice parameters of composite [3-5].

For all the samples experimental density, theoretical density and relative density were calculated using the formulae as discussed in *section 2.3.1* and all these calculated values are given in *table 4.2* for all series samples. Relative density was found to decrease with addition of Zr and with addition of ferrite phase.

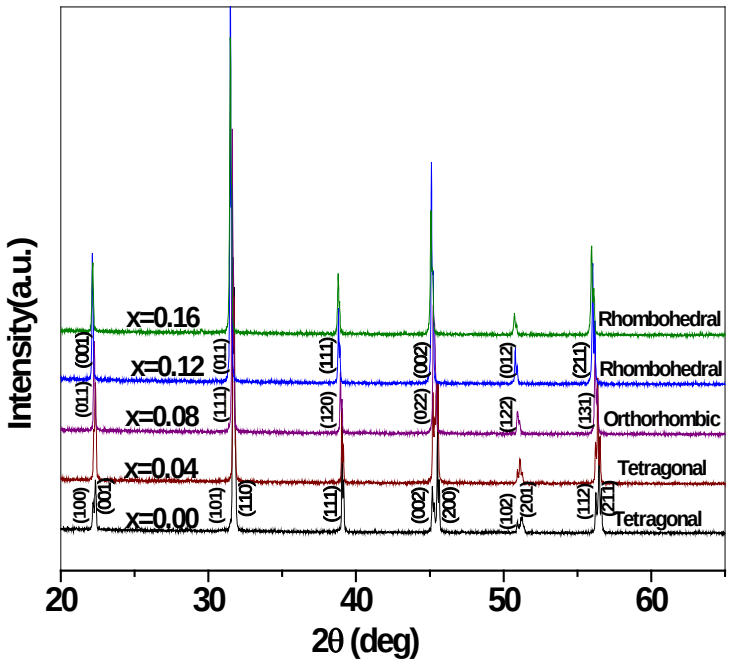

Figure 4.1 XRD pattern for **Series B1 (BSZT)**.

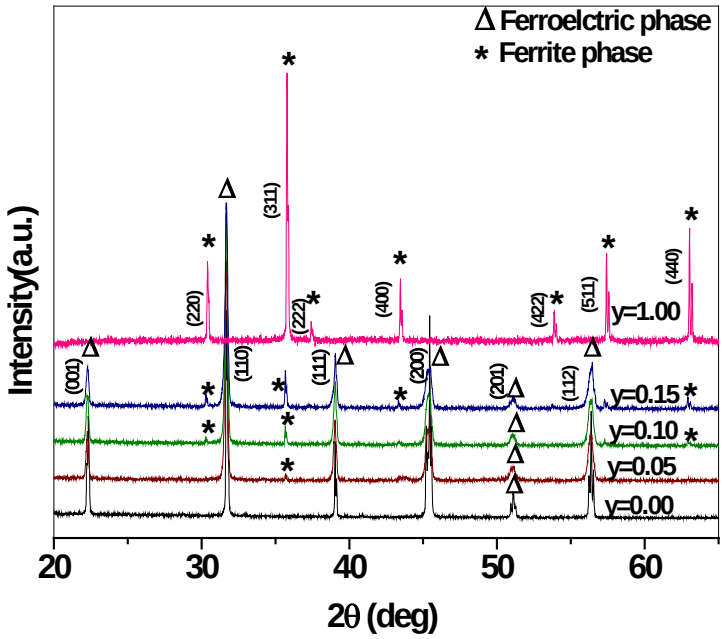

Figure 4.2 XRD pattern for **Series B2 ((y)NZF – (1-y)BSZT)**

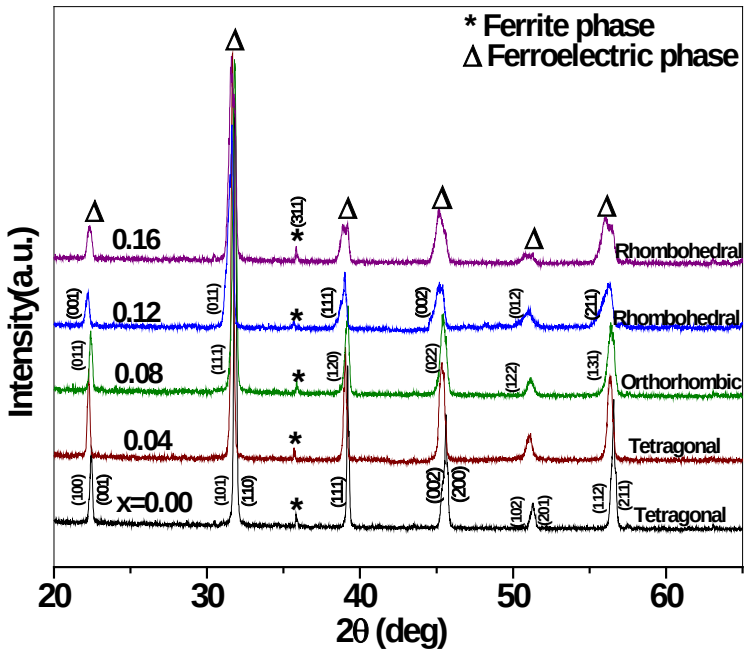

Figure 4.3 XRD pattern for **Series B3 (0.05NZF – 0.95BSZT)**

4.1 (b) Scanning Electron Microscope (SEM)

The SEM micrographs of series B1, B2 and B3 are shown in *figures 4.4, 4.5* and *4.6* respectively. All samples show well developed grain morphology. From *figure 4.4* it is observed that grain size decreases with increase in Zr content except for x= 0.04. Average grain size was calculated by using linear intercept method. The decrease in grain size with increase in Zr content can be associated with the lower grain growth rate caused by the slow diffusion of the larger Zr^{4+} ion in place of Ti^{4+} ion [6]. The decrease in grain size can also be related to reduction in tetragonality. A similar trend for grain size is also observed for Zr substituted composite samples i.e. for *series B3* as shown in *figure 4.6*. *Figure 4.5* shows the SEM micrographs of *series B2*. It is observed that grain size of samples decreases with addition of ferrite phase but we can't distinguish the grains of two phases individually due to the smaller amount of ferrite phase. Similar results have already been reported by many researchers [7-8]. The decrease in grain size

results in the decrease in mean free path of the electrons and hence causes change in resistivity of the samples.

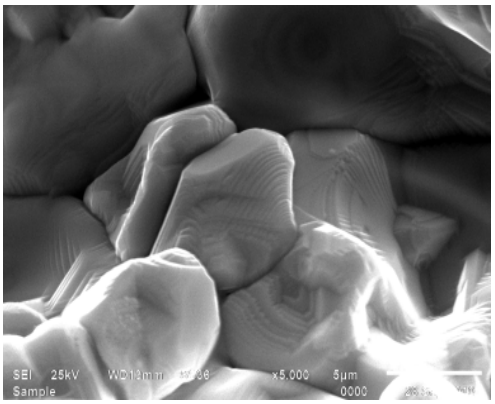

(a)

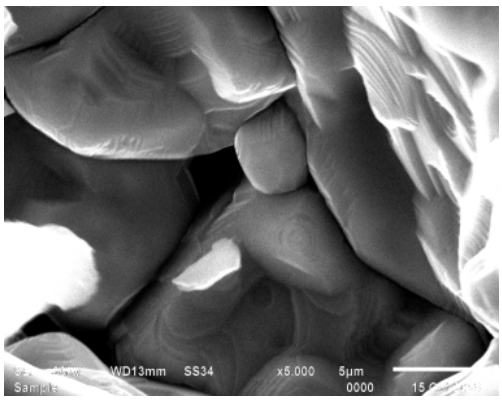

(b)

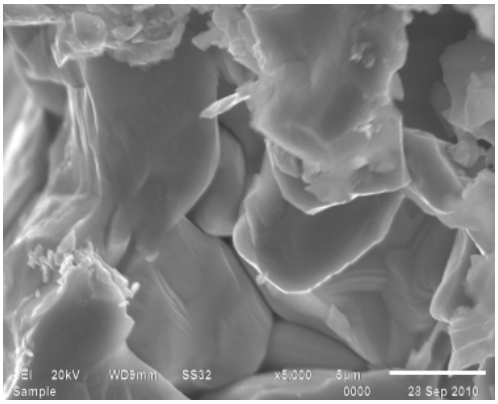

(c)

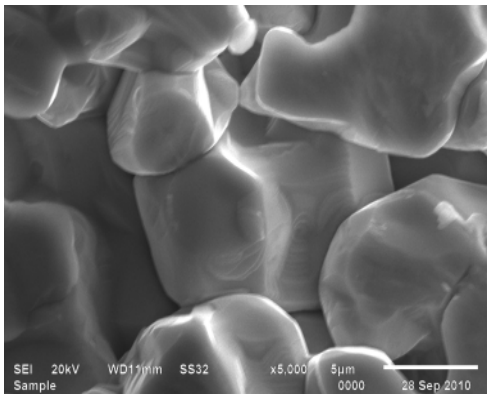

(d)

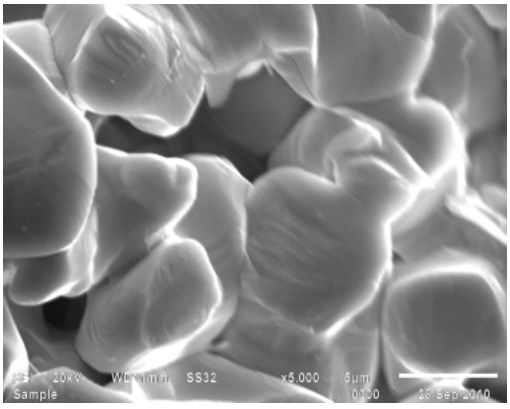

(e)

Figure 4.4 SEM micrographs of **Series B1** (BSZT) for (a) x = 0.00, (b) x=0.04, (c) x=0.08, (d) x=0.12 and (e) x=0.16

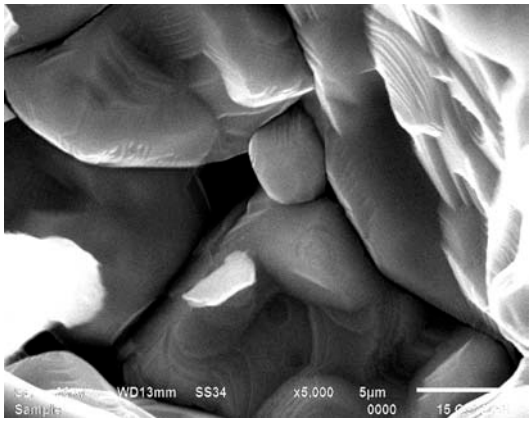

(a)

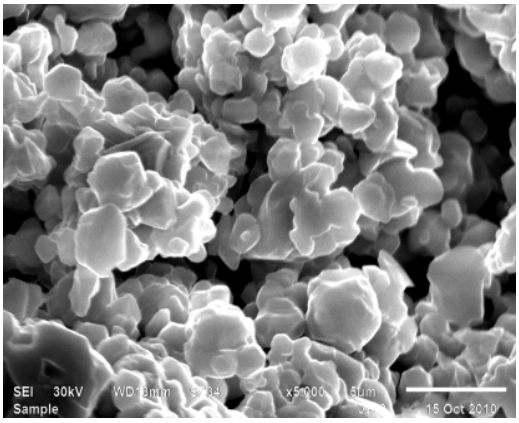

(b)

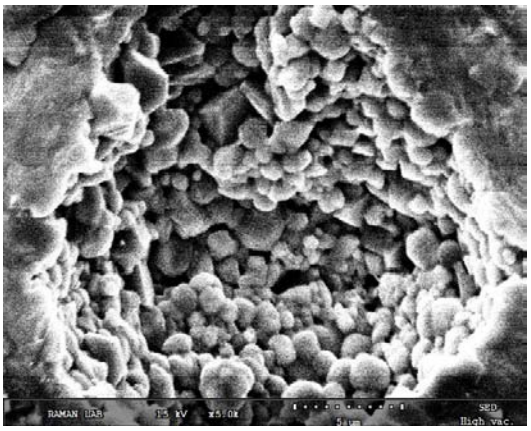

(c)

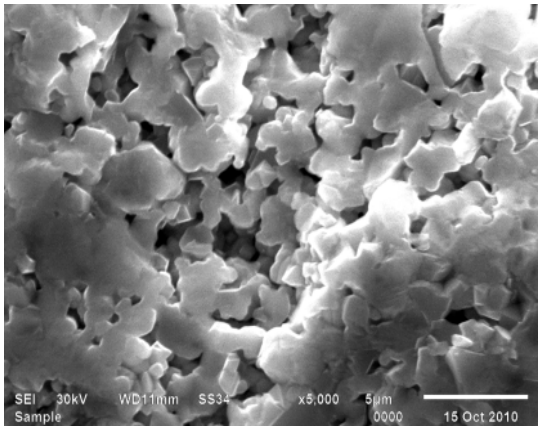

(d)

Figure 4.5 SEM micrographs of **Series B2** ((y) NZF – (1-y) BSZT) for (a) y = 0.00, (b) 0.05, (c) 0.10 and (d) 0.15

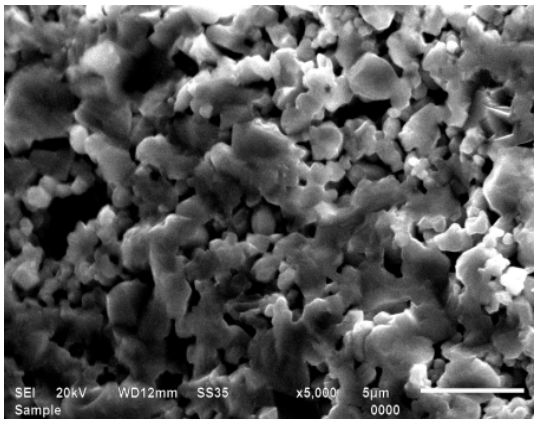

(a)

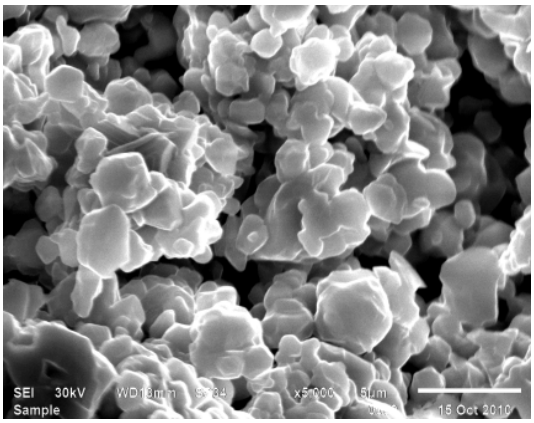

(b)

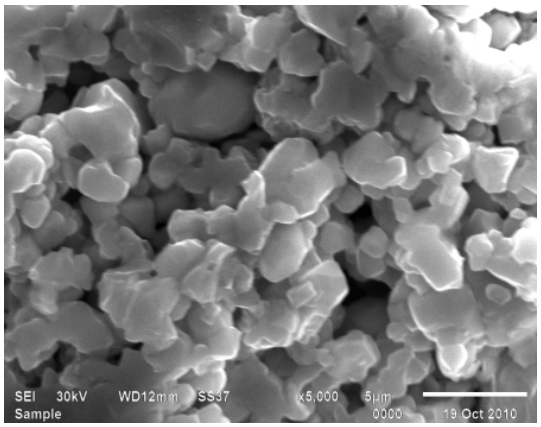

(c)

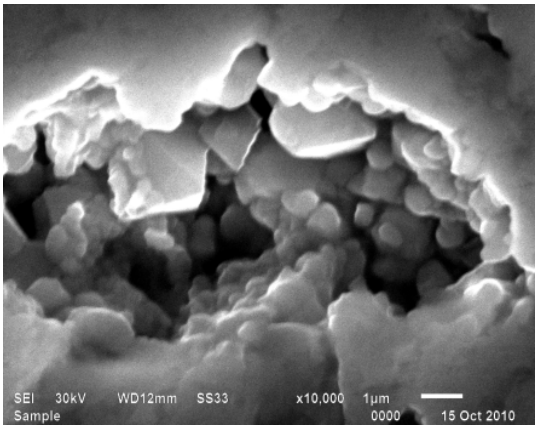

(d)

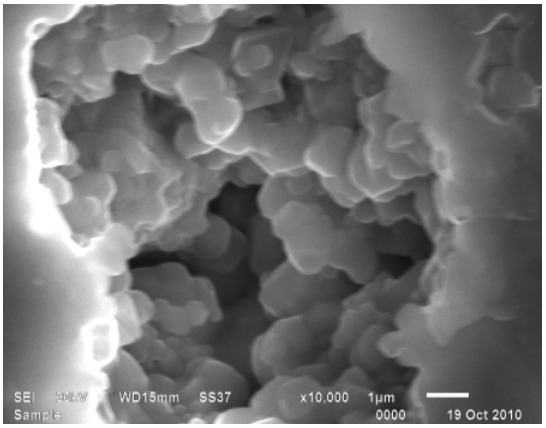

(e)

Figure 4.6 SEM micrographs of **Series B3** (0.05NZF – 0.95BSZT) for (a) x = 0.00, (b) 0.04, (c) 0.08, (d) 0.12 and (e) 0.16

Table 4.1

Lattice parameters for all series samples

Series B1 (BSZT)					Series B2 ((y)NZF- (1-y)BSZT)					Series B3 (0.05 NZF + 0.95 BSZT)				
x	Lattice parameters			Avg grain size (μm)	y	Ferroelectric			Ferrite a (Å)	x	Ferroelectric			Ferrite a (Å)
	a(Å)	c(Å)	c/a			a(Å)	c(Å)	c/a			a(Å)	c(Å)	c/a	
0.00	3.985	4.002	1004	5.68	0.00	3.987	4.003	1.004	-	0.00	3.985	4.003	1.004	8.324
0.04	3.987	4.003	1.004	5.86	0.05	3.987	4.003	1.004	8.335	0.04	3.987	4.003	1.004	8.335
0.08	3.990	4.003	1.003	5.55	0.10	3.987	4.005	1.004	8.340	0.08	3.990	4.004	1.003	8.341
0.12	4.015	4.015	1.00	5.22	0.15	3.988	4.006	1.004	8.346	0.12	4.017	4.017	1.000	8.343
0.16	4.021	4.021	1.00	4.98	--	-	-	-	--	0.16	4.022	4.022	1.000	8.344

Table 4.2

Density for all series samples

Series B1 (BSZT)				Series B2 (NZF- BSZT)				Series B3 (0.05 NZF + 0.95 BSZT)			
x	d_{exp} (g/cc)	d_{th} (g/cc)	Relative density (%)	y	d_{exp} (g/cc)	d_{th} (g/cc)	Relative density (%)	x	d_{exp} (g/cc)	d_{th} (g/cc)	Relative density (%)
0.00	5.74	5.95	96.32	0.00	5.28	5.99	88.15	0.00	5.21	5.93	87.84
0.04	5.28	5.99	88.15	0.05	5.13	5.96	86.07	0.04	5.13	5.96	86.07
0.08	5.15	6.03	85.36	0.10	4.97	5.93	83.81	0.08	5.05	5.99	84.30
0.12	4.85	5.98	81.10	0.15	5.18	5.99	86.47	0.12	4.99	5.94	84.08
0.16	4.79	6.00	79.84	-	-	-	-	0.16	5.00	5.96	83.83

4.2 Dielectric Properties

In this section variation of dielectric properties with frequency and with temperature for *series B1, B2* and *B3* are discussed.

4.2.1. Variation of ε and tanδ with Frequency

In practice, dielectric constant depends on the applied frequency due to charge transport relaxation time. The variation of dielectric constant and dielectric loss with frequency at room temperature was studied for all the series. Variation of dielectric constant and loss as a function of frequency (10^2Hz to 10^6Hz) for *series B1*, *B2* and *B3* is depicted in *figures 4.7 (a-b), 4.8 (a-b)* and *4.9(a-b)* respectively. It is found that dielectric constant decreases with the increase in frequency, the high value of dielectric constant at lower frequencies can be attributed to simultaneous presence of all types of polarizations (i.e. interfacial, ionic, dipolar, electronic, space charge etc.) in the material [9-10].

With the increase in frequency the contribution of these polarizations decreases because of their large relaxation time and hence they cease to respond at higher frequencies resulting in decrease in dielectric constant. At higher frequencies the main contribution to dielectric constant comes from the electronic polarization as other type of polarizations become less ineffective. While in case of composite samples (i.e. series B2 and B3) the dielectric dispersion observed at lower frequencies is attributed to the interfacial polarization because in case of composite samples two phases are mixed into each other that have different permittivity and conductivity [11]. In case of composites the higher values of dielectric constant can also be due to the fact that the ferroelectric regions are surrounded by non-ferroelectric regions similar to the relaxor ferroelectric materials. This gives rise to interfacial polarization which can also be related to heterogeneity of the samples like pores, impurities and grain structure in composite samples [12]. The dielectric constant remains constant at higher frequencies for all composite samples because beyond frequency of external electric field the electron exchange between Fe^{2+}/Fe^{3+} for ferrite phase cannot follow the alternating field [13-14].

From *figure 4.7* it is observed that dielectric constant increases with increase in Zr content up to x = 0.04 and after that it slightly decreases and further increases for x = 0.16. The dielectric constant follows the same trend as average grain size *(Table 4.1)* except for x = 0.16. The high value of dielectric constant for x = 0.16 is due to fact that the curie temperature of this sample is near about room temperature as will be discussed in *section 4.2.2*. A small decrease in dielectric constant is observed with frequency for all the samples, whereas pronounced dispersion is observed at higher frequencies for tanδ. From *figure 4.8* it was observed that dielectric constant decreases with increase in ferrite content (y). The decrease in dielectric constant with increase in ferrite content is similar to the behavior reported by many other researchers [15-16].

From *figure 4.9* it is also observed that value of dielectric constant varies in a random fashion for all samples. This may be due to the reason that ferrite and ferroelectric grains are randomly mixed together in parallel and series modes and it may also be due to the fact that present composites are of particulate type and hence more than one type of connectivity may exist in different parts of the same composite. Hence it is difficult to calculate the effective value of dielectric constant of composite samples [17]. It can also be observed that with the addition of Zr content in ferroelectric phase, the dielectric loss decreases and room temperature dielectric constant increases for composite samples. The variation of loss tangent with frequency for all the samples shows a similar dispersion as that of dielectric constant. But it is observed that dielectric loss increases with frequency in the higher frequency range. This dispersion in tanδ in the higher frequency range is due to some extrinsic loss phenomenon [18-19].

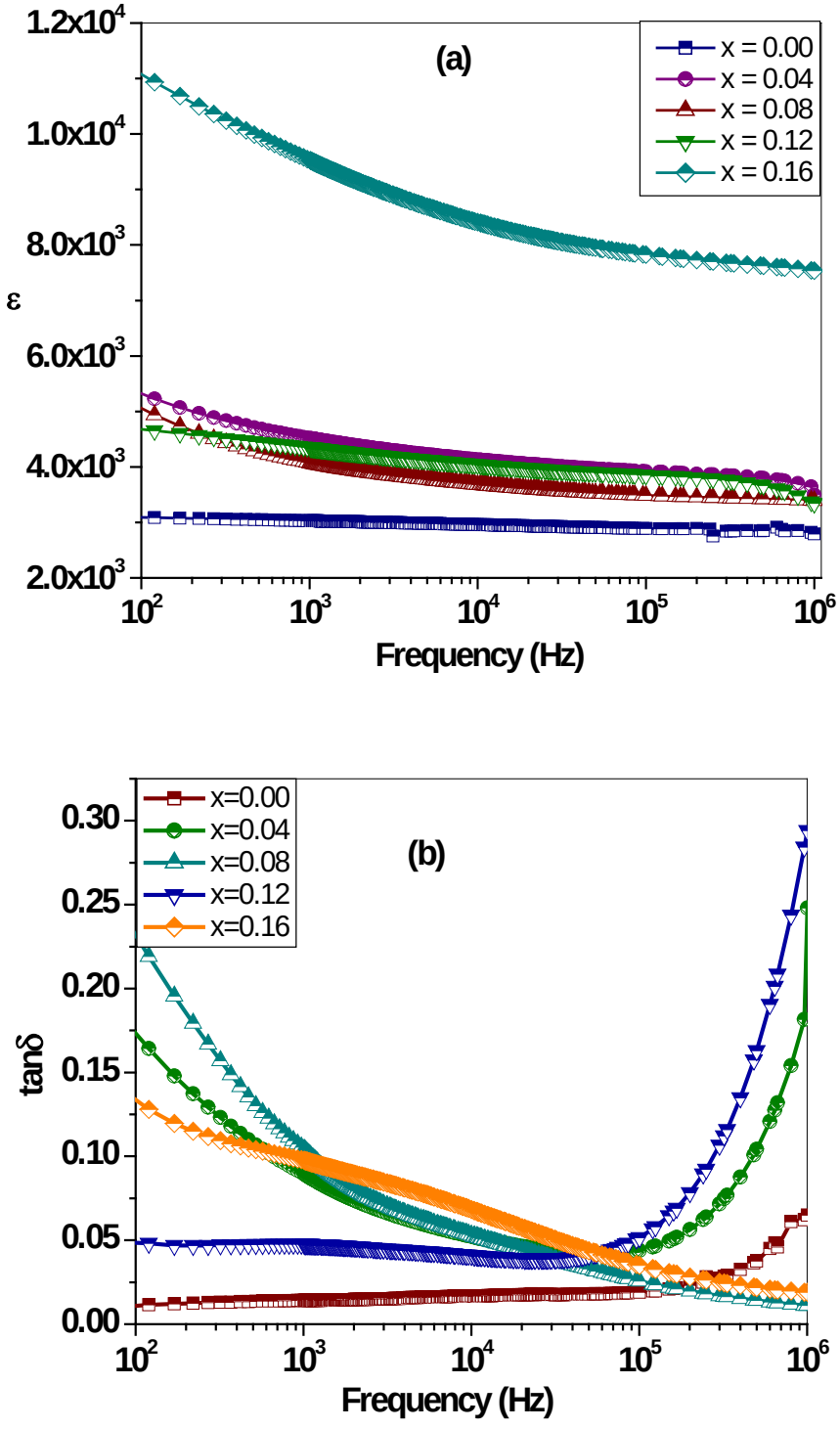

Figure 4.7 Room temperature variation of (a) dielectric constant (ε_{RT}) (b) loss tangent ($\tan\delta_{RT}$) of **Series B1** (BSZT) as a function of frequency.

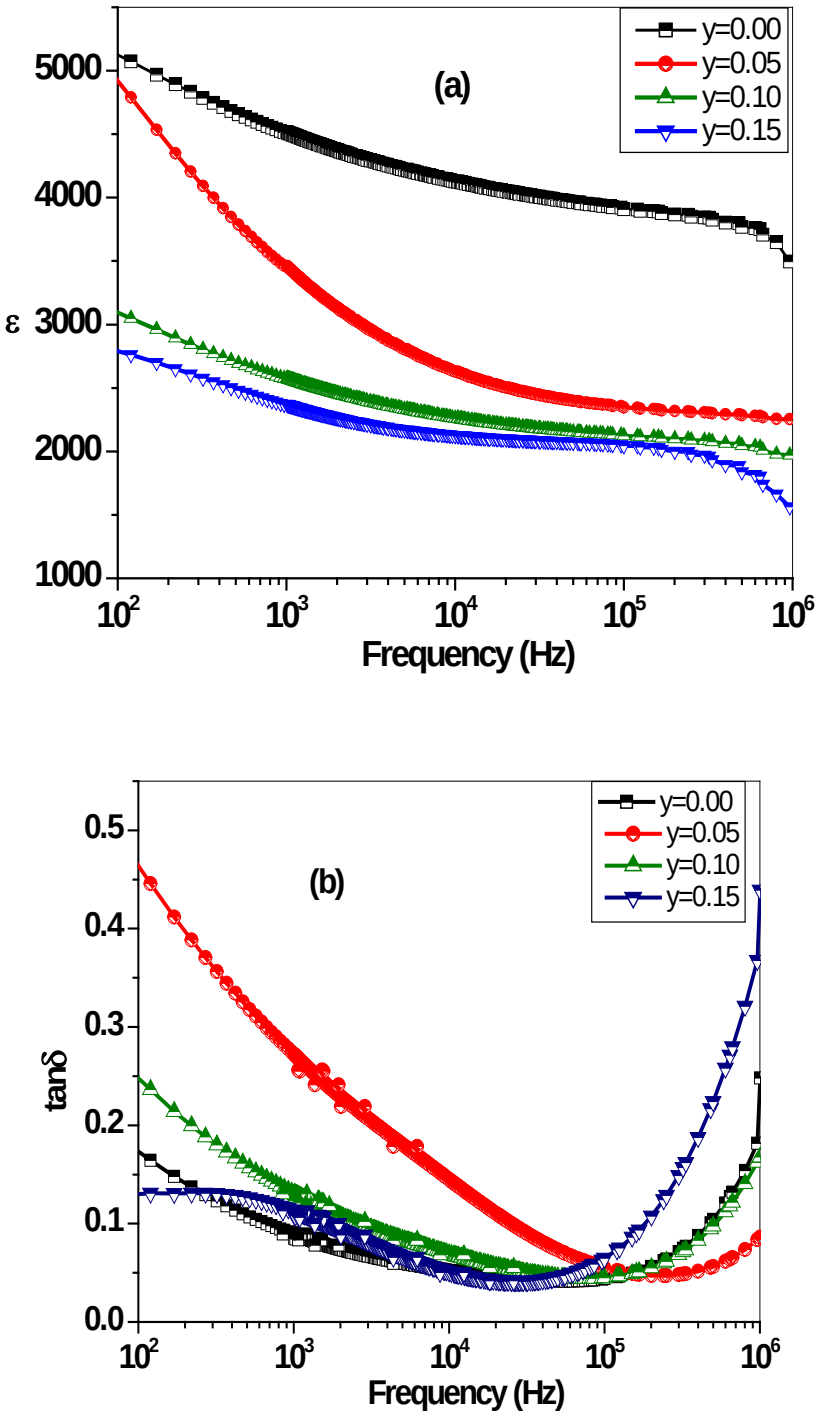

Figure 4.8 Room temperature variation of (a) dielectric constant (ε_{RT}) (b) loss tangent ($\tan\delta_{RT}$) of **Series B2** ((y) NZF- (1-y)BSZT) as a function of frequency.

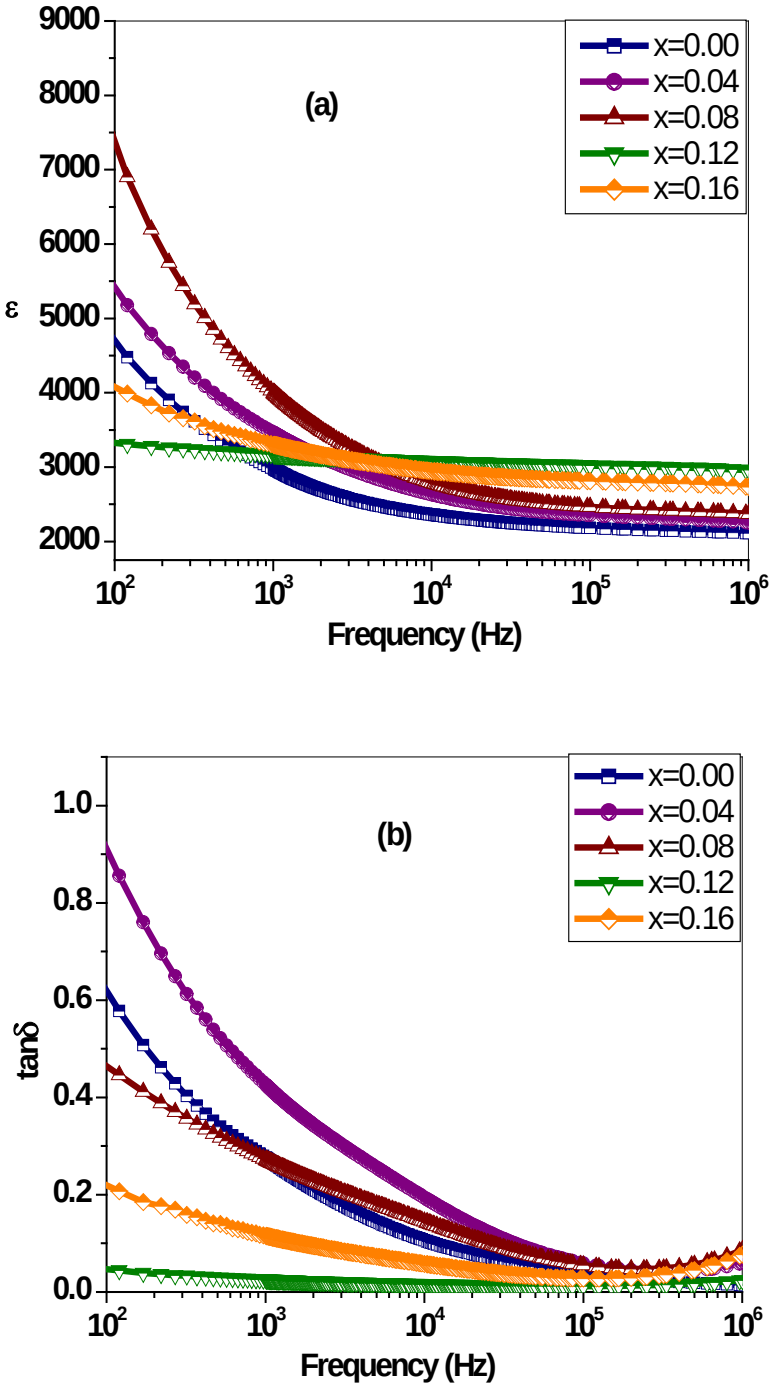

Figure 4.9 Room temperature variation of (a) dielectric constant (ε_{RT}) (b) loss tangent ($\tan\delta_{RT}$) of **Series B3** (0.05 NZF + 0.95 BSZT) as a function of frequency.

4.2.2 Temperature Dependence of ε and tanδ at Different Frequencies

In the present study, dielectric properties of all series were measured as a function of temperature at different frequencies. The variation of dielectric constant with temperature at different frequencies for *series B1, B2* and *B3* are shown in *figure 4.10, 4.11* and *4.12* respectively and all dielectric parameters like room temperature dielectric constant (ε_{RT}), dielectric loss, dielectric constant at T_c (ε_{max}), dielectric loss at T_c, and Curie temperature for *series B1, B2* and *B3* are given in *table 4.3*.

For all samples it is observed that dielectric constant increases with increase in temperature and shows a peak at particular temperature called Curie temperature (T_c) which is a characteristic of ferroelectric behavior. From *table 4.3* for series B1, T_c is observed to decrease with increase in Zr content (x). The decrease in T_c is because of larger ionic radius of Zr than that of Ti^{4+} ion. Substitution of Zr^{4+} for Ti^{4+} results in weakening of bonding force between the B-site ion and oxygen ion of the ABO_3 perovskite structure. As the B-O bond get weakened, the B-site ion can resume its position only when the tetragonal ferroelectric is at lower temperature, so the phase transition temperature (T_c) is reduced [20-23]. While for series B2 the curie temperature of samples increases with addition of ferrite phase (y).

In *series B1* for x = 0.08, a small hump can be noticed before the main peak (*figure 4.10 (c)*), which shows the ferroelectric to ferroelectric phase transition. But for x = 0.00 and x = 0.04 the ferroelectric to ferroelectric phase transition temperature is lower than the room temperature so the hump cannot be observed in the measurement range of temperature (*figure 4.10 (a-b)*). For the large amount of Zr content the two phase transitions are pinched in to one dielectric peak. This behavior of phase transitions is responsible for random variation in room temperature dielectric constant (*table 4.4*). The same trend of Curie temperature, room temperature dielectric constant and dielectric loss were observed for samples of *Series B3* but due to presence of ferrite phase the peaks of all samples get suppressed and become broadened as compare to pure ferroelectric phase and with increase in Zr content in ferroelectric phase this peak gets further broadened.

In case of Zr substituted samples the broadening of peak may be due to inhomogeneous distribution of Zr ions in the Ti- sites and mechanical stress in the grains [24]. While in case of composite samples broadening of peaks may be due to inhomogeneous structure because of the presence of two phases. From *figures 4.11* it can be observed that as the ferrite content increases the dielectric peaks get broadened and dielectric maxima decreases *(table 4.4)*.The dispersion in ε with frequency is also observed for composites for higher values of ferrite content (y). This may be due to the increase in interfacial polarization with increase in ferrite content. Composites with higher ferrite phase have high porosity, due to which increase in interfacial polarization dominates for large amount of ferrite.

The dielectric loss increases with increase in temperature for all samples which may be due to the increase in thermal conduction loss with temperature. From *table 4.3* it is also observed that dielectric loss decreases with increase in Zr content (x) (*for series B1* and *B3*). This decrease in dielectric loss can be understood as follows: The electron transport by hopping between Ti^{4+} and Ti^{3+} is one of the major factors of conduction loss. The valency of Zr^{4+} is chemically more stable than that of Ti^{4+} thus conduction by e^- hopping between Ti^{4+} and Ti^{3+} get depressed due to the substitution of Ti with Zr because Zr^{4+} blocks the path between two adjacent Ti ions and enlarge hopping distance [25]. Thus samples with less value of dielectric loss are considered to be good samples for dielectric applications.

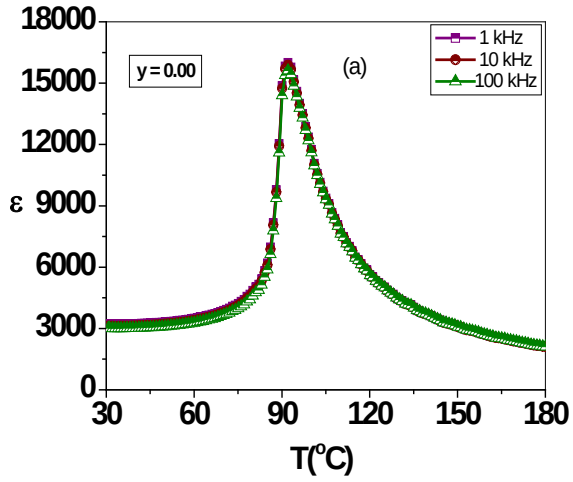
y = 0.00
(a)
1 kHz
10 kHz
100 kHz
ε
T(°C)

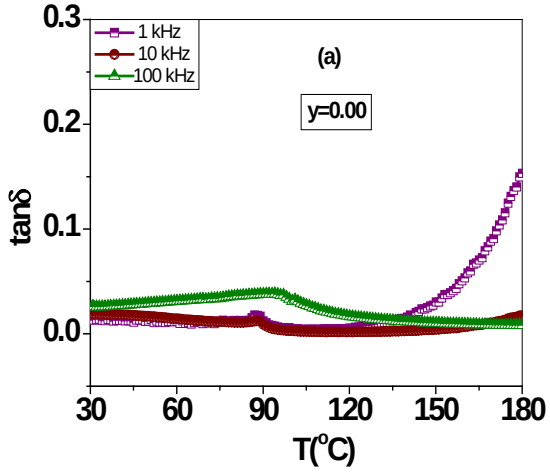
(a)
y=0.00
1 kHz
10 kHz
100 kHz
tanδ
T(°C)

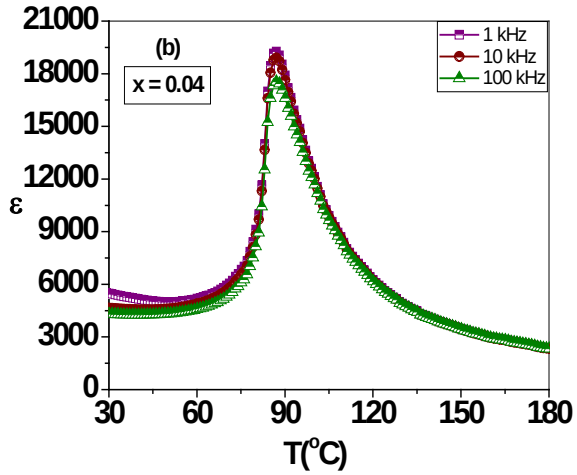
(b)
x = 0.04
1 kHz
10 kHz
100 kHz
ε
T(°C)

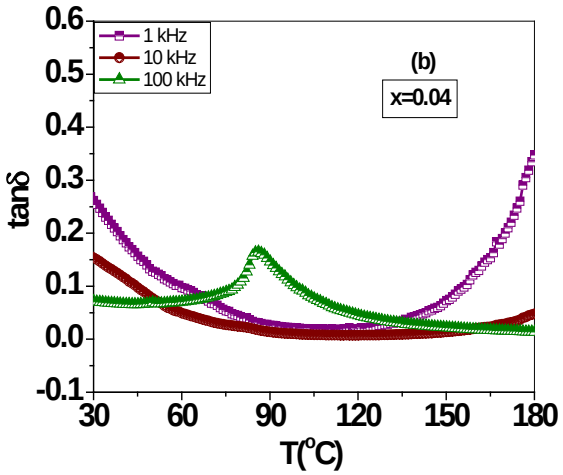
(b)
x=0.04
1 kHz
10 kHz
100 kHz
tanδ
T(°C)

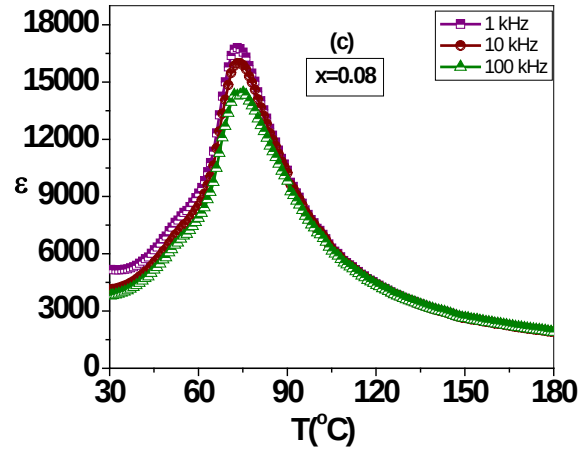
(c)
x=0.08
1 kHz
10 kHz
100 kHz
ε
T(°C)

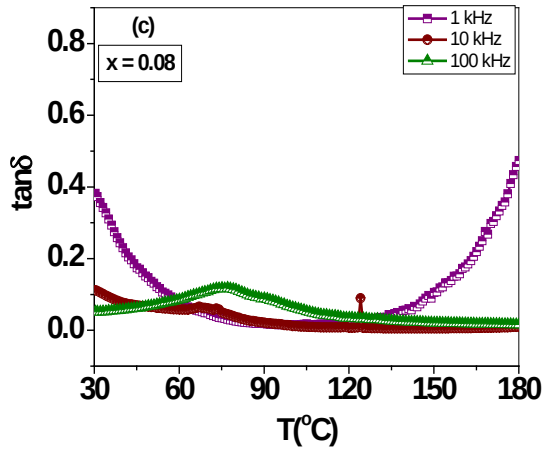
(c)
x = 0.08
1 kHz
10 kHz
100 kHz
tanδ
T(°C)

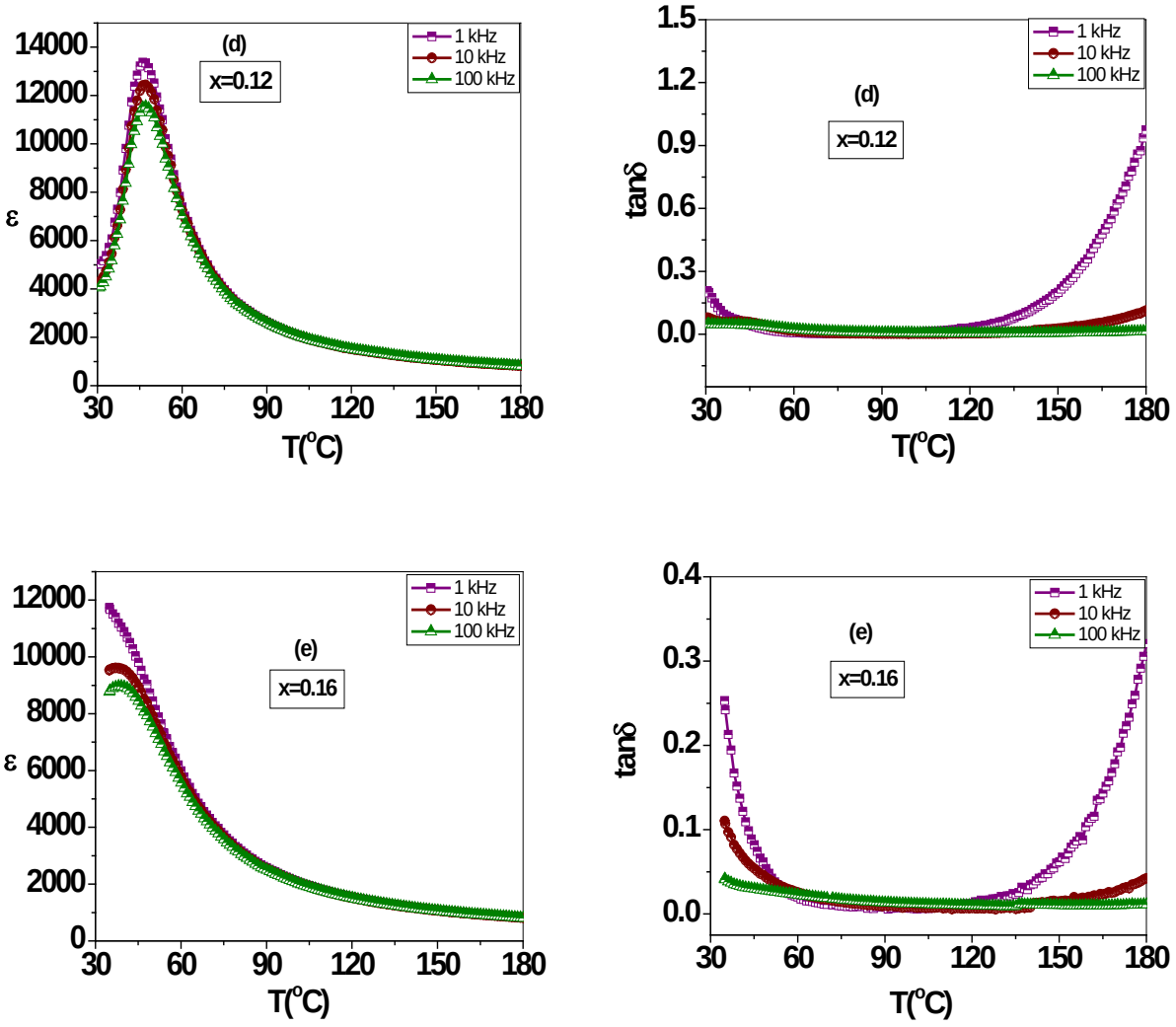

Figure 4.10 Temperature variation of ε and tanδ at different frequencies of **series B1** (BSZT)

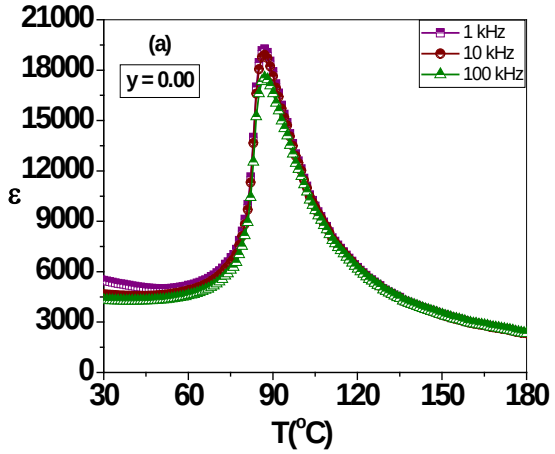
(a)
y = 0.00
1 kHz
10 kHz
100 kHz
ε
T(°C)

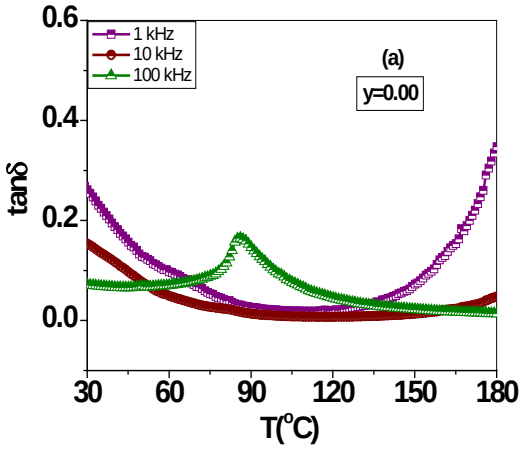
(a)
y=0.00
1 kHz
10 kHz
100 kHz
tanδ
T(°C)

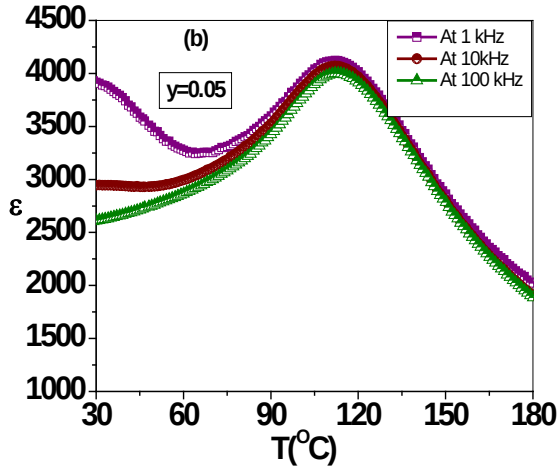
(b)
y=0.05
At 1 kHz
At 10kHz
At 100 kHz
ε
T(°C)

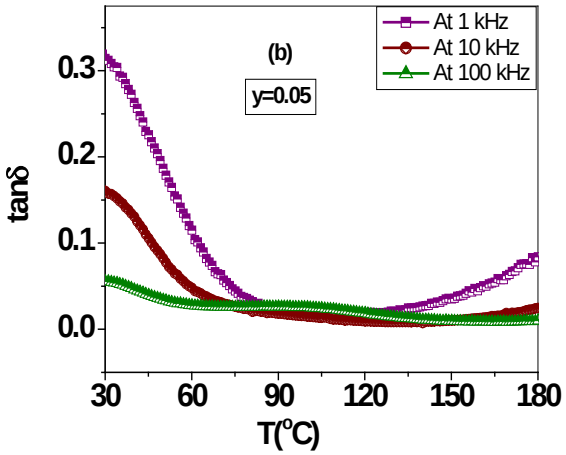
(b)
y=0.05
At 1 kHz
At 10 kHz
At 100 kHz
tanδ
T(°C)

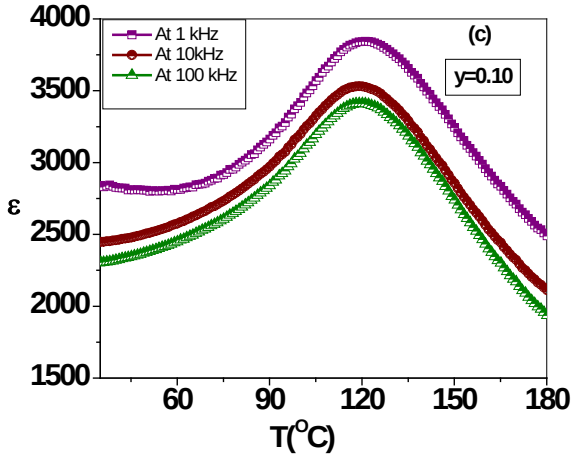
(c)
y=0.10
At 1 kHz
At 10kHz
At 100 kHz
ε
T(°C)

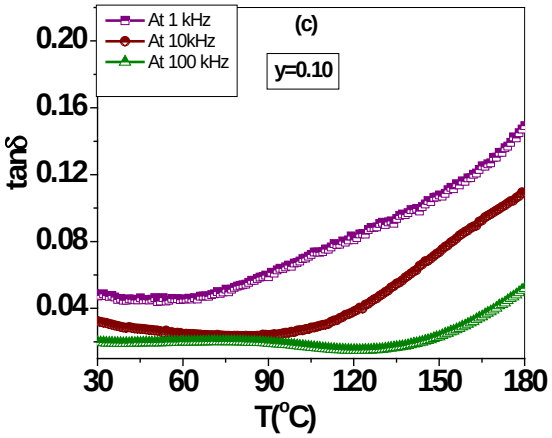
(c)
y=0.10
At 1 kHz
At 10kHz
At 100 kHz
tanδ
T(°C)

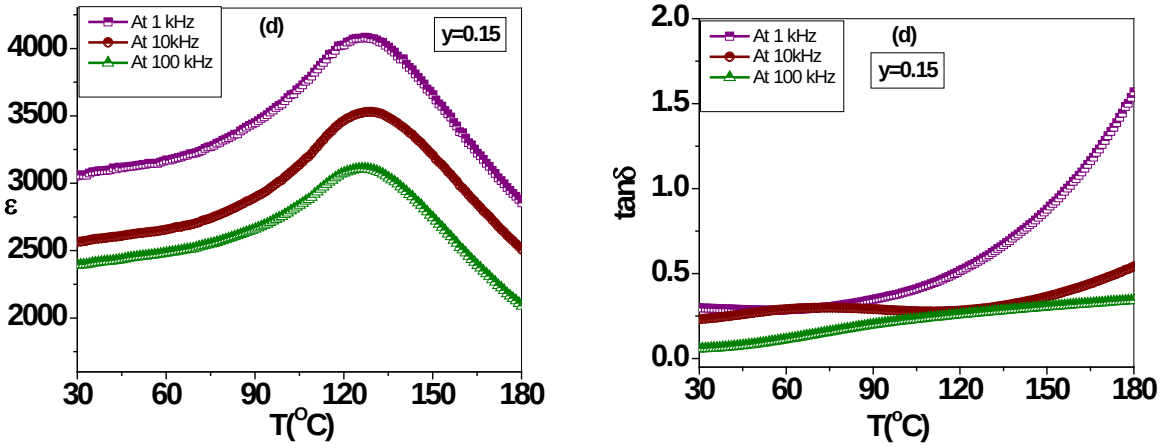

Figure 4.11 Temperature variation of ε and tanδ at different frequencies of **series B2** ((y)NZF- (1-y)BSZT)

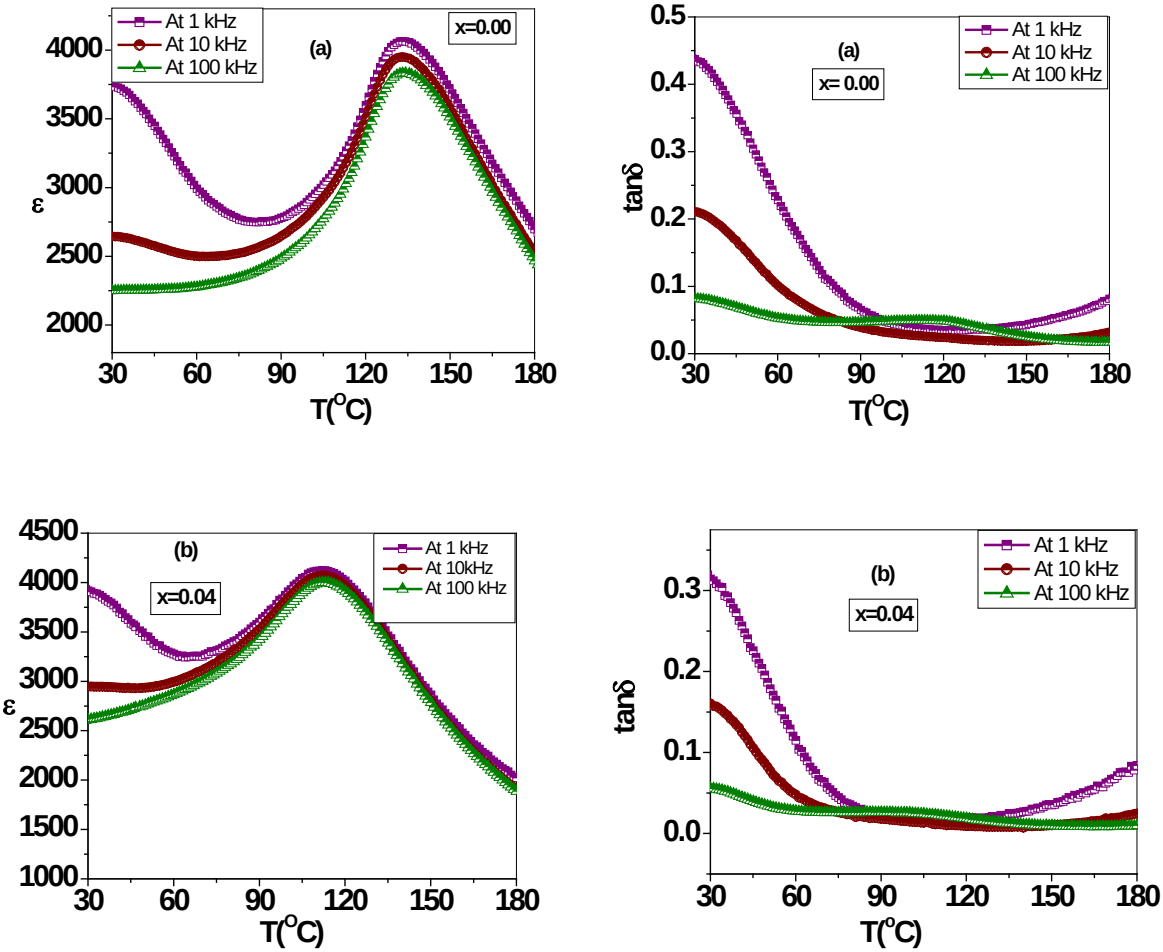

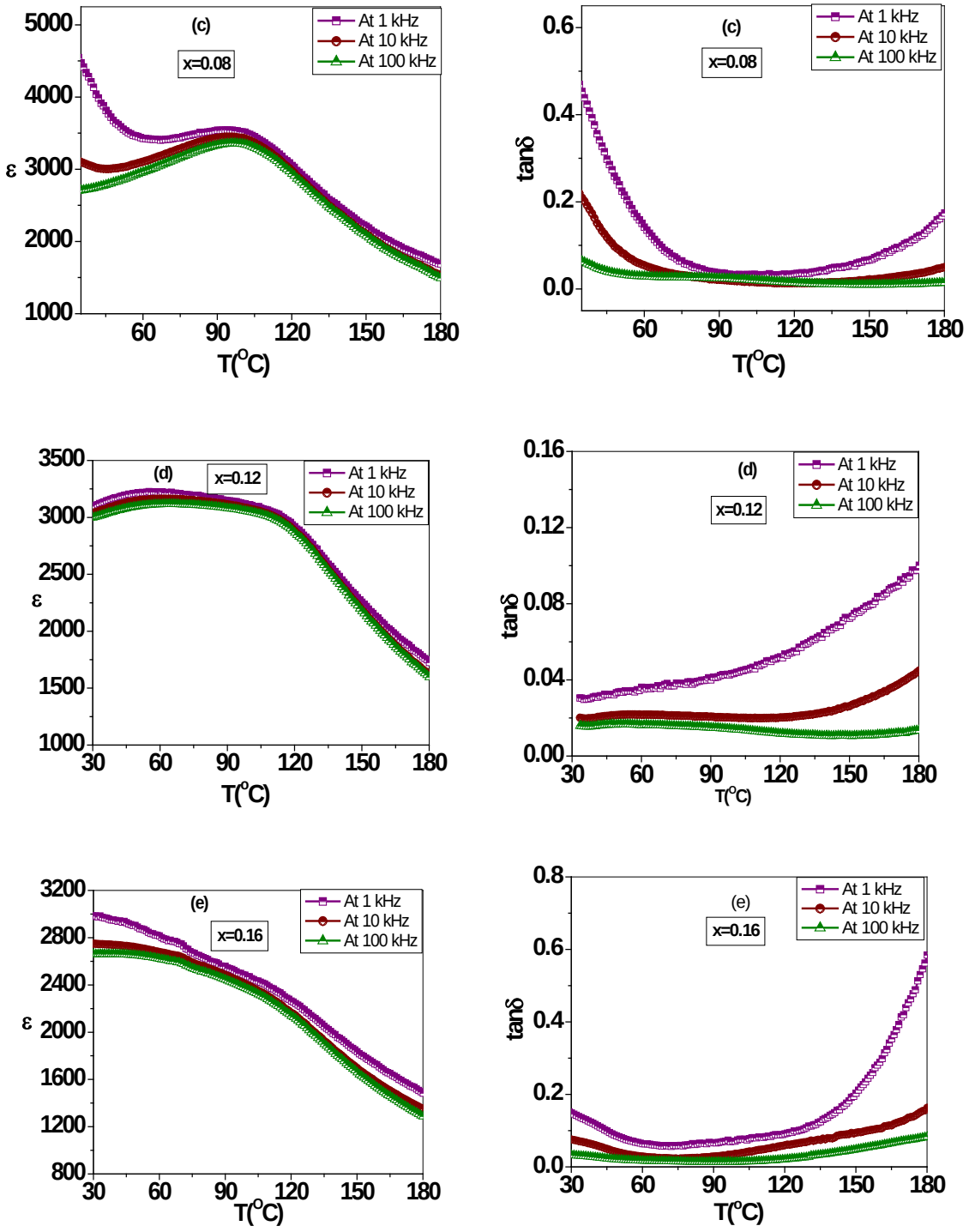

Figure 4.12 Temperature variation of ε at different frequencies of **series B3**

(0.05 NZF + 0.95 BSZT)

Table 4.3

Dielectric parameters for all series samples at 100kHz

Series B1 (BSZT)						**Series B2 (NZF- BSZT)**						**Series B3 (0.05NZF-0.95BSZT)**					
x	**ε_{RT}**	**$\tan\delta_{RT}$**	**ε_{max}**	**$\tan\delta_{max}$**	**T_c (^oC)**	**y**	**ε_{RT}**	**$\tan\delta_{RT}$**	**ε_{max}**	**$\tan\delta_{max}$**	**T_c (^oC)**	**x**	**ε_{RT}**	**$\tan\delta_{RT}$**	**ε_{max}**	**$\tan\delta_{max}$**	**T_c (^oC)**
0.00	3011	0.026	15890	0.182	92	0.00	4277	0.07	17548	0.165	87	0.00	2254	0.081	3834	0.046	134
0.04	4277	0.070	17548	0.165	87	0.05	2548	0.064	3798	0.031	112	0.04	2548	0.064	3798	0.031	112
0.08	4013	0.052	14447	0.116	73	0.10	2307	0.046	3412	0.057	120	0.08	2721	0.077	3361	0.025	96
0.12	5183	0.049	11555	0.042	47	0.15	2395	0.039	3108	0.058	127	0.12	2961	0.026	2980	0.026	54
0.16	8810	0.038	8968	0.032	39	_	_	_	_	_	_	0.16	2827	0.018	2839	0.019	41

4.3 Electrical Conductivity

In order to understand the conduction mechanisms and the type of polarons responsible for conduction, the ac conductivity of the samples was calculated from the dielectric parameters by using the relation [26]

$$\sigma_{ac} = \varepsilon\, \varepsilon_o \omega \tan\delta \qquad \text{…….. 4.2}$$

Figure 4.13 (a-c) shows the variation of ac conductivity with frequency for all series. From figures it is clear that conductivity increases linearly with increase in frequency for all the samples. From figure it is also observed that conductivity of composite samples is higher as compared to that of pure ferroelectric sample that may be due to the presence of ferrite phase. Alder and Feinleib [27] have shown that for conduction by small polarons, ac conductivity increases with frequency. Hence the present results indicate that the conduction is due to small polarons for all samples.

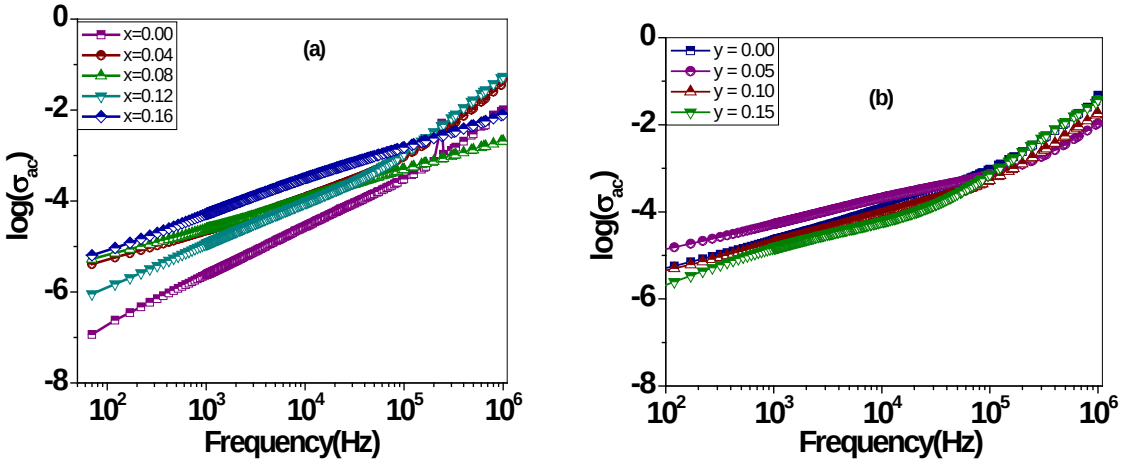

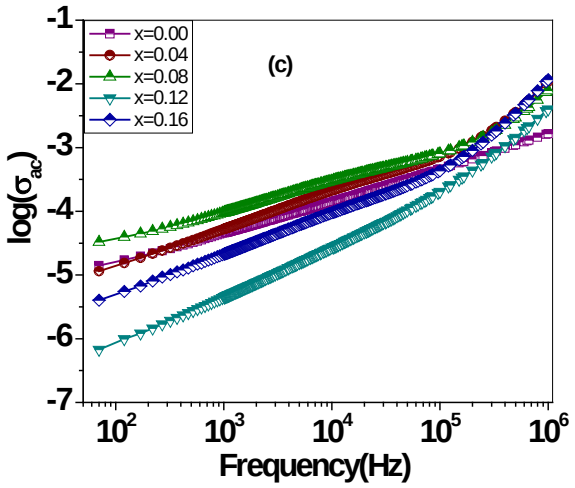

Figure 4.13 Variation of ac conductivity with frequency for **(a) series B1**, **(b**) **series B2** and **(c) series B3** samples.

4.4 Ferroelectric Properties

The P-E hysteresis loops at room temperature for *series B1*, *B2* and *B3* are shown in *figures 4.14*, *4.15* and *4.16* respectively. The value of coercive field (E_c), remanant polarization (P_r) and spontaneous polarization (P_s) were determined from the P-E loops and are given in *table 4.4* for all the samples.

From *table 4.4* it is observed *for series B1*, value of P_r, P_s and E_c decreases with increase in Zr content. Decrease in P_r can be correlated to the average grain size *(table 4.1)*. The decrease in grain size results in decrease in polarization because the number of grain boundaries increases and grain boundary is a low permittivity region it means grain boundary has poor ferroelectricity which results in decreases in polarization with decrease in grain size and vice versa [28]. It is also observed that there is increase in E_c upto x = 0.04 and after that it decreases. This is because with addition of Zr content the structure is changing from tetragonal to rhombohedral *(figure 4.1)* and the samples with rhombohedral structure have smaller principle strain, hence easier domain rotation and smaller coercive field in comparison to the samples with tetragonal symmetry [29-30].

For samples of *series B2,* the P-E hysteresis loop were studied and shown in *figure 4.15*. From *table 4.4* it is observed that value of P_r and P_s decreases with addition of ferrite content. This is because when we apply the electric field to the composite samples, the ferrite material does not respond to this field and hence results in decrease of spontaneous polarization and thus adversely affects the electrical properties and results in poor polarization. The decrease in polarization with addition of ferrite content can also be related to the increase in conductivity of the samples which results in leakage of current [31-32]. From *table 4.4* it is also observed that value of coercive field (E_c) increases with increase in ferrite phase for *series B2* which may be due to decrease in relative density of the samples *(table 4.2)* with increase in ferrite content because porosity acts as a resistance in the path of domain motion.. From *table 4.4* it is also observed that composite samples having Zr substituted ferroelectric phase show better ferroelectric properties as compared to pure BST- NZF composites *(series A, chapter 3).*

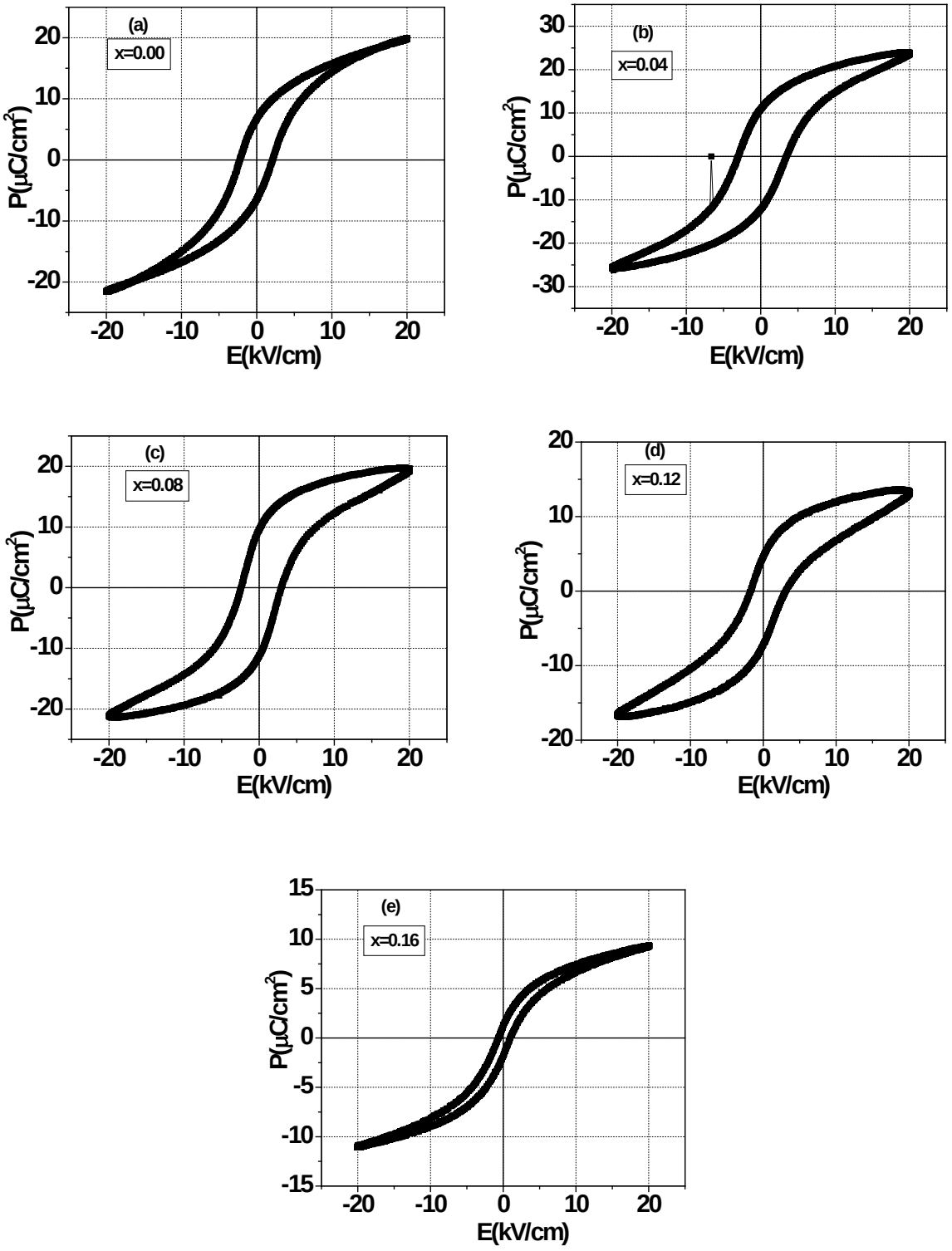

Figure 4.14 Polarization vs electric field (P-E) hysteresis loops of **series B1** (BSZT)

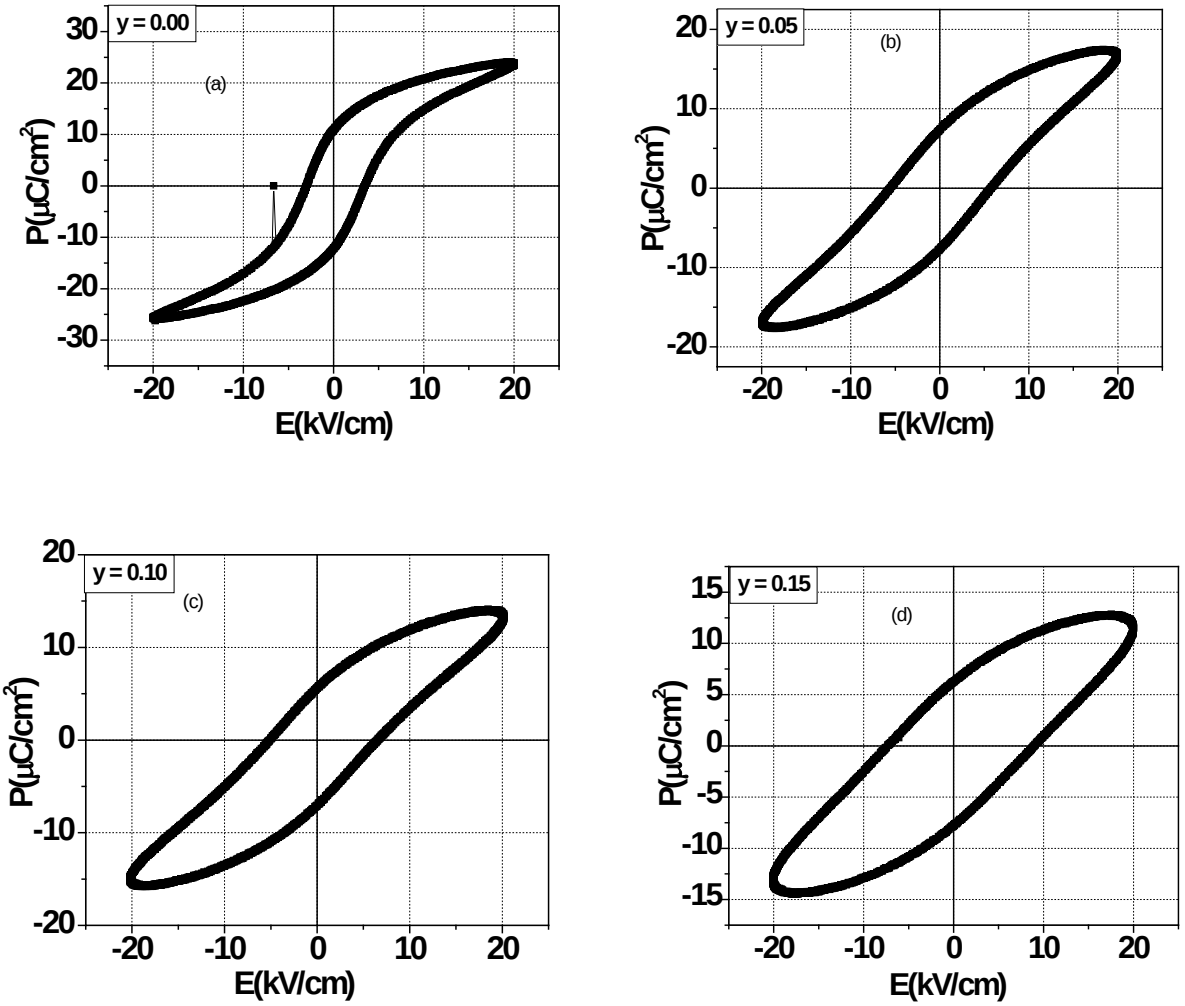

Figure 4.15 Polarization vs electric field (P-E) hysteresis loop of **series B2**

((y) NZF- (1-y) BSZT)

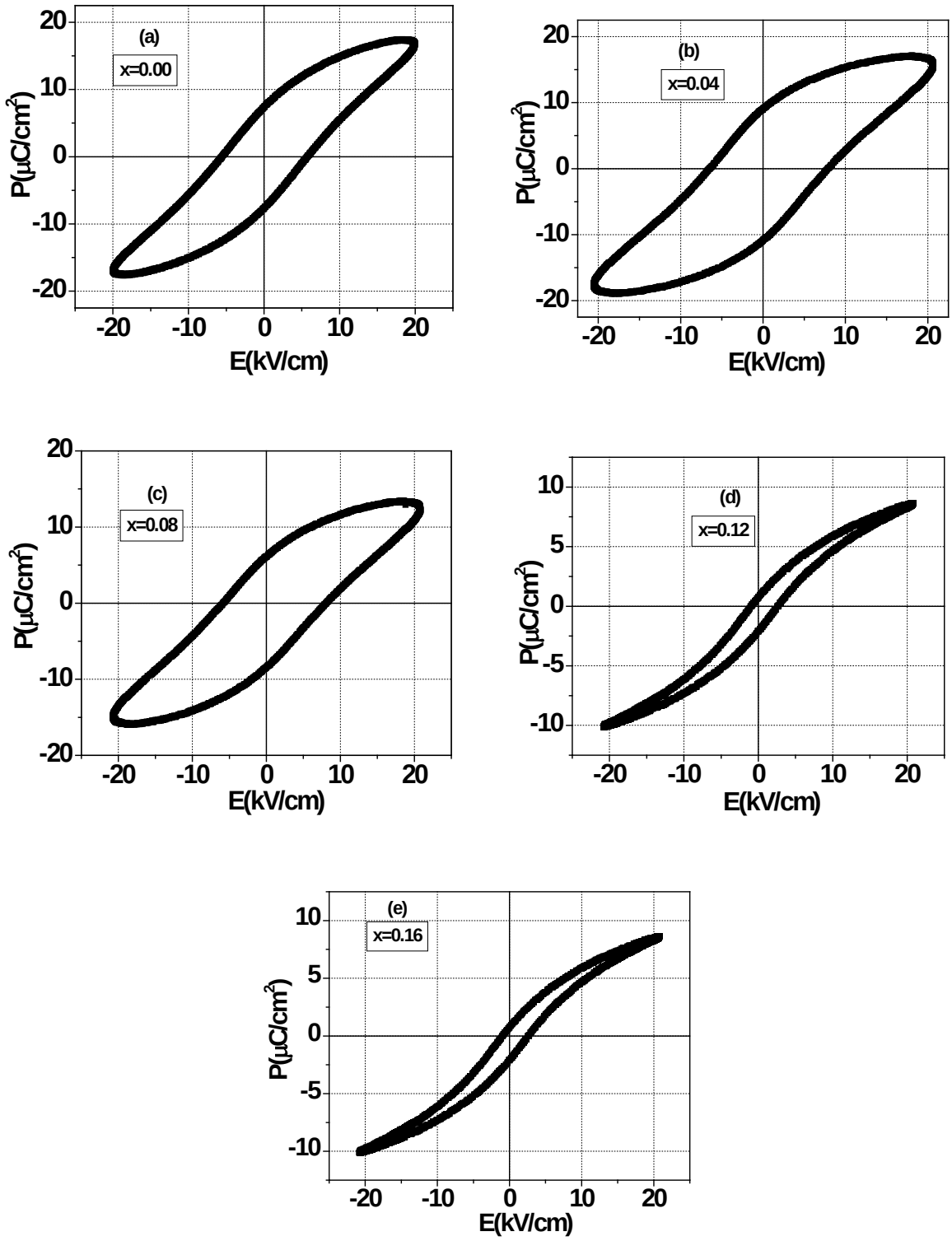

Figure 4.16 Polarization vs electric field (P-E) hysteresis loops of **series B3** (0.05NZF-0.95BSZT)

Table 4.4

Ferroelectric parameters for all series

Series B1 (BSZT)				Series B2 (NZF- BSZT)				Series B3 (0.05NZF + 0.95 BSZT)			
x	**P_r ($\mu C/cm^2$)**	**E_c (kV/cm)**	**P_{max} ($\mu C/cm^2$)**	**y**	**P_r ($\mu C/cm^2$)**	**E_c (kV/cm)**	**P_{max} ($\mu C/cm^2$)**	**x**	**P_r ($\mu C/cm^2$)**	**E_c (kV/cm)**	**P_{max} ($\mu C/cm^2$)**
0.0	6.56	2.19	20.74	0.00	11.54	3.2	25.02	0.0	7.70	7.8	16.00
0.04	11.54	3.2	25.02	0.05	7.42	5.65	17.60	0.04	7.42	5.65	17.60
0.08	10.37	2.6	20.62	0.10	5.85	6.32	14.96	0.08	7.2	6.95	14.79
0.12	5.91	2.42	15.37	0.15	7.00	8.15	13.66	0.12	1.40	1.81	9.46
0.16	1.54	0.8	10.25	--	--	--	--	0.16	1.38	2.14	8.60

4.5 Ferromagnetic Properties

In order to understand the magnetic nature of composites, magnetic hysteresis loops for all samples were taken. *Figures 4.17* and *4.18* shows the magnetic hysteresis loops for series B2 and B3 at room temperature respectively. It also confirms the existence of magnetic ordering in composite system. The value of coercive field (H_c), remanant magnetization (M_r) and spontaneous magnetization (M_s) were determined from the M-H loops and are given in *table 4.5* for all these series samples.

From *table 4.5* it is observed that there is increase in saturation magnetization and remanant magnetization increases with increase in ferrite content for series B2. This is due to the fact that ferrites are magnetic in nature and the number of domains contributing to magnetization increases with increase in ferrite content resulting in increase in net magnetization. But the values of magnetization in composites is smaller than the pure ferrite phase because ferroelectric material incorporates in to the ferrite phase and acts as pores in the presence of applied magnetic field and break the magnetic current resulting in the decrease of magnetic parameters [33] .

From *table 4.5* it is also observed that value of saturation magnetization varies in random manner although the amount of ferrite phase is fixed for *series B3*. These may be due to non-uniform mixing of two individual phases as the effective value of magnetic and electric properties of a composite material consisting of two phases can be predicted as a function of individual components [34]. *Series B1* do not shows the M-H hysteresis loops due to the absence of magnetic phase.

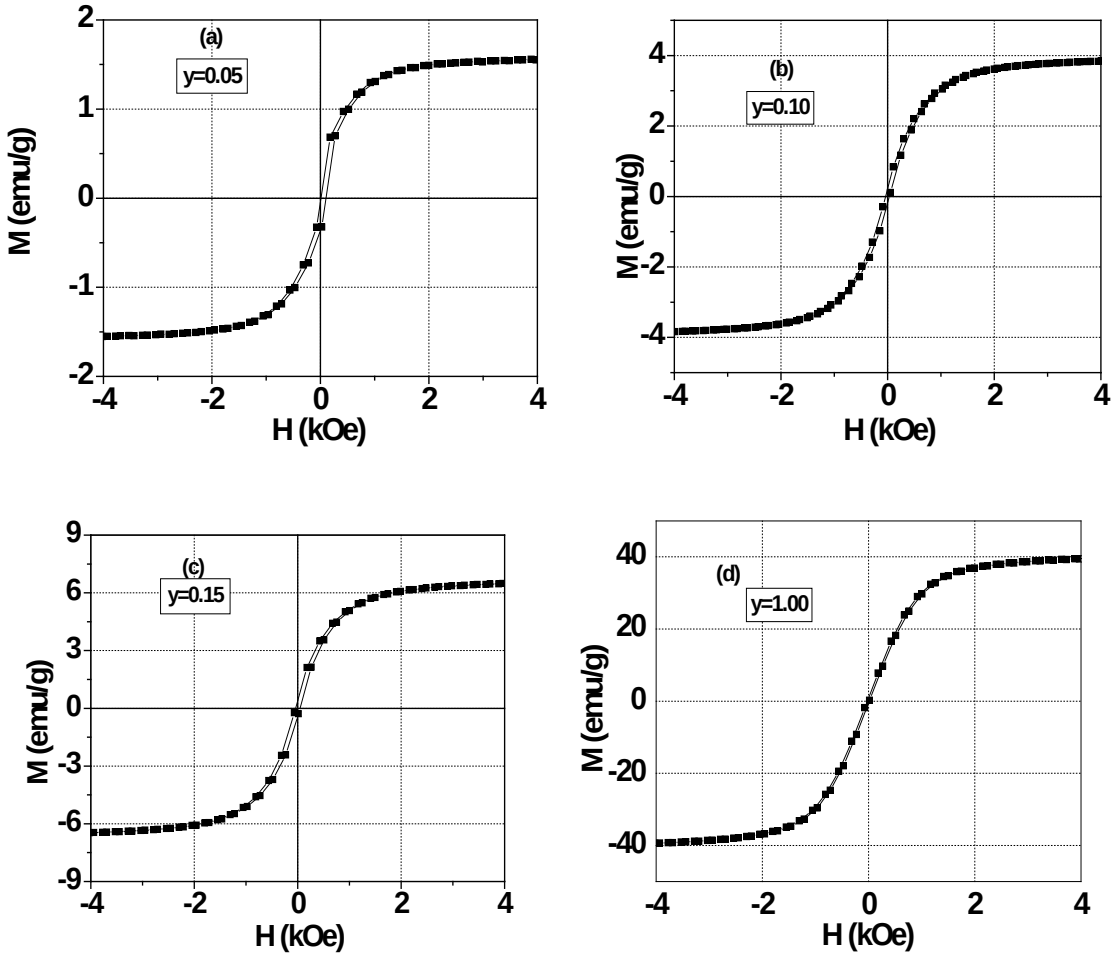

Figure 4.17 Magnetization Vs Magnetic field (M-H) hysteresis loop of **series B2** ((y)NZF- (1-y)BSZT)

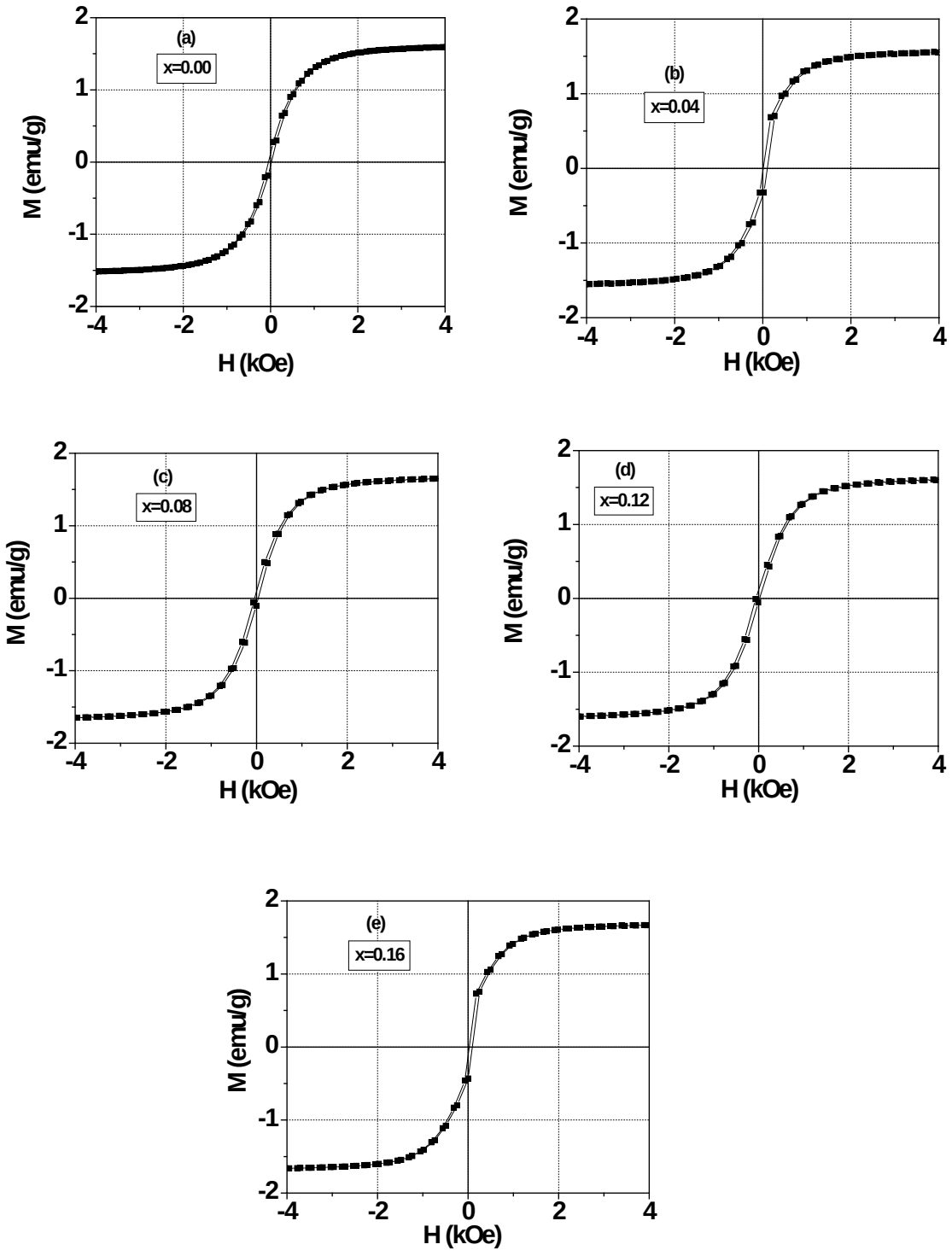

Figure 4.18 Magnetization Vs Magnetic field (M-H) hysteresis loop of **series B3** (0.05NZF + 0.95 BSZT)

Table 4.5

Ferromagnetic parameters for all series

Series B2 (NZF- BSZT)				Series B3 (0.05NZF + 0.95 BSZT)			
Y	**M_r (emu/g)**	**M_s (emu/g)**	**H_c (Oe)**	**x**	**M_r (emu/g)**	**M_s (emu/g)**	**H_c (Oe)**
0.00	_	_	_	0.0	0.162	1.60	69.82
0.05	0.156	1.56	93.08	0.04	0.156	1.56	93.08
0.10	0.394	4.0	82.23	0.08	0.159	1.66	87.70
0.15	0.798	6.5	90.26	0.12	0.153	1.62	82.20
1.00	1.34	40	32.22	0.16	0.158	1.68	90.24

4.6 Magnetoelectric Property

To study the effect of electric poling on ferromagnetic properties (magnetoelectric effect) M-H hysteresis loops were taken for both electrically poled and unpoled pieces of composite samples as already discussed in *chapter 3* and their comparison is shown in *figure 4.19 (a-c)*. Values of magnetic parameters for poled and unpoled samples are given in *table 4.6*. It can easily be observed that, there is increase in remanant magnetization and saturation magnetization for electrically poled samples which is the evidence of ME coupling.

Variation of ME coupling coefficient with dc magnetic field was also studied and is shown in *figure 4.19 (d)*. From this figure it is observed that ME coefficient goes on increasing with increase in magnetic field and after attaining a maximum value and with further increase in magnetic field it decreases, which may be due to fact that after a certain value of magnetic field the magnetostriction coefficient of ferrite phase reaches its saturation value. Hence, the strain produced in the ferrite phase would produce a constant electric field in the piezoelectric phase resulting in decrease in ME coefficient with increase in the applied dc magnetic field. This

behavior is already reported by a number of researchers [35-36]. Value of ME coefficient firstly increases with increase in ferrite content. The reason behind this can be explained on the same line as already discussed in *chapter 3*. The value of ME coefficient observed for y = 0.10 composite sample is higher as compared to those reported for bulk ferrite-ferroelectric composites in literature [37-41].

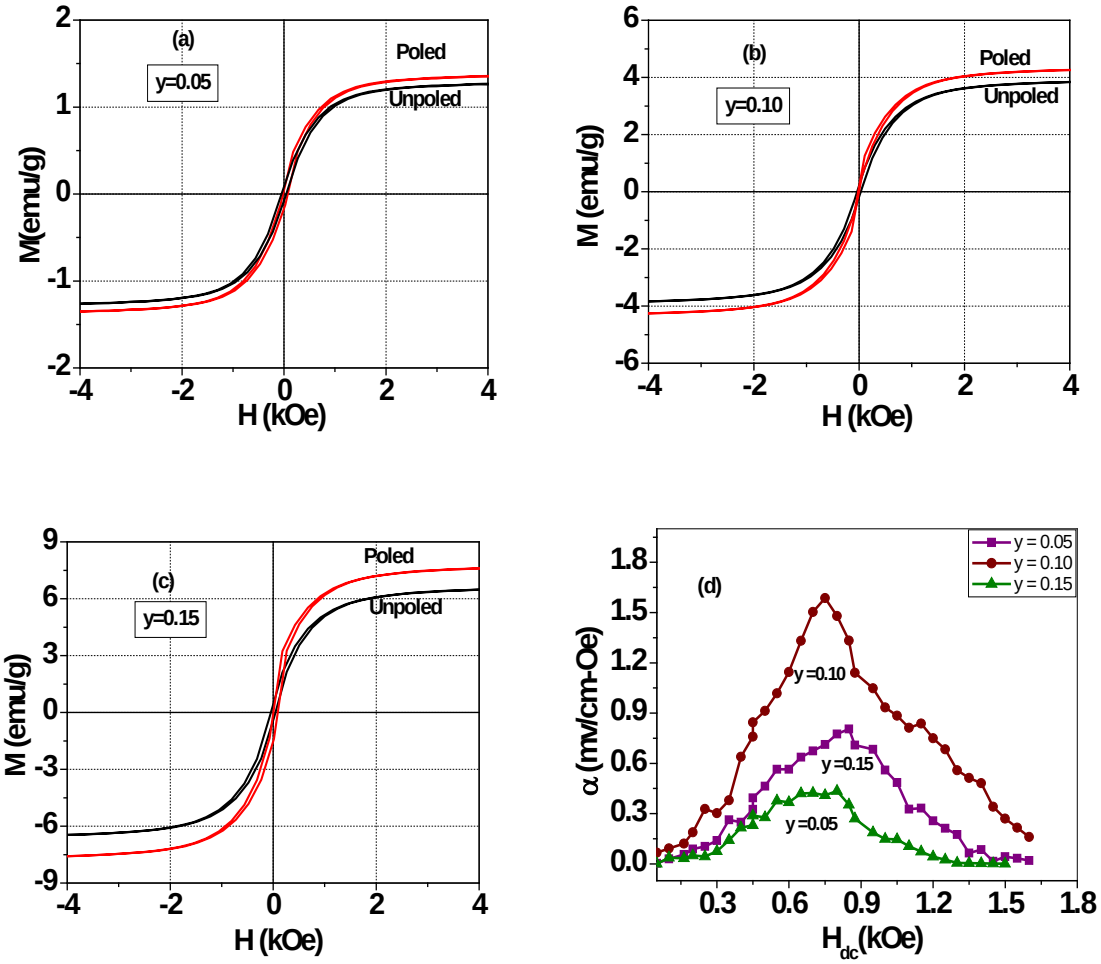

Figure 4.19 M-H hysteresis loop of **series B2** ((y)NZF- (1-y)BSZT) for poled and unpoled samples (a) y = 0.05, (b) 0.10 (c) 0.15 and (d) Variation of ME coefficient with magnetic field at room temperature

Table 4.6

Magnetic parameters of poled and unpoled samples of **Series B2**

(NZF- BSZT)

	Unpoled samples			Poled samples			ME coefficient (α) (mV/cm-Oe)
y	**M_r (emu/g)**	**M_s (emu/g)**	**H_c (Oe)**	**M_r (emu/g)**	**M_s (emu/g)**	**H_c (Oe)**	
0.05	0.156	1.3	93.08	0.160	1.34	92.21	0.4
0.10	0.394	4.0	82.23	0.411	4.27	86.61	1.65
0.15	0.798	6.5	90.26	0.830	7.62	90.00	0.78

Refrences

1) B.L. Cheng, C. Weng, S.Y. Wang and H.B. Lu, J. Europ. Ceram. Soc., **25** (2005) 2295.
2) A.S. Fawzi, A.D. Sheikh and V.L. Mathe, Phys. B, **405** (2010) 340.
3) S.S. Chougule and B.K. Chougule, Mater. Chem. Phys., **108** (2008) 408.
4) B.K. Bammannavar and L.R. Naik, J. Magn. Magn. Mater., **321** (2009) 382.
5) S.L. Kadam, K.K. Patankar, C.M. Kanamadi and B.K. Chougule, Mater. Res. Bull., **39** (2004) 2265.
6) I. Chyuan and S.L. Fu, J. Mater. Sci., **25** (1990) 4699.
7) D.R. Patil, S.A. Lokare, S.S. Chougule and B.K. Chougule, Phys. B, **400** (2007) 77.
8) D.R. Patil and B.K. Chougule, J. Alloys Compd., **470** (2009) 531.
9) O.P. Thakur and C. Prakash, Phase Transitions, **76** (2003) 567.
10) A. Dixit, S.B. Majumdar, R.S. Katiyar and A.S. Bhalla, Appl. Phys. Lett. 82 (2003) 2679.
11) M.B. Kothale, K.K. Patankar, A.V. Rao, V.L. Mathe and B.K. Chougule, Ferroelectrics, **325** (2005) 143.
12) C.M. Kanamadi, L.B. Pujari and B.K. Chougule, J. Magn. Magn. Mater., **29**5 (2005) 139.
13) N. Ponpandian, P. Balay and A. Narayanasamy, J. Cond. Mater. Phys., **14** (2002) 3221.
14) M.B. Kothale, K.K. Patankar, S.L. Kadam, V.L. Mathe, A.V. Rao and B.K. Chougule, Mater. Chem. Phys., **77** (2002) 691.
15) K.K. Patankar, S.L. Kadam, V.L. Mathe, C.M. Kanamadi, V.P. Kothavale and B.K. Chougule, Br. Ceram. Trans., **102** (2003) 19.
16) K.K. Patankar, S.A. Patil, K.V. Sivakumar, R.P. Mahajan, Y.D. Kolekar and M.B. Kothale, Mater. Chem. Phys., **65** (2000) 97.
17) K.K. Patankar, S.S. Joshi and B.K. Choughle, Phys. Let. A, **346** (2005) 337.
18) S. Singh, O.P. Thakur, C. Prakash and K.K. Raina, Phase Transitions, **78** (2005) 655.
19) L.I. Maissel and R. Glang, Handbook of Thin Film Technology, McGraw-Hill, New York, USA (1970).

20) S.G. Lee and D.S. Kang, Mater. Lett., **57** (2002) 1629.

21) P.S. Dobal, A. Dixit, R.S. Katiyar, Z. Yu, R. Guo and A.S. Bhalla, J. Appl. Phys. 89 (2001) 8085

22) N. Sawangwan, J. Barrel, K. Mackenzu and T. Tunkasiri, Appl. Phys. A, **90** (2008) 723.

23) Renu Rani, S. Singh, J.K. Juneja, C. Prakash and K.K. Raina, Ceramic Int., **37** (2011) 3755.

24) D. Hennings, H. Schell and G. Simon, J. Am. Ceram. Soc., **65** (1982) 539.

25) B.L. Cheng, Can Weng, S.Y. Wang and H.B. Lu, J. Europ. Ceram. Soc., **25** (2005) 2295.

26) S.S. Choughle and B.K. Choughle, Mater. Chem. Phys., **108** (2008) 408.

27) D. Alder and J. Feinleib, Phys. Rev. B, **2** (1970) 3112**.**

28) J. Zhai, X .Yao, J .Shen, L. Zhang and H. Chen, J. Phys. D Appl. Phys., **37** (2004) 748.

29) K. Uchino, Ferroelectric Devices, Marcel Dekker, New York (2000).

30) M. Kumar, A. Garg, R. Kumar and M.C. Bhatnagar, Phys. B, **403** (2008) 1819.

31) K. Pandey, N. Singh and S.K. Mishra, J. Pure Appl. Phys., **32** (1994) 616.

32) K.K. Patankar, S.S. Joshi and B.K. Choughle, Phys. Lett. A, **346** (2005) 337.

33) R.S. Devan and B.K. Chougule, J. Appl. Phys., **101** (2007) 0141091.

34) S. Narender Babu, S.V. Suryanarayana and T. Bhimasankaram, J. Alloys Compd. **473** (2009) 418.

35) B.K. Bammannavar and L.R. Naik, J. Magn. Magn. Mater., **321** (2009) 382.

36) S.U. Dugadsimi, B.K. Chougule, S.S. Chougule, C.H. Bhosale and S. S. Bellad, Int. J. Engg. Sci. Tech., **3** (2011) 1446.

37) A. Hanumaian, T. Bhimasankaram, S.V. Suryanarayan and G. Kumar, Bull. Mater. Sci., **17** (1994) 405.

38) D.R. Patil and B.K. Chougule, J. Alloys Compd., **470** (2009) 531.

39) D.R. Patil, S.A. Lokare, S.S. Chougule and B.K. Chougule, Phys. B, **400** (2007) 77.

40) B.K. Bammannavar and L.R. Naik, J. Magn. Magn. Mater., **321** (2009) 382.

41) S.L. Kadam, K.K. Patankar, V.L. Mathe, M.B. Kothale, R.B. Kale and B.K. Chougule, Mater. Chem. Phys., **78** (2003) 684.

Chapter - V

Synthesis and Characterizations of La Substituted NZF– BST Composites

Chapter V

Synthesis and Characterizations of La substituted NZF –BST Composites

This chapter includes study on the structural, dielectric, ferroelectric, ferromagnetic and magnetoelectric properties of La substituted (y) $Ni_{0.8}Zn_{0.2}Fe_2O_4$ - (1-y) $Ba_{0.9}Sr_{0.1}TiO_3$ ((y) NZF- (1-y) BST) composites.

The compositions discussed in the present chapter are:

Series C1 $Ba_{0.9-3x/2}Sr_{0.1}La_xTiO_3$ where x = 0.00, 0.005, 0.01, 0.015, 0.02

Series C2 (y) $Ni_{0.8}Zn_{0.2}Fe_2O_4$ - (1-y) $Ba_{0.9925}Sr_{0.1}La_{0.005}TiO_3$ where y = 0.00, 0.05, 0.10,0.15,

Series C3 0.95 $Ba_{0.9-3x/2}Sr_{0.1}La_xTiO_3$ - 0.05 $Ni_{0.8}Zn_{0.2}Fe_2O_4$ where x= 0.00, 0.005, 0.01,0.015,0.02

In *series C1* we have studied the effect of La on $Ba_{0.9-3x/2}Sr_{0.1}La_xTiO_3$ with x = 0.00 to 0.02 in steps of 0.005 for optimizing the best La substituted ferroelectric phase for composite system. In *series C1* for x = 0.005 we have observed best dielectric and ferroelectric properties hence for preparing composite samples we have selected the ferroelectric phase as $Ba_{0.9925}Sr_{0.1}La_{0.005}TiO_3$. In *series C3* the ratio of both phases (ferroelectric and ferrite) was fixed and content of La was varied in ferroelectric phase.

All samples were prepared by conventional solid state reaction method. Samples were sintered at 1325^{o}C for 4 hrs at a uniform heating of 5^{o}C/min (details are given in chapter 2). After sintering

samples were investigated for their structural, dielectric, ferroelectric, ferromagnetic and magnetoelectric properties.

5.1 Structural Properties:

5.1.1 XRD

All samples were subjected to X-ray diffraction studies. XRD patterns of *Series C1, C2* and *C3* are shown in *figure 5.1, 5.2* and *5.3* respectively. From *figure 5.1* it is observed that all samples have pure perovskite phase with tetragonal structure for *series C1*. *Figure 5.2* shows the XRD patterns of individual phases and their composites (*series C2*). From this figure it is observed that composite samples show characteristic peaks of both phases i.e. ferrite and ferroelectric phase and confirms the presence of both phases. The XRD patterns of composite samples do not show presence of any unreacted or intermediate phase which confirms that no chemical reaction took place between two phases and they maintained proper stoichiometry. From *figure 5.2* it is observed that the intensity and number of ferrite peaks increase with increase in ferrite content hence the present composite system follow the rule of mixture and from *figure 5.3* it is observed that the intensity of ferrite phase peak is very low which is due to very small percentage of ferrite phase in composite samples. The calculated values of lattice parameters for all series are given in *table 5.1*.

From table it is observed that calculated values of lattice parameters of individual phases in composite samples are in well agreement with the two pure individual phases it means structure of the material is not changing. It is also observed that for series C1 and C3 lattice parameters corresponding to ferroelectric phase decreases (c, a) with the increase in La content because larger ion Ba^{2+} (ionic radii 1.49 Å) are being replaced by smaller ion La^{3+} (ionic radii 1.17 Å) but there is very little variation in the lattice parameters of individual phases of composite samples and it may be due to the stress exerted by two phases on each other [1].

The experimental density, theoretical density and relative density for all samples of series C1, C2 and C3 are given in *table 5.2*. From table it is observed that relative density decreases with the addition of ferrite phase and La content.

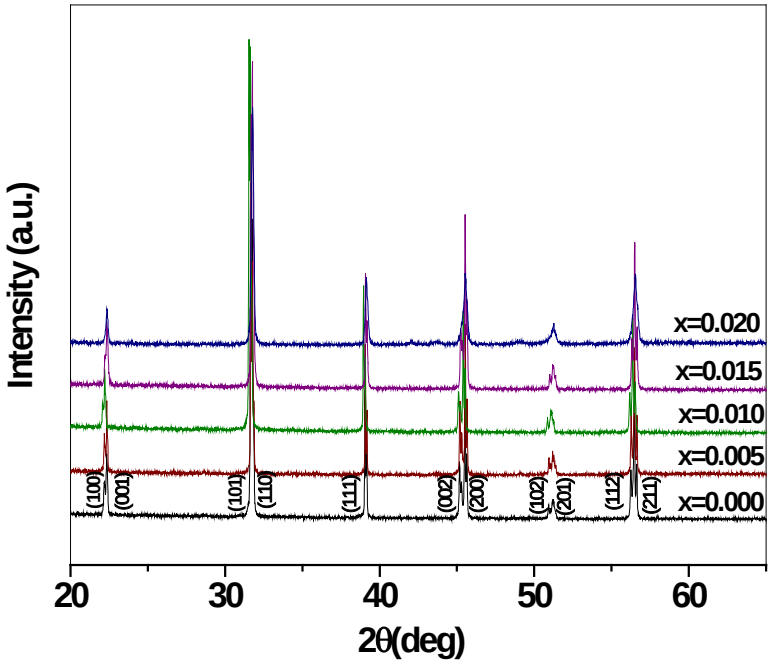

Figure 5.1 XRD pattern for **Series C1** (BSLT) for different value of x.

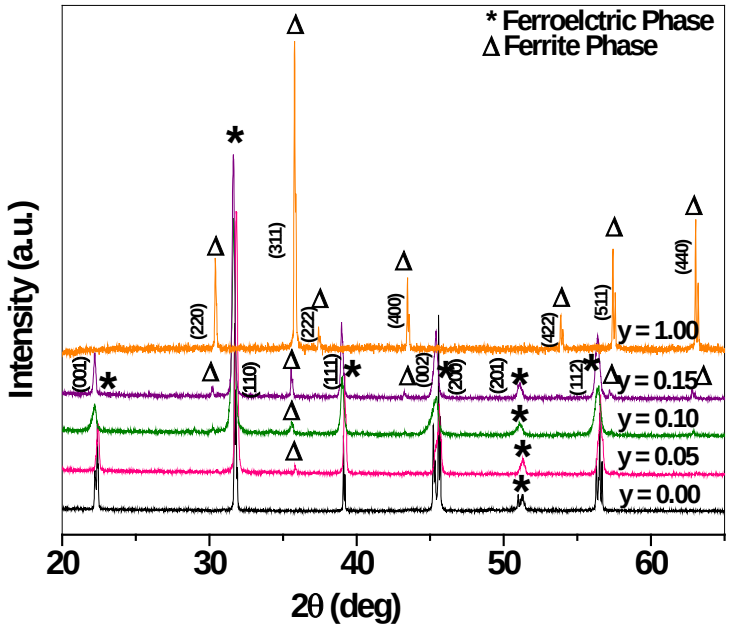

Figure 5.2 XRD pattern for **Series C2** ((y) NZF- (1-y) BSLT) for different value of y

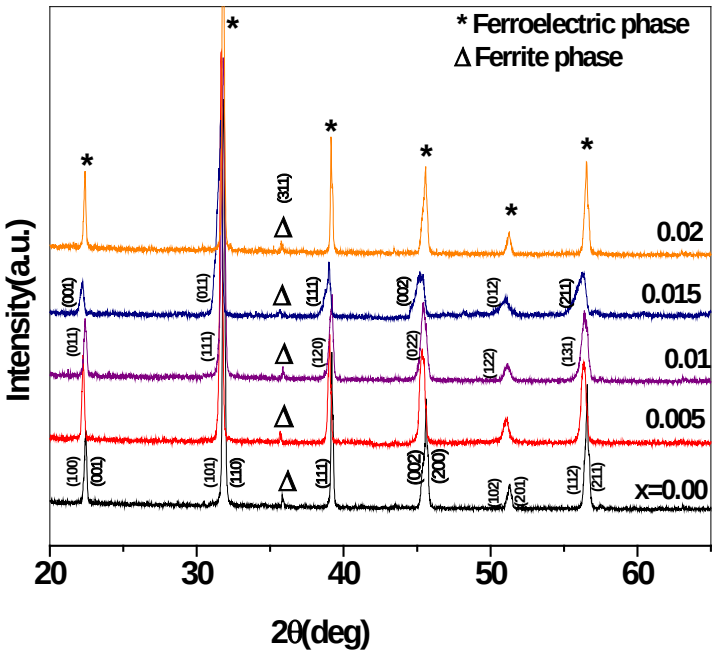

Figure 5.3 XRD pattern for **Series C3** (0.05 NZF + 0.95 BSLT) for different value of x

5.1.2 Scanning Electron Microscope (SEM)

SEM micrographs for series C1, C2 and C3 are shown in *figure 5.4*, *5.5* and *5.6* respectively. Average grain size was calculated by linear intercept method and grain size decreases with increase in La content. Grain size is larger for x = 0.005 which may be due to solubility of La and for x > 0.005 grain size decreases. This decrease may be due to segregation of La at grain boundaries resulting in inhibition of grain growth. From SEM micrographs of composite samples it is observed that grain size decreases with the addition of ferrite phase but from micrographs it is difficult to differentiate two phases individually due to small concentration of ferrite phase.

(a)

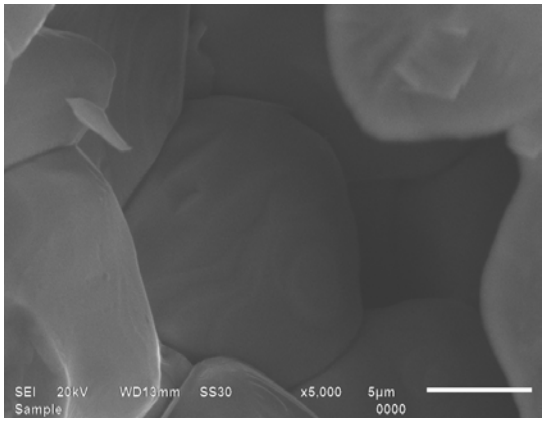

(b)

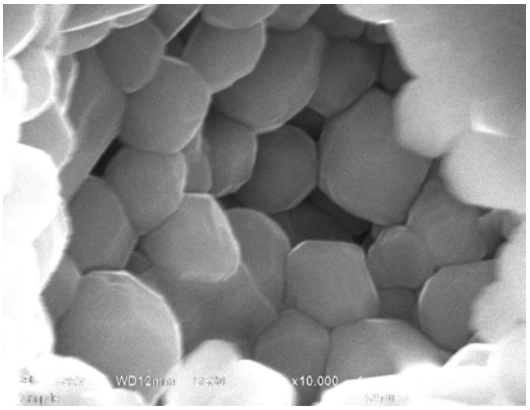

(c)

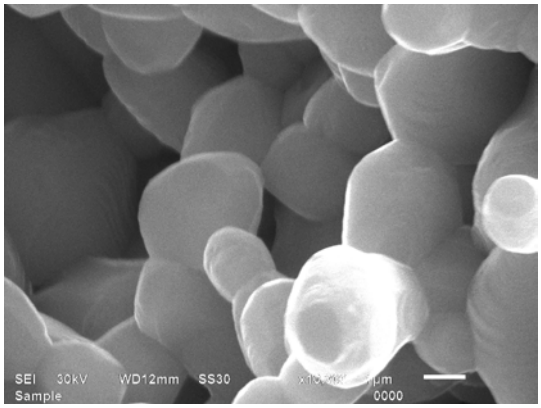

(d)

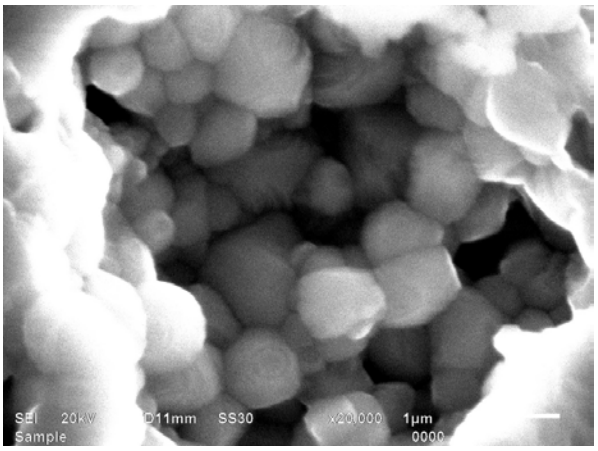

(e)

Figure 5.4 SEM micrographs of **series C1** (BSLT) for (a) x = 0.00, (b) x=0.005 (c) x=0.010 (d) x = 0.015 and (e) x = 0.020

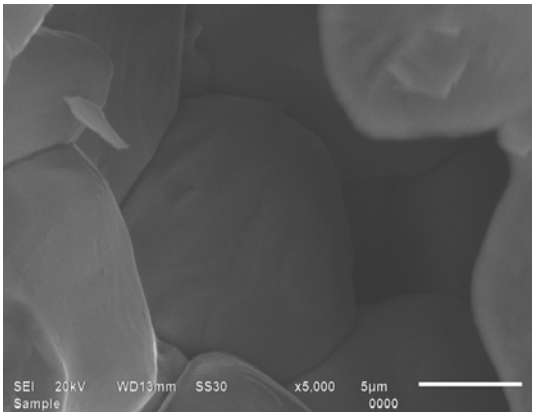

(a)

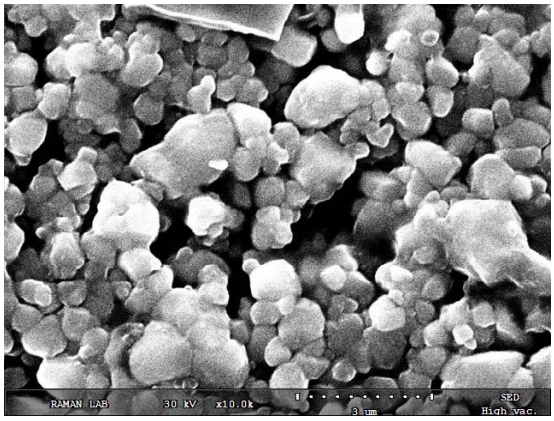

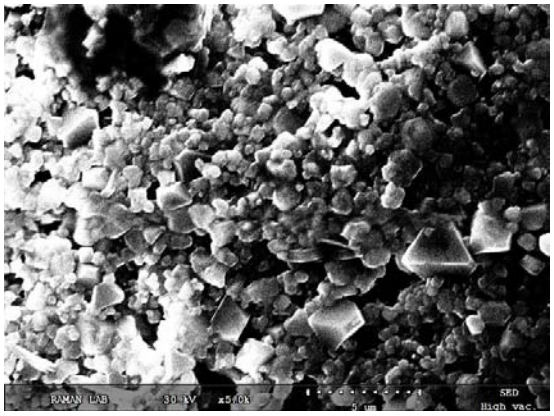

(b) **(c)**

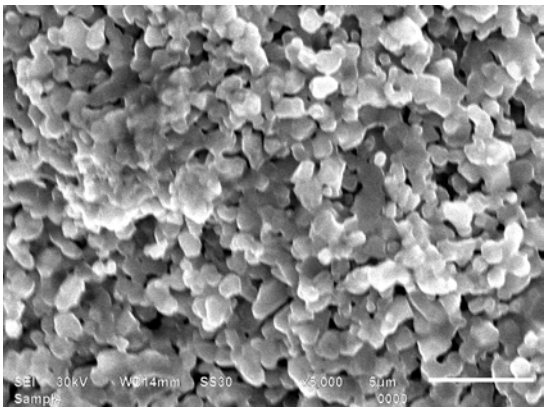

(d)

Figure 5.5 SEM micrographs of **Series C2** ((y) NZF- (1-y)BSLT) for (a) y = 0.00, (b) 0.05, (c) 0.10 and (d) 0.15

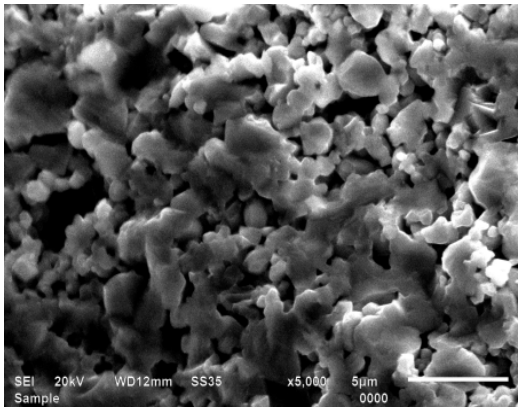

(a)

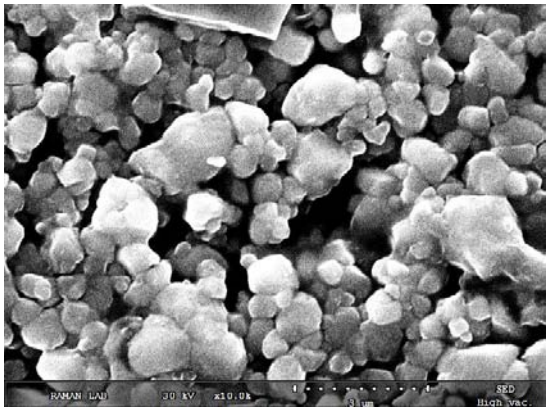

(b)

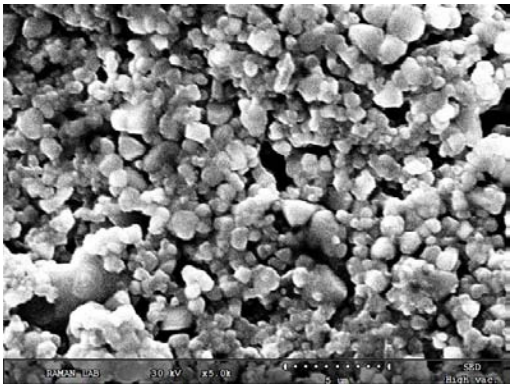

(c)

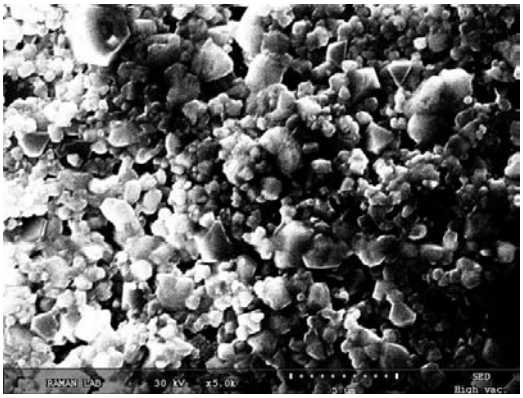

(d)

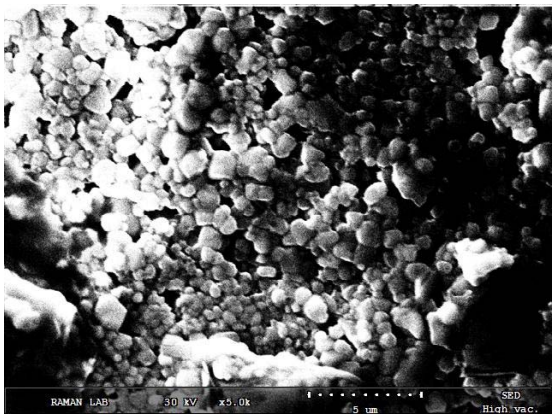

(e)

Figure 5.6 SEM micrographs of **Series C3** (0.05 NZF + 0.95 BSLT) for (a) x = 0.00, (b) x=0.005, (c) x=0.010, (d) x=0.015 and (e) x=0.020

Table 5.1

Lattice parameters for all series samples

Series C1 (BSLT)					Series C2 (NZF- BSLT)					Series C3 (0.05 NZF + 0.95 BSLT)				
x	Lattice parameters			Avg grain size (μm)	y	Ferroelectric			Ferrite	x	Ferroelectric			Ferrite
	a (Å)	c (Å)	c/a			a(Å)	c(Å)	c/a	a (Å)		a(Å)	c(Å)	c/a	a (Å)
0.00	3.986	4.002	1.004	5.68	0.00	3.987	4.003	1.004	_	0.00	3.986	4.003	1.004	8.324
0.005	3.985	4.001	1.004	6.61	0.05	3.988	4.004	1.004	8.332	0.005	3.985	4.001	1.004	8.332
0.01	3.983	3.995	1.003	3.28	0.10	3.986	4.003	1.004	8.344	0.01	3.983	3.997	1.003	8.335
0.015	3.980	3.981	1.000	1.66	0.15	3.987	4.004	1.004	8.345	0.015	3.971	3.992	1.003	8.341
0.02	3.978	3.979	1.000	1.35	--	--	--	--	--	0.02	3.976	3.988	1.003	8.339

Table 5.2

Density for all series samples

Series C1 (BSLT)				Series C2 (NZF- BSLT)				Series C3 (0.05 NZF + 0.95 BSLT)			
x	d_{exp} (g/cc)	d_{th} (g/cc)	Relative density (%)	y	d_{exp} (g/cc)	d_{th} (g/cc)	Relative density (%)	x	d_{exp} (g/cc)	d_{th} (g/cc)	Relative density (%)
0.00	5.74	5.96	96.32	0.00	5.55	5.94	93.44	0.00	5.21	5.93	87.84
0.005	5.55	5.94	93.44	0.05	5.19	6.09	85.14	0.005	5.19	6.09	85.14
0.01	5.50	5.92	93.13	0.10	5.05	6.02	84.00	0.01	5.27	6.24	84.46
0.015	5.43	5.84	92.92	0.15	5.12	6.13	83.44	0.015	5.10	6.07	84.03
0.02	5.40	5.82	92.84	--	--	--	--	0.02	5.17	6.17	83.80

5.2 Dielectric Properties

5.2.1 Variation of ε and tanδ with Frequency

Variation of dielectric constant and loss with frequency for *series C1, C2* and *C3* are shown in *figures 5.7 (a-b), 5.8 (a-b)* and *5.9 (a-b)* respectively. From these figures it is observed that dielectric constant decreases with frequency and remains constant at higher frequencies. The higher values of dielectric constant at lower frequencies and low value at higher frequencies indicate large dispersion and that may be due to Maxwell- Wagner type interfacial polarization in agreement with Koops phenomenological theory [2-4]. In case of pure ferrite and ferroelectric materials the large value of dielectric constant is due to the heterogeneity of the samples [5-6]. However in case of composite samples it is ascribed to the fact that ferroelectric regions are surrounded by non-ferroelectric regions. This give rise to interfacial polarization and at lower frequencies contribution of this polarization is maximum. The dielectric constant remains constant at higher frequencies for all composite samples because beyond frequency of external electric field the electron exchange between Fe^{2+}/Fe^{3+} and $Ni^{2+}/Ni^{3+}$for ferrite phase cannot follow the alternating field [7-8].

From *figure 5.7* and *5.9* for *series C1* and *C3* it is also observed that value of room temperature dielectric constant increases and dielectric loss decreases with addition of La content. From *figure 5.9* it is also observed that La substitution in ferroelectric phase decrease the dielectric dispersion of composite samples hence La substitution not only results in improved dielectric properties of pure ferroelectric series (*series C1*) but also improves dielectric properties of composite samples (*series C3*). From *figure 5.8* it is also observed that room temperature dielectric constant decreases with addition of ferrite content. The similar trend is observed by many researchers [9-10]. The variation of dielectric loss with frequency shows similar dispersion as that of dielectric constant for all series samples.

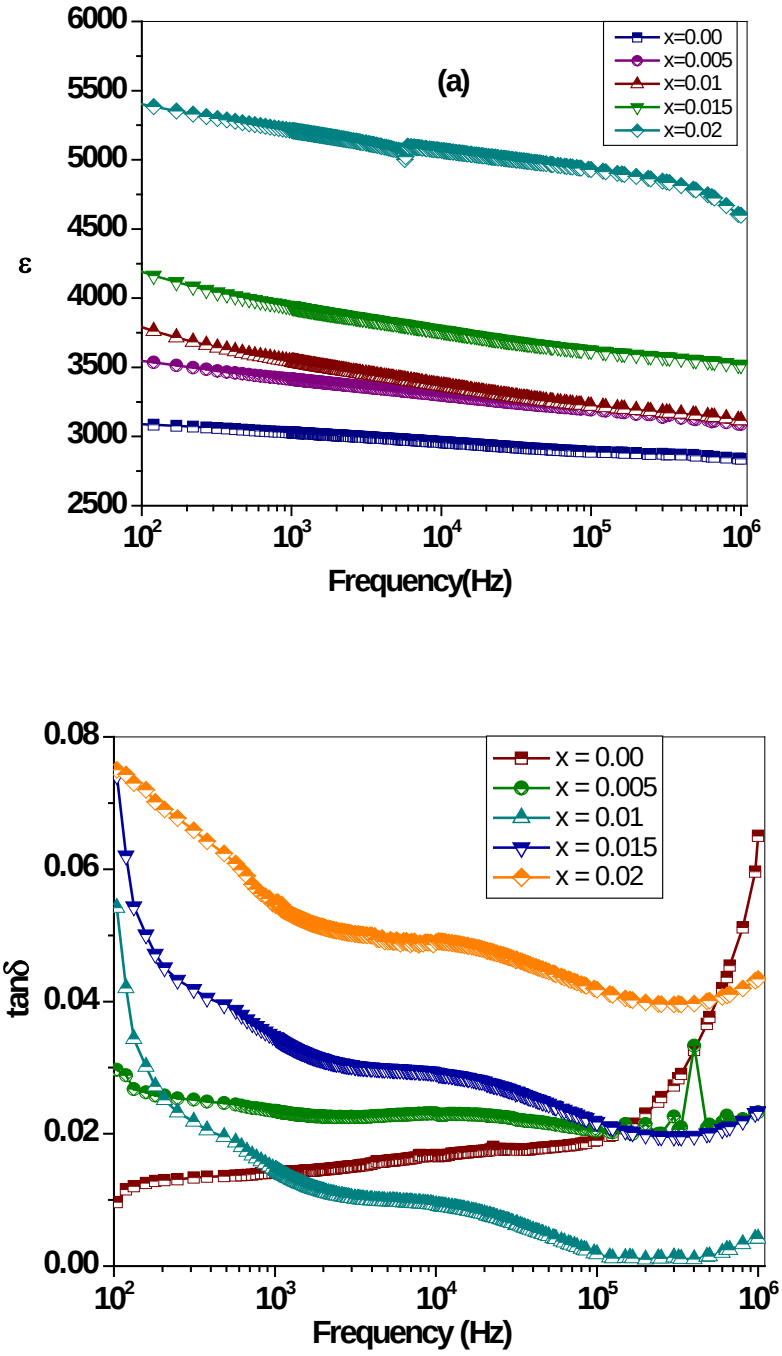

Figure 5.7 Room temperature variation of (a) dielectric constant (ε_{RT}) (b) loss tangent ($\tan\delta_{RT}$) of Series C1 (BSLT) as a function of frequency.

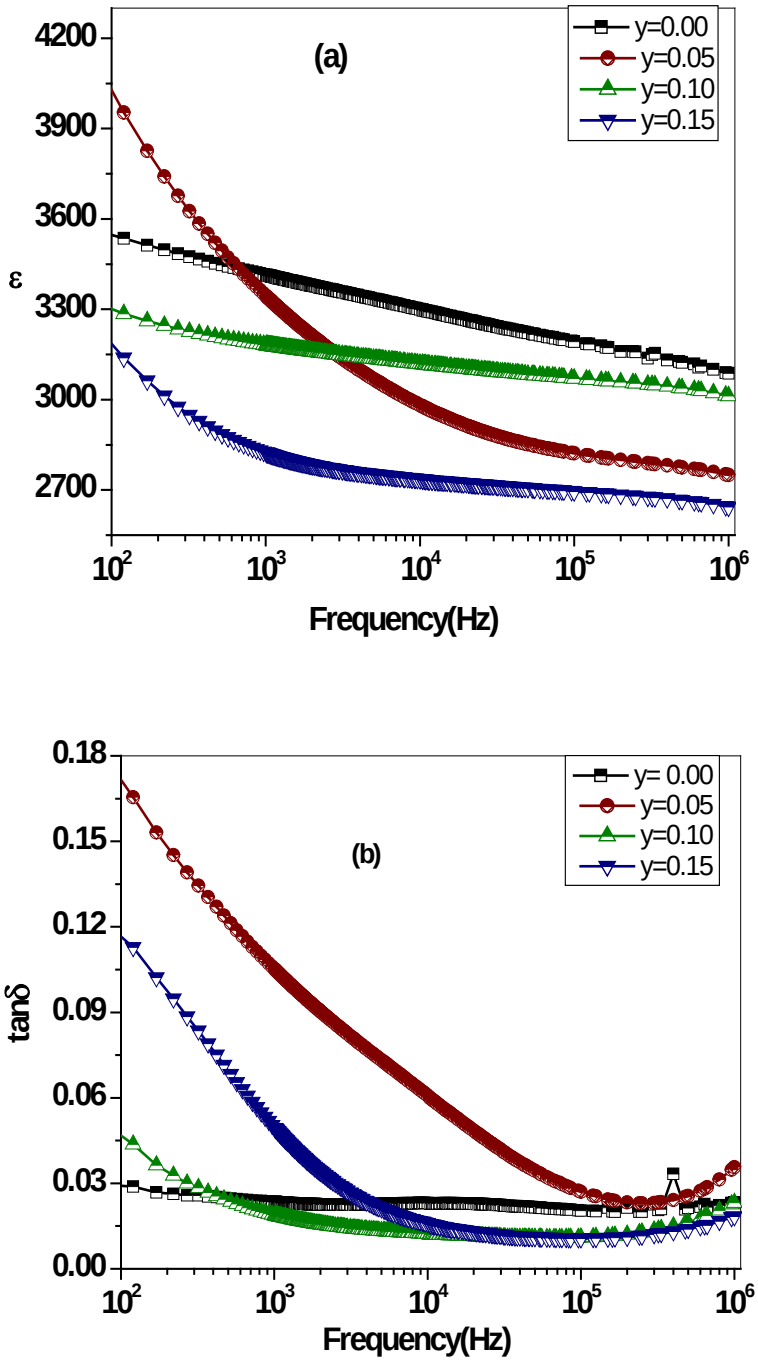

Figure 5.8 Room temperature variation of (a) dielectric constant (ε_{RT}) (b) loss tangent ($\tan\delta_{RT}$) of Series C2 ((y) NZF- (1-y) BSLT) as a function of frequency

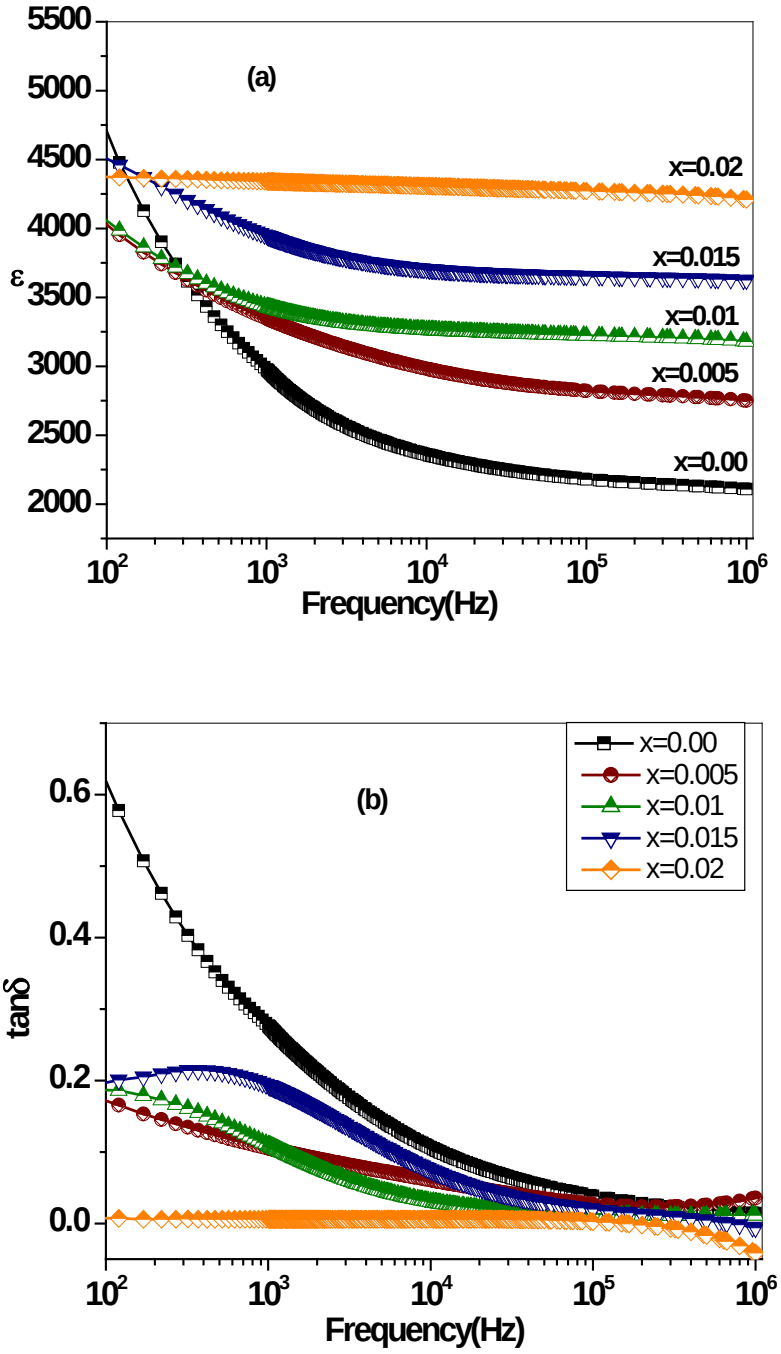

Figure 5.9 Room temperature variation of (a) dielectric constant (ε_{RT}) (b) loss tangent ($\tan\delta_{RT}$) of Series C3 (0.05 NZF - 0.95 BSLT) as a function of frequency.

5.2.2 Temperature Dependence of ε and tanδ at Different Frequencies

The variation of dielectric constant and loss with temperature at different frequencies (1 kHz, 10 kHz and 100 kHz) for *series C1, C2* and *C3* are shown in *figure 5.10, 5.11* and *5.12* respectively. It is observed that all samples show increase in dielectric constant with increase in temperature and reaching to maximum at a particular temperature called Curie temperature of ferroelectric phase and with further increase in temperature dielectric constant decreases. This is a typical characteristic of ferroelectric materials. The increase in dielectric constant with temperature may be due to temperature dependent characteristics of domain wall motion. The dielectric loss increases with temperature for all samples this is due to increase in thermal conduction loss with temperature.

All dielectric parameters like room temperature dielectric constant (ε_{RT}), room temperature dielectric loss, dielectric constant at T_c (ε_{max}), dielectric loss at T_c, and Curie temperature for *series C1, C2* and *C3* are given in *table 5.3*. From table 5.3, it is observed that for *series C1* and *C3,* La has very prominent effect on the dielectric properties of pure ferroelectric series as well as of composite samples. T_c is observed to decrease with increase in La content because the origin of the transition from paraelectric to ferroelectric phase lies in the vibrations in the Ti-O bonds. Since the substitution of La^{3+} causes the reduction of Ti^{4+} ion to Ti^{3+} ion due to their donor nature which results in the weakening of Ti-O bonds. Thus the dielectric peak shift towards room temperature with increase in lanthanum content and thereby room temperature dielectric constant increases (table 5.3) [11-12].

From table 5.3 it is also observed that dielectric loss decreases for both series (series C1 and C3) with increase in lanthanum content. The decrease in dielectric loss can be understood as follows: The electron transport by hopping between Ti^{4+} and Ti^{3+} is one of the major factors of conduction loss. As La^{3+} substitutes for the A-site acts as a donor additive and vacancies for Ba- site will be produced. These Ba-sites vacancy and donor nature of La^{3+} results in the reduction of Ti^{4+} ions into Ti^{3+} ions.

From *figure 5.10* it is also observed that width of the dielectric peak increases with increase in La content, which is a characteristic of diffused phase transition. This diffusion is due to the compositional fluctuations and structural disordering in the arrangement of cations , which results in microscopic inhomogeneity in the samples with local Curie points [13]. It is also observed that value of dielectric constant is less for *series C3* as compared to pure ferroelectric series (series C1) this is due to the presence of ferrite phase which dilute the ferroelectric nature of the samples. From *table 5.3* for *series C2*, it is observed that the values of dielectric parameters are strongly dependent on the content of individual phases also. The decrease in dielectric constant and broadness of the peak originate from the incorporation of non-ferroelectric phase in pure ferroelectric phase and detailed reasoning is already discussed in previous chapters. If we compare the dielectric property of series A (unsubstituted series), series B2 (Zr substituted) and series C2 (La substituted) it is found that composite samples having La substituted ferroelectric phase (series C2) shows improved dielectric properties as compared to other series.

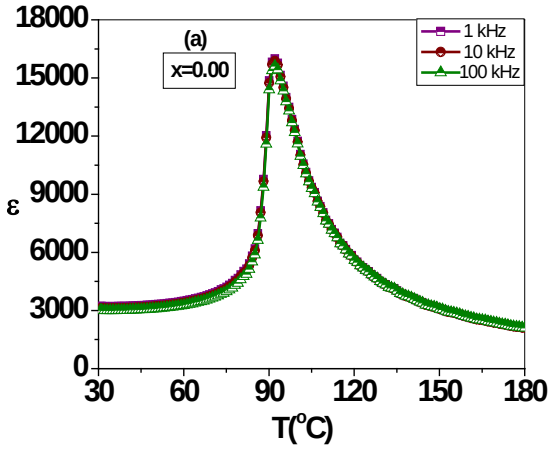
(a)
x=0.00
1 kHz
10 kHz
100 kHz
ε
T(°C)

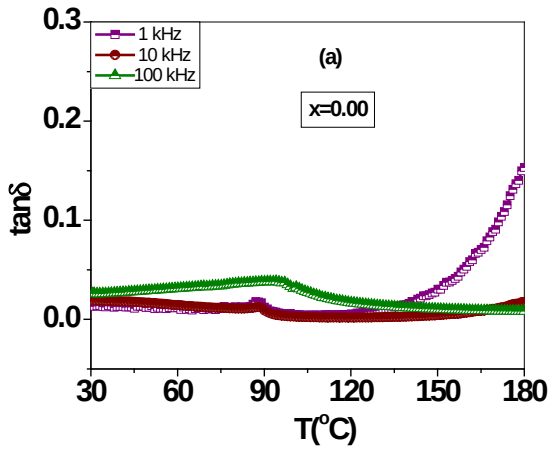
(a)
x=0.00
1 kHz
10 kHz
100 kHz
tanδ
T(°C)

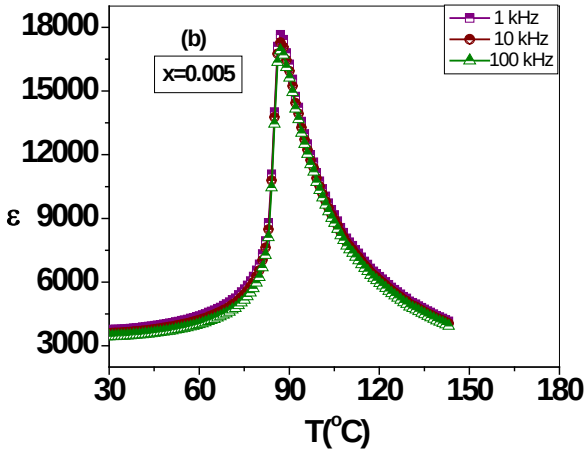
(b)
x=0.005
1 kHz
10 kHz
100 kHz
ε
T(°C)

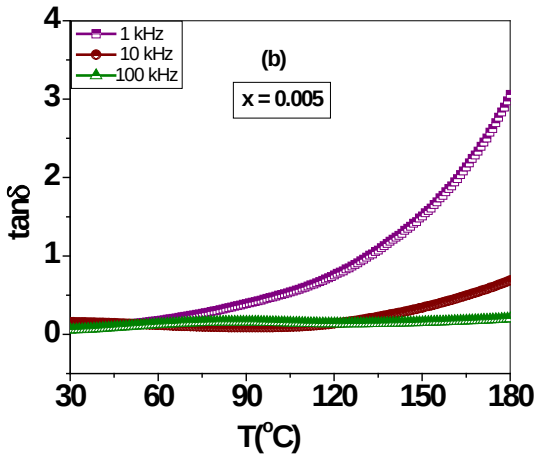
(b)
x = 0.005
1 kHz
10 kHz
100 kHz
tanδ
T(°C)

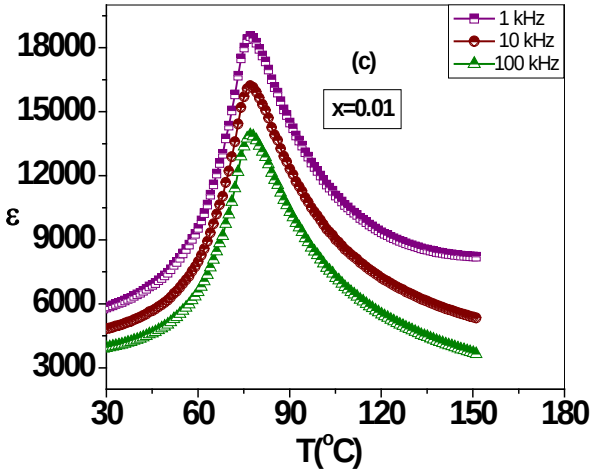
(c)
x=0.01
1 kHz
10 kHz
100 kHz
ε
T(°C)

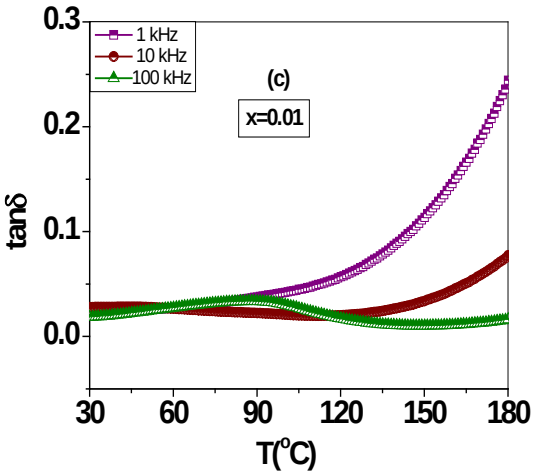
(c)
x=0.01
1 kHz
10 kHz
100 kHz
tanδ
T(°C)

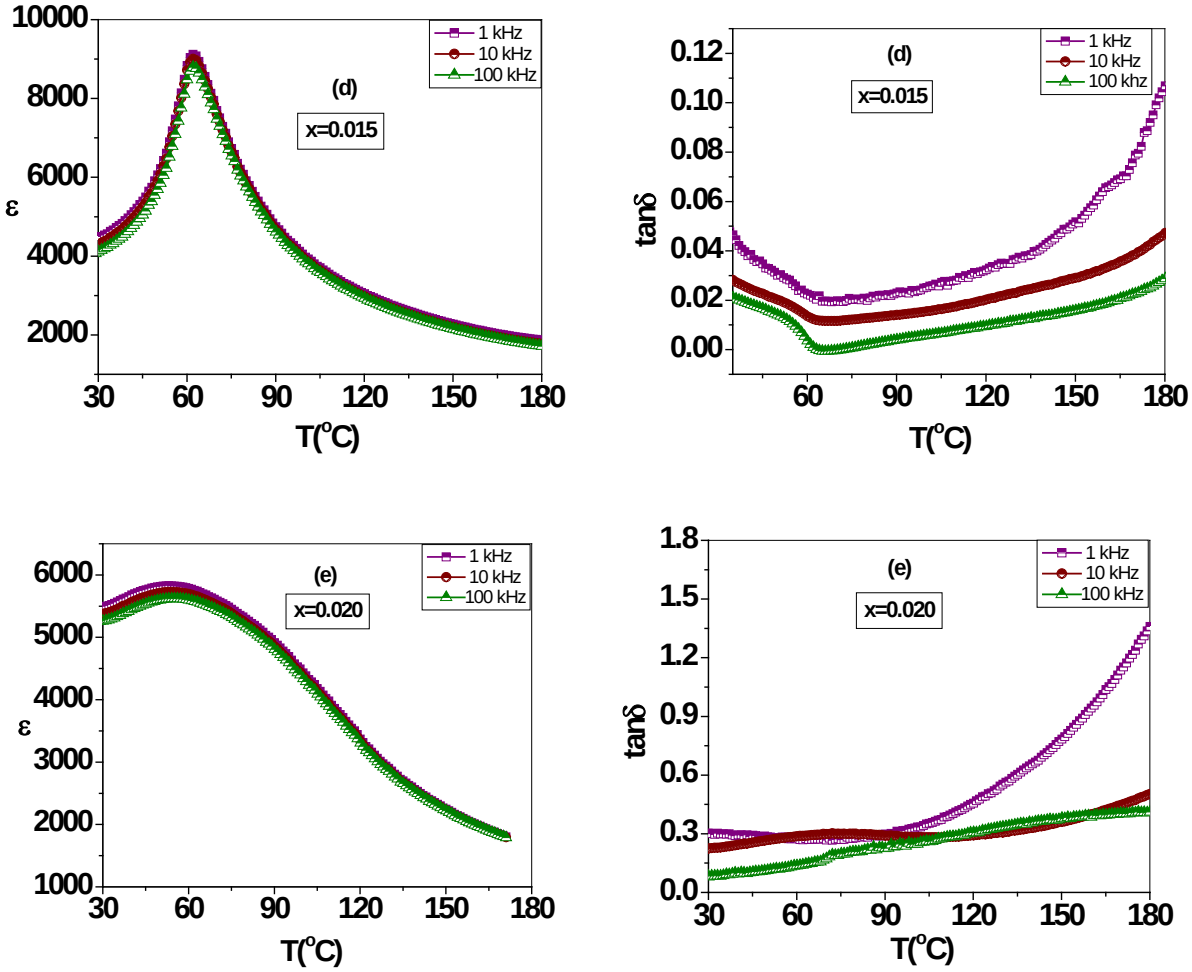

Figure 5.10 Temperature variation of ε and tanδ at different frequencies for **series C1** (BSLT)

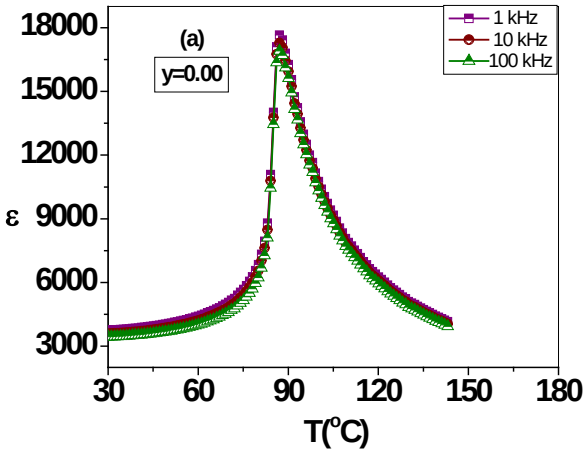
(a)
y=0.00
1 kHz
10 kHz
100 kHz
ε
T(°C)

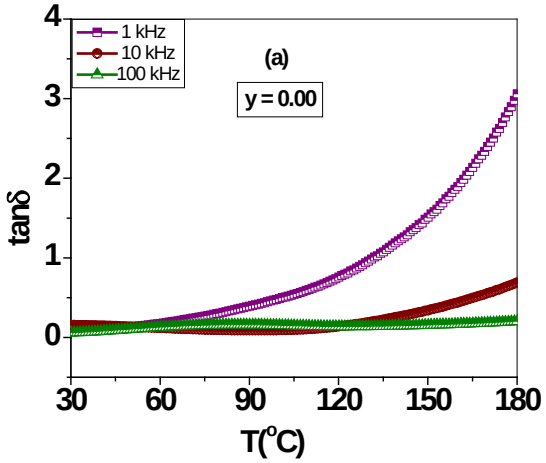
(a)
y = 0.00
1 kHz
10 kHz
100 kHz
tanδ
T(°C)

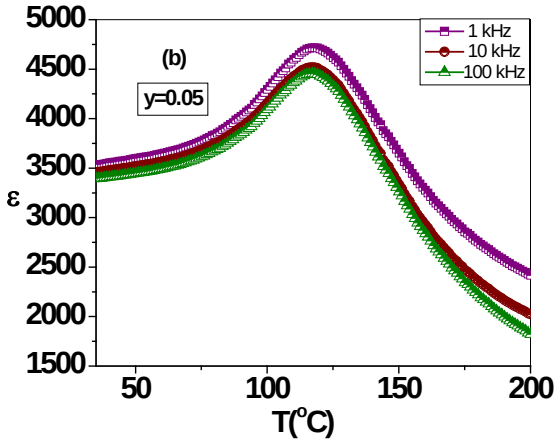
(b)
y=0.05
1 kHz
10 kHz
100 kHz
ε
T(°C)

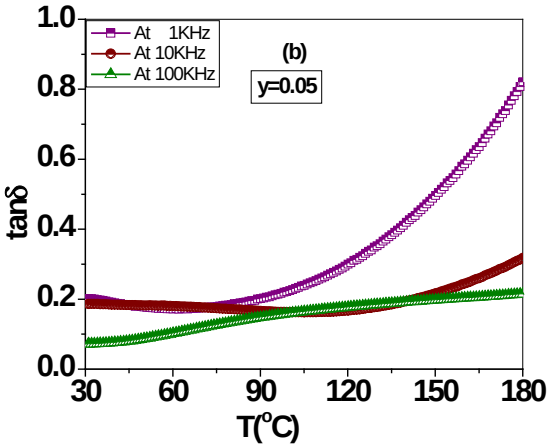
(b)
y=0.05
At 1KHz
At 10KHz
At 100KHz
tanδ
T(°C)

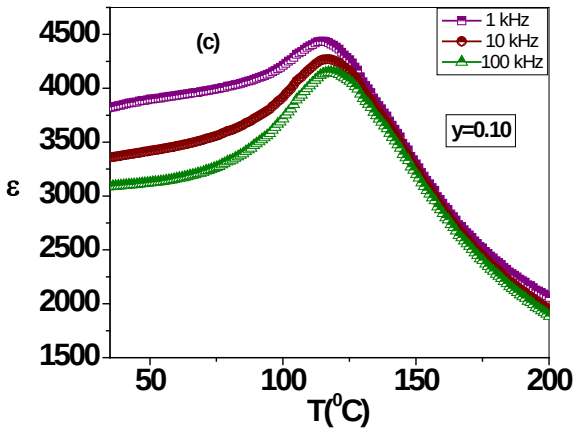
(c)
y=0.10
1 kHz
10 kHz
100 kHz
ε
T(°C)

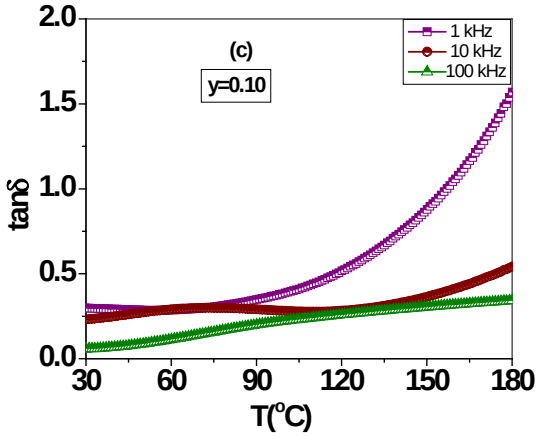
(c)
y=0.10
1 kHz
10 kHz
100 kHz
tanδ
T(°C)

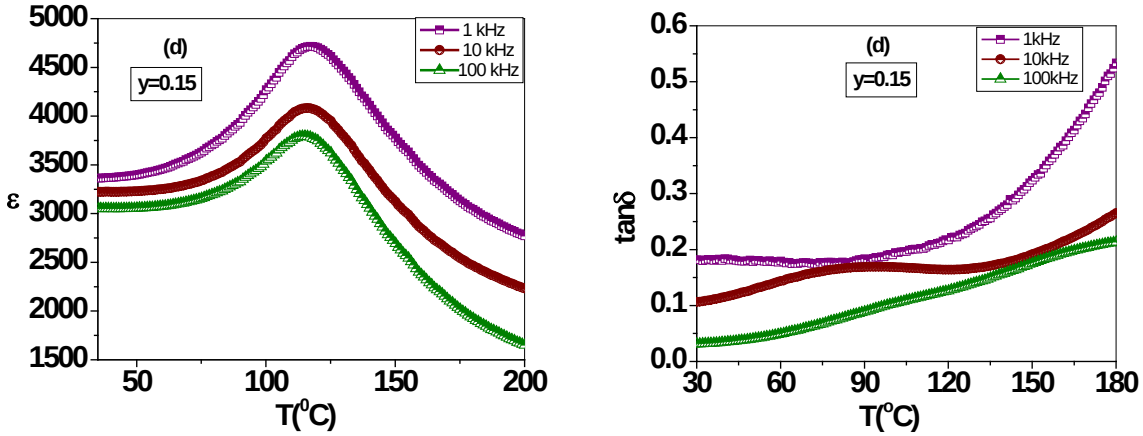

Figure 5.11 Temperature variation of ε and tanδ at different frequencies for **series C2** ((y) NZF- (1-y) BSLT)

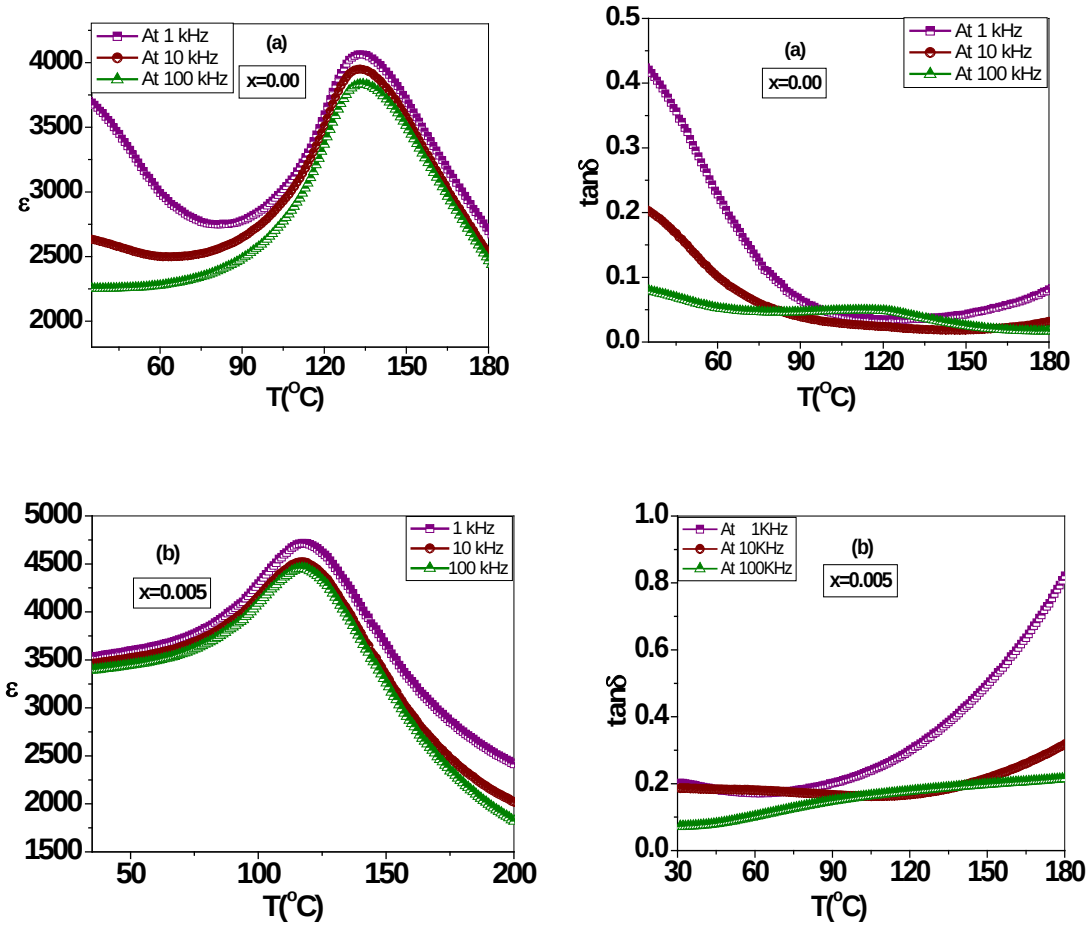

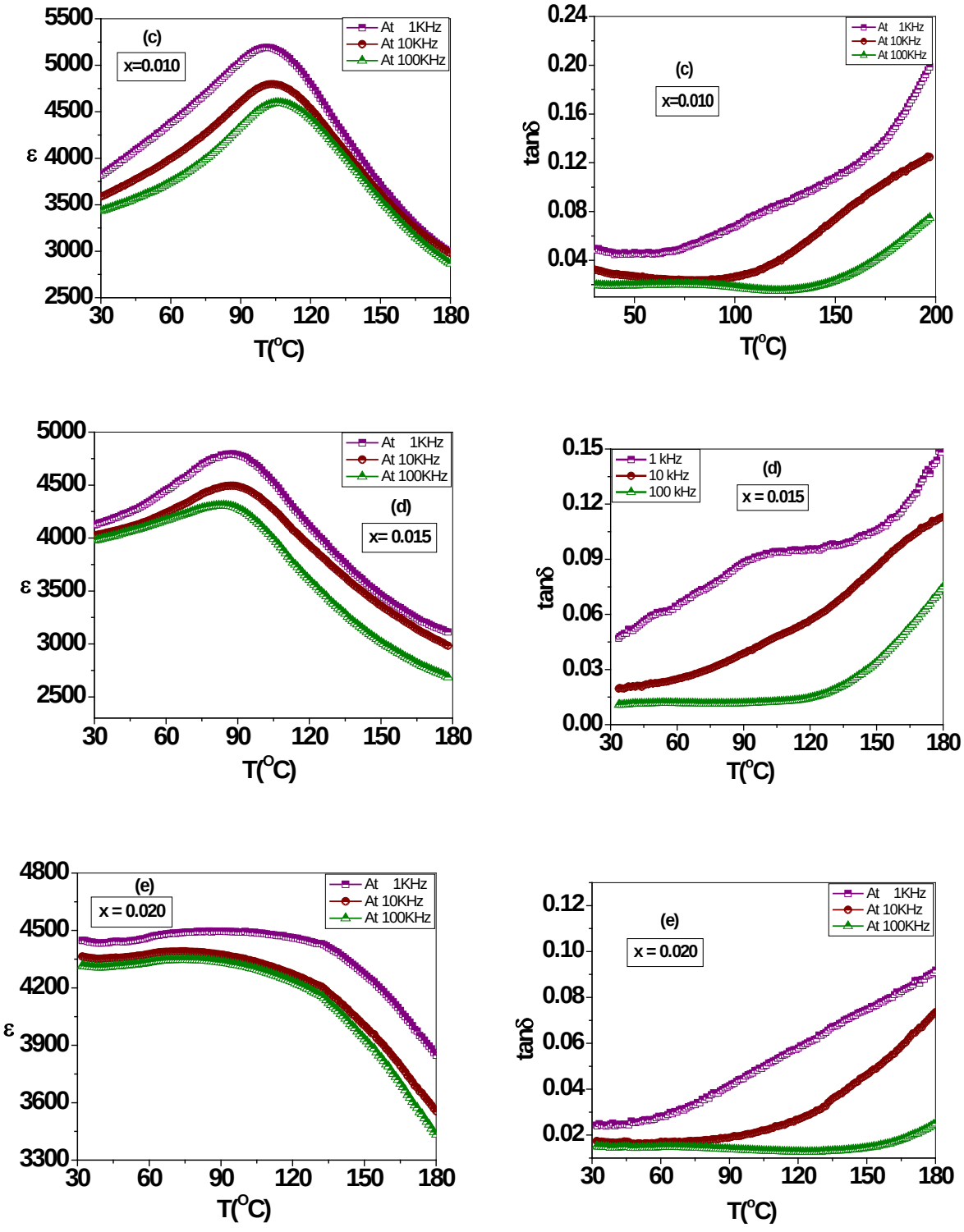

Figure 5.12 Temperature variation of ε at different frequencies for **series C3**

(0.05 NZF - 0.95 BSLT)

Table 5.3

Dielectric parameters for all series samples at 100 kHz

Series C1 (BSLT)						**Series C2 (NZF- BSLT)**						**Series C3 (0.05NZF-0.95BSLT)**					
x	**ε_{RT}**	**$\tan\delta_{RT}$**	**ε_{max}**	**$\tan\delta_{max}$**	**T_c (^oC)**	**y**	**ε_{RT}**	**$\tan\delta_{RT}$**	**ε_{max}**	**$\tan\delta_{max}$**	**T_c (^oC)**	**x**	**ε_{RT}**	**$\tan\delta_{RT}$**	**ε_{max}**	**$\tan\delta_{max}$**	**T_c (^oC)**
0	3011	0.026	15890	0.182	92	0.00	3444	0.06	16703	0.032	88	0	2254	0.081	3834	0.046	134
0.005	3444	0.06	16703	0.160	88	0.05	3395	0.072	4455	0.170	117	0.005	3395	0.072	4455	0.17	117
0.010	3936	0.018	13904	0.032	77	0.10	3084	0.057	4146	0.261	119	0.010	3441	0.019	4598	0.016	106
0.015	4113	0.023	8793	0.021	62	0.15	3053	0.031	3794	0.121	115	0.015	3992	0.010	4309	0.015	84
0.020	5262	0.030	5623	0.018	55	--	--	--	--	--	--	0.020	4314	0.015	4346	0.020	70

5.3 Electrical Conductivity

Figure 5.13 shows the variation of ac conductivity with frequency for all series samples. From figures it is clear that conductivity increases linearly with increase in frequency for all the samples. The results are similar to the one observed by other workers [14-15]. It is also observed that conductivity of composite samples is high as compared to pure ferroelectric phase that is due to the presence of ferrite phase. For the present system plots are linear confirming small polarons type of conduction.

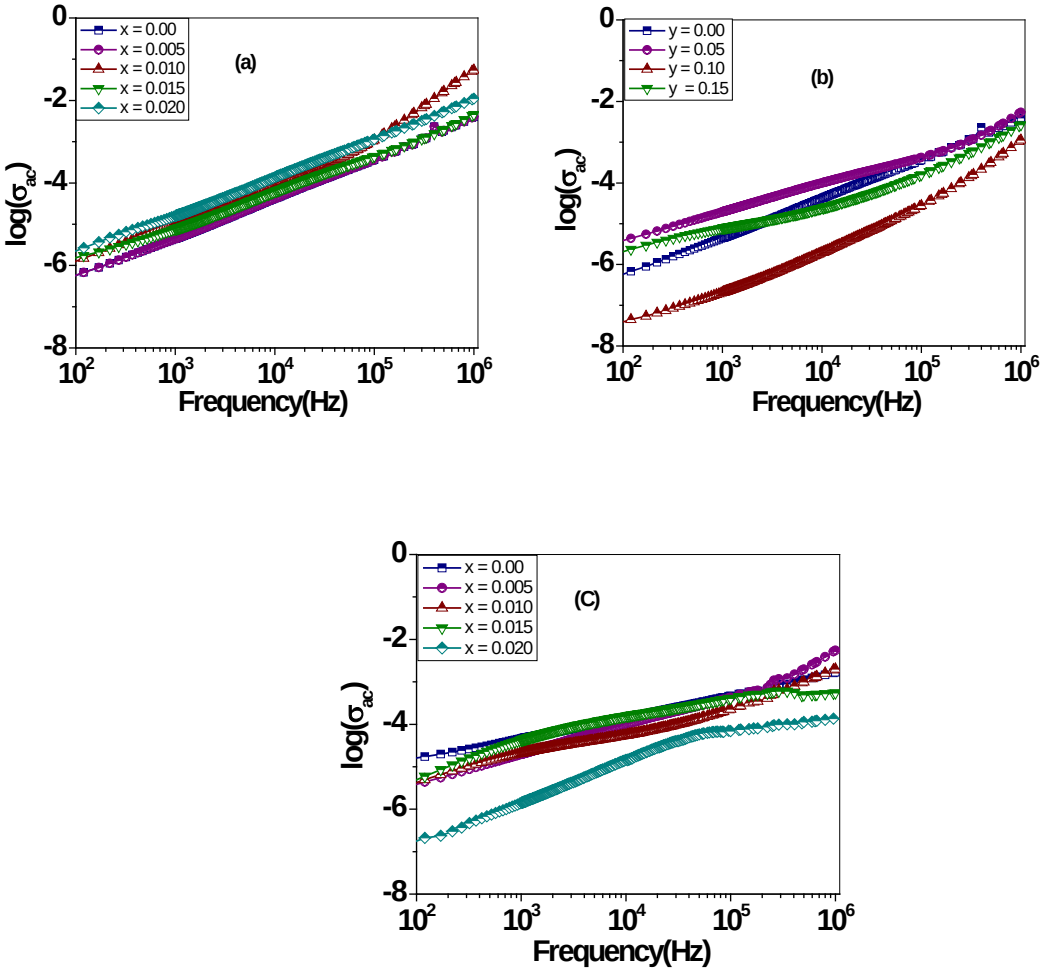

Figure 5.13 Variation of ac conductivity with frequency for (a) series C1, (b) series C2 and (c) series C3 samples

5.4 Ferroelectric Properties

To study ferroelectric properties P-E hysteresis loops were recorded for all series samples. P-E hysteresis loops of *series C1, C2* and *C3* are shown in *figure 5.14, 5.15* and *5.16* respectively. The value of coercive field (E_c), remanant polarization (P_r) and spontaneous polarization (P_s) were determined from the P-E loops for all samples and are given in *table 5.4*.

From *table 5.4* for series C1, it is observed that coercive field (E_c), and spontaneous polarization (P_s) decreases with increase in La content. The decrease in coercive field (E_c) with increase in La content is an evidence of the donor nature of La^{3+} ions at Ba sites. The reduction in tetragonality is also responsible to the decrease in E_c . But the value of spontaneous polarization increases up to x = 0.005 and after that decreases with further increase in La. This trend can be attributed to the fact that La substitution resulted in enhanced dipole moment up to x = 0.005 and beyond that grain size plays its role as smaller polarization exist in finer grains. The similar trend is observed for *series C3* but the value of polarization is less as compared to pure series (*series C1*) that may be due to the presence of ferrite phase.

From *table 5.4* it is also observed that values of P_r and P_s decrease with increase in ferrite content for series C2 and from *figure 5.15* it can also be seen that hysteresis loops become more unsaturated with increasing ferrite content. The decrease in polarization with addition of ferrite content can also be related to the increase in conductivity of the samples which results in leakage of current [16-17]. The reasoning for this in detail has already been discussed in chapter 4 but it is found that composite samples having La substituted ferroelectric phase shows improved ferroelectric properties as compared to *series A* (unsubstituted series) and *series B2* (Zr substituted series).

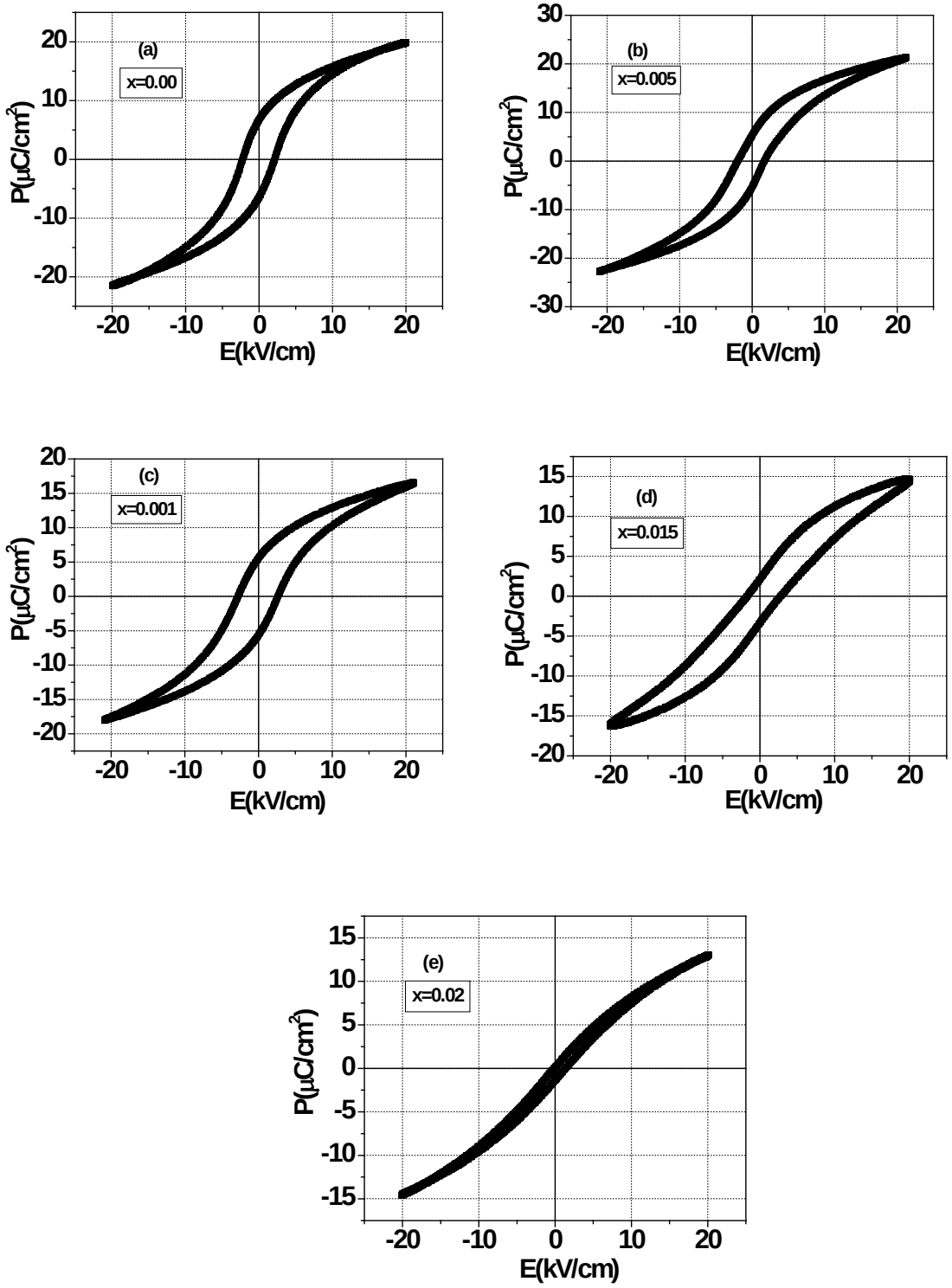

Figure 5.14 Polarization vs electric field (P-E) hysteresis loops for **Series C1** (BSLT)

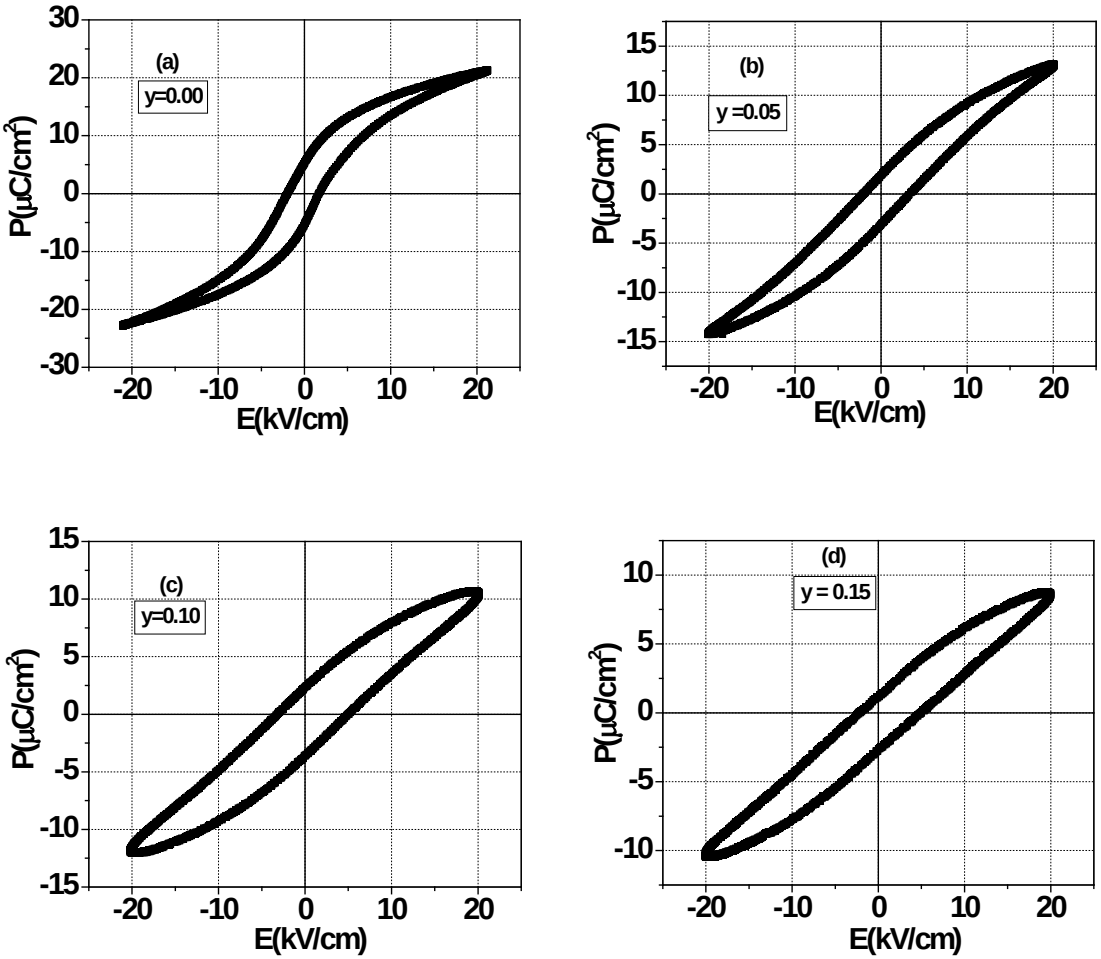

Figure 5.15 Polarization vs electric field (P-E) hysteresis loop for **series C2** ((y)NZF- (1-y)BSLT)

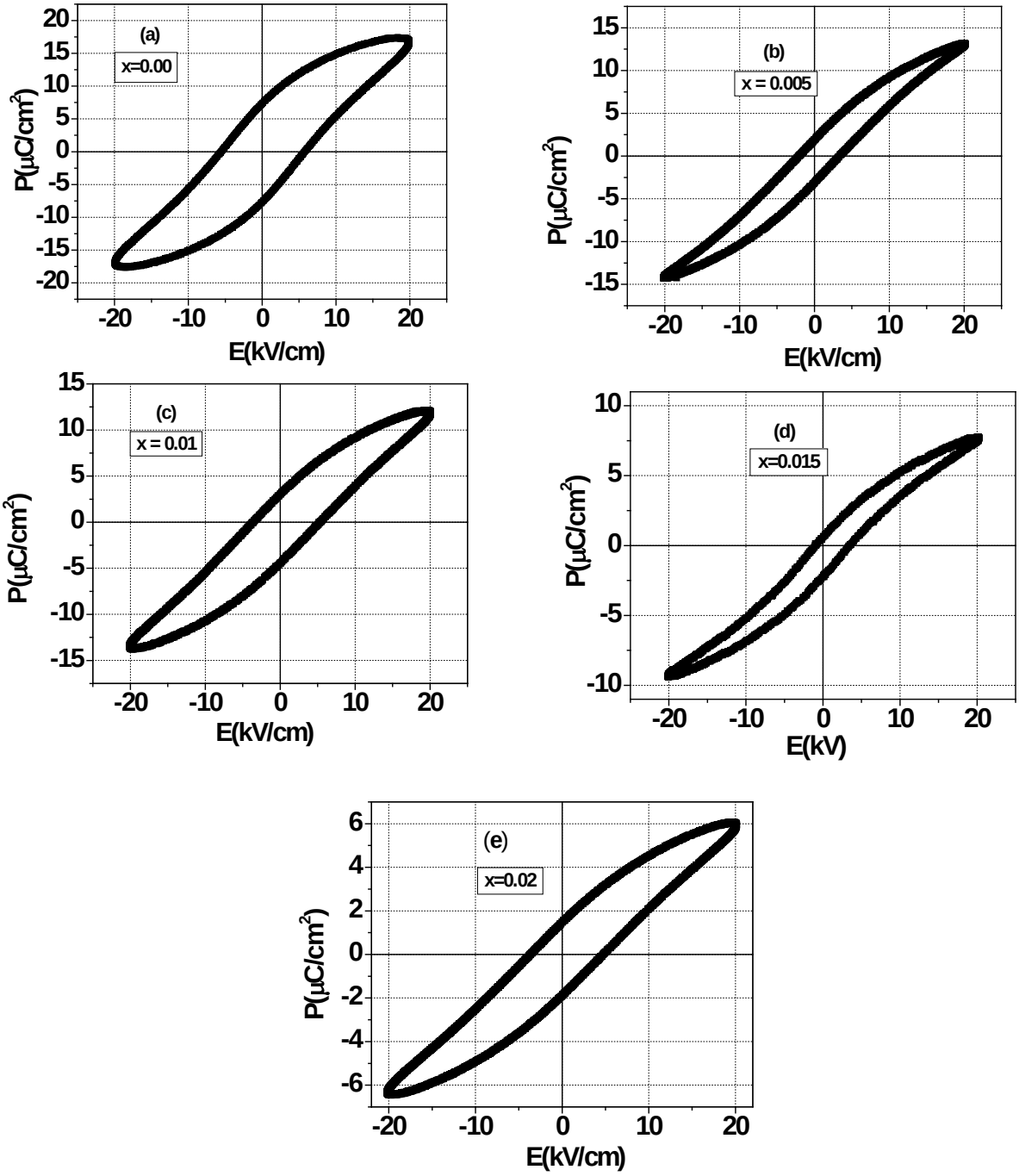

Figure 5.16 Polarization vs electric field (P-E) hysteresis loops of **series C3** (0.05 NZF + 0.95BSLT)

Table 5.4

Ferroelectric parameters for all series samples

Series C1 (BSLT)				Series C2 (NZF - BSLT)				Series C3 (0.05 NZF + 0.95 BSLT)			
x	**P_r ($\mu C/cm^2$)**	**E_c (kV/cm)**	**P_{max} ($\mu C/cm^2$)**	**y**	**P_r ($\mu C/cm^2$)**	**E_c (kV/cm)**	**P_{max} ($\mu C/cm^2$)**	**x**	**P_r ($\mu C/cm^2$)**	**E_c (kV/cm)**	**P_{max} ($\mu C/cm^2$)**
0.0	6.558	2.192	20.74	0.00	5.304	1.831	22.06	0.0	7.70	7.8	16.00
0.005	6.304	1.831	22.06	0.05	2.58	2.697	13.75	0.005	2.58	2.697	13.75
0.01	3.102	1.424	17.36	0.10	2.49	3.92	11.44	0.01	4.43	3.74	12.96
0.15	2.742	1.392	15.56	0.15	1.94	3.48	9.69	0.15	2.14	1.41	8.60
0.02	1.420	0.775	13.86	-	-	-	-	0.02	4.22	1.68	6.26

5.5 Ferromagnetic Properties

In order to understand the magnetic nature of composites, M-H hysteresis loops for all composite samples were studied. The magnetic hysteresis loops for *series C2* and *C3* at room temperature are shown in *figures 5.17* and *5.18* respectively. *Series C1* does not show M-H loops due to absence of ferrite phase. The value of coercive field (H_c), remanant magnetization (M_r) and spontaneous magnetization (M_s) are determined from the M-H loops and are given in table 5.5 for all these samples.

From table 5.5 it is observed that there is increase in saturation magnetization and remanant magnetization with increase in ferrite content for *series C2*. This is due to the fact that ferrites are magnetic in nature and the number of domains contributing to magnetization increases with increase in ferrite content that result in increase of net magnetization. But the values of magnetization in composites is smaller than the pure ferrite phase because ferroelectric material incorporates in to the ferrite phase and acts as pores in the presence of applied magnetic field resulting in the decrease of these magnetic parameters [18] .

From *table 5.5* for *series C3*, it is also observed that value of saturation magnetization varies in random manner while the amount of ferrite phase is fixed that may be due to non-uniform mixing of two individual phases as discussed in chapter 4 [19].

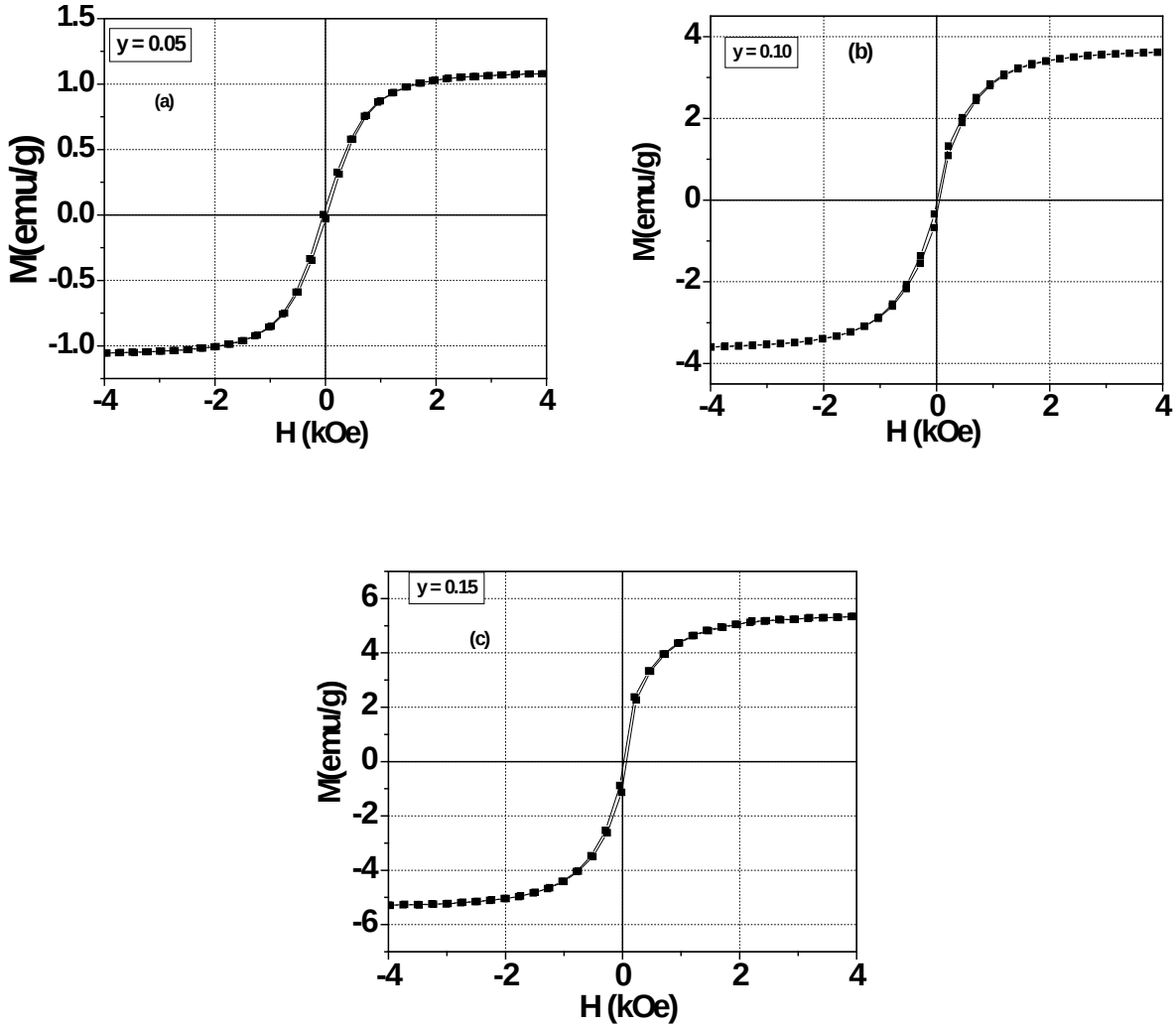

Figure 5.17 Magnetization vs Magnetic field (M-H) hysteresis loop of series C2 ((y) NZF- (1-y) BSLT) measured at room temperature

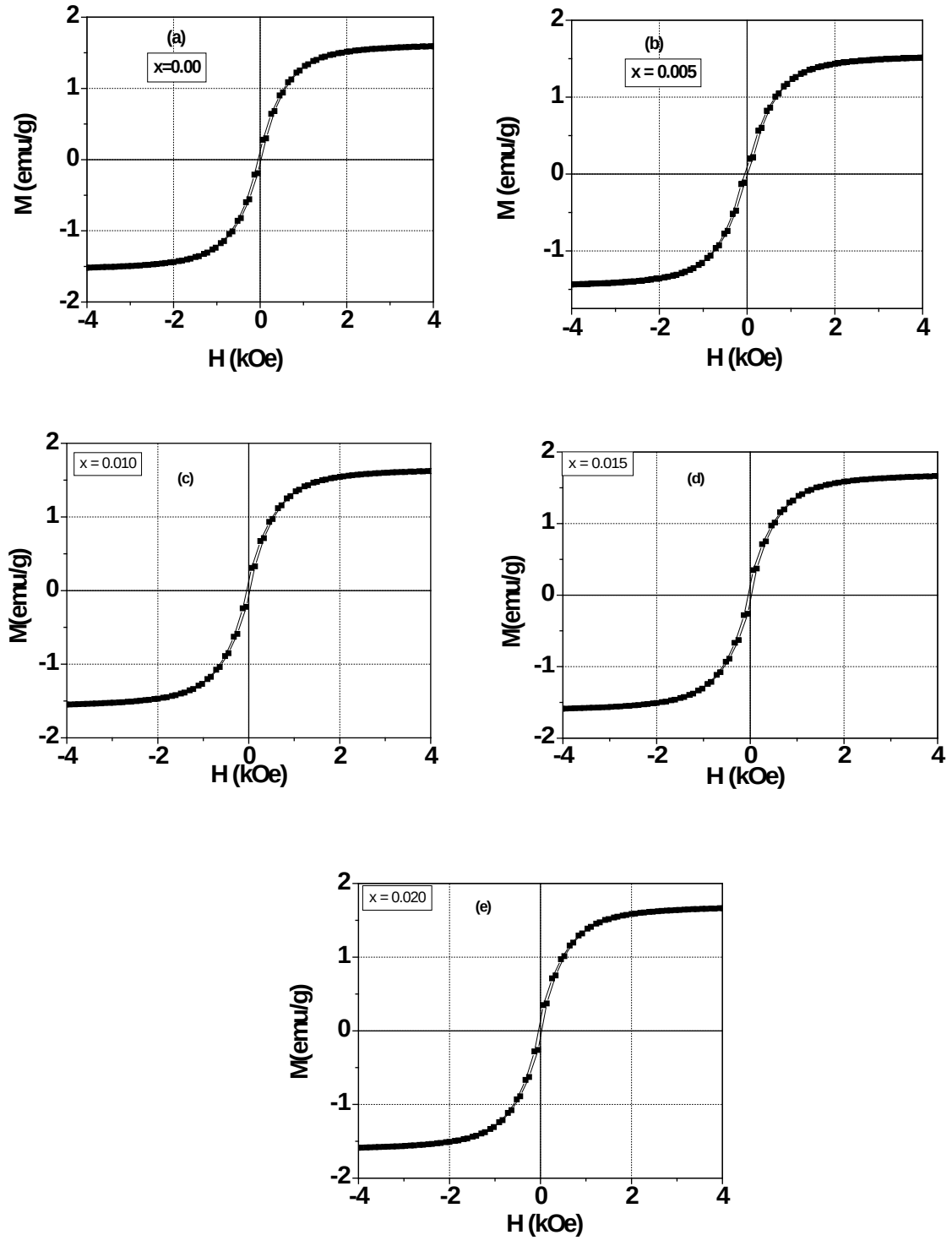

Figure 5.18 Magnetization Vs Magnetic field (M-H) hysteresis loop of **seriesC3** (0.05 NZF–0.95 BSLT) measured at room temperature

Table 5.5

Ferromagnetic parameters for all series samples

Series C2 (NZF- BSLT)				Series C3 (0.05 NZF + 0.95 BSLT)			
y	**M_r (emu/g)**	**M_s (emu/g)**	**H_c (Oe)**	**x**	**M_r (emu/g)**	**M_s (emu/g)**	**H_c (Oe)**
0.00	--	---	---	0.0	0.162	1.60	69.82
0.05	0.12	1.52	63.61	0.005	0.115	1.52	63.61
0.10	0.26	3.32	72.25	0.01	0.196	1.64	74.37
0.15	0.47	4.60	65.96	0.15	0.154	1.55	70.443
--	--	--	---	0.02	0.22	1.68	70.27

5.6 Magnetoelectric Property

Figure 5.19 shows the comparison of M-H loops for both electrically poled and unpoled samples and values of magnetic parameters for poled and unpoled samples are given in *table 5.6*. It can be observed that, there is increase in remanant magnetization and saturation magnetization for electrically poled samples which is the evidence of ME coupling.

The variation of magnetoelectric coupling coefficient as a function of dc magnetic field was also studied and shown in *figure 5.19 (b)*. From this figure it is observed that ME output goes on increasing with increase in magnetic field and after attaining a maximum value it decreases with further increase in magnetic field. The decrease in ME output with increase in magnetic field is due to the fact that after a certain value of magnetic field the magnetostriction coefficient of ferrite phase reaches its saturation value. Hence, the strain produced in the ferrite phase would produce a constant electric field in the piezoelectric phase as discussed in the previous chapters.

The value of M-E coefficient is given in *table 5.6*. From this table it is observed that the maximum value of magnetoelectric coefficient is obtained for y = 0.10 and its value is 2.4 mV/cm-Oe. The lower value of ME output for large value of ferrite content (y = 0.15) is due to

low resistivity of ferrite phase as compared to ferroelectric phase resulting in the leakage of the charges developed in the ferroelectric grains due to the presence of conductive ferrite grains [20].

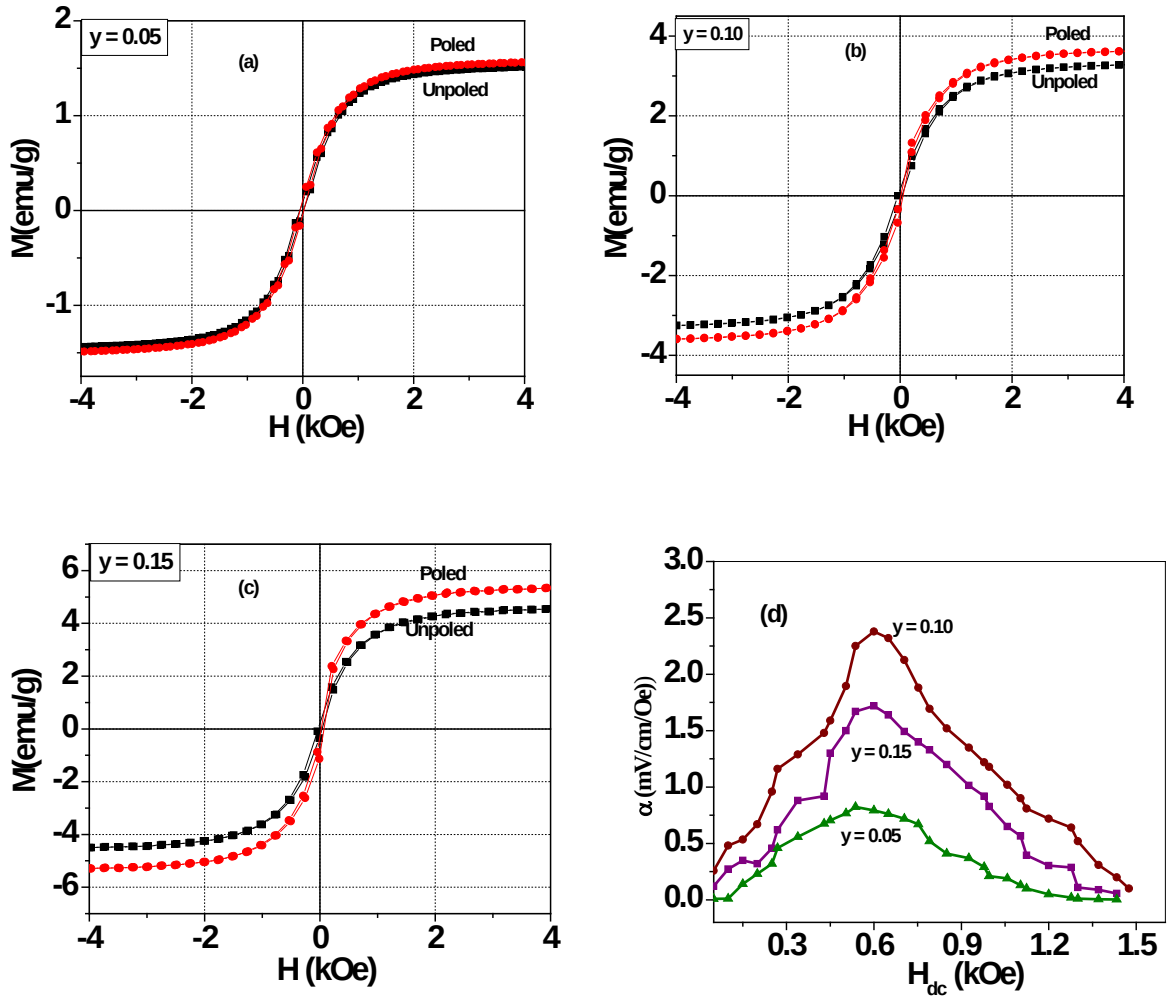

Figure 5.19 M-H hysteresis loop of **series C2** ((y)NZF- (1-y)BSLT) for poled and unpoled samples (a) y = 0.05, (b) 0.10 (c) 0.15 and (d) Variation of ME coefficient with magnetic field at room temperature

Table 5.6

Magnetic parameters of poled and un-poled samples and magnetoelectric coefficient for series C2.

	Unpoled samples			Poled samples			ME coefficiet (mV/cm-Oe)
y	M_r (emu/g)	M_s (emu/g)	H_c (Oe)	M_r (emu/g)	M_s (emu/g)	H_c (Oe)	
0.05	0.12	1.52	63.61	0.16	1.57	62.6	0.7
0.10	0.26	3.32	72.25	0.32	3.66	78.34	2.4
0.15	0.47	4.60	65.96	0.53	5.4	64.32	1.6

Refrences

1) A.S. Fawzi, A.D. Sheikh and V.L. Mathe, Phys B, **405** (2010) 340.
2) J.C. Maxwell, Electricity and Magnetism, Oxford University Press, London (1973).
3) K.W. Wagner, Ann. Phys., **40** (1993) 818.
4) C.G. Koops, Phys. Rev., **83** (1951) 121.
5) S. Upadhyaya, D. Kumar and Om Prakash, Bull. Mater. Sci., **19** (1996) 513.
6) C.M. Kanamadi, L.B. Pujari and B.K. Chougule, J. Magn. Magn. Mater., **295** (2005) 139.
7) N. Ponpandian, P. Balay and A. Narayanasamy, J. Phys. Conds. Matter., **14** (2002) 3221.
8) M.B. Kothale, K.K. Patankar, S.L. Kadam, V.L. Mathe, A.V. Rao and B.K. Chougule,, Mater. Chem. Phys., **77** (2002) 691.
9) K.K. Patankar, S.L. Kadam, V.L. Mathe, C.M. Kanamadi, V.P. Kothavale and B.K. Chougule, Br. Ceram. Trans., **102** (2003) 19.
10) K.K. Patankar, S.A. Patil, K.V. Sivakumar, R.P. Mahajan, Y.D. Kolekar and M.B. Kothale, Mater. Chem. Phys., **65** (2000) 97.
11) Y.L. Li and Y.F. Qu, Mater. Chem. Phys., **110** (2008) 157.
12) P. Kumar, S. Singh, J.K. Juneja, C. Prakash and K.K. Raina, Modern Phys. Lett. B, **23** (2009) 3419.
13) K. Prasad, Indian J. Engg. Mater. Sci., **7** (2000) 446.
14) K.K. Patankar, V.L. Mathe, R.P. Mahajan, S.A. Patil, Ram Manohar Reddy and K.V. Siva Kumar, Mater. Chem. Phys., **72** (2001) 23.
15) R.P. Mahjan, K.K. Patankar, M.B. Kothale and S.A. Patil, Bull. Mater. Sci., **23** (2000) 273.
16) K. Pandey, N. Singh and S.K. Mishra, J. Pure Appl. Phys., **32** (1994) 616.
17) K.K. Patankar, S.S. Joshi and B.K. Choughle, Phys. Letter A, **346** (2005) 337.
18) R.S. Devan and B.K. Chougule, J. Appl. Phys., **101** (2007) 0141091.
19) S. Narender Babu, S.V. Suryanarayana and T. Bhimasankaram, J. Alloys Compd., **473** (2009) 418.
20) A. Hanumaian, T. Bhimasankaram, S.V. Suryanarayan and G. Kumar, Bull. Mater. Sci., **17** (1994) 405.

Chapter - VI

Synthesis and Characterizations of Microwave Sintered NZF – BSZT Composites

Chapter VI

Synthesis and Characterizations of Microwave Sintered NZF – BSZT Composites

Microwave processing is an innovative technique in the field of ceramic processing and material synthesis. Sintering of ceramic materials by microwave has been studied by many researchers [1-5] and is reported to be superior as compared to the conventional sintering. The reason may be attributed to a different heating mechanism in microwave sintering. During microwave processing, heat is generated internally within the material instead of originating from external sources and hence there is an inverse heating profile as compared to conventional sintering or we can say in the microwave sintering material is heated by energy conversion rather than the energy transfer so the heating is very rapid and uniform.

The difference in energy transfer mechanism is found to be advantageous for processing of materials through microwave technique and thus heat can be generated throughout the volume of the material therefore there is always a great potential to reduce processing time and enhance overall quality as compared to conventional heating. In addition to volumetric heating, energy transfer at a molecular level may have some additional advantages [6-9].

In the present chapter, composites of (y) $Ni_{0.8}Zn_{0.2}Fe_2O_4$ + (1-y) $Ba_{0.9}Sr_{0.1}Zr_{0.04}Ti_{0.96}O_3$ (where y = 0.00, 0.05, 0.10, 0.15 and 1.00 wt%) *(Series D)* were prepared by using microwave sintering (MWS). The samples were sintered at 1325^{o}C for 20 mins., and the sintered samples were characterized for their structural, dielectric, ferroelectric, ferromagnetic and magnetoelectric properties. The properties of same composites series prepared by conventional

sintering have already been discussed in *chapter 4 (Series B2*). Comparison of the properties of conventional and microwave sintered samples are also discussed in this chapter. *Figure 6.1* shows the comparison of sintering time profile for conventional and microwave sintering and it is observed that processing time in case of microwave sintering is very short as compared to conventional sintering.

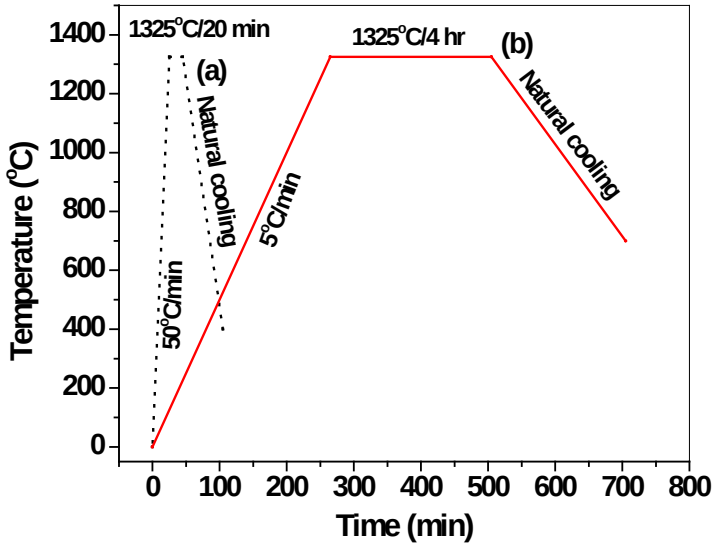

Figure 6.1 Sintering schedule of (a) microwave and (b) conventional sintering

6.1 Structural Properties

6.1(a) XRD

Figure 6.2 shows the XRD patterns of individual phases i.e. ferroelectric (y = 0.00) and ferrite phase (y =1.00) and their composites with y = 0.05, 0.10 and 0.15 prepared by microwave sintering. XRD patterns of composite samples exhibit the characteristic peaks of both phases i.e. (110) for ferroelectric phase and (311) for ferrite phase and hence confirms the presence of both phases. For all samples, all peaks were indexed and no extra peak was observed hence it is clear that no chemical reaction took place between two phases and they maintained proper stoichiometry. From XRD patterns it is also clear that there is increase in the intensity and

number of ferrite peaks with increase in ferrite content (y) indicating that present composite system follows the rule of mixture as in case of conventional sintered samples discussed in chapter 4 (*Series B2*). The calculated values of lattice parameters for all the samples are given in *table 6.1*. It is observed that in case of composites sample there is a very slight change in the lattice parameter of ferroelectric and ferrite phase. This change may be due to stress exerted on each other by two phases [10].

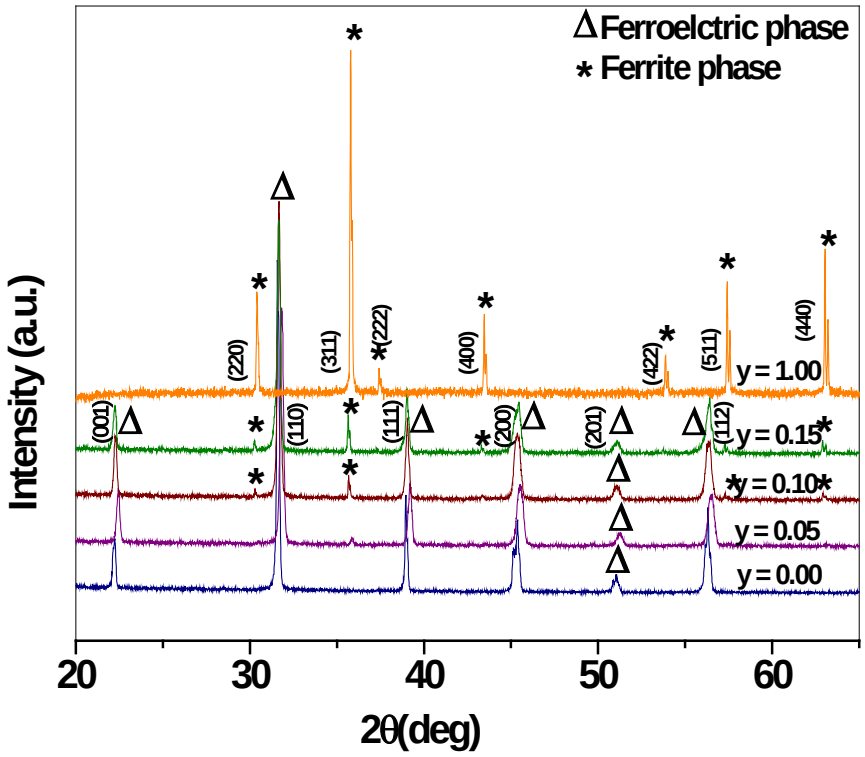

Figure 6.2 XRD patterns for different values of y

6.1(b) Scanning Electron Microscope (SEM)

Figure 6.3 shows the comparison of SEM micrographs of freshly broken surfaces of microwave sintered and conventional sintered samples. From this figure it is observed that samples prepared by using microwave sintering technique are more homogeneous and dense as

compared to the conventional sintered sample. It is also observed that grain size in microwave sintered samples is small as compared to conventional sintered sample and this may be due to the faster heating and cooling rates in the microwave sintering process. The calculated values of average grain size and experimental density of microwave and conventional sintered samples are given in *table 6.1*. From table it is observed that, a higher value of experimental density is observed in case of microwave sintered samples as compared to the density of similar compositions sintered by conventional furnace. Hence larger densification can be achieved in short interval of time by microwave sintering.

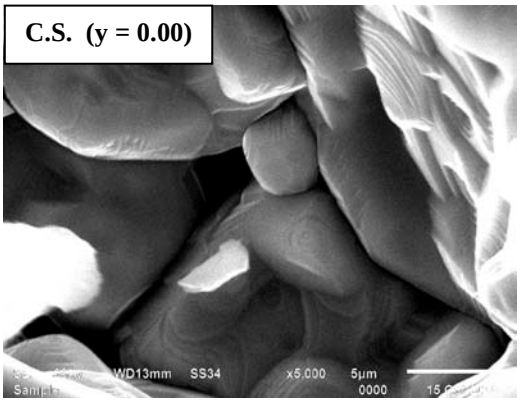

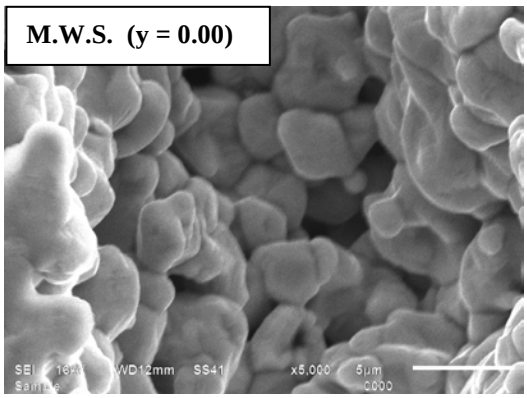

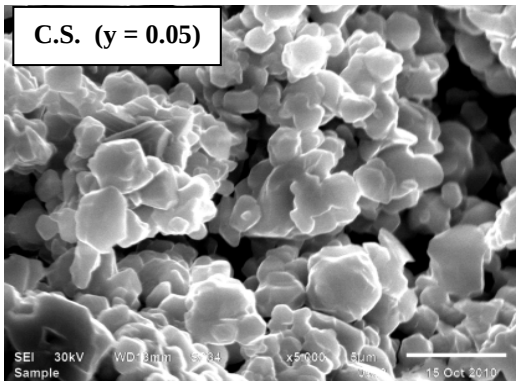

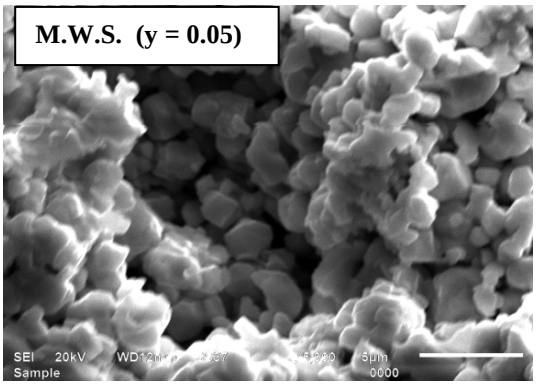

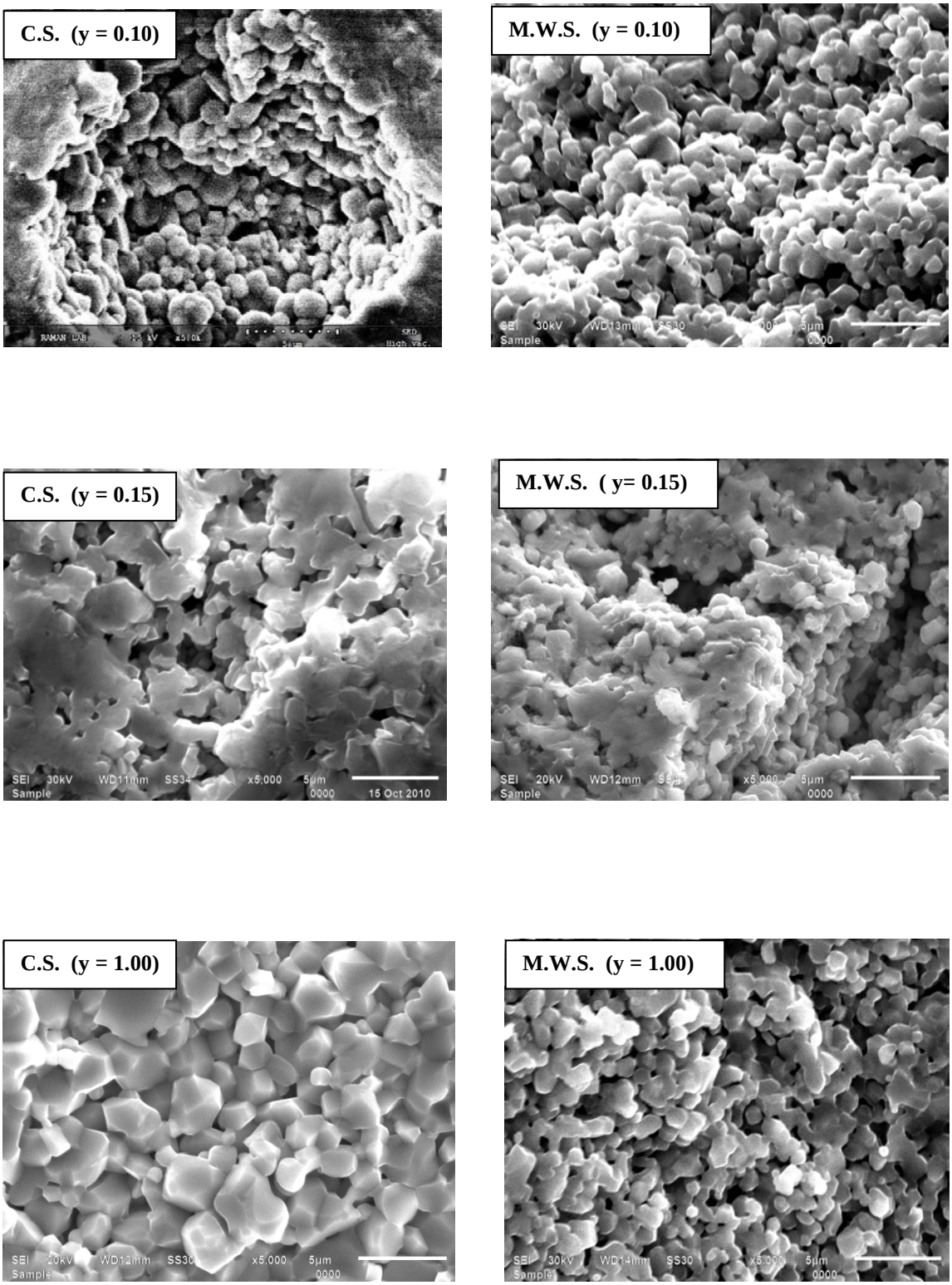

Figure 6.3 Comparison of SEM micrographs of conventional and microwave sintered (1-y) BSZT- (y) NZF composite samples

Table 6.1

Structural parameters of (1-y) BSZT- (y) NZF (Series D)

y	d_{exp} (g/cc) CS	d_{exp} (g/cc) MWS	Ferroelectric			Ferrite a (Å)	Avg. grain size (μm)
			a(Å)	c(Å)	c/a		
0.00	5.28	5.82	3.98	4.00	1.005	-	3.03
0.05	5.13	5.38	3.98	4.01	1.007	8.33	2.19
0.10	4.97	5.31	3.98	4.00	1.005	8.34	1.46
0.15	5.18	5.34	3.98	4.01	1.007	8.34	1.35
1.00	4.93	5.02	_	_	_	8.33	1.40

6.2 Dielectric Properties

6.2.1 Variation of ε and tanδ with Frequency

Figure 6.4(a-b) shows the variation of dielectric constant (ε) and dielectric loss (tanδ) with frequency for all microwave sintered samples at room temperature. Inset of figure 6.4 (b) shows the variation of dielectric loss with frequency for y = 1.00. The value of dielectric constant decreases with increase in frequency because in a dielectric material, polarization occurs due to contributions of electronic, ionic, dipolar and space charge polarization as the frequency increases, contribution of different polarization decreases and only electronic polarization contributes at higher frequencies so the dielectric constant is found to decrease with increase in frequency for all samples [11]. It is also observed that room temperature dielectric constant decreases with addition of ferrite phase. This behavior of dielectric constant with frequency for all microwave sintered samples is same as that of conventional sintered samples and can be explained on the same lines as discussed in *chapter 4* in *section 4.2.1* for *series B2*.

6.2.2 Temperature Dependence of ε at Different Frequencies

The temperature dependence of dielectric constant at three different frequencies (1 kHz, 10 kHz and 100 kHz) for all microwave sintered composite samples is shown in *figure 6.5*. From this figure it is observed that, all samples exhibit similar temperature dependence of dielectric constant as those prepared by conventional sintering process *(figure 4.11)*. For all samples dielectric constant increases with increase in temperature and shows a peak at a particular temperature called Curie temperature (T_c), which is a characteristic of ferroelectric behavior. From this figure it is also observed that with the increase in ferrite contents dielectric peaks get broadened and dielectric maxima decreases (values are given in table 1). For y =1.00 the dielectric constant increases continuously which is characteristics of pure ferrite phase. The incorporation of non-ferroelectric phase in the pure ferroelectric phase dilutes the ferroelectric properties of the composites, resulting in the reduction of the dielectric constant and broadening of the peak. The broadening of peak may also be due to microscopic heterogeneity in the composites [12-13].

Comparison of all dielectric parameters like room temperature dielectric constant (ε_{RT}), dielectric loss ($\tan\delta_{RT}$), dielectric constant at T_c (ε_{max}) and dielectric loss at T_c of conventional sintered and microwave sintered samples are given in *table 6.2*. From this table it is observed that, with microwave sintering we get comparable dielectric constant to the conventional sintered samples but there is a decrease in dielectric loss in microwave sintered samples as compared to the conventional sintered samples which may be attributed to the low porosity and dense microstructure in the case of MWS ceramic samples. Hence we get samples with low loss and comparable dielectric constant in a short sintering time by using microwave. But it is also observed that for y = 1.00 there is large difference in value of dielectric constant that may be due to the presence of large amount of Fe^{2+} ions in conventional sintered samples as compared to microwave sintered samples and the presence of Fe^{2+} ion in ferrite material always contributes to high dielectric constant. The rapid and enhanced reaction process in microwave

sintering may have given less opportunity for material loss and reducing the chance for formation of Fe^{2+}.

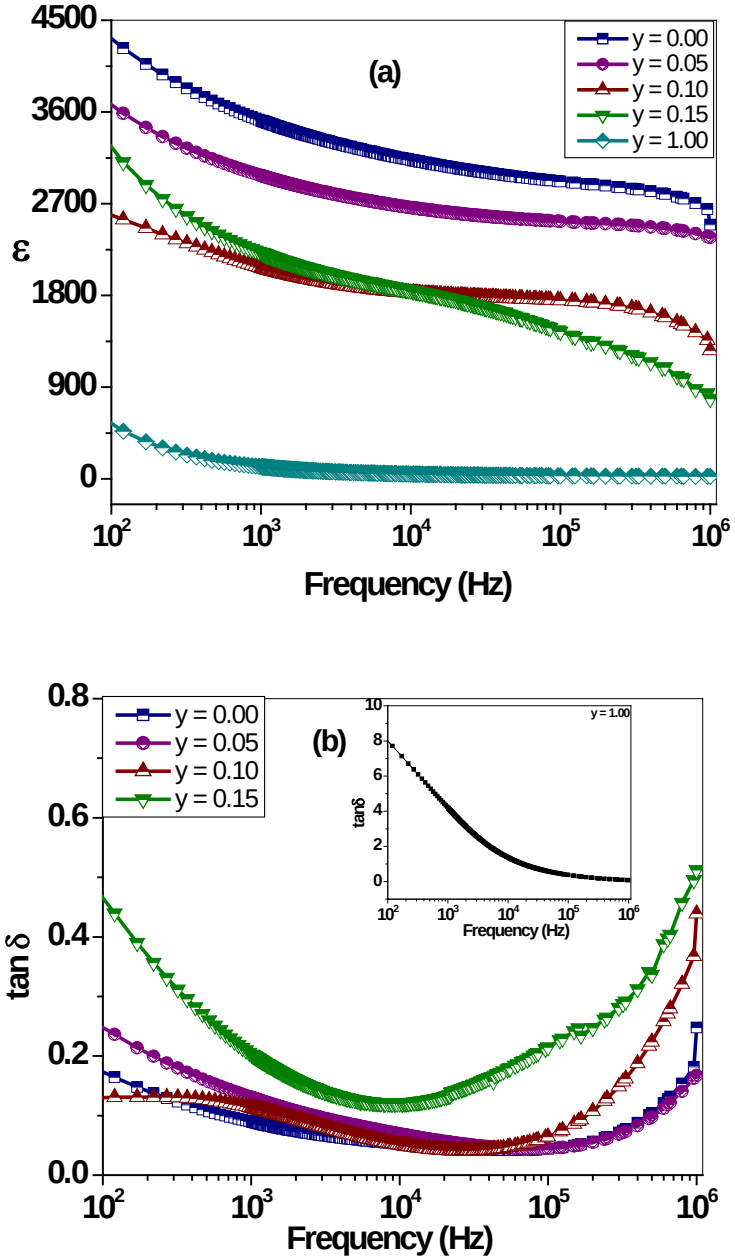

Figure 6.4 Variation of (a) dielectric constant and (b) dielectric loss as a function of frequency at room temperature of (1-y) BSZT- (y) NZF composites prepared by microwave sintering

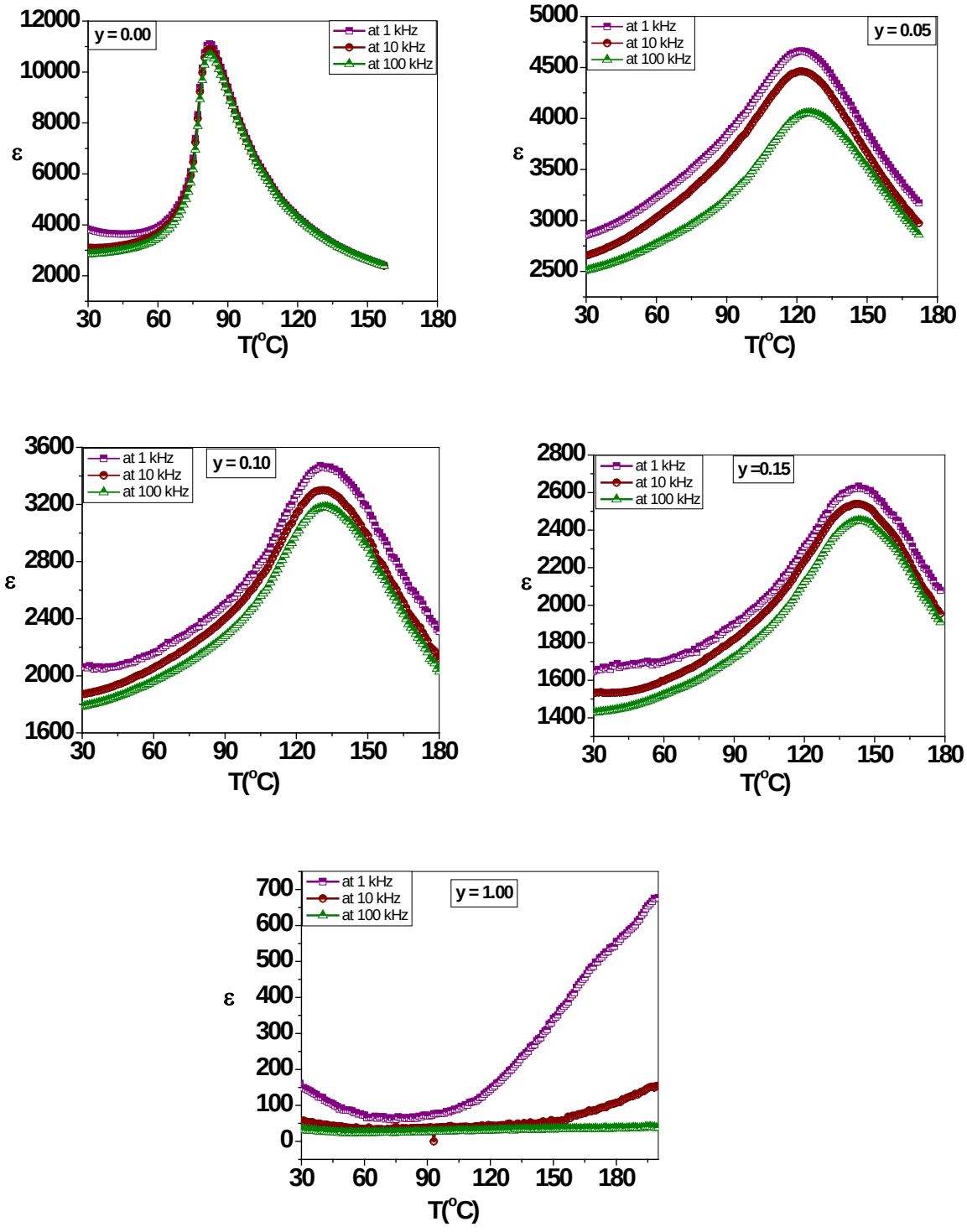

Figure 6.5 Temperature variation of ε at different frequencies for (1-y) BSZT- (y) NZF composites prepared by microwave sintering

Table 6.2

Comaprison of dielectric parameters of conventional and microwave sintered samples at 100kHz

	Conventional sintered				Microwave sintered			
y	ε_{RT}	$\tan\delta_{RT}$	ε_{max}	$\tan\delta_{max}$	ε_{RT}	$\tan\delta_{RT}$	ε_{max}	$\tan\delta_{max}$
0.00	4277	0.07	17548	0.165	2852	0.03	10671	0.145
0.05	2548	0.064	3798	0.031	2521	0.053	4056	0.060
0.10	2307	0.046	3412	0.057	1792	0.049	3184	0.052
0.15	2395	0.039	3108	0.058	1429	0.032	2451	0.049
1.00	556	4.00	-	-	35	0.60	-	-

6.3 Ferroelectric Properties

We have already discussed in detail (*chapter 4, series B2*) the ferroelectric properties of NZF-BSZT composites prepared by conventional solid state route. In this section ferroelectric properties of same compositions which were synthesized by microwave sintering route are discussed. Comparison of room temperature *P-E* hysteresis loops for NZF-BSZT composite prepared by microwave and conventional sintering process are shown in figure *6.6 (a-d)* and their comparison of all ferroelectric parameters are given in *table 6.3*. From this table it is observed that microwave sintered and conventional sintered samples show comparable ferroelectric properties while the processing time of microwave sintering was very less as compared to conventional sintering. But there is decrease in coercive field in case of microwave sintered samples. From table 6.3 it is also observed that, variation in polarization with ferrite content for microwave sintered composite samples is same as that of conventional sintered samples and can be explained on the same lines as discussed in *chapter 4 (Section 4.4, series B2).*

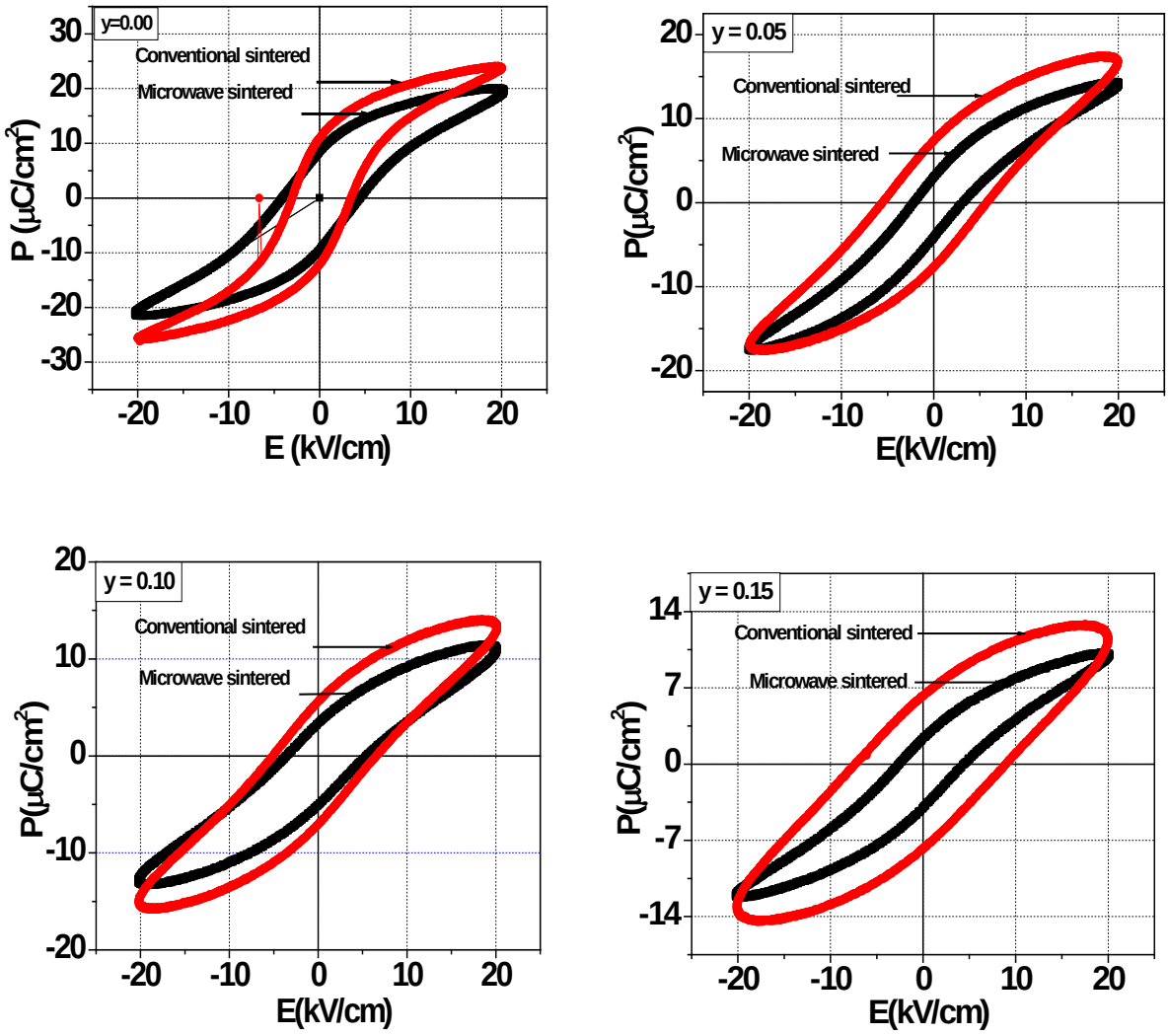

Figure 6.6 Comparison of conventional and microwave sintered P-E hysteresis loops of (1-y) BSZT- (y) NZF composites

6.4 Ferromagnetic Properties

The comparison of room temperature M-H graphs of microwave and conventional sintered samples are shown in *figure 6.7*. All samples exhibit low coercivity values, which is typical nature of soft ferrites. Comparison of all ferromagnetic parameters of conventional sintered and microwave sintered samples are given in *table 6.3*. From this table it is observed that variation of remanant magnetization and saturation magnetization with ferrite content is

similar to as observed for conventional sintered samples (*chapter 4* for *series B2)*. It is also observed that the magnetization of microwave sintered samples is more as compared to the conventional sintered samples. The higher value of magnetization in microwave sintered samples can be related to the porosity of the samples. The conventional sintered samples are porous and porosity causes the discontinuity which prevents the movement of domain walls and hence shows low value of magnetization [14].

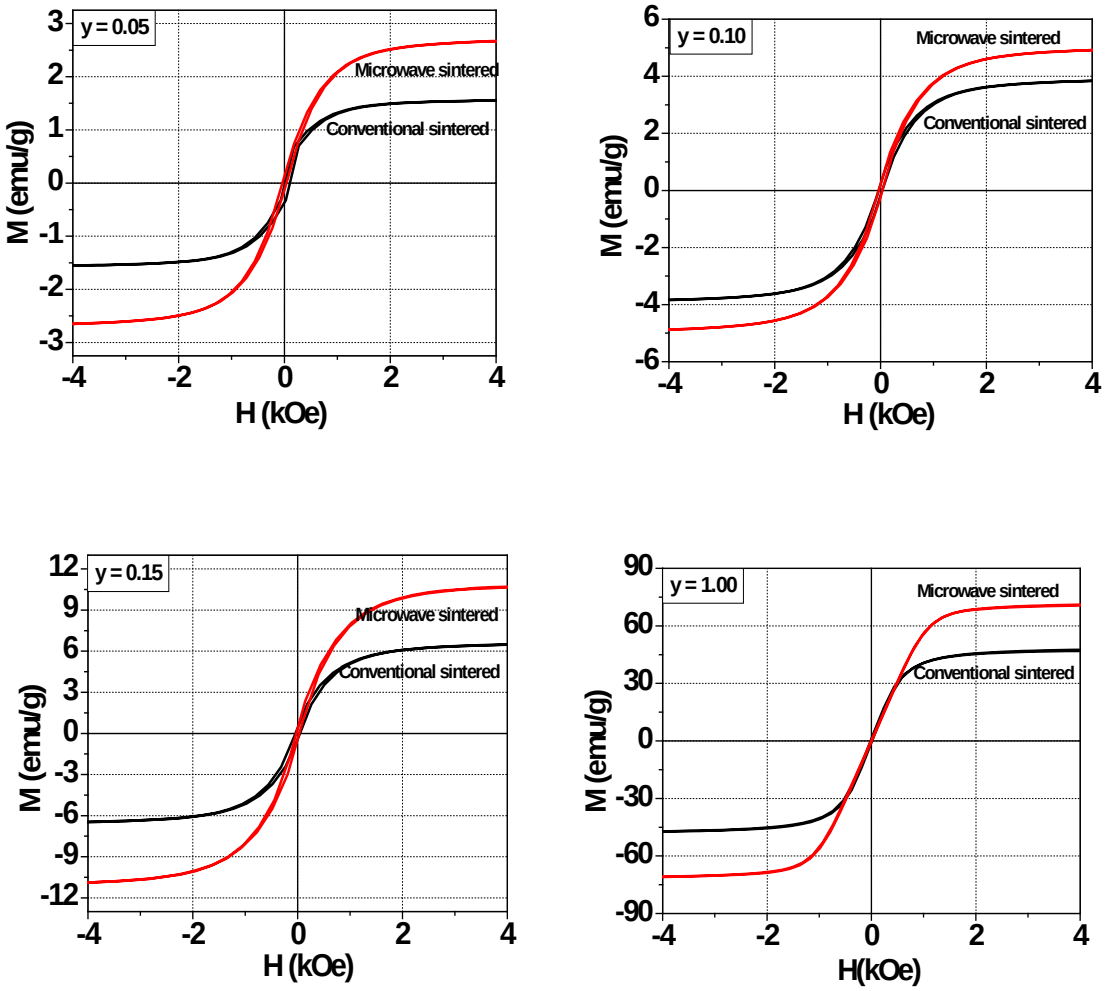

Figure 6.7 Comparison of conventional and Microwave sintered M-H hysteresis loops of (1-y) BSZT- (y) NZF composites

Table 6.3

Comparison of ferroelectric and ferromagnetic parameters of conventionally sintered and microwave sintered composites of (y) NZF - (1-y) BSZT

y	Ferroelectric Parameters						Ferromagnetic Parameters					
	Conventional sintered			Microwave sintered			Conventional sintered			Microwave sintered		
	P_r (μC/cm²)	E_c (kV/cm)	P_{max} (μC/cm²)	P_r (μC/cm²)	E_c (kV/cm)	P_{max} (μC/cm²)	M_r (emu/g)	M_s (emu/g)	H_c (Oe)	M_r (emu/g)	M_s (emu/g)	H_c (Oe)
0.00	11.54	3.2	25.02	9.01	4.26	22.30	_	_	_	_	_	_
0.05	7.42	5.65	17.60	4.20	2.66	16.04	0.156	1.56	93.08	0.238	2.688	72.80
0.10	5.85	6.32	14.96	3.61	4.53	12.45	0.394	4.0	82.23	0.427	4.956	68.67
0.15	7.00	8.15	13.66	3.18	3.55	11.32	0.741	6.5	90.26	0.798	10.94	63.76
1.00	_	_	_	_	_	_	2.91	47.20	30.21	3.4	71.30	21.7

6.5 Magnetoelectric Property

Room temperature M-H hysteresis loops were taken for both electrically poled and unpoled pieces of composite sample. Comparison for poled and unpoled sample (y= 0.10) for conventionally sintered and microwave sintered samples is shown in figure 6.8. It can be easily observed that, there is increase in remanant magnetization and saturation magnetization for electrically poled samples which is the evidence of ME coupling [15]. This enhancement for electrically poled samples is large in microwave sintered sample as compare to conventional sintered sample.

The variation of magnetoelectric coupling coefficient as a function of dc magnetic field was also studied and comparative graph for conventional and microwave sintered sample is shown in *figure 6.9* From this figure it is observed that the variation of ME coupling coefficient with dc magnetic field for microwave sintered sample is similar to the one as observed for conventional sintered samples and this can be explained on the same line as discussed in chapter 4 in section 4.6. From *figure 6.9* it is also observed that the value of ME coefficient is large for microwave sintered sample as compare to conventional sintered sample. The maximum value of magnetoelectric coefficient for microwave sintered sample is due to high resistivity of ferrite phase in microwave sintered sample (because of presence of low number of Fe^{2+} ions) resulting in the decrease in leakage of charge developed in ferroelectric regions.

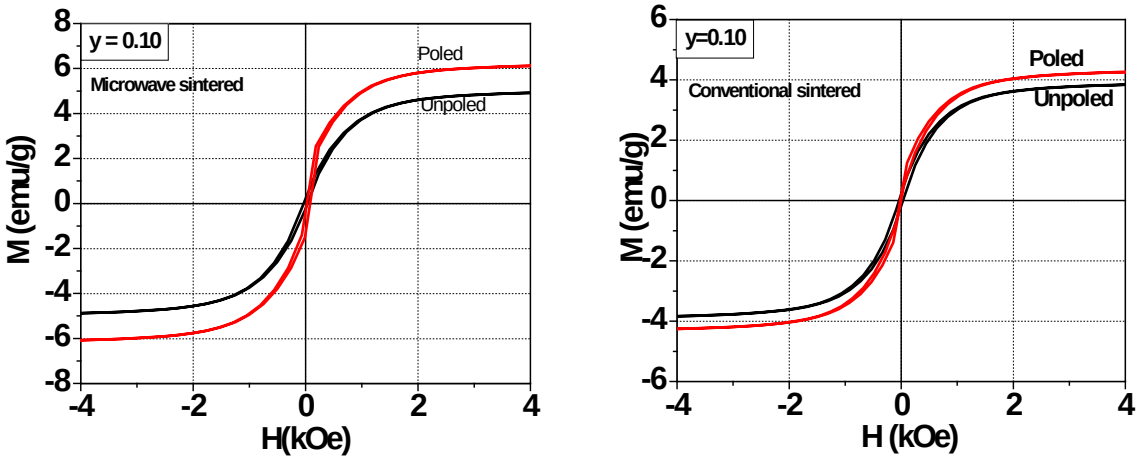

Figure 6.8 Comparison of M-H hysteresis loop for poled and unpoled samples for microwave and conventional sintered sample

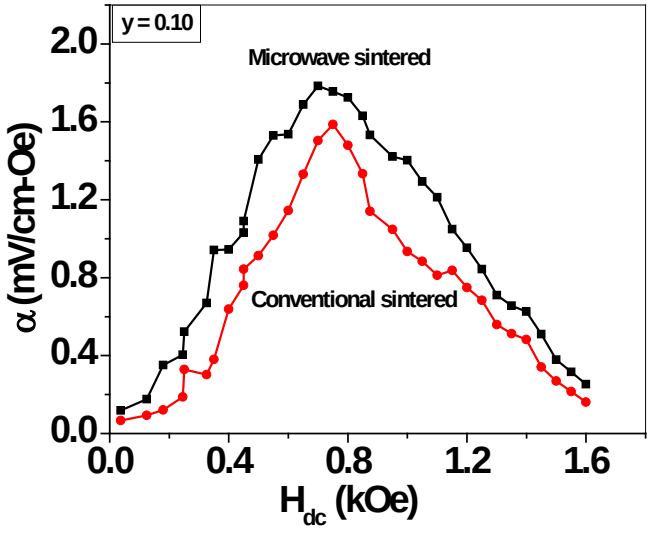

Figure 6.9 Variation of ME coefficient with magnetic field at room temperature for conventional and microwave sintered sample for y = 0.10

Refrences

1) R. Roy, S. Komarneni and J.L. Yang, J. Am. Ceram. Soc., **68** (1985) 392.
2) S. Komarneni and R. Roy, Mater. Lett., **4** (1986) 107.
3) O.P. Thakur, C. Prakash and D.K. Aggarwal, Mater. Sci. Engg. B, **96** (2002) 221
4) R.L. Beatty, W.H. Sutton and M.F. Iskander, Mater. Res. Soc. Proceed, USA **269**, (1992).
5) D.E. Clark, W.R. Tinga and J.R. Laia, Ceram. Trans., **36** (1993) 110.
6) O.P. Thakur, C. Prakash and D.K. Aggarwal, J. Ceram. Process. Res., **3** (2002) 75.
7) R. Roy, S. Komarneni and J.L. Yang, J. Am. Ceram. Soc., **68** (1985) 392.
8) E. Marand, H.R. Baker and J.D. Graybeal, Macromolecules, **25** (1992) 2243.
9) D.K. Aggarwal, Strong Microwaves in Plasma, **2** (2006).
10) A.S. Fawzi, A.D. Sheikh and V.L. Mathe, Phys. B, **405** (2010) 340.
11) O.P. Thakur and C. Prakash, Phase Transitions, **76** (2003) 567.
12) K.K. Patankar and V.L. Mathe, J. Electroceramics, **6** (2001)115.
13) S. Upadhyay, D. Kumar and O. Prakash, Bull. Mater. Sci., **19** (1996) 513.
14) A.R. Reddy, R.G. Mohn, D. Ravinder and B. Boyanov, J. Mater. Sci., **34** (1999) 3169.
15) A. Singh and R. Chatterjee, Appl. Phys. Lett., **93** (2008) 182908.

Chapter - VII

Summary and Recommendation for Future Work

Chapter 7

Summary and Recommendation for Future Work

This chapter summarized the accomplishments demonstrated in this thesis and provides recommendation for future work on ferrite-ferroelectric composites (M-E composites) and their devices. Present work deals with the synthesis and characterizations of modified BST-NZF composites i.e. ferrite-ferroelectric composites in bulk form. The modification was carried out by substituting Zr at B site and La at A site in the ferroelectric phase (BST) of present composite. This substitution was undertaken in a view to understand the suitability of the substituting elements for the enhancement of various properties of these composites. The samples in the bulk form were synthesized by conventional solid state route and one of the series also by using novel techniques namely; microwave sintering. The advantage of microwave sintering over conventional sintering are also discussed. Characterized results are suggestive for suitability of modified ferrite-ferroelectric composites for various applications.

7.1 Summary of the Results

The important results and achievements from the present work are summarized below:

- The sintering temperature of composite samples is always a matter of concern and a systematic study for the optimization of sintering temperature has been carried out in the present work. The Porosity was observed to be lowest for composition sintered at 1325^{o}C. The spontaneous polarization (P_s), room temperature dielectric constant (ε_{RT}) and spontaneous magnetization was observed to be highest for composition sintered at same

temperature. Hence, optimum temperature for sintering for composite samples at which dielectric, ferroelectric and ferromagnetic properties are better is 1325^{o}C.

- Structural properties were studied by using XRD patterns and SEM micrographs. Confirmation of both phases was carried out by using XRD patterns. The XRD peaks corresponding to ferrite phase become more pronounced with increase in ferrite content. In case of Zr substituted composite, structure of the material changes from tetragonal to rhombohedral and lattice parameter was found to increase with increase in Zr content while in case of La substituted composite, the structure of the material remains same i.e. tetragonal structure but lattice parameter was found to decreases with increase in La content. Variation in the lattice parameter was explained in terms of different ionic radii of substituents. In SEM micrographs it is difficult to differentiate between two individual phases. Grain size was found to decrease with increase in Zr content and also with La content.
- La and Zr substitution in BST-NZF composites provides many interesting features in the dielectric properties of the material, such as shifting in Curie temperature and modification of dielectric properties. It was found that room temperature dielectric constant increases and dielectric loss decreases with increase in Zr content and make sample suitable for good memory devices applications. The increase in room temperature dielectric constant may be due to shifting of Curie temperature towards room temperature. The dielectric peaks get broadened with increase in Zr content. The similar trend is observed with variation of La content in composite samples. If we compare the dielectric, ferroelectric and magnetoelectric properties of unsubstituted series (BST-NZF), Zr substituted series (BSZT-NZF) and La substituted series (BSLT-NZF), it was found that composite samples having La substituted ferroelectric phase shows improved properties as compared to other series.
- It was found that Zr and La substitution had very prominent effect on the ferroelectric and magnetoelectric properties of composite samples. Electrical polarization was found to decrease with increase in Zr and La content but for Zr = 0.04% and La = 0.005% it was found to be maximum. Magnetoelectric coefficient was found to be increase up to 10% ferrite content and after that decreases with further increase in ferrite content for all series

samples. But La substituted composite samples show improved ferroelectric and magnetoelectric properties as compare to unsubstituted and Zr substituted composite samples. Hence, from the results we can conclude that Zr and La modified composites can be used for memory devices over a temperature range, sensors, transducers due to their low dielectric loss and high magnetoelectric coefficient. They can also be exploited as sensors, wave guide, transducers and actuators due to their improved properties.

- Series D was sintered by microwave technique and characterized for various properties. It was found that XRD patterns show well defined peaks and no extra peak was observed irrespective of whether the material was densified by conventional or microwave techniques. Higher value of experimental density was found in case of microwave sintered samples as compared to the density values of similar compositions obtained by conventional process. Hence we conclude that larger densification can be achieved in short interval of time by microwave sintering. It was also found that with microwave sintering we get comparable dielectric constant to the conventional sintered samples with decrease in dielectric loss. Hence we get samples with low loss and comparable dielectric constant in a short interval of time by microwave sintering. It was observed that microwave sintered samples also shows comparable ferroelectric properties to conventional sintered samples while the processing time of microwave sintering was very less as compared to conventional sintering. Magnetization was found to be more in microwave sintered samples as compared to the conventional sintered samples. From all these results we conclude that microwave sintering not only improves properties of the samples but also save energy and time.

7.2 Recommendation forFuture Work:

The thesis explored several aspects of ferrite-ferroelectric composite materials in modified BST-NZF system. As these materials show magnetoelectric property thus they have received continuous attention as potential sensors for magnetic field measurements and transducers for magnetoelectric conversion and actuators. These composites are of interest for a variety of device applications including electrically controlled electro-optic or piezoelectric

devices, actuators and magnetoelectric memory devices. The modified BST-NZF compositions needed to be investigated for other applications as well. Accordingly, it is quite interesting to explore the ways and means to improve the various properties in our future research work. The studies suggested for these materials for future work are as follows:

- In the present work, only compositions of BST-NZF with Ba/Sr ratio 90/10 and Ni/Zn ratio 80/20 have been studied. Composition with different ratio and with different substituents can be studied systematically for further improvement in their properties.
- The same work can be done by other processing techniques like mechano-chemical alloying and chemical methods. This may result in better improvement in their various properties.
- Dielectric property with dc magnetic field can be studied. This may give further more information about magnetoelectric coupling.

****